Compton Scattering by Nuclei *

M.-Th. Hütt [a,1], A.I. L'vov [b,2], A.I. Milstein [c,3], M. Schumacher [a,4]

[a] *Zweites Physikalisches Institut, Universität Göttingen, D-37073 Göttingen, Germany*
[b] *P.N. Lebedev Physical Institute, Leninsky Prospect 53, Moscow 117924, Russia*
[c] *Budker Institute of Nuclear Physics, 630090 Novosibirsk, Russia*

Abstract

The concept of Compton scattering by even-even nuclei from giant-resonance to nucleon-resonance energies and the status of experimental and theoretical researches in this field are outlined. The description of Compton scattering by nuclei starts from different complementary approaches, namely from second-order S-matrix and from dispersion theories. Making use of these, it is possible to incorporate into the predicted nuclear scattering amplitudes all the information available from other channels, *viz.* photon-nucleon and photon-meson channels, and to efficiently make use of models of the nucleon, the nucleus and the nucleon-nucleon interaction. The total photoabsorption cross section constrains the nuclear scattering amplitude in the forward direction. The specific information obtained from Compton scattering therefore stems from the angular dependence of the nuclear scattering amplitude, providing detailed insight into the dynamics of the nuclear and nucleon degrees of freedom and into the interplay between them. Nuclear Compton scattering in the giant-resonance energy-region provides information on the dynamical properties of the in-medium mass of the nucleon. Most prominently, the electromagnetic polarizabilities of the nucleon in the nuclear medium can be extracted from nuclear Compton scattering data obtained in the quasi-deuteron energy-region. In our description of this latter process special emphasis is laid upon the exploration of many-body and two-body effects entering into the nuclear dynamics. Recent results are presented for two-body effects due to the mesonic seagull amplitude and due to the excitation of nucleon internal degrees of freedom accompanied by meson exchanges. Due to these studies the in-medium electromagnetic polarizabilities are by now well understood, whereas the understanding of nuclear Compton scattering in the Δ-resonance range is only at the beginning. Furthermore, phenomenological methods how to include retardation effects in the scattering amplitude are discussed and compared with model predictions.

*Supported by Deutsche Forschungsgemeinschaft (Schu222, SFB201, 436RUS113/510) and DAAD
[1] e-mail: huett@bio.tu-darmstadt.de
[2] e-mail: lvov@x4u.lebedev.ru
[3] e-mail: A.I.Milstein@inp.nsk.su
[4] e-mail: Martin.Schumacher@phys.uni-goettingen.de

Contents

1 Introduction

The discovery made by Compton in 1922 [1] that photons are scattered by free electrons is one of the mile-stones of modern physics. In this process an energy shift of the photon was observed which quantitatively could be explained by assuming an elastic collision between particles. Later on, the term Compton scattering has been transferred to photon scattering by other objects as there are atoms, nucleons and nuclei. An essential difference between free electrons and these other objects is that the latter have an internal structure so that excitation and particle emission processes become possible. In that case the term Compton scattering is used to denote coherent-elastic photon scattering where the scattering object coincides in all (internal) quantum numbers in the initial and final states. In case of atoms the term Compton scattering occasionally is replaced by the term Rayleigh scattering [2]. This is of advantage in cases where the coherent-elastic scattering process (Rayleigh scattering) is discussed together with the incoherent scattering process (also called Compton Scattering), where one bound electron is ejected from the electron cloud into the continuum. This process then resembles the one discovered by Compton [1] except for the appearance of binding effects [3]. The term Raman scattering is used in the case where the atom or nucleus does not return to the initial state but no particle emission is taking place. Another related photon scattering process is coherent-elastic scattering in the Coulomb field of nuclei termed Delbrück scattering [4,5]. The three coherent-elastic photon scattering processes, *viz.* atomic Rayleigh scattering, Delbrück scattering and nuclear Compton scattering are expected to interfere with each other. This has been observed in several investigations [5].

1.1 Early work on nuclear Compton scattering in the giant-resonance region

Scattering of photons in the region of the "giant resonance" of the nucleus was probably first observed by Gaerttner and Yeater [6] and Dressel, Goldhaber, and Hanson [7]. These works were motivated by Goldhaber and Teller [8] who proposed to understand a pronounced structure in the photoabsorption cross section between 10 and 30 MeV in terms of a collective motion of protons against neutrons. The experiments were made feasible by the advent of betatrons delivering photons of sufficient energy but suffered from the lack of efficient photon detectors. More refined experiments became possible with the advent of NaI(Tl) scintillation counters which were first applied by Stearns [9] and Fuller and Hayward [10, 11]. Stearns used monochromatic photons of 17.6 MeV from the ^{7}Li(p,γ) nuclear reaction whereas Fuller and Hayward used continuous photons produced by a betatron.

A remarkable progress was made by Hayward et al. in 1973 [12] with the first application of monochromatic linearly polarized photons. These photons were produced by resonance fluorescence of the well-known 1^+ state at 15.1 MeV in ^{12}C. With these experiments a discrimination was possible between nuclear Compton scattering and nuclear Raman scattering, the latter being especially strong for deformed nuclei.

1.2 Nuclear Compton scattering experiments from the mid-1970th to the present

The breakthrough in investigations of nuclear Compton scattering came with the advent of large-volume NaI(Tl) detectors and the availability of quasimonochromatic photons [13–48]. As a first step the technique of positron-annihilation-in-flight has been applied to produce quasimonochromatic photons. In early uses of bremsstrahlung two different techniques have been developed. In one of these the total spectrum of bremsstrahlung photons was used. By applying very narrow collimators in front of the NaI(Tl) detectors the low-energy tails of the response functions were largely suppressed so that large portions of the spectra of scattered photons could be interpreted in terms of Compton scattering. This method was efficiently used by B. Ziegler et al. [25, 26, 30] and led to insight into

general properties of nuclear scattering amplitudes below meson photoproduction threshold, *viz.*the importance of formfactors, the possibility to investigate the electromagnetic polarizabilities of nucleons in the nuclear medium (*cf.* also [24]), *etc.* When using wider collimators in front of the NaI(Tl) detectors the response functions generate a low-energy tail. In this case only a narrow energy range at the upper end of the bremsstrahlung spectrum can be interpreted in terms of Compton scattering.

The techniques described in the foregoing paragraph have been more and more replaced by tagged photons either from bremsstrahlung or from backscattered laser light. In this technique the energy of the secondary electron is measured in a magnetic spectrometer so that the energy of the primary photon is known through a coincidence condition with the Compton scattered photon or some other reaction product. This technique was first applied to nuclear Compton scattering experiments at the University of Illinois [49] and is now standard in all laboratories — *viz.* Brookhaven [50], Lund [51,52], Mainz [53,54], Saskatoon [55] — where experiments on Compton scattering by nuclei are carried out. Back scattering of laser light [50] and coherent bremsstrahlung from diamond crystals [56–58] are also efficient sources of linearly polarized photons. At low energies (5–100 MeV) also the method of off-axis tagging [33, 59] leads to reasonable degrees of linear polarization.

An other type of experiments which has to be mentioned here has achieved very high energy resolution ($\approx$ 10 keV) due to the use of Ge(Li) detectors and due to the use of photons from nuclear reactions [60–66]. These experiments were restricted to energies from about 5 MeV [61] to 17.4 MeV [63]. The high energy-resolution was of essential help in cases where Compton scattered photons had to be discriminated from photons stemming from nuclear resonance fluorescence or nuclear Raman scattering.

1.3 Motivations for studying nuclear Compton scattering

Several experiments on Compton scattering by nuclei were concerned with multipole decompositions of giant resonances [13, 15, 16, 18, 19, 21, 25, 26, 30, 33, 64]. The comparatively weak electric quadrupole amplitude is enhanced through interference with the dominant electric-dipole amplitude. Therefore, nuclear Compton scattering became a tool to study the properties of the isovector electric quadrupole resonance. In fact, this is the only model independent method existing for this purpose. The status of this research will be discussed in section 4.

An interesting feature of nuclear Compton scattering below meson photoproduction threshold which has been realized very early is its strong sensitivity to meson exchange currents (MEC) between nucleons [67–83]. In this respect Compton scattering is of essential superiority to electron scattering at similar momentum transfers which is to a large extent insensitive to this phenomenon. The study of MEC degrees of freedom and their interplay with nuclear degrees of freedom have attracted strong interest in many investigations, and different schools have approached these phenomena in different ways. Meson exchange currents have long been realized to be the origin for the enhancement of the integrated dipole strength in comparison with the prediction Σ_{TRK} of the usual Thomas-Reiche-Kuhn (TRK) sum rule [67]. The integrated strength of the giant-dipole resonance (GDR) overshoots the TRK sum rule prediction by the factor $(1 + \kappa^{GDR})$. The quasi deuteron (QD) photoabsorption process which can be interpreted as the absorption by correlated proton-neutron pairs inside the nucleus, provides an additional strength [84] $\kappa^{QD}\Sigma_{TRK}$. It was a great progress to show [68] that due to gauge invariance MEC also have to modify the non-resonant contribution to the scattering amplitude, i.e. the so-called seagull amplitude, which accompanies resonant scattering through intermediate excited nuclear-structure states. In the absence of MEC the seagull amplitude would simply be the superposition of the Thomson scattering amplitudes of the protons in the nucleus forming the "kinetic seagull amplitude". Accordingly it was discussed in what way the modification of the total seagull amplitude through an additional "exchange" or "mesonic" seagull amplitude could possibly be understood as

Thomson scattering by pions in nuclei [71–75, 78, 83]. According to Siegert's theorem [85] there is no charge-density modification due to mesons in a nucleus (except for a small relativistic correction) but an additional (two-body) current due to the exchange of charged mesons. Therefore, the interpretation of the MEC contribution to the seagull amplitude requires special care (*cf.* sections 3.3 and 7). It turns out that the giant-resonance part of the mesonic seagull amplitude is closely related to the in-medium mass of the nucleon [63, 66, 86–97] which is a special case of the general Brown and Rho scaling [91–94, 96–98]. One motivation to study nuclear Compton scattering, therefore, is to get further insight into the properties of the in-medium mass of the nucleon.

Below meson photoproduction threshold the internal excitation of the nucleon enters into the nuclear Compton scattering amplitude via the electromagnetic polarizabilities of the nucleon [99–101]. The electromagnetic polarizabilities are fundamental constants, characterizing the response of the nucleon to an external electromagnetic field and, thus, the dynamical structure of the nucleon. The advantage of the electromagnetic polarizabilities of the nucleon is that they can precisely be measured for the free and the bound nucleon by carrying out Compton scattering experiments. Because of this property, the electromagnetic polarizabilities are an ideal observable for exploring possible in-medium modifications of the nucleon structure. Some fundamental theoretical aspects of the in-medium electromagnetic polarizabilities have been discussed on the basis of quark models [102, 103] and pion-cloud models [80, 82, 104]. In recent time essential progress has been made in this field of research both experimentally and theoretically (*cf.* sections 5 and 9).

For energies in the resonance range of the nucleon above meson photoproduction threshold only first steps have been made in the investigation of nuclear Compton scattering. One reason for this delay is that only a very fragmentary set of data was available, even for the nucleus ^{4}He which was the subject of principal interest for experimental researches [20, 23, 29, 35, 40, 44, 45]. On the experimental side considerable progress has been made very recently by the Göttingen-Mainz collaboration at MAMI (Mainz) [44, 46] and by the LEGS collaboration at Brookhaven [45] where differential cross sections for Compton scattering by ^{4}He have been measured in large angular and energy intervals. These experiments showed that the widely accepted theoretical description of Compton scattering in terms of the Δ-hole model [105–109] is in serious disagreement with experimental data [46]. This leads to the conclusion that the in-medium excitation of the Δ resonance is not fully understood and possibly may lead to new insights into the structure of the bound nucleon.

1.4 Fields related to nuclear Compton scattering

In addition to nuclear Compton scattering, nuclear Raman scattering and nuclear resonance fluorescence have remained branches of photon scattering researches up to present days. For deformed nuclei with ground-state spins $I \geq 1$ Raman scattering is possible as an incoherent (non-interfering) elastic scattering process ending up with a nonexcited nucleus, but in a spin-state differing from that of the initial state. Raman scattering into excited states [49, 110–115] is also possible as an inelastic scattering process. The theoretical framework appropriate to describe Raman scattering is the concept of generalized polarizabilities [116–122] leading in a natural way to a discrimination between scalar (Compton) and tensorial (Raman) scattering and — as a third possibility — vector scattering.

Nuclear resonance fluorescence takes place at energies below particle threshold of the nucleus as an elastic photon scattering process through the excitation of isolated nuclear states [123]. The study of this process serves as a tool of low-energy nuclear spectroscopy which is not considered here in detail.

1.5 Organization of the present paper

The topic of Compton scattering by nuclei cannot be covered completely in one article. Therefore, this paper is strongly biased by our own preferences and results. Historical aspects and lines of development going back to previous researches have briefly been covered in the foregoing parts of this section, or will be mentioned in introductory parts of sections to come. To supplement on this we recommend to take notice also of previous reports [121, 124–130]. We believe that the present report differs from the previous ones by the fact that subnuclear and retardation phenomena of nuclear Compton scattering have received a much better understanding due to recent — partly unpublished — researches. Also, due to very recent experimental and theoretical results Compton scattering in the Δ resonance range has received a wider coverage than before.

The present article is concerned with Compton scattering by spin-saturated nuclei. This restriction involves that the lightest nucleus to be discussed here is ^{4}He. Other nuclei of experimental interest are ^{12}C, ^{16}O, ^{40}Ca and ^{208}Pb. These are the nuclei where a reasonable amount of experimental data on Compton scattering are available. In comparison to these the investigations of the deuteron — though being the most fundamental ones — are at the very beginning and we give here only few references to recent experimental and theoretical works [131–136].

In **section 2** we give a definition of the degrees of freedom of nucleons in a nucleus. Our main goal is to get a clear-cut distinction between the external (nuclear structure) and the internal degrees of freedom of the bound nucleon. It is pointed out that the "classical subnuclear degrees of freedom" viz. meson exchange currents (MEC) are not specific for the one or the other part but separately enter into both.

In **section 3** we formulate an outline of the theoretical aspects of Compton scattering below meson photoproduction threshold. We start from relativistic second-order perturbation theory, point out how MEC and the "negative energy states" of the nucleus can be taken care of, and show how dispersion theory can be used to make links to experimental data.

Section 4 is devoted to our present understanding of giant-resonances. Since previous work has been covered in previous reviews [121, 126, 127] we concentrate on our own regions of researches, as there are enhancement and retardation effects and the dynamics of the giant-resonance mode. Furthermore, we give a detailed description of the retardation problem which is sizable in nuclear Compton scattering because the wavelengths of the photon $1/\omega$, where ω is the photon energy, and the nuclear radius R are of the same order of magnitude. The solution of the retardation problem which we present may appear as a preliminary guess at a first sight. Nevertheless, the results we obtain are quite precise numerically, as will be shown in section 10 through a model calculation.

Section 5 is devoted to effects which are observed in the quasideuteron range of the nucleus. Since the quasideuteron process itself does not make large contributions to the nuclear scattering amplitude this section is mainly concerned with the polarizabilities of the bound nucleon which belong to the most interesting aspects of nuclear Compton scattering.

Section 6 describes our present knowledge in the Δ-resonance region. Unfortunately, the study of nuclear Compton scattering above meson photoproduction threshold is only at the beginning and very interesting properties of nuclear Compton scattering in this energy range have not yet been investigated quantitatively. Accordingly, this section only provides a brief description of recent points of discussion.

Section 7 again is concerned with the giant-resonance region but describes interpretations of subnuclear effects in terms of effective masses and effective currents of nucleons in the framework of the Fermi liquid theory. This section also refers to modern views, *e.g.* the general Brown and Rho scaling [96, 97].

The following three sections 8–10 are devoted to recent theoretical developments. **Section 8** describes a dispersion theory at fixed momentum transfer for nuclear Compton scattering. In **section 9** a diagrammatic model of meson exchange currents is discussed, which essentially clarifies the most important properties of the mesonic seagull amplitude and, in addition, leads to quantitative results for exchange form factors and meson-induced polarizability modifications. In **section 10** retardation effects are studied within a relativistic oscillator model.

We do not include a discussion of nuclear Compton scattering in the asymptotic range beyond 1.5–2.0 GeV into this article, because there has been no recent research and because there are comprehensive reviews of this field [137]. Access to literature is given in [128] for diffractive Compton scattering taking place at small scattering angles. Large-angle Compton scattering takes place via direct photon-quark coupling which is described in [138–141].

Summary: Our main motivation for studying nuclear Compton scattering was to investigate in-medium properties of nucleons as there are
(i) the in-medium mass of the nucleon,
(ii) the in-medium electromagnetic polarizabilities,
(iii) the in-medium Δ excitation.
During these studies it turned out that some theoretical aspects which are essential for the data analysis were not understood with the desirable clarity and, therefore, had to be investigated along with the in-medium properties.
These are
(iv) the relation between retardation and higher multipoles,
and
(v) the effects of meson-exchange currents on the in-medium electromagnetic polarizabilities.
Further work has to be done to understand
(vi) the effects of meson exchange currents on Compton scattering in the Δ-range.

2 The absorption of photons and the degrees of freedom of the nucleus

Compton scattering is closely related to the process of photoabsorption, since the Compton amplitude for forward scattering can be expressed via the total absorption cross section with the help of the optical theorem and a dispersion relation. In this sense the total photoabsorption cross section is a special case of Compton scattering and, therefore, a detailed understanding of nuclear photoabsorption is of essential help for the discussion of Compton scattering. Our goal is to investigate the nuclear and subnuclear degrees of freedom of the nucleus in a consistent way. This means that we first have to consider the properties of free nucleons and then we have to ask what the modifications are which enter into the picture as a consequence of nuclear binding. As a result of this discussion we arrive at a clear-cut distinction between the external (nuclear structure) and internal degrees of freedom of the bound nucleon.

2.1 Photoabsorption by the nucleon

For illustration Fig. 2.1 shows the photoabsorption cross section of the proton separated into partial cross sections. The photoabsorption cross section of the nucleon starts at the meson photoproduction threshold and continues through different regions of photo-excitation mechanisms. In the region of nucleon resonances which terminates at photon energies of about 1.5 to 2 GeV we find three broad lines corresponding to the $\Delta(1232)P_{33}$, $N(1520)D_{13}$ and $N(1680)F_{15}$ nucleon resonances located at photon energies of 320 MeV, 740 MeV and 1020 MeV, respectively. The excitation of these resonances proceeds through photons of, respectively, $M1$, $E1$ and $E2$ multipolarities. The properties of these resonances and also those of the weaker ones have successfully been understood in terms of three constituent quarks located in a binding potential. In addition we find a nonresonant background corresponding to one-pion photoproduction up to about 400 MeV and to more complicated mechanisms above.

Figure 2.1: *Photoabsorption cross section of the proton schematically separated into partial cross sections [142] containing nucleon resonances and a nonresonant component.*

The range of energies beyond about 2 GeV is frequently called the asymptotic range of the photoabsorption cross section. Here we find vector mesons, i.e. ω, ρ, ϕ etc. in the intermediate state. This means that there is no direct interaction of the photon with the constituents of the nucleon. In addition, the interaction of these vector mesons with the nucleon also is not direct but proceeds peripheral through t-channel exchanges. The main candidates for these t-channel exchanges are the isoscalar tensor meson $f_2(1270)$, the isovector tensor meson $a_2(1320)$ and the Pomeron $\mathcal{P}$, where the Pomeron takes care of the energy independent part of the photoabsorption cross section, while the two tensor mesons take care of its energy dependent part. The isovector meson $a_2(1320)$ has to be introduced in addition to the isoscalar meson $f_2(1270)$ because proton and neutron differ slightly in the energy-dependent part of the cross section [142]. The t-channel exchanges entering into the description of forward-direction Compton scattering have spin 2 in accordance with general conservation rules.

In considering the properties of the nucleon photoabsorption cross section in the asymptotic range, we have to be aware that the total photoabsorption cross section is subject to inclusive reactions where there is no detection of the particles in the final state. In this case we predominantly observe those processes which make the largest contributions to the photoabsorption cross section. These are the processes at small transverse momentum, i.e. the peripheral processes mentioned above. On the other hand, in exclusive reactions where particles in the final state are detected, processes with

large transverse momenta may be separated experimentally. Here we again observe direct couplings of photons with constituents which now are the individual valence quarks. Some more detailed discussions of this aspect can be found in articles contained in [143] and in [138, 139].

2.2 Photoabsorption by the nucleus

When combining nucleons to form a nucleus three major changes are observed:

(i) The photoabsorption cross section extends below pion photoproduction threshold to form two nuclear-structure modes of photo excitation, *viz.* the giant resonance (GR) mode and the quasideuteron (QD) mode. In order to understand these two modes of excitation, the internal structure of the nucleon probably may not be of explicit relevance — although we do not know this for sure. To start with, we may use a picture where unmodified nucleons in their ground states and mesons being exchanged between them are the only nuclear constituents to deal with.

Figure 2.2 gives a schematic view of the photoabsorption cross section of ^{208}Pb between the giant resonance range and the Δ range. The giant resonance range is dominated by the giant-dipole resonance (GDR). The photoabsorption cross section is well described by a Lorentzian line which extends below the particle threshold of the nucleus in the form of narrow lines [145]. The strengths contained in these individual narrow lines is given through the interplay between the Lorentzian tail of the GDR and the density of levels. This leads to the consequence that there is a minimum in the individual strengths close to the particle threshold as indicated in Fig. 2.2. The quasideuteron cross section starts at the p-n two-particle threshold and extends into the Δ range above the pion threshold.

Figure 2.2: *Schematic view of the nuclear photoabsorption cross section of ^{208}Pb from the giant resonance to the Δ resonance range. GDR: giant-dipole resonance, GQR: isovector giant-quadrupole resonance, QD: quasideuteron mode, Δ: Delta resonance of nucleons in the nucleus, Born: nonresonant photoexcitation of nucleons in the nucleus through the Born terms of the photo-pion amplitudes [144].*

(ii) Above pion photoproduction threshold in the resonance range of the nucleon we find a broadening of the resonances increasing with mass number A. This is shown in Fig. 2.3 where the normalized photoabsorption cross section for the proton is compared with those of the three lightest nuclei. The solid line represents the normalized photoabsorption cross section of complex nuclei ($A \gtrsim 4$). In this universal curve there is no indication left of a $D_{13}(1520)$ resonance. Irrespective of this, there seems to be a conservation of the integrated photoabsorption strength when going from free to bound nucleons [147].

Figure 2.3: *Total photoabsorption cross sections per nucleon. Data are shown for ^{1}H (black circles), ^{2}H (gray circles), ^{3}He (open circles) and ^{4}He (grey squares) [146]. The solid line represents the universal curve for complex nuclei.*

(iii) In the asymptotic range of the nucleon photoabsorption cross section (beyond 1.5 - 2 GeV) the scaling of the photoabsorption cross section with mass number A observed through the universal curve of Fig. 2.3 is no longer valid. Instead we find a proportionality of the photoabsorption cross section with A^α with α lying somewhere between 1 and 2/3, i.e. between a proportionality to the nuclear volume and the area of the nuclear cross-section. This change in proportionality is due to the fact that the interaction of the intermediate-state vector mesons with the nucleus is of very short range. This property of the photoabsorption cross section is called shadowing which is illustrated by Fig. 2.4.

Figure 2.4: *Fits to the total nuclear photoabsorption cross sections per nucleon as an example of shadowing in the asymptotic region [148].*

Further properties of giant resonances:
Giant resonances may be viewed as nuclear transitions in the shell model from occupied states below the Fermi level to unoccupied states above it. For a given multipolarity these transitions occur coherently, which may be visualized in terms of a collective model [149]. A further aspect is the strong interaction between nucleons. This leads to the need of replacing particle-hole excitations by quasiparticle-quasihole excitations, where the latter may be described in terms of the Fermi liquid theory of finite nuclei. This aspect will be covered in section 7.

As contributions to Compton scattering, the giant resonances can be characterized by their electromagnetic multipolarity. In this way a definite dependence on the scattering angle is assigned to each resonance. The most prominent contribution to giant resonances stems from the isovector giant-dipole resonance (GDR) which is seen in all nuclei including ^{4}He. In heavy nuclei this giant dipole resonance has successfully been parameterized in terms of one Lorentzian line in case of spherical nuclei, or in terms of the superposition of two Lorentzian lines in case of deformed nuclei [150, 151]. Axially deformed means prolate deformation as far as we know. There seems to be only one case of an investigation of an oblate deformed nucleus [115], *viz.* ^{127}I. However, in this case it turned out that the giant resonance did not behave like a collective motion with respect to two independent axes.

Most of the available information on photoabsorption cross sections of medium-mass to heavy nuclei has been obtained by photo-neutron experiments [152]. For light to medium-mass nuclei photoabsorption cross sections in the GR and QD ranges have been measured by photon attenuation experiments [84], because for these nuclei photoneutron experiments do not lead to information on the total absorption cross section due to sizable contributions from proton channels.

It is interesting to note that the Lorentzian shape of the GDR extends below the particle threshold where we find individual nuclear levels instead of a continuum. Some details concerning the properties of strengths of individual nuclear levels has already been discussed in connection with Fig. 2.2. In order to prove these expected properties, rather sophisticated methods had to be applied [145]. A series of narrow γ lines ($\Delta E \approx 10$ eV) produced via the neutron capture reaction was used to investigate nuclear resonance fluorescence due to a random overlap of photons with nuclear levels. Using statistical methods it was possible to get insight into the properties of $E1$ excitations in the tail region of giant resonances. It may be of interest to note that the same statistical ansatz applied to the giant-resonance tail also explains the observed distributions of electric-dipole strengths in nuclei [153].

Figure 2.5 gives a schematic view of the giant-resonance structure of ^{208}Pb for the first three multipoles, *viz.* E1, M1 and E2 [95]. Each multipole is split up into an isoscalar and an isovector component. For the E1 multipole the isoscalar component is identical with Thomson scattering of the whole nucleus and therefore does not show up as a separate excitation mode.

Figure 2.5: *Schematic representation of giant resonance multipoles for ^{208}Pb. $(E1)_1$: isovector giant electric-dipole resonance (GDR), $(M1)_0$: isoscalar giant magnetic-dipole resonance, $(M1)_1$: isovector giant magnetic-dipole resonance,$(E2)_0$: isoscalar giant electric-quadrupole resonance, $(E2)_1$: isovector giant electric-quadrupole resonance [95].*

To summarize, the GR degree of freedom of the nucleus corresponds to the complete set of one-quasiparticle one-quasihole states in a shell model. This allows us to introduce a scattering amplitude T_{GR} for the giant-resonance degree of freedom which separately is gauge invariant, if the non-resonant (seagull) contributions are treated properly.

Further properties of quasideuterons:
Quasideuterons (QD) are proton-neutron pairs correlated through the exchange of charged mesons. Therefore, QD are the smallest cluster states in nuclei which may show up in the interaction with photons. There are several approaches to a description of QD excitations of which we mention the approaches of Levinger [154], Gottfried [155] and Laget [156]. From the point of view of a proper treatment of degrees of freedom and sum rules, the Laget model is the most appropriate one , because it relates the total QD strength to exchange currents via the relation

$$\sigma_{QD} = L\frac{NZ}{A}\sigma_D^{ex}, \tag{2.1}$$

where σ_{QD} is the quasideuteron cross section, σ_D^{ex} the exchange part of the deuteron photoabsorption cross section, Z and N are the charge number and the neutron number, respectively, of the nucleus and L is a parameter. This means that the total classical or non-mesonic (Thomas-Reiche-Kuhn) dipole strength is contained in the giant resonances as is also suggested by shell model considerations. Then meson exchange currents provide us with an enhancement of the giant resonance strength and — in addition — with the QD strength. Beyond this favorable property the Laget formula has not to be taken too literally because considerable differences are expected between deuterons and quasi-deuterons.

For the analysis of Compton scattering data it is most convenient to use a Lorentzian representation as proposed by Ziegler [15].

Similar to the giant-resonance (GR) degree of freedom the (QD) degree of freedom may be related to a complete set of isovector 2-particle 2-hole states, allowing us to introduce a separately gauge invariant amplitude T_{QD}, again with the prerequisite that this amplitude is properly accompanied by non-resonant (seagull) contributions.

Further properties of the Δ range of the nucleus:
Figure 2.6 shows the photoabsorption cross section of a complex nucleus split up into different contributing components. The two nonresonant components are due to the quasideuteron effect and due to the Born term of the photo-pion amplitude. The Δ resonance contribution is split up into two components. The high energy part with its maximum around 350 MeV corresponds to real-meson photoproduction whereas the low energy part with its maximum around 260 MeV to virtual-meson photoproduction.

Figure 2.6: *Total nuclear photoabsorption cross sections per nucleon. Data are shown for nuclei between ^{4}He and ^{238}U [148]. In addition the result of a model calculation for the universal photoabsorption curve is shown [157]. The left curve extending underneath the Δ resonance is the QD cross section. The Δ-resonance cross section is partitioned into two curves, into a non-mesonic part (left resonant curve) and a mesonic part (right resonant curve). The nonresonant curve in the Δ range corresponds to the Born term of meson photoproduction.*

This latter phenomenon is well known from photodisintegration experiments on the deuteron where a bump-like structure is observed in the non-mesonic cross section at energies above meson threshold. This bump-like structure occurs through excitation of the Δ resonance with subsequent two-nucleon disintegration of the deuteron. In recent experimental investigations on ^{4}He [158] with the subsequent theoretical investigations [157] on complex nuclei it was shown that — after a Δ excitation — there is a branching of strength into the non-mesonic channel and into the mesonic channel with a conservation of strength as compared to the free nucleon. This consideration shows that the resonance-like structure in the non-mesonic *pn* channel is not part of the QD degree of freedom but of the nucleon internal degrees of freedom which will be described by the amplitude T_N. Such a decomposition of the nuclear photoabsorption cross section at Δ-resonance energies into a mesonic and a non-mesonic channel is very well understood due to its manifestation in nucleon knock-out reactions [159–164].

2.3 Summary on the degrees of freedom of the nucleus

The most clear-cut distinction between external and internal degrees of freedom of nucleons in a nucleus is contained in the Compton scattering amplitudes of the individual nucleon, where the Born terms T^{Born} [101] correspond to the external degree of freedom and the non-Born terms $T^{non-Born}$ to the internal ones. The leading Born term is given by the Thomson scattering amplitude of a point-like particle. This term is independent of the photon energy. There are other contributions to the Born terms which simultaneously depend on the charge and the anomalous magnetic moment of the nucleon and on the photon energy ω. These latter terms do not contribute to the nuclear scattering amplitude in the GR energy region but are in principle observable in the QD energy range, though the effects are very small (see section 5).

To summarize, we have to discriminate between nuclear degrees of freedom (A), which may be giant resonance states (GR) or quasideuteron states (QD), and nucleon (N) degrees of freedom, which may be resonant nucleon states or asymptotic nucleon states. The correspondence between the nucleon-structure independent and nucleon-structure dependent terms of the nucleon and nuclear Compton scattering amplitudes is illustrated by Eqs. (2.2) and (2.3)

$$\begin{array}{ccccc} T^{nucleon} & = & T^{Born} & + & T^{non-Born} \\ \Updownarrow & & \Updownarrow & & \Updownarrow \\ T_{tot} & = & T_A & + & T_N \end{array} \qquad (2.2)$$

$$(2.3)$$

with

$$T_A = T_{GR} + T_{QD}. \qquad (2.4)$$

The first terms in Eqs. (2.2) and (2.3) are similar in the respect that they both show contributions which are connected to low-energy effective degrees of freedom of the object involved.

As an overview, the different degrees of freedom and their main characteristics are summarized in Table 2.1. From the discussion given above it is clear that the resonant peak at the high-energy end of the non-mesonic $\gamma\, {}^{A}X \rightarrow {}^{A-2}Y + p + n$ cross section is not part of the QD degree of freedom but belongs to the nucleon-internal (N) degree of freedom of the nucleus.

Table 2.1: *Excitation modes and degrees of freedom of the nucleus*

excitation mode of the nucleus	corresponding amplitude of the nucleon	excitation mode of the nucleon	nuclear objects and phenomena
giant resonances (GR)	Born terms	–	quasi-p quasi-h states in an average potential
quasi deuteron excitations (QD)	Born terms	–	proton-neutron pairs correlated by charged meson exchange
scaling range $\sigma \propto A$ (N)	non-Born amplitude in the resonance range	meson-isobar structure of the nucleon	baryon resonances and mesons in the nuclear medium
shadowing range $\sigma \propto A^{\alpha},\ \alpha < 1$ (N)	non-Born amplitude in the asymptotic range	vector dominance and t-channel exchanges & direct γ-quark couplings	in-medium vector dominance & direct γ-quark couplings

2.4 The role of Compton scattering in investigations of the degrees of freedom of the nucleus

At first sight Compton scattering simply appears to be one further reaction channel among many others which — in addition — is very difficult to measure. This view would lead to the conclusion that Compton scattering is not capable of providing any new information in addition to that obtained from other reaction channels. This, of course, is not the case. On the contrary, Compton scattering is a reaction channel with unique properties as will be outlined in the following.

Differing from photoparticle physics, Compton scattering is concerned with the first step of the excitation process only, since the same matrix element $\langle n|H_{int}|0\rangle$ of the first-step transition from the ground state $|0\rangle$ to the excited state $|n\rangle$ enters into the absorption and the emission processes. This favorable feature of Compton scattering makes it possible to study the photoabsorption process without the disturbing effects of subsequent processes, taking place between the initial photoabsorption and the final particle emission. For this reason it is possible to discuss the photoabsorption processes in terms of the initial photoabsorption process only, and forget about all the other processes. This property leads to a smaller model dependence of Compton scattering than observed in photoparticle experiments. The next favorable property of Compton scattering is its unambiguous relation to the total photoabsorption cross section via the optical theorem and the forward-angle dispersion relations. These relations fix the Compton differential cross section in the forward direction so that additional properties of the photoexcitation mechanisms and additional genuine two-photon properties (*e.g.* seagull amplitudes and electromagnetic polarizabilities) may be studied through measurements of the angular distribution of Compton scattered photons.

3 Compton scattering below pion threshold: general aspects

At present no quantitative consistent description of nuclear Compton scattering below pion threshold exists which is based on first principles. Over the years a variety of phenomenological models has been developed, which provide insight into the physical mechanisms responsible for contributions to the scattering amplitude. Many important results were obtained by applying dispersion relations to the Compton amplitude (see *e.g.* [165, 166]). For those parts of the amplitude, which are not easily accessible by dispersion theory, microscopic calculations have been attempted, *e.g.* for distinct multipole excitations [167], for mesonic effects [70,80,82,83,168] and for the contribution from nucleon excitations [102]. In this way nuclear Compton scattering can contribute to the understanding of such subnuclear aspects as mesonic currents between the nuclear constituents and virtual excitations of the nucleons. In the last few years several important pieces of information have been extracted from the experimental data. At low energies the relative strengths of electromagnetic multipoles were analyzed [13, 16, 19, 25, 33, 64, 95, 169] for comparison with predictions from multipole sum rules. The interesting question, whether the electromagnetic polarizabilities of the nucleon inside the nucleus essentially differ from those of the free nucleon, has been theoretically addressed [80, 82, 104, 166, 168] and experimentally studied with good accuracy [39, 43, 48, 170].

In the process of nuclear Compton scattering the exchange of mesons between nucleons, which represents the nucleon-nucleon interaction, leads to specific observable phenomena in the whole energy region considered here. This can be understood from the fact that mesons, themselves, may be charged and can, therefore, interact directly with photons. Best known among these phenomena is the modification of the Thomas-Reiche-Kuhn (TRK) sum rule [67], i.e. the appearance of the so-called enhancement constant κ. Originally, the quantity κ was calculated [67] to be about 0.4 and this value was not in an obvious disagreement with the experimental data then available. These data [150, 151] were mainly obtained for heavy nuclei and extended up to energies of about 30 MeV, thus including mainly the giant-resonance region. Later on it was shown that a considerable amount of photoabsorption strength is located above the giant resonance region [84, 152]. This strength is due to the excitation of quasideuterons, i.e. of clusters consisting of proton-neutron pairs correlated through the exchange of charged mesons. Due to this, the enhancement of giant-multipole strength is increased to $\kappa \sim 1.0$ in total. A wide variety of model calculations has been carried out for the total enhancement constant κ as well as for the different contributions to it, which are theoretically or experimentally accessible [87, 171, 172], see also [126]. Parts of κ could be related to parameters of Fermi liquid theory and to the notion of quasi-particle masses [96]. A compilation of results can be found in [173]. The contributions to κ have also been studied in a diagrammatic form [80, 83], similar to the approach described in section 9. In addition, mesonic exchange currents can imitate a modification of the nucleon polarizabilities [168]. This contribution may be subtracted in order to single out a change of the bound nucleon's polarizabilities from its free values. The advantage of this subtraction is related to the fact that meson-exchange contributions are not a local effect and are accompanied with two-body form factors. The latter ones are distinctly different from the one-body form factor which presumably accompanies all single-nucleon contributions, including polarizabilities of the bound nucleon. For a more detail discussion see sections 5 and 9.

The effect of mesonic exchange currents on the different electromagnetic properties of nuclei has been the subject of a large number of research articles, books and review papers. The reviews by Riska [174] and Arenhövel [121], as well as the book by Ericson and Weise [173] give an excellent introduction to this field. The description of mesonic exchange effects strongly depends on the physical process considered. In this review only the scattering of real photons is discussed. As no complete underlying theory of mesonic effects in this process exists, most of the results are model-dependent. Nevertheless, it is possible to obtain a qualitative description of various features of the Compton amplitude within the approaches, which will be discussed in this section.

3.1 The photon-nucleus scattering amplitude in second-order perturbation theory

Similar to the case of atomic physics [2] the discussion of nuclear photon scattering may start from second-order perturbation theory. But dissimilar to atomic physics this approach does not lead to predictions which directly may be compared with experiments because of the complexity of the physical situation. Nevertheless second-order perturbation theory is an essential building block for the construction of the general phenomenological theory. In principle, there is no limitation of this approach with respect to the degrees of freedom taken into account. However, in the present section we restrict the application of this method to the energy region of giant resonances (GR). Other effects, like the quasideuteron (QD) contribution and the internal excitation of nucleons, will be accounted for by alternative approaches.

The amplitude for the scattering of a photon γ by a nucleus A in its ground state $\gamma + A \to \gamma' + A'$ to the order e^2 (we set $\hbar = c = 1$; e is the charge of the proton and $e^2 = 1/137$ is the fine-structure constant) reads

$$\mathcal{T}_{fi} = (2\pi)^4 \delta^{(4)}(p_i + k_1 - p_f - k_2) V \epsilon_1^\mu \epsilon_2^{\nu *} \left(T_{\mu\nu} + S_{\mu\nu}\right) \tag{3.1}$$

where V is the total (infinite) volume, $T^{\mu\nu}$ is given by

$$\begin{aligned} & (2\pi)^4 \delta^{(4)}(p_i + k_1 - p_f - k_2) V \epsilon_1^\mu \epsilon_2^{\nu *} T_{\mu\nu} \\ = \; & -2\pi \delta(E_0 + \omega_1 - E_f - \omega_2) \epsilon_1^\mu \epsilon_2^{\nu *} \int d\mathbf{x}\, d\mathbf{y} e^{i\mathbf{k}_1 \cdot \mathbf{x}} e^{-i\mathbf{k}_2 \cdot \mathbf{y}} \\ & \times \sum_n \left\{ \frac{\langle f | j_\nu(\mathbf{y}) | n \rangle \langle n | j_\mu(\mathbf{x}) | i \rangle}{E_0 - E_n + \omega_1 + i0} + \frac{\langle f | j_\mu(\mathbf{x}) | n \rangle \langle n | j_\nu(\mathbf{y}) | i \rangle}{E_0 - E_n - \omega_2 + i0} \right\} \end{aligned} \tag{3.2}$$

and $S^{\mu\nu}$ is the seagull amplitude [68, 126] which provides the gauge invariance for the amplitude $\mathcal{T}_{fi}$. Therefore, one has

$$k_1^\mu \left(T_{\mu\nu} + S_{\mu\nu}\right) = \left(T_{\mu\nu} + S_{\mu\nu}\right) k_2^\nu = 0. \tag{3.3}$$

Representations of $S_{\mu\nu}$ will be discussed below. In Eq. (3.2) ϵ_1^μ and ϵ_2^ν denote the polarization vector of the incoming and outgoing photon, respectively. In the following we will use the Coulomb gauge, in which the photon polarization vector is given by $\epsilon_i^\mu = (0, \boldsymbol{\epsilon}_i)$ with $\boldsymbol{\epsilon}_i \cdot \mathbf{k}_i = 0$. Furthermore, for the sake of simplicity we consider the case of linearly polarized photons and, therefore, omit the complex conjugation for the polarization vector $\boldsymbol{\epsilon}_2$. The four-momenta of the incoming and outgoing photon are denoted by $k_1 = (\omega_1, \mathbf{k}_1)$ and $k_2 = (\omega_2, \mathbf{k}_2)$, respectively, while the corresponding quantities for the nucleus are p_i and p_f. The function $\mathbf{j}(x)$ is the electromagnetic current associated with the interaction of the photon with the nucleus, as will be discussed a little later on. The summation in (3.2) is performed over a complete set of eigenstates $|n\rangle$ of the nuclear Hamiltonian with eigenvalues E_n. The state $|i\rangle$ of the energy E_0 stands for the nuclear ground state and $|f\rangle$ for the final nuclear excited state in the laboratory system. In the case of Compton scattering initial and final states are equal to each other except for the total kinetic energy of the nucleus. In the laboratory frame the photon energies ω_1 and ω_2 are related via the Compton formula

$$\omega_2 = \frac{\omega_1}{1 + \dfrac{\omega_1}{AM}(1 - \cos\theta)} \tag{3.4}$$

where M is the nucleon mass, A again is the mass number of the nucleus and θ is the scattering angle.

The seagull amplitude $S^{\mu\nu}$ is identically equal to zero in the case of a relativistic description of the nucleus and the absence of exchange currents (or velocity dependent potentials in more general terms [68, 126]). This case has extensively been investigated for Compton scattering by atoms where electrons are described as Dirac particles in a self-consistent central potential [2]. These investigations have provided us with an insight into the general properties of the amplitude given in Eq. (3.2).

In the following, a non-vanishing seagull amplitude enters into the scattering amplitude for two reasons. First, we pass to the nonrelativistic form of the second-order perturbation theory. Then the negative-energy intermediate states in Eq. (3.2) give rise to a seagull amplitude $B(\omega,\theta)$. The other reason are exchange currents which are a consequence of the isovector nucleon-nucleon interaction. In this case gauge invariance may be restored by introducing the mesonic seagull amplitude $S(\omega,\theta) = \varepsilon_\mu \varepsilon_\nu^{*'} S^{\mu\nu}$. The appearance of a seagull-like contribution B in a nonrelativistic description of photon-nucleus scattering can easily be seen when the photon interaction is introduced in the nonrelativistic nuclear Hamiltonian via minimal substitution.

3.2 The nonrelativistic photon-nucleus interaction and the concept of currents

In a nonrelativistic description [81, 121, 130, 175, 176] the interaction between a nucleon and an electromagnetic field is given by the Hamiltonian

$$\begin{aligned} H_{int} &= \sum_{i=1}^{A} \left[\frac{1}{2}(1+\tau_3^{(i)}) \left(eA_0(\mathbf{r}_i) - \frac{e}{2M}[\,\mathbf{p}_i \cdot \mathbf{A}(\mathbf{r}_i) + \mathbf{A}(\mathbf{r}_i) \cdot \mathbf{p}_i\,] + \frac{e^2}{2M}\mathbf{A}(\mathbf{r}_i)\cdot\mathbf{A}(\mathbf{r}_i) \right) \right. \\ &\quad \left. - \frac{e\hbar}{2M}\left(\mu_p \frac{1}{2}(1+\tau_3^{(i)}) + \mu_n \frac{1}{2}(1-\tau_3^{(i)}) \right) \boldsymbol{\sigma}^{(i)} \cdot (\boldsymbol{\nabla}\times\mathbf{A}) \right], \end{aligned} \tag{3.5}$$

where $\boldsymbol{\sigma}^{(i)}/2$, $\tau_3^{(i)}/2$, $\mathbf{p}_i$ and $\mathbf{r}_i$ are the spin operator, the third component of the isospin operator, the three-momentum and the coordinate vector of the ith nucleon, respectively. The quantities μ_p and μ_n are the magnetic moments of the nucleons.

The term quadratic in $\mathbf{A}(\mathbf{r})$ is related to the kinetic seagull amplitude $B(\omega,\theta)$. All terms linear in $\mathbf{A}(\mathbf{r})$ contribute to the one-nucleon electromagnetic current. The terms depending on the magnetic moments give rise to spin currents which are responsible for magnetic spin-flip transitions in a nucleus. With the help of the usual relation

$$j_\mu(\mathbf{r}) = \left. \frac{\delta H_{int}}{\delta A^\mu(\mathbf{r})} \right|_{A_\nu = 0} \tag{3.6}$$

one obtains the following representation of the one-body contribution to the nuclear charge density $\rho(\mathbf{r})$ and current $\mathbf{j}(\mathbf{r})$:

$$\begin{aligned} \rho^{[1]}(\mathbf{r}) &\equiv \sum_i \rho_i^{[1]}(\mathbf{r}) = e\sum_i \frac{1+\tau_3^{(i)}}{2}\delta(\mathbf{r}-\mathbf{r}_i) \\ \mathbf{j}^{[1]}(\mathbf{r}) &= e\sum_i \frac{1+\tau_3^{(i)}}{2}\left(\frac{\mathbf{p}_i}{2M}\delta(\mathbf{r}-\mathbf{r}_i) + \delta(\mathbf{r}-\mathbf{r}_i)\frac{\mathbf{p}_i}{2M} \right) \\ &- \frac{e}{2M}\sum_i \left(\mu_p \frac{1+\tau_3^{(i)}}{2} + \mu_n \frac{1-\tau_3^{(i)}}{2} \right) \boldsymbol{\sigma}_i \times \boldsymbol{\nabla}\ \delta(\mathbf{r}-\mathbf{r}_i) \end{aligned} \tag{3.7}$$

The exchange of charged mesons between proton and neutron leads to an additional contribution to the electromagnetic current. The total electromagnetic current fulfills a continuity equation, which can be decomposed into a relation for the one-body part,

$$\boldsymbol{\nabla}\cdot\mathbf{j}^{[1]}(\mathbf{r}) = -i\left[H_0, \rho^{[1]}(\mathbf{r}) \right], \tag{3.8}$$

and a similar expression for the two-body current

$$\boldsymbol{\nabla}\cdot\mathbf{j}^{[2]}(\mathbf{r}) = -i[\sum_{i<j} V_{ij}^{(ex)}, \rho^{[1]}(\mathbf{r})]. \tag{3.9}$$

Here H_0 stands for the kinetic and central part of the nuclear Hamiltonian H, while $V_{ij}^{(ex)}$ is the two-nucleon exchange potential. In Eq. (3.9) it was taken into account that in the limit of point-like, static nucleons the two-body charge density $\rho^{[2]}$ vanishes since $\rho^{[2]}(\mathbf{r}) \propto 1/M$. The vanishing of $\rho^{[2]}$ in the static limit is known as Siegert's theorem [85]. From $\rho^{[1]}(\mathbf{r})$ one obtains a representation of the operator $\mathbf{D}$ for the total dipole moment

$$\mathbf{D} = \int d\mathbf{r}\, \rho^{[1]}(\mathbf{r})\, \mathbf{r} = e \sum_i \frac{1+\tau_3^{(i)}}{2}\, \mathbf{r}_i. \tag{3.10}$$

Using this expression, Eq. (3.9) and representing the exchange potential as $V_{ij}^{(ex)} = \boldsymbol{\tau}^{(i)} \cdot \boldsymbol{\tau}^{(j)}\ v_{ij}^{(ex)}$, where $v_{ij}^{(ex)}$ does not depend on the isospin variables, one finds the following form of the total two-body current

$$\mathbf{J}^{[2]} = \int d\mathbf{r}\, \mathbf{j}^{[2]}(\mathbf{r}) = i[\sum_{i<j} V_{ij}^{(ex)},\ \mathbf{D}] = -e \sum_{i<j} \left(\boldsymbol{\tau}^{(i)} \times \boldsymbol{\tau}^{(j)}\right)_3 (\mathbf{r}_i - \mathbf{r}_j) v_{ij}^{(ex)}. \tag{3.11}$$

The largest contribution to the two-body current comes from the π and ρ meson exchange parts of the two-nucleon potential $V_{ij}^{(ex)}$, which in momentum space are given by

$$\begin{aligned} V_{ij}^{(\pi)}(\mathbf{q}) &= -\frac{f^2}{m_\pi^2} (\boldsymbol{\tau}^{(i)} \cdot \boldsymbol{\tau}^{(j)}) \frac{(\boldsymbol{\sigma}_i \cdot \mathbf{q})(\boldsymbol{\sigma}_j \cdot \mathbf{q})}{\mathbf{q}^2 + m_\pi^2}, \\ V_{ij}^{(\rho)}(\mathbf{q}) &= -\frac{f_\rho^2}{m_\rho^2} (\boldsymbol{\tau}^{(i)} \cdot \boldsymbol{\tau}^{(j)}) \frac{(\boldsymbol{\sigma}_i \times \mathbf{q}) \cdot (\boldsymbol{\sigma}_j \times \mathbf{q})}{\mathbf{q}^2 + m_\rho^2}. \end{aligned} \tag{3.12}$$

Here m_π and m_ρ is the pion and ρ-meson mass, respectively, $f^2/4\pi \simeq 0.08$ and $f_\rho^2/4\pi \sim 4.5 - 5.5$.

It is convenient to introduce the two-body current in momentum space via

$$\mathbf{j}^{[2]}(\mathbf{r}) = \frac{1}{2} \sum_{i \neq j} \int \frac{d\mathbf{k}_1}{(2\pi)^3} \int \frac{d\mathbf{k}_2}{(2\pi)^3}\ \exp\left(i\mathbf{k}_1 \cdot (\mathbf{r}_i - \mathbf{r}) + i\mathbf{k}_2 \cdot (\mathbf{r}_j - \mathbf{r})\right) \mathbf{j}_{ij}^{[2]}(\mathbf{k}_1, \mathbf{k}_2). \tag{3.13}$$

The simplest way to arrive at an explicit form of the contribution of pion exchange to the current $\mathbf{j}_{ij}^{[2]}(\mathbf{k}_1, \mathbf{k}_2)$ is a direct calculation of the Feynman diagrams shown in Figure 9.1 (*cf.* section 9). In these diagrams the vertices are obtained via a minimal substitution in the corresponding Hamiltonians. As a result one finds [174]:

$$\begin{aligned} \mathbf{j}_{ij}^{[2]}(\mathbf{k}_1, \mathbf{k}_2) &= -ie \frac{f^2}{m_\pi^2} \left(\boldsymbol{\tau}^{(i)} \times \boldsymbol{\tau}^{(j)}\right)_3 \left\{ \frac{\boldsymbol{\sigma}_i\, (\boldsymbol{\sigma}_j \cdot \mathbf{k}_2)}{m_\pi^2 + \mathbf{k}_2^2} - \frac{\boldsymbol{\sigma}_j\, (\boldsymbol{\sigma}_i \cdot \mathbf{k}_1)}{m_\pi^2 + \mathbf{k}_1^2} + \right. \\ &\left. (\mathbf{k}_2 - \mathbf{k}_1) \frac{(\boldsymbol{\sigma}_i \cdot \mathbf{k}_1)}{m_\pi^2 + \mathbf{k}_1^2} \frac{(\boldsymbol{\sigma}_j \cdot \mathbf{k}_2)}{m_\pi^2 + \mathbf{k}_2^2} \right\}. \end{aligned} \tag{3.14}$$

Similar expressions can be obtained for the contribution of ρ-meson exchange [174].

In a nonrelativistic second-order perturbation theory the resonance amplitude $R(\omega, \theta)$ is given by the contribution to $\epsilon_1^\mu \epsilon_2^\nu T_{\mu\nu}$ of only positive-energy intermediate states in the r.h.s. of Eq. (3.2). This corresponds to using a nonrelativistic Hamiltonian as a starting point.

In the nonrelativistic approach gauge invariance is provided by introducing a non-resonant (seagull) amplitude, which is non-zero even in the absence of mesonic exchange currents. This part of the seagull amplitude corresponds to the contribution of negative-energy intermediate states in Eq. (3.2) in the nonrelativistic approximation. This so-called kinetic seagull amplitude can be written as

$$\begin{aligned} B(\omega, \theta) &= -\frac{1}{M}\, \boldsymbol{\epsilon}_1 \cdot \boldsymbol{\epsilon}_2\ \langle f | \sum_j \int d\mathbf{x}\, d\mathbf{y}\ e^{i\mathbf{k}_1 \cdot \mathbf{x}} e^{-i\mathbf{k}_2 \cdot \mathbf{y}} \rho_i^{[1]}(\mathbf{x} - \mathbf{r}_i)\, \rho_i^{[1]}(\mathbf{y} - \mathbf{r}_i)\, | i \rangle \\ &= -\frac{e^2}{M}\, \boldsymbol{\epsilon}_1 \cdot \boldsymbol{\epsilon}_2\ \langle f | \sum_j \frac{1+\tau_3^{(j)}}{2} \exp\left[i(\mathbf{k}_1 - \mathbf{k}_2) \cdot \mathbf{r}_j\right]\ | i \rangle = -\frac{Ze^2}{M} \boldsymbol{\epsilon}_1 \cdot \boldsymbol{\epsilon}_2 F_1(q), \end{aligned} \tag{3.15}$$

where $\mathbf{q} = \mathbf{k}_1 - \mathbf{k}_2$ and $F_1(q)$ is the form factor describing the distribution of protons inside the nucleus.

This representation of the kinetic seagull amplitude is frequently used in predictions of nuclear photon scattering. Using (3.15) to represent the negative-energy states in (3.2) certainly is only an approximation. However, below meson photoproduction threshold the possible uncertainty is only of the order of a few percent as discussed in [95]. Furthermore, the possibility of using a modified form factor which incorporates binding effects has been discussed in [166]. This modified form is given by [2]

$$F_1^{(mod)}(q) = \frac{1}{Z}\ \langle f|\sum_j \frac{1+\tau_3^{(j)}}{2}\ \exp\left[i\mathbf{q}\cdot\mathbf{r}_j\right]\frac{M}{E-V(\mathbf{r}_j)}\ |i\rangle \tag{3.16}$$

where E is the total energy of the nucleon bound in the potential $V(r)$ which is assumed to be the 4th component of a Lorentz vector. The modified form factor has been introduced in connection with atomic Rayleigh scattering [177] and later was investigated and explained by Brown et al. [178]. The predictions of Brown et al. [178] concerning the modified form factor were experimentally confirmed by Schumacher [179], who showed that atomic Rayleigh scattering data require the application of the modified form factor at least for the helicity non-flip amplitude.

In the hypothetical case of structureless nucleons and the absence of exchange currents the cross section for nuclear photoabsorption would contain only giant resonances and, hence, go to zero at about 30 to 40 MeV. The amplitude $R_{GR}(\omega,\theta) + B(\omega,\theta)$ would provide a complete description of nuclear photon scattering. Furthermore, the integral over the total photoabsorption cross section would fulfill the usual Thomas-Reiche-Kuhn (TRK) sum rule without any enhancement. Relativistic corrections, which could in principle destroy this relation, are negligibly small in the giant resonance region. If we keep the nucleons structureless but take into account meson exchange currents the giant resonance amplitude R_{GR} is modified. Furthermore, an additional contribution R_{QD} to the resonance amplitude appears, the so-called quasi-deuteron scattering, which will be discussed in section 5. This new amplitude $R_{GR} + R_{QD} + B$ is no longer gauge invariant by itself and a counter term $S(\omega,\theta)$, which is usually called the mesonic seagull amplitude, is needed to restore gauge invariance. The total amplitude T_A corresponding to all nuclear degrees of freedom is then given by

$$T_A = R_{GR} + R_{QD} + B + S = R_{GR} + R_{QD} + S_{tot}, \tag{3.17}$$

where S_{tot} is the sum of the kinetic and mesonic seagull amplitudes. The contribution T_N of nucleon-internal degrees of freedom to the nuclear Compton amplitude, which is not included in (3.17), will be discussed in sections 5 and 6. As will be seen, below pion threshold the main contribution to this amplitude is due to the electric and magnetic polarizabilities of the bound nucleon.

The microscopic consideration of meson exchange has lead to explicit calculations of the amplitude S. Such calculations have been carried out by Alberico and Molinari [75] based on expressions derived by Christillin [68,71,72] and Friar [69], as well as by Hütt and Milstein [168,193]. In the static limit the mesonic seagull amplitude at ω=0 is of the following form:

$$\begin{aligned}\tilde{S}(\omega,\theta)\Big|_{\omega=0} &= \frac{i}{2}\left\{\langle f|\left[\boldsymbol{\epsilon}_1\cdot\mathbf{D}\,,\ \boldsymbol{\epsilon}_2\cdot\mathbf{J}^{[2]}\right] + \left[\boldsymbol{\epsilon}_2\cdot\mathbf{D}\,,\ \boldsymbol{\epsilon}_1\cdot\mathbf{J}^{[2]}\right]|i\rangle\right\} \\ &= \frac{2e^2}{3}\,\boldsymbol{\epsilon}_1\cdot\boldsymbol{\epsilon}_2\ \langle f|\sum_{j<k}\left(\tau_+^{(j)}\tau_-^{(k)} + \tau_-^{(j)}\tau_+^{(k)}\right)\ (\mathbf{r}_j-\mathbf{r}_k)^2\ v_{jk}^{(ex)}\,|i\rangle\,,\end{aligned} \tag{3.18}$$

where $\tau_\pm^{(j)} = 1/2\ (\tau_1^{(j)} \pm i\,\tau_2^{(j)})$ are the isospin raising and lowering operators. Here and in the following we use the symbol $\tilde{S}(\omega,\theta)$ to denote a static approximation of $S(\omega,\theta)$. Due to the isospin structure of the matrix elements in Eq. (3.18) only proton-neutron pairs contribute to the mesonic seagull

amplitude. Taking into account the effect of retardation, but still neglecting any other dependence on the photon energy ω, which is connected with the ω- and $\mathbf{k}$-dependence of the mesonic propagators, one has

$$\tilde{S}(\omega,\theta) = \frac{2e^2}{3}\,\boldsymbol{\epsilon}_1\cdot\boldsymbol{\epsilon}_2\;\langle f|\sum_{j<k}\left(\tau_+^{(j)}\tau_-^{(k)}+\tau_-^{(j)}\tau_+^{(k)}\right)\;(\mathbf{r}_j-\mathbf{r}_k)^2\;v_{jk}^{(ex)}\exp\left[-i\mathbf{q}\cdot(\mathbf{r}_j+\mathbf{r}_k)/2\right]|i\rangle \qquad (3.19)$$

It is convenient to write this limit of the mesonic seagull amplitude in the form

$$\tilde{S}(\omega,\theta) = -\boldsymbol{\epsilon}_1\cdot\boldsymbol{\epsilon}_2\frac{NZ}{A}\frac{e^2}{M}\kappa F_2(q) \qquad (3.20)$$

where κ is the enhancement constant and $F_2(q)$ is the two-body form factor, which characterizes the distribution of correlated proton-neutron pairs inside the nucleus. The function F_2 is normalized in such a way that $F_2(0)$=1. A first attempt to qualitatively discuss two-body or exchange form factors within a microscopic model has been made by Alberico and Molinari [75] for the case of ^{208}Pb. In section 9 the construction of such form factors is described on more general grounds within a modified Fermi gas. To this end the full mesonic seagull amplitude can be represented as a convolution of a spin-isospin correlation function with matrix elements arising from amputated diagrams for meson exchange.

3.3 Low-energy behavior of the scattering amplitude and dispersion relation

In this section we discuss another view towards a decomposition of the Compton scattering amplitude into a sum of resonant and non-resonant parts. While in the previous section the consideration was based on second-order perturbation theory and the requirement of gauge invariance, here our starting point is a dispersion relation for the scattering amplitude in forward direction. At the end of the last section the nuclear Compton amplitude T_A presented itself as a sum of three contributions (3.17) provided by different physical mechanisms (see also [127, 166, 170]): the collective nuclear excitations (giant resonances), $R_{GR}(\omega,\theta)$, the scattering by quasi-deuteron clusters, $R_{QD}(\omega,\theta)$, and the so-called seagull amplitude, $S_{tot}(\omega,\theta)$. The physical background of this separation is the following: Via optical theorem and a subtracted dispersion relation the scattering amplitude in the forward direction is up to an additive constant determined by the total photoabsorption cross section. This cross section contains resonant structures, which at different energies correspond to the two different excitation mechanisms (*cf.* Fig. 2.2) which we call giant-resonance (GR) and quasideuteron (QD), as was discussed in section 2.

An experimental separation of GR and QD excitations is relatively easy for heavy nuclei where the giant-dipole resonance (GDR) cross section containing by far most of the total GR strength is given by a Lorentzian line in case of spherical nuclei as discussed in section 2. In case of the validity of a Lorentzian shape rather precise information on the integrated strength in the giant resonance may be obtained because this Lorentzian shape may be used to separate the GDR cross section from the QD cross section.

On the other hand also the shape of the QD cross section [154–156] is known either in the form of the Levinger parameterization [154], the Laget parameterization [156] or a (QD) Lorentzian representation (*cf.* sections 2 and 5). Then the shape of the QD cross section extrapolated to above the pion threshold may be used to separate the QD excitation from the nucleon internal excitation. In practice this is achieved with sufficient precision by adjusting a Lorentzian curve to the QD cross section below pion threshold.

In this sense the nuclear photoabsorption cross section $\sigma_A(\omega)$ below pion threshold and slightly above can experimentally be separated into two parts,

$$\sigma_A(\omega) = \sigma_{GR}(\omega) + \sigma_{QD}(\omega).$$

This serves as a means to construct the resonance parts of the scattering amplitude R_{GR} and R_{QD} as

$$\mathrm{Re}\left(R_{GR}(\omega,0)-R_{GR}(0,0)\right)=\frac{\omega^2}{2\pi^2}\,\mathcal{P}\int\limits_0^\infty\frac{\sigma_{GR}(\omega')\,d\omega'}{\omega'^2-\omega^2} \tag{3.21}$$

and

$$\mathrm{Im}R_{GR}(\omega,0)=\frac{\omega}{4\pi}\,\sigma_{GR}(\omega). \tag{3.22}$$

The same is valid for R_{QD}. This widely used procedure corresponds to the application to the once-subtracted forward-angle dispersion relation and of the optical theorem to partial cross sections. This procedure is legitimate because the GR and QD excitations correspond to separate degrees of freedom.

The application of dispersion relations to the total nuclear Compton cross section dates back to the early work of Gell-Mann, Goldberger and Thirring [165]. There it was shown that for the total scattering amplitude $T_{tot}(\omega,\theta)$, which — in our language — includes all degrees of freedom of the nucleus a subtracted dispersion relation may be formulated:

$$\mathrm{Re}\left(T_{tot}(\omega,0)-T_{tot}(0,0)\right)=\frac{\omega^2}{2\pi^2}\mathcal{P}\int_0^\infty\frac{\sigma_{tot}(\omega')}{\omega'^2-\omega^2}d\omega', \tag{3.23}$$

where $T_{tot}(0,0)=-Z^2e^2/AM$. For convenience in the further discussion we introduce a "free-nucleon photoabsorption cross section" via

$$A\sigma_N^{free}(\omega)=Z\sigma_p(\omega)+N\sigma_n(\omega), \tag{3.24}$$

where $\sigma_p(\omega)$ and $\sigma_n(\omega)$ are the free proton and neutron photoabsorption cross sections, respectively. The cross section of Eq. (3.24) defines a "free-nucleon scattering amplitude" for the ensemble of nucleons in a nucleus through

$$\mathrm{Re}\left(T_N^{free}(\omega,0)-T_N^{free}(0,0)\right)=\frac{\omega^2}{2\pi^2}\mathcal{P}\int_0^\infty\frac{A\sigma_N^{free}(\omega')}{\omega'^2-\omega^2}d\omega' \tag{3.25}$$

with $T_N^{free}(0,0)=-Ze^2/M$. Similarly, one may think of the difference between the total photoabsorption cross section σ_{tot} and the one σ_A, where only nuclear degrees of freedom contribute, as a bound-nucleon cross section:

$$\sigma_N^{bound}(\omega)=\frac{1}{A}(\sigma_{tot}(\omega)-\sigma_A(\omega)). \tag{3.26}$$

From (3.23), (3.25) and (3.26) we obtain

$$\begin{aligned}\mathrm{Re}\left(T_{tot}(\omega,0)-T_N^{free}(\omega,0)\right) &= \frac{NZ}{A}\frac{e^2}{M}+\frac{\omega^2}{2\pi^2}\mathcal{P}\int_0^\infty\frac{\sigma_A(\omega')}{\omega'^2-\omega^2}d\omega' \\ &+ \frac{\omega^2}{2\pi^2}\mathcal{P}\int_0^\infty\frac{A\left(\sigma_N^{bound}(\omega')-\sigma_N^{free}(\omega')\right)}{\omega'^2-\omega^2}d\omega'\end{aligned} \tag{3.27}$$

which is the basis of our further conclusions.

For $\omega\to\infty$ Eq. (3.27) provides us with the Gell-Mann-Goldberger-Thirring (GGT) sum rule[1], *viz.*

$$\begin{aligned}\int_0^\infty\sigma_A(\omega)d\omega=2\pi^2\frac{NZ}{A}\frac{e^2}{M} &+ 2\pi^2\mathrm{Re}\left(T_{tot}(\infty,0)-T_N^{free}(\infty,0)\right) \\ &+ \int_0^\infty A(\sigma_N^{free}(\omega)-\sigma_N^{bound}(\omega))d\omega.\end{aligned} \tag{3.28}$$

[1]In the original work the nuclear (A) and nucleon internal (N) d.o.f. were simply separated through a cut at pion threshold.

In the original paper [165] it was assumed that the asymptotic term in Eq. (3.28) is equal to zero. Then Eq. (3.28) has a very attractive interpretation by stating that the enhancement of strength contained in the integral over the nuclear photoabsorption cross section $\sigma_A(\omega)$ is equal to the reduction of strength in the nucleon photoabsorption cross section due to nuclear binding. Later on it was realized [180,181] that the basic assumption of GGT about the properties of the asymptotic term in (3.28) is not correct because of vector dominance phenomena. Due to this fact the GGT sum rule needs refinements. The refinement discussed by Ahrens et al. [182] fixes the dispersion integral in the second line of (3.27) at $\omega = 314$ MeV instead of $\omega \to \infty$ thus making use of zero crossings of the real parts of scattering amplitudes. Although in this way reasonable numbers are obtained for the enhancement constant κ the interesting physical content of the original GGT sum rule [165] is not preserved. Furthermore, there seem to be no indications for a reduction of photoabsorption strength above pion threshold which might show up as an enhancement of photoabsorption strength below pion threshold [147].

Some new aspects of the GGT-sum rule may be obtained by showing that this sum rule is not a property of the photoabsorption cross section but rather a property of the mesonic seagull-amplitude $S(\omega,\theta)$. The arguments leading to this conclusion are as follows. The total seagull amplitude S_{tot}, which is the sum of the kinetic and mesonic seagull amplitudes, has an imaginary part only above pion threshold. From Eq. (3.27), together with (3.21) one obtains a dispersion representation of the mesonic seagull amplitude in the form [80, 166]

$$\mathrm{Re}S(\omega,0) - S(0,0) + \mathrm{Re}T_N(\omega,0) = \frac{\omega^2}{2\pi^2}\mathcal{P}\int_{m_\pi}^{\infty} \frac{A\sigma_N^{bound}(\omega')}{\omega'^2-\omega^2}d\omega', \tag{3.29}$$

where on the l.h.s. the energy is restricted to the range below meson threshold where the amplitudes are real. This relation has the following interpretation. The difference $S(\omega,0) - S(0,0)$ is the "dynamic" part of the mesonic seagull amplitude at zero angle, i.e. that part which is energy dependent in the forward direction, corresponding to meson exchanges beyond the static limit of the meson exchange potential. In the order ω^2 the l.h.s. of Eq. (3.29) corresponds to the electromagnetic polarizabilities of the nucleon and their modification due to binding. From (3.29) we are led to the supposition that the quantity $\sigma_N^{bound}(\omega)$ should consist of two different parts one, ${\sigma'}_N^{bound}(\omega)$, related to T_N and an other, $\Delta\sigma^{(S)}(\omega)$, related to $S(\omega,0)-S(0,0)$. Below meson photoproduction threshold the amplitude T_N may be expressed in terms of the in-medium electromagnetic polarizabilities $\tilde{\alpha}_N$ and $\tilde{\beta}_N$ (see section 5.2 for more details) via

$$T_N(\omega,\theta) = A\left(\tilde{\alpha}_N g_{E1}(\theta) + \tilde{\beta}_N g_{M1}(\theta)\right)\omega^2 F_1(q) + \mathcal{O}(\omega^4). \tag{3.30}$$

Then the supposition implies that only the part ${\sigma'}_N^{bound}(\omega)$ is responsible for the *genuine* in-medium electromagnetic polarizabilities $\tilde{\alpha}_N$ and $\tilde{\beta}_N$ whereas the rest, $\Delta\sigma^{(S)}(\omega)$, leads to the relations

$$\begin{aligned} \mathrm{Re}S(\omega,0) - S(0,0) &= \frac{\omega^2}{2\pi^2}\mathcal{P}\int_{m_\pi}^{\infty}\frac{-\Delta\sigma^{(S)}(\omega')}{\omega'^2-\omega^2}d\omega' \\ \mathrm{Im}S(\omega,0) &= -\frac{\omega}{4\pi}\Delta\sigma^{(S)}(\omega). \end{aligned} \tag{3.31}$$

The sign of $\Delta\sigma^{(S)}(\omega)$ in (3.31) has been chosen negative in order to make this quantity itself positive. The proof of this statement is given by Eq. (3.33) where the positive right side of the equation is consistent with a negative signs in (3.31). In the case that

$$\lim_{\omega\to\infty} S(\omega,0) = 0 \tag{3.32}$$

which appears to us plausible, we are lead to a sum rule in the following form

$$\int_{m_\pi}^{\infty}\Delta\sigma^{(S)}(\omega')d\omega' = 2\pi^2\frac{NZ}{A}\frac{e^2}{M}\kappa \tag{3.33}$$

where use has been made of Eq. (3.20). In a formal sense the sum rule (3.33) is exactly identical to what Gell-Mann Goldberger and Thirring [165] had in mind, but the physical interpretation is different in two essential points:
(i) The sum rule (3.33) does not describe a property of the photoabsorption cross section but rather a property of the mesonic seagull amplitude $S(\omega,\theta)$. This is an important difference, because due to this, $\Delta\sigma^{(S)}(\omega)$ may not be interpreted in terms of a reduction of photoabsorption strength of the individual nucleons through a transfer to energies below π-threshold by some mechanism. Instead, $\Delta\sigma^{(S)}(\omega)$ has to be understood as being due to an additional two-body effect.
(ii) The condition for the validity of the sum rule (3.33) is not the equality of absorption cross-sections for the free and bound nucleon in the high-energy limit, but instead is given by the property (3.32) of the mesonic seagull amplitude which should already be fulfilled in the resonance region of the nucleon photoabsorption cross-section. This point has been cleared up by Schumacher et al. [166]. A favorable consequence of this finding is that the sum rule (3.33) does not interfere with the shadowing effect as suspected in [180–182].

In addition to the fulfillment of a dispersion relation, the main constraint on the nuclear Compton amplitude is the low-energy theorem [69, 183, 184]. It states that the Compton scattering amplitude at $\omega = 0$ is equal to the (coherent) Thomson limit

$$T_A(0,\theta) = -\,\boldsymbol{\epsilon}_1 \cdot \boldsymbol{\epsilon}_2\, \frac{Z^2 e^2}{AM}. \tag{3.34}$$

Let us represent the low-energy limit of the resonance part of the Compton amplitude in a form which is convenient for the further discussion:

$$R_{GR}(0,\theta) = \boldsymbol{\epsilon}_1 \cdot \boldsymbol{\epsilon}_2\, \frac{e^2}{M}\, \frac{ZN}{A}\,(1+\kappa^{GR}), \tag{3.35}$$

where κ^{GR} is a constant which, as it will become clear later, is the essential parameter characterizing all phenomena connected with the enhancement of sum rules due to mesonic effects in the giant resonance region. Taking into account the fact that $R_{GR}(\omega,0)$ vanishes as ω tends to infinity, with the help of the dispersion relation (3.21) one has

$$\frac{1}{2\pi^2}\int\limits_0^\infty \sigma_{GR}(\omega)d\omega = R_{GR}(0,0) = \frac{NZ}{A}\frac{e^2}{M}(1+\kappa^{GR}). \tag{3.36}$$

In the limit of $\omega = 0$, one could expect that only the electric dipole operator contributes to scattering and that only unretarded quantities should appear. Therefore, one might think that the unretarded $E1$ resonance amplitude

$$\overset{\circ}{R}_{GDR}(0,\theta) = \boldsymbol{\epsilon}_1 \cdot \boldsymbol{\epsilon}_2\, \frac{e^2}{M}\, \frac{ZN}{A}\,(1+\overset{\circ}{\kappa}{}^{GDR}), \tag{3.37}$$

which introduces the unretarded enhancement parameter $\overset{\circ}{\kappa}{}^{GDR}$ given by the unretarded electric-dipole photoabsorption cross section $\overset{\circ}{\sigma}_{GDR}$ (again GDR stands for "giant dipole resonance"),

$$\frac{1}{2\pi^2}\int\limits_0^\infty \overset{\circ}{\sigma}_{GDR}(\omega)d\omega = \overset{\circ}{R}_{GDR}(0,0) = \frac{NZ}{A}\frac{e^2}{M}(1+\overset{\circ}{\kappa}{}^{GDR}), \tag{3.38}$$

coincides with the dispersion amplitude (3.35). The appropriate equation

$$R_{GR}(0,\theta) = \overset{\circ}{R}_{GDR}(0,\theta) \tag{3.39}$$

and its consequence

$$\kappa^{GR} = \mathring{\kappa}^{GDR} \tag{3.40}$$

make the essence of Gerasimov's argument [185], which is one of the most frequently cited (and critisized [186–190]) properties of the multipole contributions to giant resonance excitations. It states that the corrections due to retardation and the effects of multipoles higher than electric dipole cancel in the integrated total photoabsorption cross section. Gerasimov's argument is not precisely valid in nonrelativistic models because they do not maintain the strict validity of dispersion relations [186–188]. Even in relativistic models which obey the constraints of dispersion relations (see [186, 188, 189] and section 10), Eq. (3.39) does not hold as an identity (see section 10.4). Nevertheless, expected deviations are rather small, as will be discussed in some more detail in section 4.4. Data analyses given in section 4 supports the assumption that the difference between κ^{GR} and $\mathring{\kappa}^{GDR}$ can be neglected in practical applications. In the following discussion in section 3 we disregard the difference between κ^{GR} and $\mathring{\kappa}^{GDR}$.

Returning to the remaining low-energy contributions to the amplitude T_A we now define the quasideuteron amplitude at zero energies, $R_{QD}(0,\theta)$, in a similar way to Eq. (3.36) as

$$R_{QD}(0,\theta) = \boldsymbol{\epsilon}_1 \cdot \boldsymbol{\epsilon}_2 \; \frac{e^2}{M} \frac{ZN}{A} \kappa^{QD}. \tag{3.41}$$

Therefore, one has

$$\frac{1}{2\pi^2} \int_0^\infty \sigma_{QD}(\omega) d\omega = \frac{NZ}{A} \frac{e^2}{M} \kappa^{QD}. \tag{3.42}$$

From comparing (3.34) with (3.35) and (3.41) one obtains

$$S_{tot}(0,\theta) = -\boldsymbol{\epsilon}_1 \cdot \boldsymbol{\epsilon}_2 \; \frac{Ze^2}{M} \left(1 + \frac{N}{A}\kappa\right) \tag{3.43}$$

for the low-energy limit of the seagull amplitude, where $\kappa = \kappa^{GR} + \kappa^{QD}$.

Early attempts [68, 71, 72, 74, 75, 83] to understand the term proportional to κ in (3.43) were based on the idea that this term may be interpreted as Thomson scattering by charged pions in the nucleus. This effect cannot be seen in electron scattering experiments, because this is a one-photon process which averages over the positive and negative charges of the pions. Thomson scattering on the other hand is related to the squares of pion charges and, therefore, there is no cancellation. In consequence it should be possible give a number for the pion excess per nucleon which was derived [83] to be $n_\pi \approx 0.07$. However, this idea dating back to a work of Christillin and Rosa-Clot [72] implies a special interpretation of Siegert's theorem [85] in the sense that there is a number density of pions without a charge density. In some sense this may be in line with Siegert's theorem because there are positive and negative pions so that the two charges may cancel to zero. By following Siegert's arguments literally also number densities should be excluded. This latter point of view has been substantiated by Weyrauch and Arenhövel [78] who realized that pion charges only occur as "transition charges". In other words, the term proportional to κ does not appear due to a modification of the number of particles in the nucleus but due to a modification of the electromagnetic current.

3.4 Multipole expansion of the scattering amplitude for giant resonances

Via a dispersion relation and the optical theorem the resonance structure of the Compton scattering amplitude in forward direction is completely determined by nuclear photoabsorption. However, in order to obtain the angular dependence of the scattering amplitude, it is necessary to consider the

multipolarity of the resonances. The multipole-dependent transition operators are obtained by expanding the photon field $\mathbf{A}$ into multipole components. For this purpose let us consider a circularly polarized photon with a polarization vector $\boldsymbol{\xi}_\mu$ equal to

$$\boldsymbol{\xi}_{\pm 1} = \mp \frac{1}{\sqrt{2}} (\mathbf{e}_x \pm i \mathbf{e}_y) \tag{3.44}$$

where $\mathbf{e}_x$, $\mathbf{e}_y$ are two orthogonal unit vectors in the plane perpendicular to the photon momentum $\mathbf{k}$, which is directed along the axis z, $\mathbf{k} = \omega \mathbf{e}_z$, and $\mu = \pm 1$ denotes the helicity of the photon. The multipole decomposition of the photon wave function for a fixed helicity μ is then given by

$$\boldsymbol{\xi}_\mu \, e^{i\,\mathbf{k}\cdot\mathbf{r}} = \sum_{L=1}^{\infty} i^L \sqrt{2\pi(2L+1)} \; \{\mu \mathbf{A}_{L\mu}(\mathbf{r}, M) + \mathbf{A}_{L\mu}(\mathbf{r}, E)\}. \tag{3.45}$$

Here, at any angular momentum projection μ, $|\mu| \leq L$,

$$\begin{aligned} \mathbf{A}_{L\mu}(\mathbf{r}, M) &= j_L(kr)\, \mathbf{Y}_{LL\mu}(\hat{\mathbf{r}})\,, \\ \mathbf{A}_{L\mu}(\mathbf{r}, E) &= \frac{1}{\omega} \boldsymbol{\nabla} \times (j_L(kr)\, \mathbf{Y}_{LL\mu}(\hat{\mathbf{r}})) \\ &= i \sqrt{\frac{L}{2L+1}} j_{L+1}(kr) \mathbf{Y}_{L\ L+1\ \mu} - i \sqrt{\frac{L+1}{2L+1}} j_{L-1}(kr) \mathbf{Y}_{L\ L-1\ \mu} \end{aligned} \tag{3.46}$$

are the vector potentials for the magnetic and electric multipoles, respectively, $j_L(kr)$ is the spherical Bessel function. The vector spherical harmonic $\mathbf{Y}_{JlM}(\hat{\mathbf{r}})$ is related to the usual spherical harmonics $Y_{lm}(\hat{\mathbf{r}})$ via

$$\mathbf{Y}_{JlM}(\hat{\mathbf{r}}) = \sum_{m\mu} C^{JM}_{1\mu,lm}\, Y_{lm}(\hat{\mathbf{r}})\, \boldsymbol{\xi}_\mu$$

with $\boldsymbol{\xi}_0 = \mathbf{e}_z$ and with $C^{JM}_{j_1 m_1, j_2 m_2}$ denoting the Clebsch-Gordan coefficient for the coupling of angular momenta $\mathbf{j}_1$ and $\mathbf{j}_2$ to $\mathbf{J}$. The quantity $\hat{\mathbf{r}}$ is the unit vector in the direction of $\mathbf{r}$.

Choosing the axis z along the momentum $\mathbf{k}_1$ of the initial photon in Compton scattering, we can use the above expressions (with $\mathbf{k} = \mathbf{k}_1$) to write the multipole transition operators as

$$Q_{\lambda L} = \sum_\mu \left(\boldsymbol{\xi}^*_\mu \cdot \boldsymbol{\epsilon}_1 \right) \, Q^{(\mu)}_{\lambda L}\,, \tag{3.47}$$

where

$$Q^{(\mu)}_{\lambda L} = (2\pi)^{1/2} (2L+1)^{1/2} i^L \int d\mathbf{x}\, \mathbf{j}(\mathbf{r}) \cdot \mathbf{A}_{L\mu}(\mathbf{r}, \lambda), \quad \lambda = E, M. \tag{3.48}$$

Strictly speaking, such a multipole decomposition makes a sense in the center-of-mass of the nucleus. In a more general situation the operators (3.48) carry both convectional (center-of-mass) and intrinsic electromagnetic currents. Since the nucleus enters to the initial, final and intermediate states in the direct and crossed term of the Compton scattering amplitude with different velocities, the convectional current cannot be completely excluded. However, for low energies and heavy nuclei which we only consider here such complications are irrelevant, and we can safely assume in most situations that the transition operators always transform the ground state of the nucleus, $|0\rangle$, into an excited state $|\nu\rangle$ with $\nu \neq 0$.

In Eq. (3.48) each operator contains all orders in ω starting from ω^L for the magnetic multipoles and from ω^{L-1} for the electric ones. When in Eqs. (3.46), (3.48) the substitution $j_L(\omega r) \to (\omega r)^L/(2L+1)!!$ is made, one obtains the corresponding transition operators in the long-wavelength limit which we call unretarded and denote by $\overset{\circ}{Q}{}^{(\mu)}_{\lambda L}$ and $\overset{\circ}{Q}_{\lambda L}$. In particular,

$$\overset{\circ}{Q}_{E1} = \int d\mathbf{x}\, \mathbf{j}(\mathbf{r}) \cdot \boldsymbol{\epsilon}_1 = i[H, \boldsymbol{\epsilon}_1 \cdot \mathbf{D}]. \tag{3.49}$$

The amplitude resulting from the unretarded operators will be called "unretarded", while the exact operators are understood to lead to the "retarded" amplitude. If the wavelength of the incoming photon is of the same order as the nuclear radius, it is not effective to expand the photon plane wave with respect to ωr since many powers of ωr and many multipoles contribute. At these photon energies the effect of retardation is essential. The problem of retardation is one of the main topics of our review and will be discussed in sections 4 and 10.

For the final photon which is not directed along the axis z, similar expressions can be used with a rotation $R : \mathbf{k}_1 \to \mathbf{k}_2$ applied to the polarizations $\boldsymbol{\xi}_\mu$ and multipoles $\mathbf{A}_{L\mu}(\mathbf{r}, \lambda)$:

$$\tilde{Q}^R_{\lambda L} = \sum_\mu \left(\boldsymbol{\xi}^{R*}_\mu \cdot \boldsymbol{\epsilon}_2 \right) Q^{(\mu)\,R}_{\lambda L}, \tag{3.50}$$

where

$$Q^{(\mu)\,R}_{\lambda L} = (2\pi)^{1/2}(2L+1)^{1/2} i^L \int d\mathbf{x}\, \mathbf{j}(\mathbf{r}) \cdot \mathbf{A}^R_{L\mu}(\mathbf{r}, \lambda). \tag{3.51}$$

The rotated and unrotated operators are related by ordinary D-functions of Wigner,

$$Q^{(\mu)\,R}_{\lambda L} = \sum_{\mu'} Q^{(\mu')}_{\lambda L} D^L_{\mu\mu'}(R). \tag{3.52}$$

Following the general idea that it is possible to represent the total scattering amplitude as a sum, where each contribution corresponds to a different physical mechanism of excitation, we now consider the scattering by giant resonances only, together with the corresponding counterparts coming from the seagull amplitude. Therefore, $T_{GR} = R_{GR} + B + S_{GR}$ with $S_{GR} = S(\kappa \to \kappa^{GR})$ and S from Eq. (3.20). One then arrives at the following decomposition of the giant resonance scattering amplitude:

$$\begin{aligned} T_{GR}(\omega, \theta) \;=\; & -\boldsymbol{\epsilon}_1 \cdot \boldsymbol{\epsilon}_2 \frac{Ze^2}{M} F_1(q) - \boldsymbol{\epsilon}_1 \cdot \boldsymbol{\epsilon}_2 \frac{NZ}{A} \frac{e^2}{M} \kappa^{GR} F_2(q) \\ & - \sum_{\lambda L} \sum_\nu g^{\lambda L}(\theta) \left\{ \frac{|\langle \nu | Q_{\lambda L} | 0 \rangle^2|}{E_0 - E^{\lambda L}_\nu + \omega + i\Gamma^{\lambda L}_\nu/2} + \frac{|\langle \nu | Q_{\lambda L} | 0 \rangle^2|}{E_0 - E^{\lambda L}_\nu - \omega - i\Gamma^{\lambda L}_\nu/2} \right\}, \end{aligned} \tag{3.53}$$

where unrotated transition operators are used (with any polarization which is irrelevant) and all the angular and polarization dependence of the resonance amplitude is translated into the angular functions $g^{\lambda L}(\theta)$ which incorporate the D-function in (3.52) and the factors of μ in (3.45) for each photon. If both photons are circularly polarized and have the helicities $\mu_1 = \pm 1$ and $\mu_2 = \pm 1$, then

$$g^{EL}(\theta) = \left[D^L_{\mu_1 \mu_2}(R) \right]^*, \quad g^{ML}(\theta) = \mu_1 \mu_2 \left[D^L_{\mu_1 \mu_2}(R) \right]^*. \tag{3.54}$$

Since we consider Compton scattering, where the final and initial internal nuclear states are equal, and restrict ourselves to spin-0 nuclei, it follows from angular momentum and parity conservation that only products of multipole components with the same λL contribute to Eq. (3.53). For simplicity, we have skipped recoil corrections in the energy denominator, which are negligibly small in the giant resonance region. We also neglected the additional ω-dependent terms in the kinetic seagull amplitude (relativistic corrections, which are related to negative-energy intermediate states) and in the mesonic seagull amplitude (modifications of the electromagnetic polarizabilities). Such corrections are small in the giant resonance region. The separation of the scattering amplitude into multipoles and its application to giant resonances has been discussed by Arenhövel, Danos and Greiner [118]. If the transition operators are used in the long-wavelength approximation and, at the same time, the dependence of the resonance denominators on the photon energy is neglected, one observes a strict cancellation for each electric multipole $EL \neq E1$ between the contributions to the resonance amplitude and those coming from the multipole expansion of the seagull amplitude. This general property of scattering

amplitudes is a consequence of low-energy theorems [69] and may be traced back to low-energy expansions of spherical Bessel functions. The terms from the electric dipole give rise to the Thomson limit, in accordance with the low-energy theorem.

The interpretation of Eq. (3.53) in terms of individual nuclear levels is inappropriate in the nuclear continuum because of the formation of giant resonances [191], where the strength of a large number of individual nuclear states n (including the continuum) is concentrated into one GR nuclear state ν. That is why we use in Eq. (3.53) the sum over $\nu\lambda L$ rather than a sum over n standing in the first-principle Eq. (3.2). In contrast to the continuum states n, the collective states ν have finite widths $\Gamma_\nu^{\lambda L}$ which give an imaginary part to the resonance amplitude R_{GR} as is also prescribed by Eq. (3.2). Note that the presence of the widths in the crossed term in (3.53) is not supported by Eq. (3.2), in which the crossed term has no imaginary part at positive energies ω at all. However, the Lorentzian form of (3.53) is a rather popular approximation often used to describe dispersion effects in dissipative systems like an oscillator with a friction. The form given in Eq. (3.53) could arise if one uses the widths $\Gamma_\nu^{\lambda L}$ depending on the photon energy, like, for example, the radiative widths $\Gamma_\gamma \sim (\hbar\omega)^3$ [192], and naively extrapolates them to negative ω (where the widths, strictly speaking, must be zero). A mathematical advantage of the Lorentzian approximation to partial resonance amplitudes is that the Lorentzian function

$$R_L(\omega) = \frac{1}{\omega_r^2 - \omega^2 - i\omega\Gamma_0} = -\frac{1}{2\omega_0}\left(\frac{1}{\omega - \omega_0 + i\Gamma_0/2} - \frac{1}{\omega + \omega_0 + i\Gamma_0/2}\right), \tag{3.55}$$

with $\omega_0 = \sqrt{\omega_r^2 - \Gamma_0^2/4}$, has no singularities in the upper semiplane $\mathrm{Im}\,\omega > 0$ of the complex energy and thus obeys the causality condition. It exactly satisfies the dispersion relation

$$\mathrm{Re}R_L(\omega) = \frac{2}{\pi}\mathcal{P}\int_0^\infty \mathrm{Im}R_L(\omega')\frac{\omega'\,d\omega'}{\omega'^2 - \omega^2},$$

what makes its use especially convenient in dispersion calculations. A disadvantage is that the crossing symmetry $R_L(\omega) = R_L(-\omega)$ is not fulfilled for the imaginary part of R_L. However, this does not create problems as long as the Lorentzian approximation for absorption cross sections is used for positive ω only. On the experimental side it is well known that heavy nuclei show GDR photoabsorption cross-sections in the form of Lorentzian curves for spherical nuclei. These Lorentzian photoabsorption cross sections can be generated in a formal way from the sum in Eq. (3.53) by keeping only one level.

The coupling of giant resonance modes and collective nuclear surface modes has been discussed by Arenhövel et al. [118, 119]. In this case the terms in (3.53) are the components into which the giant resonances are fragmented due to the coupling of collective surface and volume modes. In this case a relation between widths Γ_ν and energies E_ν of the components of the form $\Gamma_\nu \sim E_\nu^{3/2}$ is assumed.

In a collective model, giant resonances which we are dealing with here are due to collective motions of nucleons. In case of the giant-dipole resonance (GDR) this is the isovector electric-dipole motion of protons against neutrons for which the dynamic model of Steinwedel and Jenssen [149] has been developed. In a shell model this same GDR phenomenon corresponds to $1p{-}1h$ excitations of nucleons between neighboring oscillator shells ($1\hbar\omega$ transitions) (*cf.* *e.g.* [126]). The most elegant way to incorporate two-body currents into this one-body picture is provided by the Fermi liquid theory. In this model the strong interaction between nucleons leads to an effective mass M^* of quasiparticles and a modification of the isovector current. Because of the special importance of this aspect for the understanding of subnuclear degrees of freedom in isovector giant-resonances we devote a special section to this problem (section 7).

Other important GR modes are the isoscalar and isovector giant-quadrupole resonances. Enhancement effects on these GR modes have not been discussed except for a first approach in one of our

previous works [95]. Following the essential ideas of this approach we will discuss the enhancement of higher multipoles in the present work on more general grounds.

As pointed out above, giant resonances may be considered as nuclear states which themselves are coupled to a very large number of strongly overlapping individual nuclear states. These GR states may be viewed as coherent superpositions of transitions of a given multipolarity between occupied and unoccupied shell model states located below and above the Fermi level, respectively. In the following we slightly rearrange the resonance part of the GR amplitude, Eq. (3.53). We introduce the resonance energy $(E_\nu^{\lambda L})_r$ of the GR states instead of $E_\nu^{\lambda L}$ via $(E_\nu^{\lambda L})_r^2 = (E_\nu^{\lambda L} - E_0)^2 + (\Gamma_\nu^{\lambda L})^2/4$. Furthermore, we separate the ω-independent contribution coming from the $E1$ transition. Using Eqs. (3.35) and (3.49), we may transform the resonance part in such a way that the low-energy limit appears explicitly:

$$\begin{aligned} R_{GR}(\omega,\theta) &= \frac{e^2}{M}\frac{NZ}{A}(1+\kappa^{GR})\, g^{E1}(\theta) \\ &\quad + \sum_{\lambda L}\sum_{\nu} 2\,(E_\nu^{\lambda L} - E_0)\frac{(E_\nu^{\lambda L})_r^2 - \omega^2 + i\omega\Gamma_\nu^{\lambda L}}{\left((E_\nu^{\lambda L})_r^2 - \omega^2\right)^2 + (\omega\Gamma_\nu^{\lambda L})^2}\,\Theta_\nu^{\lambda L}(\omega)\, g^{\lambda L}(\theta), \end{aligned} \tag{3.56}$$

where

$$\begin{aligned} \Theta_\nu^{\lambda L} &= |\langle\nu|\, Q_{\lambda L}\,|0\rangle|^2\ , \quad \lambda L \neq E1 \\ \Theta_\nu^{E1} &= |\langle\nu|\, Q_{E1}\,|0\rangle|^2 - \left|\langle\nu|\, \overset{\circ}{Q}_{E1}\,|0\rangle\right|^2 + \frac{\omega^2}{3}|\langle\nu|\mathbf{D}|0\rangle|^2 \end{aligned} \tag{3.57}$$

are energy-dependent coefficients and the operator $\mathbf{D}$ is the dipole moment.

In the following the subscript r of $(E_\nu^{\lambda L})_r$ will be omitted for convenience. Due to the transformation of the electric dipole contribution, the lowest multipoles in the sum, $E1$, $M1$ and $E2$, are all proportional to ω^2 in the low-energy limit. Close to resonance energies a good approximation for the angular dependence of the amplitude R_{GR} can be obtained by multiplying each term in the sum with respect to λL in Eq. (3.56) by the multipole angular functions $g^{\lambda L}(\theta)$. Using (3.54) and (8.7), one can obtain that

$$g^{EL}(\theta) = A_L(z)\,\boldsymbol{\epsilon}_1\cdot\boldsymbol{\epsilon}_2 + B_L(z)\,\mathbf{s}_1\cdot\mathbf{s}_2, \quad g^{ML}(\theta) = A_L(z)\,\mathbf{s}_1\cdot\mathbf{s}_2 + B_L(z)\,\boldsymbol{\epsilon}_1\cdot\boldsymbol{\epsilon}_2, \tag{3.58}$$

where $\mathbf{s}_i = \hat{\mathbf{k}}_i \times \boldsymbol{\epsilon}_i$, $\hat{\mathbf{k}}_i = \mathbf{k}_i/\omega$, $z = \hat{\mathbf{k}}_1\cdot\hat{\mathbf{k}}_2$ and

$$A_L(z) = \frac{2}{L(L+1)}(P_L'(z) + zP_L''(z)), \quad B_L(z) = -\frac{2}{L(L+1)}P_L''(z). \tag{3.59}$$

Here $P_L(z)$ are Legendre polynomials. For the lowest multipoles the functions $g^{\lambda L}(\theta)$ are given by:

$$\begin{aligned} g^{E1}(\theta) &= \boldsymbol{\epsilon}_1\cdot\boldsymbol{\epsilon}_2 \\ g^{M1}(\theta) &= \mathbf{s}_1\cdot\mathbf{s}_2 \\ g^{E2}(\theta) &= 2(\boldsymbol{\epsilon}_1\cdot\boldsymbol{\epsilon}_2)\,(\hat{\mathbf{k}}_1\cdot\hat{\mathbf{k}}_2) - \mathbf{s}_1\cdot\mathbf{s}_2 \\ g^{M2}(\theta) &= 2(\mathbf{s}_1\cdot\mathbf{s}_2)\,(\hat{\mathbf{k}}_1\cdot\hat{\mathbf{k}}_2) - \boldsymbol{\epsilon}_1\cdot\boldsymbol{\epsilon}_2 \\ g^{E3}(\theta) &= \frac{1}{4}\left[15\left(\hat{\mathbf{k}}_1\cdot\hat{\mathbf{k}}_2\right)^2 - 1\right]\boldsymbol{\epsilon}_1\cdot\boldsymbol{\epsilon}_2 - \frac{5}{2}\left(\hat{\mathbf{k}}_1\cdot\hat{\mathbf{k}}_2\right)(\mathbf{s}_1\cdot\mathbf{s}_2)\,. \end{aligned} \tag{3.60}$$

In order to obtain the angular distribution at energies outside the resonance region, it is necessary to use further properties of the scattering amplitude, which are closely related to the problem of retardation. In other words, it is necessary to discuss the energy dependence of the quantity $\Theta_\nu^{\lambda L}$ entering into (3.56). This energy dependence is quite different at small energies, in the center of the GR region and in the high-energy limit.

3.5 Multipole and isospin decomposition of the seagull amplitude

For the further consideration it is useful to understand the isospin structure of the seagull amplitude, as well as its multipole decomposition. The underlying idea has been adopted from the hydrodynamic model of giant resonances, introduced by Steinwedel and Jensen [149] which describes the isovector motion of protons against neutrons in a giant-dipole resonance excitation. In this model the relevant dynamic quantity is the square of the difference of proton and neutron densities $(\rho_p - \rho_n)^2$ leading to an increase in potential energy in case of a local deviation from the average. In a similar way also the in-phase, or isoscalar, variation of the local density leads to giant resonance modes with the isoscalar giant-dipole mode being equivalent to Thomson scattering of the whole nucleus.

In accordance with Eq. (3.18) the total seagull amplitude S_{tot} in the static limit is equal to

$$S_{tot} = \frac{i}{2}\Big\{\langle f|\,[\boldsymbol{\epsilon}_1\cdot\mathbf{D}\,,\ \boldsymbol{\epsilon}_2\cdot(\mathbf{J}^{[1]}+\mathbf{J}^{[2]})] + [\boldsymbol{\epsilon}_2\cdot\mathbf{D}\,,\ \boldsymbol{\epsilon}_1\cdot(\mathbf{J}^{[1]}+\mathbf{J}^{[2]})]\,|i\rangle\Big\} \tag{3.61}$$

with

$$\mathbf{J}^{[1]} = \frac{e}{M}\sum_i \frac{1+\tau_3^{(i)}}{2}\ \mathbf{p}_i$$

and $\mathbf{J}^{[2]}$ from Eq. (3.11). In order to single out the isoscalar and isovector contributions to Eq. (3.61) we represent the dipole moment operator in the following form:

$$\mathbf{D} = e\sum_i \frac{1+\tau_3^{(i)}}{2}\ \mathbf{r}_i = \left(e\,\frac{N}{A}\sum_i \frac{1+\tau_3^{(i)}}{2}\ \mathbf{r}_i - e\,\frac{Z}{A}\sum_i \frac{1-\tau_3^{(i)}}{2}\ \mathbf{r}_i\right) + eZ\,\frac{1}{A}\sum_i\ \mathbf{r}_i. \tag{3.62}$$

The term in round brackets in Eq. (3.62) is the intrinsic dipole moment operator. It depends on relative coordinates of protons and neutrons and hence has an isovector structure. The remaining term in (3.62) represents the dipole moment of the nucleus as a whole. It does not distinguish coordinates of protons and neutron and, therefore, is an isoscalar operator.[2] It is evident from Eq. (3.11) that the commutator of $\mathbf{J}^{[2]}$ with the isoscalar part of the dipole moment vanishes. Therefore, exchange currents do not contribute to the isoscalar part of the seagull amplitude. The commutator of $\mathbf{J}^{[1]}$ with the isoscalar part of the dipole operator is nonzero and leads to the isoscalar part of the seagull amplitude:

$$S_{tot}^{(is)} = -\frac{Z^2}{A}\ \frac{e^2}{M}\boldsymbol{\epsilon}_1\cdot\boldsymbol{\epsilon}_2. \tag{3.63}$$

The isovector part of the dipole moment has a nonzero commutator with both $\mathbf{J}^{[1]}$ and $\mathbf{J}^{[2]}$ and, as a result, the isovector seagull amplitude in the static limit is given by

$$S_{tot}^{(iv)} = -\frac{ZN}{A}\frac{e^2}{M}\ (1+\kappa)\ \boldsymbol{\epsilon}_1\cdot\boldsymbol{\epsilon}_2. \tag{3.64}$$

In Eq. (3.64) we use the quantity κ instead of κ^{GR} for the formal reason that the current operators introduced in Eq. (3.61) do not discriminate between GR and QD excitations. Nevertheless, the application of the results obtained here may be restricted giant resonances, as will be done in the next section when discussing GR sum rules.

As soon as retardation corrections are included via the photon plane wave the corresponding form factors appear in the seagull amplitude with F_1 being related to the current $\mathbf{J}^{[1]}$ and F_2 to $\mathbf{J}^{[2]}$ (*cf.* Eqs. (3.15) and (3.19)):

$$S_{tot}^{(is)} = -\frac{Z^2}{A}\ \frac{e^2}{M}F_1(q)\ \boldsymbol{\epsilon}_1\cdot\boldsymbol{\epsilon}_2\ , \quad S_{tot}^{(iv)} = -\frac{ZN}{A}\frac{e^2}{M}\ (F_1(q)+\kappa\,F_2(q))\ \boldsymbol{\epsilon}_1\cdot\boldsymbol{\epsilon}_2. \tag{3.65}$$

[2] Using these terms in such a context we ignore that the electric charge of the nucleus itself, Z, has an isovector component.

In order to obtain a multipole decomposition of the seagull amplitude S_{tot}, we introduce one- and two-body densities $\rho_{1,2}$, which are related to the form factors $F_{1,2}$ via

$$\rho_i(r) = \int \frac{d\mathbf{q}}{(2\pi)^3} F_i(q) \, \exp\left(i\mathbf{q}\cdot\mathbf{r}\right). \tag{3.66}$$

Then

$$\boldsymbol{\epsilon}_1 \cdot \boldsymbol{\epsilon}_2 F_i(q) = \sum_{l=0}^{\infty} f_l^{(i)}(\omega) G_l(\theta) \tag{3.67}$$

with

$$f_l^{(i)}(\omega) = 4\pi \int_0^{\infty} dr r^2 \rho_i(r) j_l^2(\omega r), \tag{3.68}$$

$G_0(\theta) = g^{E1}(\theta)$ and, for $l > 0$,

$$G_l(\theta) = \frac{1}{2}(l+2) g^{E(l+1)}(\theta) + \frac{1}{2}(2l+1) g^{Ml}(\theta) + \frac{1}{2}(l-1) g^{E(l-1)}(\theta). \tag{3.69}$$

Here $g^{\lambda L}(\theta)$ is the angular distribution function for the multipole λL, as before. A derivation of the expansion given in Eqs. (3.67) and (3.69) can be found in appendix C. Substitution of these relations into Eq. (3.65) leads to the multipole decomposition of the seagull amplitude $S_{tot} = S_{tot}^{(is)} + S_{tot}^{(iv)}$:

$$\begin{aligned} S_{tot} &= \sum_{\lambda L} S_{tot}^{\lambda L}(\omega)\, g^{\lambda L}(\theta)\ , \quad S_{tot}^{EL}(\omega) = -\frac{Ze^2}{M}\left(\frac{(L+1) f_{L-1}(\omega) + L f_{L+1}(\omega)}{2}\right)\ , \\ S_{tot}^{ML}(\omega) &= -\frac{Ze^2}{M}\left(\frac{2L+1}{2}\right) f_L(\omega)\ , \quad f_l(\omega) = f_l^{(1)}(\omega) + \frac{N}{A}\kappa f_l^{(2)}(\omega). \end{aligned} \tag{3.70}$$

When one uses only the lowest-order terms with respect to ω for each multipole, one obtains expressions for the unretarded multipole amplitudes entering into S_{tot}:

$$\mathring{S}_{tot}^{EL}(\omega) = -\frac{Ze^2}{M}\frac{(L+1)\,\omega^{2L-2}}{2\,[(2L-1)!!]^2}\left(\left\langle r^{2L-2}\right\rangle_1 + \frac{N}{A}\,\kappa\,\left\langle r^{2L-2}\right\rangle_2\right), \tag{3.71}$$

$$\mathring{S}_{tot}^{ML}(\omega) = -\frac{Ze^2}{M}\frac{(2L+1)\,\omega^{2L}}{2\,[(2L+1)!!]^2}\left(\left\langle r^{2L}\right\rangle_1 + \frac{N}{A}\,\kappa\,\left\langle r^{2L}\right\rangle_2\right)\ , \quad \left\langle r^{2l}\right\rangle_{1,2} = 4\pi \int\limits_0^{\infty} dr\, r^{2l+2}\rho_{1,2}.$$

As was already pointed out all contributions from electric multipoles in Eq. (3.71) except for $E1$ cancel the corresponding low-energy expansion of the resonance amplitude. In the case of magnetic multipoles such cancellations do not appear. This asymmetry between electric and magnetic multipoles becomes important when we discuss sum rules in section 4. There it will become evident that sum rules in a strict sense are only possible for electric multipoles.

4 Compton scattering by giant resonances

In the present section we discuss the status of Compton scattering by giant resonances. The usual way of constructing the resonance (positive energy) scattering amplitude of Compton scattering by giant resonances is given by the Lorentzian representation of photoabsorption cross sections and the application of the optical theorem and the once-subtracted dispersion relation. The amplitudes obtained in this way are valid close to the peaks of the resonances but quite obviously fail in the low-energy and high-energy limits. These deficiencies can be cured by introducing nonretarded amplitudes which are valid in the low-energy limit and by introducing retardation formfactors to take into account retardation effects [95, 176]. This procedure is in accordance with the nonrelativistic Hamiltonian but violates the requirements dispersion relations which may be understood as a violation of causality [165]. When correcting for this effect a satisfactory representation of the resonance (positive energy) amplitude including the effects of retardation is obtained as will be shown in section 10 through a model calculation. On the basis of this theoretical approach we discuss recent theoretical and experimental results obtained for the giant resonances.

Before proceeding further it is worth to briefly explain why the second-order perturbation theory, which results in Eq. (3.56) for the resonance amplitude R_{GR}, is not fully suitable for data analyses and why dispersion relations are invoked for an alternative construction for R_{GR}. The main practical problem with a use of Eq. (3.56) is that an evaluation of this equation involves both the spectrum of excited states and the energy dependences of the transition matrix elements $\langle\nu|Q_{\lambda L}|0\rangle$. These matrix elements are not known with the necessary precision when $\omega R \simeq 1$ (here R is the nuclear radius), *i.e.* when the energy ω lies well above the region of the giant dipole and giant quadrupole resonances and when retardation effects come fully into play. At such energies matrix elements between the ground state $|0\rangle$ and excited states $|\nu\rangle$ with $L \sim \omega R$ are no longer suppressed by threshold factors like $(\omega R)^L$ or $(\omega R)^{L-1}$. Therefore, these excited states, being fully negligible in Eq. (3.56) in the low-energy region $\omega R \ll 1$, do give an essential contribution to the real part of R_{GR} at high energies. We refer to section 10 for a model example.

On the other hand, the dispersion relation (3.21) suggests that the high-energy behavior of $R_{GR}(\omega, 0)$ is controlled by photoabsorption in the low energy region at $\omega R \ll 1$, where the giant dipole and quadrupole resonances are located, so that the knowledge of details of the high-energy behavior of the transition matrix elements should be unnecessary. From this reason it is attractive to try to formulate the resonance amplitude R_{GR} by using dispersion relations and to extend Eq. (3.21) to nonzero angles. One possible extension based on fixed-t dispersion relations is considered in section 8. As we will see, it can be developed for low t (or small angles) but also runs into trouble when the region of high t, *i.e.* $-tR^2 \gtrsim 1$, is considered.

In this situation a phenomenological approach was developed [95] which combines the advantages of the two approaches and is apparently applicable at all energies of practical interest — up to the pion photoproduction threshold — as confirmed by a model study in section 10. To help with the understanding of the different steps and to provide a dictionary of the notation used, we briefly summarize the procedure of finding the partial resonance amplitudes $R_{GR}^{\lambda L}$. To avoid confusion note that all the partial amplitudes used in this section do not include the constant $R_{GR}(0,0)$, Eq. (3.35), so that all of them vanish at $\omega = 0$.

At the first stage naive once-subtracted dispersion relations for partial amplitudes are postulated and the corresponding "dispersion" amplitudes $\tilde{R}_{GR}^{\lambda L}$ are obtained as a sum of few Lorentzians with parameters given by the structure of the total photoabsorption cross section. These "dispersion" amplitudes are not assumed to be identical with the proper amplitudes $R_{GR}^{\lambda L}$ because they have either a wrong threshold (at $\omega \to 0$) or a wrong asymptotic (at $\omega \to \infty$) behavior, or both. They are only used to construct unretarded, $\mathring{R}_{GR}^{\lambda L}$, and retarded, $\hat{R}_{GR}^{\lambda L}$, amplitudes and to fix their scale. It is

assumed that the (total) retarded amplitude $\hat{R}_{GR}$ is nothing but the full unretarded amplitude $\overset{\circ}{R}_{GR}$ multiplied by retardation form factor squared, $F^2_{(ret)}(\omega)$. The matching of the "dispersion" amplitude $\tilde{R}_{GR}$ and the retarded amplitude $\hat{R}_{GR}$ is done in such a way that these two amplitudes yield the same absorption cross sections at the giant-resonance peaks. The retarded amplitudes have theoretically sound behavior both at low and high energies as long as one stays on the real axis of complex ω-plane. Being also correct at the resonance peaks, they are assumed to be in general very close to the proper amplitudes $R^{\lambda L}_{GR}$. However, a comparison with the requirement of the forward-angle dispersion relation reveals a mismatch $\Delta R(\omega)$ between the total "dispersion" amplitude $\tilde{R}_{GR}(\omega, 0)$ and the total retarded amplitude $\hat{R}_{GR}(\omega, 0)$. In order to remove this mismatch, the electric dipole amplitude R^{E1}_{GR} is appropriately corrected with ΔR, and this gives the final resonance amplitude R_{GR}. The whole construction is chosen to ensure vanishing of the resulting resonance amplitude R_{GR} in the high-energy limit at any angle.

The described procedure cannot be strictly derived from first principles. Moreover, some features of thus obtained resonance amplitude R_{GR} are in contrast to those found in relativistic models; among them is the absence of a q-dependent form factor $F(q)$ in the asymptotics of $R_{GR}(\omega, \theta)$ (see section 10). Nevertheless, that is the best what was proposed to describe Compton scattering through the giant resonance region, and this Ansatz finds a numerical confirmation both experimentally and through model studies.

Now we proceed with giving details of the described approach.

4.1 The giant resonance amplitude in the Lorentzian representation

The general form of the resonance amplitude for the forward direction given in (3.56) consists of a Lorentzian part and a coefficient $\Theta^{\lambda L}_{\nu}$, which is energy dependent and is expected to be different at low energies, in the center of the giant-resonance region and in the high-energy limit, respectively. In the following we, therefore, will discuss three different regimes of the resonance amplitude corresponding to the three energy regions.

The great advantage of Compton scattering experiments is the fact that in the forward direction the amplitude is fixed through the optical theorem, the dispersion relation and the low-energy theorem. Then the specific information of Compton scattering is contained in the angular distribution of the differential cross section. For applications this means that the resonance amplitudes as formulated in Eq. (3.56) has to be replaced by a more practical version. In the vicinity of the giant resonances this is obtained through the following procedure. We consider the total photoabsorption cross section as a superposition of Lorentzian lines

$$\sigma(\omega) = \sum_{\lambda L} \sigma^{\lambda L}(\omega) = \sum_{\lambda L} \sum_{\nu} \sigma^{\lambda L}_{\nu} \frac{(\omega \Gamma^{\lambda L}_{\nu})^2}{\left[(E^{\lambda L}_{\nu})^2 - \omega^2\right]^2 + \omega^2 (\Gamma^{\lambda L}_{\nu})^2} \tag{4.1}$$

where the sum with respect to ν is taken over all Lorentzians contributing to the multipoles λL. The quantities $E^{\lambda L}_{\nu}$, $\Gamma^{\lambda L}_{\nu}$ and $\sigma^{\lambda L}_{\nu}$ denote the resonance energies, widths and peak cross sections of the Lorentzians, respectively. A resonance amplitude $\tilde{R}_{GR}$, which is applicable in the resonance region and corresponds to the photoabsorption cross section of (4.1), then has the form

$$\begin{aligned} \tilde{R}_{GR}(\omega, \theta) &= \frac{NZ}{A} \frac{e^2}{M} (1 + \kappa^{GR}) g^{E1}(\theta) + \sum_{\lambda L} \tilde{R}^{\lambda L}(\omega, \theta) \qquad (4.2) \\ &= \frac{NZ}{A} \frac{e^2}{M} (1 + \kappa^{GR}) g^{E1}(\theta) + \frac{\omega^2}{4\pi} \sum_{\lambda L, \nu} \sigma^{\lambda L}_{\nu} \Gamma^{\lambda L}_{\nu} \frac{(E^{\lambda L}_{\nu})^2 - \omega^2 + i\omega \Gamma^{\lambda L}_{\nu}}{\left[(E^{\lambda L}_{\nu})^2 - \omega^2\right]^2 + \omega^2 (\Gamma^{\lambda L}_{\nu})^2} g^{\lambda L}(\theta). \end{aligned}$$

Here and below $\tilde{R}^{\lambda L}(\omega,\theta)$ means the product $\tilde{R}^{\lambda L}(\omega)\, g^{\lambda L}(\theta)$. In the low and high energy limit a special discussion of the amplitude's properties is required.

The energy-dependent multipole amplitudes $\tilde{R}^{\lambda L}$ in (4.2) are built in such a way that they satisfy the optical theorem,

$$\mathrm{Im}\tilde{R}^{\lambda L}(\omega,0) = \frac{\omega}{4\pi}\sigma^{\lambda L}(\omega), \tag{4.3}$$

and obey the naive subtracted dispersion relations

$$\mathrm{Re}\tilde{R}^{\lambda L}(\omega,0) = \frac{\omega^2}{2\pi^2}\mathcal{P}\int_0^\infty \frac{\sigma^{\lambda L}(\omega')}{(\omega')^2-\omega^2}\, d\omega'. \tag{4.4}$$

Here the subtraction is replaced by zero, what is allowed because the subtractions for all multipoles are contained in the first term of the r.h.s. of (4.2) and, furthermore, are of electric-dipole multipolarity.

In the high-energy limit $\omega \to \infty$, the dispersion resonance amplitudes (4.4) are given by

$$\mathrm{Re}\tilde{R}^{\lambda L}(\infty,0) = -\frac{1}{2\pi^2}\int_0^\infty \sigma^{\lambda L}(\omega')\, d\omega' = -\sum_\nu \frac{\sigma_\nu^{\lambda L}\Gamma_\nu^{\lambda L}}{4\pi}, \tag{4.5}$$

where the explicit form of the partial absorption cross sections, Eq. (4.1), was used. Since the giant resonance amplitude has to vanish in the high-energy limit, we obtain from (4.2) and (4.5) the GGT sum rule:

$$\sum_{\lambda L}\int_0^\infty \sigma^{\lambda L}(\omega')d\omega' = \sum_{\lambda L,\nu}\frac{\pi}{2}\sigma_\nu^{\lambda L}\Gamma_\nu^{\lambda L} = 2\pi^2\frac{NZ}{A}\frac{e^2}{M}(1+\kappa^{GR}). \tag{4.6}$$

A further useful property of the scattering amplitude in the Lorentzian form concerns the second negative momentum of the integrated cross section. We discuss this property here as a reference for further applications. One has

$$\lim_{\omega\to 0}\frac{\mathrm{Re}\tilde{R}^{\lambda L}(\omega,0)}{\omega^2} = \frac{1}{2\pi^2}\int_0^\infty \frac{\sigma^{\lambda L}(\omega')}{(\omega')^2}d\omega' \equiv \frac{1}{2\pi^2}\sigma_{-2}^{\lambda L} = \frac{1}{4\pi}\sum_\nu \frac{\sigma_\nu^{\lambda L}\Gamma_\nu^{\lambda L}}{(E_\nu^{\lambda L})^2}, \tag{4.7}$$

where in the last step the explicit (Lorentzian) form of the amplitudes $\tilde{R}^{\lambda L}$ has been used again.

It is possible to relate the resonance amplitude, Eq. (4.2), to the forward-direction form, Eq. (3.56), which yields a representation of the matrix elements $\Theta_\nu^{\lambda L}$ applicable *in the resonance region*:

$$\Theta_\nu^{\lambda L}(\omega) = \frac{\omega^2\sigma_\nu^{\lambda L}\Gamma_\nu^{\lambda L}}{8\pi\, E_\nu^{\lambda L}}. \tag{4.8}$$

Note that in this form of the matrix elements $\Theta_\nu^{\lambda L}$ all effects of retardation are included. Such effects are important, when the product of the photon energy ω with the nuclear radius R is of the order of unity, which is the case in an actual experiment.

4.2 The unretarded resonance amplitude

The dispersion amplitude (4.2) is built in such a way that it vanishes at high energies in the forward direction. Such vanishing appears as a result of the exact balance between the first term in (4.2) and the partial amplitudes $\tilde{R}^{\lambda L}(\infty,0)$, as is stated by Eq. (4.6). However, this balance is destroyed at angles $\theta \neq 0$, when the angular coefficients $g^{\lambda L}(\theta)$ of different multipoles become different. Accordingly, Eq. (4.2) does not vanish in the high-energy limit. Another deficiency of Eq. (4.2) which has to be cured is

that the multipole amplitudes $\tilde{R}^{\lambda L}(\omega,0)$ do not have the proper ω dependence at low energies except for the lowest multipoles $\lambda L = E1, E2, M1$.

As the first step to remove these deficiencies we introduce now an unretarded form $\overset{\circ}{R}_{GR}$ of the giant resonance amplitude R_{GR}, where each multipole transition operator is taken into account only in its lowest order in ω and manifestly results in the correct low-energy behavior. Our construction is as follows. In the low-energy limit each multipole (electric and magnetic) in the total nuclear scattering amplitude $T_A(\omega,\theta)$ is proportional to ω^{2L} (except for the Thomson $E1$ amplitude). This property can be obtained from general considerations based on analytical properties of the amplitude, as will be seen in section 8. The amplitude $R_{GR}(\omega,\theta)$ in the form of Eq. (3.56), together with (3.48) teaches us that in the low-energy limit each electric multipole component is proportional to ω^{2L-2}, while the magnetic multipole starts from ω^{2L}. As was pointed out above the EL multipole contributions of the order ω^{2L-2} in the seagull amplitude cancel the corresponding terms in the resonance amplitude, which leads to the correct low-energy behavior for the sum. Taking into account these properties we may write

$$\overset{\circ}{R}_{GR}(\omega,\theta) = \frac{NZ}{A}\frac{e^2}{M}(1+\overset{\circ}{\kappa}^{GDR})g^{E1}(\theta) + \sum_{\lambda L}\overset{\circ}{R}^{\lambda L}(\omega,\theta) = \tag{4.9}$$
$$\frac{NZ}{A}\frac{e^2}{M}(1+\overset{\circ}{\kappa}^{GDR})g^{E1}(\theta) + \frac{\omega^2}{4\pi}\sum_{\lambda L,\nu}\overset{\circ}{\sigma}{}^{\lambda L}_{\nu}\Gamma^{\lambda L}_{\nu}\frac{(E^{\lambda L}_{\nu})^2-\omega^2+i\omega\Gamma^{\lambda L}_{\nu}}{\left[(E^{\lambda L}_{\nu})^2-\omega^2\right]^2+\omega^2(\Gamma^{\lambda L}_{\nu})^2}\Omega^{\lambda L}_{\nu}(\omega)g^{\lambda L}(\theta),$$

where

$$\begin{aligned}\Omega^{E1}_{\nu}(\omega) &= 1\\ \Omega^{EL}_{\nu}(\omega) &= (\omega/E^{EL}_{\nu})^{2L-4} \quad \text{for } L\geq 2\\ \Omega^{ML}_{\nu}(\omega) &= (\omega/E^{ML}_{\nu})^{2L-2} \quad \text{for } L\geq 1.\end{aligned} \tag{4.10}$$

In accordance with Eq. (3.37), the unretarded enhancement parameter $\overset{\circ}{\kappa}^{GDR}$ stands in the unretarded amplitude (4.9). Assuming that the $E1$ component of Eq. (4.9) vanishes at high energies, we find the (modified) TRK sum rule

$$\int_0^{\infty}\overset{\circ}{\sigma}{}^{E1}(\omega')d\omega' = \sum_{\nu}\frac{\pi}{2}\overset{\circ}{\sigma}{}^{E1}_{\nu}\Gamma^{E1}_{\nu} = 2\pi^2\frac{NZ}{A}\frac{e^2}{M}(1+\overset{\circ}{\kappa}^{GDR}). \tag{4.11}$$

Here the corresponding unretarded absorption cross section is

$$\overset{\circ}{\sigma}(\omega) = \sum_{\lambda L}\overset{\circ}{\sigma}{}^{\lambda L}(\omega) = \sum_{\lambda L,\nu}\overset{\circ}{\sigma}{}^{\lambda L}_{\nu}\frac{(\omega\Gamma^{\lambda L}_{\nu})^2}{\left[(E^{\lambda L}_{\nu})^2-\omega^2\right]^2+\omega^2(\Gamma^{\lambda L}_{\nu})^2}\Omega^{\lambda L}_{\nu}(\omega). \tag{4.12}$$

The difference between this expression for $\overset{\circ}{\sigma}(\omega)$ and the corresponding quantity $\sigma(\omega)$ from Eq. (4.1) lies in the appearance of the ω-dependent factor $\Omega^{\lambda L}_{\nu}$ and in the unretarded peak cross sections $\overset{\circ}{\sigma}{}^{\lambda L}_{\nu}$. A comparison of $\overset{\circ}{\sigma}{}^{\lambda L}(\omega)$ and $\sigma^{\lambda L}(\omega)$ will be given in section 10 in the framework of a specific model. It should be noted that the energy-dependent factor $\Omega^{\lambda L}_{\nu}$ becomes effective for electric octupoles, magnetic quadrupoles and higher multipoles. At energies much larger than the resonance energies this form of the unretarded multipole cross sections cannot be applied. Nevertheless, in the case of electric multipoles energy-weighted sum rules can be derived, which serve as a guideline in the interpretation of experimental data.

The cancellation between the leading terms in the unretarded resonance amplitudes $\overset{\circ}{R}^{\lambda L}$ and in the expansion of the seagull amplitude leads to sum rules for electric multipoles. Since different mechanisms of excitation are involved, it is possible to formulate such sum rules independently for the

isoscalar (is) and the isovector (iv) contributions. Due to the fact that we are restricting ourselves to giant resonance phenomena, it is necessary to understand which part of the total seagull amplitude S_{tot} corresponds to this degree of freedom. Clearly, the kinetic seagull amplitude B has to be included. Therefore, as mesonic effects appear in the isovector part only (*cf.* Eq. (3.64)), the isoscalar sum rules can straightforwardly be written down:

$$\overset{\circ}{\sigma}{}^{EL,(is)}_{-(2L-2)} = 2\pi^2 \lim_{\omega\to 0} \frac{\overset{\circ}{R}{}^{EL,(is)}(\omega,0)}{\omega^{2L-2}} = \pi^2 \frac{Z^2e^2}{AM} \frac{L+1}{[(2L-1)!!]^2} \left\langle r^{2L-2} \right\rangle_1 , \quad L>1. \tag{4.13}$$

The r.h.s. of Eq. (4.13) follows from the decomposition of the seagull amplitude, Eq. (3.71), together with Eq. (3.63). Note that no such sum rule exists for $E1$, as the observed electric dipole resonance is an isovector excitation. In the case of isovector sum rules the situation is more complicated. In section 3.2 we discussed the full mesonic seagull amplitude obtained in the static limit. Clearly, only a part of this amplitude, previously denoted by S_{GR}, enters into the giant resonance amplitude T_{GR}, which we discuss now. However, it is impossible to extract S_{GR} from S without further assumptions, as long as we basically argue in the framework of the Fermi gas model which cannot discriminate between GR and QD modes of excitation. Strictly speaking, it is not sufficient to only pass from κ to $\overset{\circ}{\kappa}{}^{GDR}$ in the amplitude S, but also the dependence on momentum transfer is modified. This means that the form factor F_2^{GR} entering into S_{GR} is different from the two-body form factor F_2 appearing in the amplitude S. Such a modification can only be discussed in a model-dependent way, *e.g.* by following the frequently applied (see *e.g.* [173]) line of thought that the main contribution to S_{GR} comes from the central part of the exchange potential. We discuss the quantitative consequences of this assumption in appendix B. Here we denote the normalized density, which corresponds to the form factor F_2^{GR} by ρ_2^{GR} and write the isovector sum rule as

$$\begin{aligned} \overset{\circ}{\sigma}{}^{EL,(iv)}_{-(2L-2)} &= 2\pi^2 \lim_{\omega\to 0} \left(\frac{\overset{\circ}{R}{}^{EL,(is)}(\omega,0)}{\omega^{2L-2}} + \frac{NZ}{A}\frac{e^2}{M}(1+\overset{\circ}{\kappa}{}^{GDR})\delta_{L,1} \right) \\ &= \pi^2 \frac{NZ}{A}\frac{e^2}{M}\frac{L+1}{[(2L-1)!!]^2} \left(\left\langle r^{2L-2} \right\rangle_1 + \overset{\circ}{\kappa}{}^{GDR} \left\langle r^{2L-2} \right\rangle_2^{GR} \right). \end{aligned} \tag{4.14}$$

The label GR given here to the two-body formfactor F_2^{GR}, the two-body density ρ_2^{GR} and the two-body averaged radius $\left\langle r^{2L-2} \right\rangle_2^{GR}$ indicates that these quantities now are restricted to the GR d.o.f. and, therefore, may be slightly different from the corresponding quantities introduced in section 3.5 where no distiction between the GR and QD d.o.f. has been made. The upper indices (is) and (iv) for the absorption cross section correspond to restricting the sum with respect to ν in Eq. (4.12) to isoscalar and isovector giant resonance excitations, respectively. It should be stressed that these sum rules are valid for the unretarded photoabsorption cross sections and not immediately for the experimental (retarded) photoabsorption cross sections. Sum rules for the latter case will be discussed below in section 4.5 and in section 8. A useful relation for the purpose of data analysis as well as for the following discussion is the sum of Eqs. (4.13) and (4.14) for the case of the electric quadrupole. One has

$$\overset{\circ}{\sigma}{}^{E2}_{-2} = \overset{\circ}{\sigma}{}^{E2,(is)}_{-2} + \overset{\circ}{\sigma}{}^{E2,(iv)}_{-2} = \frac{\pi^2}{3}\frac{Ze^2}{M} \left(\left\langle r^2 \right\rangle_1 + \frac{N}{A}\overset{\circ}{\kappa}{}^{GDR} \left\langle r^2 \right\rangle_2^{GR} \right). \tag{4.15}$$

In the particular case $L=1$, Eq. (4.14) gives the sum rule (4.11).

4.3 The retardation problem

The principal goal of a theoretical investigation of nuclear Compton scattering is to obtain a consistent description of the energy and angular dependence of the scattering amplitude in a wide energy region.

In the previous section different quantities have been introduced. The "dispersion" amplitudes $\tilde{R}^{\lambda L}$ provide a formulation of Compton scattering in the resonance region only. Since their parameters are taken from experiment, these amplitudes are retarded quantities. The corresponding unretarded amplitudes $\overset{\circ}{R}{}^{\lambda L}$ were designed to correctly describe the low-energy Compton scattering, but they were expressed in terms of unretarded quantities. Therefore, in order to obtain in a wide energy region (also including high energies) a representation of the Compton scattering amplitude expressed only via observable quantities, it is necessary to establish a relation between unretarded and retarded quantities. A formulation of this retardation problem in terms of the Bessel functions entering into the multipole transition operators has been given in section 3.4 in the following way: In an expansion [194] of the plane wave for the photon into terms with definite parity and total angular momentum L, Eq. (3.45), each term contains a spherical Bessel function $j_L(\omega r)$. An amplitude obtained using the exact multipole operators is called "retarded", while in the case where the substitution $j_L(\omega r) \to (\omega r)^L/(2L+1)!!$ is made, the resulting amplitude is called "unretarded". The importance of retardation effects is different in the different energy regions, i.e. at low energies, in the resonance region and in the high-energy limit, which for our present purpose can be identified with the pion threshold. Only at very low energies the parameter of expansion ωR, with the nuclear radius R, is small. In the resonance region this parameter is still smaller than unity, but no longer negligible, while at high energies one has $\omega R \sim 1$.

Let us consider again the representation of the (retarded) scattering amplitude T_{GR} coming from second-order perturbation theory. In Eq. (3.53) the seagull part of the scattering amplitude includes the effects of retardation through the form factors. A further important property of (3.53) is that in the high-energy limit the last term, i.e. the resonance amplitude, vanishes and, therefore, the high-energy limit of the scattering amplitude is represented by the first two (seagull) terms. Our solution of (i.e. the Ansatz for) the retardation problem with respect to the resonance amplitude consists of two parts. We have to fix (i) how the low-energy form $\overset{\circ}{R}_{GR}(\omega,\theta)$ of Eq. (4.9) and the retarded Lorentzian form $\tilde{R}_{GR}(\omega,\theta)$ of Eq. (4.2) are related to each other, and (ii) through which mechanism the high-energy form of the resonance amplitude tends to zero. We follow the ideas of our previous work [95] and then — in later sections — discuss the predictions of fixed-t dispersion relations and calculations within a relativistic harmonic-oscillator model.

The interpolation between $\overset{\circ}{R}_{GR}(\omega,\theta)$ and $\tilde{R}_{GR}(\omega,\theta)$ starts with the introduction of a "retarded" resonance amplitude

$$\hat{R}_{GR}(\omega,\theta) = \overset{\circ}{R}_{GR}(\omega,\theta)\, F^2_{(ret)}(\omega). \tag{4.16}$$

This retarded resonance amplitude $\hat{R}_{GR}(\omega,\theta)$ reflects our "classical" expectation of the retardation effect. The quantity $F_{(ret)}(\omega)$ is a form factor due to the spatial distribution of quasiparticles. It takes into account the different phases of the electromagnetic wave with respect to the location of these quasiparticles. In a classical picture one form factor in Eq. (4.16) appears as a result of calculating the total force acting on an extended charged object. The second form factor results from the calculation of the photon radiation off this extended object due to acceleration. This picture is confirmed by the consideration of the relativistic oscillator model (*cf.* section 10). As a consequence (4.16) is the logical form of a retarded amplitude in a classical picture. This type of retardation has already been discussed by Barashenkov and Kaiser [196] in the case of the nucleon and by Petrun'kin [197] and Ericson and Hüfner [175] in a quantum-mechanical treatment of Thomson scattering. More recently it has been derived by Baron et al. [176] in a nonrelativistic model calculation of retardation effects on the resonance part of the giant dipole resonance.

Strictly speaking, due to the close structural relation between the resonance and seagull parts of the amplitude, it is not obvious, what type of form factor should be used for $F_{(ret)}(\omega)$ in Eq. (4.16). One may expect that different types of excitations lead to different form factors. For example, while

for isoscalar excitations the one-body form factor F_1 seems appropriate, isovector excitations should be related to an isovector form factor $F^2_{(iv)} = (F_1^2 + \mathring{\kappa}^{GDR}(F_2^{GR})^2)/(1 + \mathring{\kappa}^{GDR})$.

In order to fix the coefficients $\mathring{\sigma}_\nu^{\lambda L}$ contained in the low-energy form, Eq. (4.9), of the resonance amplitude $\mathring{R}_{GR}(\omega,\theta)$, we use the condition that the retarded amplitude yields through the optical theorem the correct magnitude of the absorption cross section at the resonance peaks:

$$\mathrm{Im}\,\hat{R}^{\lambda L}_{GR}(E^{\lambda L}_\nu,\theta) = \mathrm{Im}\,\tilde{R}^{\lambda L}_{GR}(E^{\lambda L}_\nu,\theta). \tag{4.17}$$

This gives relations

$$\mathring{\sigma}_\nu^{\lambda L}\, F^2_{(ret)}(E^{\lambda L}_\nu) = \sigma_\nu^{\lambda L} \tag{4.18}$$

between the unretarded $\mathring{\sigma}_\nu^{\lambda L}$ and the experimental peak cross sections $\sigma_\nu^{\lambda L}$.

Thus defined, the retarded resonance amplitude $\hat{R}_{GR}(\omega,\theta)$ fulfills one of the most essential conditions we are looking for since it apparently vanishes in the high-energy limit owing to the factor $F_{(ret)}(\omega)$. In spite of this and in spite of its classical plausibility, the resonance amplitude $\hat{R}_{GR}(\omega,\theta)$ in the form of (4.16) is not fully acceptable because it violates causality. This can easily be seen if for example the proton density is approximated by a Gaussian distribution, i.e. $F_{(ret)}(\omega) = \exp(-\omega^2/(4\lambda))$ where the parameter λ is fixed by demanding that it reproduces the usual mean square nuclear charge radius [176]. In this particular form one can easily derive that $\hat{R}(\omega,\theta)$ of Eq. (4.16) tends to infinity in part of the upper complex-ω half-plane for $|\omega| \to \infty$. Consequently, this form of the resonance amplitude violates causality [165]. Similar difficulties (*e.g.* additional poles in the upper half-plane of ω) may appear for other distributions of quasiparticles. However, as it will be seen in section 10 within the relativistic oscillator model, it is possible that such energy-dependent form factors are compensated by the sum over all intermediate states, if all matrix elements are taken into account exactly. In this way the correct analytical properties of the total amplitude may in principle be restored. Since it is necessary to approximate these matrix elements in all applications of the general formalism, a different approach for overcoming the difficulties of an incorrect analytical behavior has been suggested in [95].

The incorrect analytical behavior of the "retarded" amplitude (4.16) manifests itself in that it does not obey the GGT dispersion relation at the forward angle. That means that there is a mismatch

$$\Delta R(\omega) = \tilde{R}_{GR}(\omega,0) - \hat{R}_{GR}(\omega,0) \tag{4.19}$$

between the exact (dispersion) amplitude $\tilde{R}_{GR}(\omega,0)$ and the "retarded" amplitude (4.16). It was proposed in [95] to consider this difference as an electric dipole correction to the "retarded" amplitude and to finally write the resonance amplitude $R_{GR}(\omega,\theta)$ including the effects of retardation in the following form:

$$R_{GR}(\omega,\theta) = \hat{R}_{GR}(\omega,\theta) + \boldsymbol{\epsilon}_1\cdot\boldsymbol{\epsilon}_2\,\Delta R(\omega). \tag{4.20}$$

By construction, the amplitude (4.20) is in agreement with forward-direction dispersion theory, just because of the above specific choice of $\Delta R(\omega)$. Simultaneously, the amplitude (4.20) preserves all the favorable properties of the retarded amplitude $\hat{R}(\omega,\theta)$. The high-energy limit of the resonance amplitude (4.20) is determined by $\tilde{R}_{GR}(\omega,0)$ and has the form

$$\begin{aligned} R_{GR}(\omega,\theta) &\approx \tilde{R}_{GR}(\omega,0)\, g^{E1}(\theta) \\ &= \left(\frac{NZ}{A}\frac{e^2}{M}(1+\kappa^{GR}) + \frac{\omega^2}{4\pi}\sum_{\lambda L,\nu}\sigma_\nu^{\lambda L}\Gamma_\nu^{\lambda L}\frac{(E_\nu^{\lambda L})^2-\omega^2+i\omega\Gamma_\nu^{\lambda L}}{((E_\nu^{\lambda L})^2-\omega^2)^2+\omega^2(\Gamma_\nu^{\lambda L})^2}\right) g^{E1}(\theta) \\ &\to \frac{1}{4\pi\omega^2}\sum_{\lambda L,\nu}\sigma_\nu^{\lambda L}\Gamma_\nu^{\lambda L}\left((\Gamma_\nu^{\lambda L})^2-(E_\nu^{\lambda L})^2+i\omega\Gamma_\nu^{\lambda L}\right) g^{E1}(\theta). \end{aligned} \tag{4.21}$$

For the last line in Eq. (4.21) the sum rule (4.6) has been used. The Ansatz (4.20) implies that we attributed an electric dipole characteristic to this high-energy limit.[3] In section 8 the properties of Eq. (4.20) are discussed within the framework of fixed-t dispersion relations.

The adopted procedure is equivalent to using the dispersion relation for the dipole $E1$ amplitude (however not with only the $E1$ cross section but rather with a modified one) and to introducing threshold ($\Omega_\nu^{\lambda L}$) and retardation ($F_{(ret)}$) factors to other "dispersion" multipoles. This is explicitly shown by another form of Eq. (4.20) which summarizes all different peaces of the amplitude:

$$\begin{aligned} R_{GR}(\omega,\theta) &= \frac{NZ}{A}\frac{e^2}{M}(1+\kappa^{GR})g^{E1}(\theta) \\ &\quad + \frac{\omega^2}{4\pi}\sum_{\lambda L,\nu}\sigma_\nu^{\lambda L}\Gamma_\nu^{\lambda L}\frac{(E_\nu^{\lambda L})^2-\omega^2+i\omega\Gamma_\nu^{\lambda L}}{\left[(E_\nu^{\lambda L})^2-\omega^2\right]^2+\omega^2(\Gamma_\nu^{\lambda L})^2}\left[\Omega_\nu^{\lambda L}(\omega)g^{\lambda L}(\theta)\right]_{(ret)}, \end{aligned} \tag{4.22}$$

where

$$\left[\Omega_\nu^{\lambda L}(\omega)g^{\lambda L}(\theta)\right]_{(ret)} = g^{\lambda L}(\theta)+\left[\frac{F_{(ret)}^2(\omega)}{F_{(ret)}^2(E_\nu^{\lambda L})}\Omega_\nu^{\lambda L}(\omega)-1\right]\left(g^{\lambda L}(\theta)-g^{E1}(\theta)\right). \tag{4.23}$$

We may note that the unretarded enhancement parameter $\mathring{\kappa}^{GDR}$ standing in the unretarded amplitude $\mathring{R}_{GR}(\omega,\theta)$ and in the retarded amplitude $\hat{R}_{GR}(\omega,\theta)$ does not appear in the final amplitude (4.22). Instead, only the retarded quantity κ^{GR} appears as it should, owing to the constraint of the GGT sum rule. So, the parameter $\mathring{\kappa}^{GDR}$ cannot be *directly* determined from Compton scattering data. Given, however, the absorption cross section and the form factor, one can calculate $\mathring{\kappa}^{GDR}$ through Eq. (4.11) and compare it with κ^{GR}. This will be done in the following sections.

The above-mentioned replacement of the unretarded enhancement parameter $\mathring{\kappa}^{GDR}$ by the retarded one, κ^{GR}, in Eq. (4.22) takes place only, because the correction $\Delta R(\omega)$ in Eq. (4.20) was attributed to the $E1$ multipolarity. Therefore, one can conclude that the electric dipole factor appearing in Eq. (4.20) and persisting up to the asymptotics (4.21) is obligatory at low energies. At high energies it might be modified, and this is exactly what is observed in the model considered in section 10, where an additional form factor appears in the asymptotics of R_{GR}. However, we have to repeat again (see footnote [3]) that the same model suggests that such modifications are not important numerically. (See section 10.5 for more detail.)

The resonance amplitude R_{GR}, Eqs. (4.20) or (4.22), together with the total giant-resonance seagull contribution

$$B(\omega,\theta)+S_{GR}(\omega,\theta) = -\frac{e^2}{M}\Big(Z\,F_1(q)+\frac{NZ}{A}\,\kappa^{GR}F_2^{GR}(q)\Big)\,g^{E1}(\theta), \tag{4.24}$$

composes the part of the total amplitude T_A, Eq. (3.17), related to the giant-resonance degrees of freedom. The remaining contributions in Eq. (3.17) are discussed in section 5.

The effects of retardation on the giant-multipole amplitudes are illustrated in Fig.4.1. The imaginary parts are not noticeably affected by the retardation factor $F_{(ret)}^2(\omega)$ whereas the effect on the real parts is very large, as can be seen from the differences between the solid and the dotted curves. However, it is important to realize that the damping of the scattering amplitude through $F_{(ret)}^2(\omega)$ is a physical effect only for multipoles other than electric dipole. For the electric dipole this damping (solid curve in the upper figure) is an artifact of a nonrelativistic theory which violates the requirements of dispersion theory. The corresponding correction given by $\Delta R(\omega)$ of (4.20) not only restores the

[3] Within the relativistic model considered in section 10, the asymptotics of the amplitude $R_{GR}(\omega,\theta)$ is more complicated and contains also a retardation form factor dependent on the momentum transfer q. Numerically, however, such a form factor is not very important, because it becomes only effective when the asymptotic amplitude is already small (see section 10.5).

nondamped dotted curve of the upper figure but — even more — enhances this amplitude by adding constructively those parts of the real amplitudes of the higher multipoles which have been damped away by $F^2_{(ret)}(\omega)$. As a consequence, retardation does not lead to a decrease of the real amplitude as a whole but to a change in its multipolarity. The real amplitudes of the higher multipoles vanish in the high-energy limit and the electric-dipole amplitude becomes larger by the same amount. The total resonance amplitude $R_{GR}(\omega,\theta)$ vanishes in the high-energy linit due to a cancellation of the two terms on the r.h.s. of the first line of (4.21).

Figure 4.1: *Scattering amplitudes for the giant-dipole resonances (upper figure) and isovector giant-quadrupole resonance (lower figure) of* ^{208}Pb *in the forward direction: Im* $R^{\lambda L}(\omega,\theta=0)$ *(dashed), Re* $\tilde{R}^{\lambda L}(\omega,\theta=0)$ *(dotted) and Re* $\hat{R}^{\lambda L}(\omega,\theta=0)$ *(solid).*

4.4 Gerasimov's argument

The developed model for nuclear Compton scattering in the giant-resonance region allows one to determine the parameter $\overset{\circ}{\kappa}{}^{GDR}$ which is of great importance for understanding the effective mass of the nucleon in a nucleus. As was emphasized above, the integrated strength of the unretarded $E1$ absorption cross section is determined through experimental data on photon absorption indirectly, *viz.* by virtue of an extrapolation based on the specific form of retardation corrections, Eq. (4.18), implemented in the model. In the next subsections we will see that such an extrapolation gives a result very close to that predicted by Gerasimov's argument [185] which is therefore considered here.

Gerasimov's argument [185] says that the photoabsorption cross section integrated over all multipole components is equal to the integrated unretarded dipole strength and that, therefore, retardation corrections pertinent to the $E1$ absorption of real photons are compensated in the integral by other multipoles. This argument has been criticized in a number of papers [186–190] (see also section 10) for not being valid in general. In those papers it was explicitly shown that the alleged compensation does not happen for a particle bound in a potential (without meson-exchange forces) and that relativistic corrections destroy Gerasimov's argument.

It is instructive to see where exactly a flaw is in the Gerasimov's original derivation. It is in an illegal combination of the dispersion relation (3.21) and the time-ordered perturbation theory (3.2) which give seemingly similar but nevertheless different resonance amplitudes when applied in the usual context of low energies $\omega \ll M$. The same total scattering amplitude T is represented differently in the dispersion and perturbation theory:

$$T(\omega,0) = S^{disp}(\omega,0) + R^{disp}(\omega,0) = S^{p.t.}(\omega,0) + R^{p.t.}(\omega,0) \tag{4.25}$$

(in this discussion we omit subscripts like GR or GDR and assume that S means the total seagull amplitude including the kinetic part B; for the sake of clarity, we denote the "dispersion" amplitude $\tilde{R}(\omega,0)$ by $R^{disp}(\omega,0)$ here). Considering as an example Compton scattering on a Dirac particle of mass M bound in a potential and restricting oneself to energies $\omega \ll M$, one includes all negative-energy intermediate states in Eq. (3.2) to the (effective) seagull $S^{p.t.}$, so that $R^{p.t.}$ is given by positive-energy components of the total amplitude T:

$$R^{p.t.}(\omega,0) = T_+(\omega,0). \tag{4.26}$$

When the retardation is turned off and only electric dipole transitions are included (this limit corresponds to a formal use of $\mathbf{k}=0$ but $\omega \neq 0$ in Eq. (3.2)), the corresponding unretarded $E1$ resonance scattering amplitude $\overset{\circ}{R}{}^{p.t.}_{E1}(\omega,0) = \overset{\circ}{T}{}_{+,E1}(\omega,0)$ vanishes at "high" energies $\omega \sim \omega_m$, where ω_m is an

arbitrary energy which is much smaller than M but much larger than the binding energy of the particle involved. Therefore the unretarded resonance amplitude satisfies an *unsubtracted* dispersion relation

$$\mathrm{Re}\,\overset{\circ}{R}{}^{p.t.}_{E1}(\omega,0)=\frac{1}{2\pi^2}\mathcal{P}\int_0^{\omega_m}\overset{\circ}{\sigma}_{E1}(\omega')\,\frac{\omega'^2\,d\omega'}{\omega'^2-\omega^2}, \tag{4.27}$$

which gives

$$R^{p.t.}(0,0)\equiv\overset{\circ}{R}{}^{p.t.}_{E1}(0,0)=\frac{1}{2\pi^2}\int_0^{\omega_m}\overset{\circ}{\sigma}_{E1}(\omega)\,d\omega. \tag{4.28}$$

As a simple analysis shows (see section 10.3 and Eq. (4.35) below), the positive-energy part alone of the total amplitude T does not satisfy the unsubtracted dispersion relation, because T_+ does not vanish at "high" $\omega\sim\omega_m$. Therefore, in order to have the unsubtracted dispersion relation valid for the "dispersion" resonance amplitude R^{disp},

$$\mathrm{Re}\,R^{disp}(\omega,0)=\frac{1}{2\pi^2}\mathcal{P}\int_0^{\omega_m}\sigma(\omega')\,\frac{\omega'^2\,d\omega'}{\omega'^2-\omega^2} \tag{4.29}$$

(note that the "dispersion" amplitude was *defined* through this dispersion integral) and accordingly to have the relation

$$R^{disp}(0,0)=\frac{1}{2\pi^2}\int_0^{\omega_m}\sigma(\omega)\,d\omega, \tag{4.30}$$

the amplitude R^{disp} has to include, at least partly, negative-energy contributions of T. Since the total amplitude satisfies the GGT dispersion relation, we conclude that

$$R^{disp}(\omega,0)=T(\omega,0)-T(\omega_m,0), \tag{4.31}$$

where the constant $T(\omega_m,0)$ ensures vanishing of the "dispersion" resonance amplitude at "high" energies. In this equation the amplitude $T(\omega,0)$ includes both positive and negative energy contributions and therefore $R^{disp}(\omega,0)$ does so.[4] Comparing Eqs. (4.26) and (4.31), we conclude that their difference at zero energy,

$$\begin{aligned}\Delta R^{Gerasimov}(0,0) &= R^{disp}(0,0)-R^{p.t.}(0,0)\\ &= T_-(0,0)-T(\omega_m,0)=T_-(0,0)-T_-(\omega_m,0)-T_+(\omega_m,0),\end{aligned} \tag{4.32}$$

is determined by the energy dependence of the negative-energy contribution (if any) and by the asymptotics of the positive-energy one. Just this difference prevents the integrals (4.28) and (4.30) to be identical and generally leads to a violation of Gerasimov's argument.

As an illustration of what happens, let us consider positive and negative energy parts of the amplitude $T(\omega,0)$ in the case of a free Dirac particle having a momentum $\mathbf{p}$ [95]. Such a case is easy for a treatment, and it is relevant because it shows the behavior of the scattering amplitude at energies much higher than the binding energy. It is clear from scale arguments that the "high"-energy ($\omega\sim\omega_m$) asymptotics of the scattering amplitude is determined by a coherent sum of local scattering contributions found for different points in the potential well with a constant local potential. Therefore it is sufficient to consider scattering off free particles (with a local mass $M(r)=M+V_s(r)$) and then to take a proper average. We can disregard a possible Lorentz-vector potential V_v, because it makes only local shifts of energies $E\to E+V_v(r)$ which do not change any local observables including the scattering amplitude (*cf.* [187, 195]).

[4] Since the Lorentzian parameterization of the "dispersion" amplitude R^{disp}, Eq. (4.2) at $\theta=0$, is constructed exactly in a way to ensure its vanishing at high energies, this parameterization is an approximation to Eq. (4.31). Therefore it intrinsically includes a part of the negative-energy contribution T_-.

Considering the case of forward scattering on the free Dirac particle, we have

$$\begin{aligned} T_+ &= e^2 U^+ \left[\frac{(\boldsymbol{\alpha}\cdot\boldsymbol{\epsilon}_2)\,\Lambda^+_{\mathbf{p}+\mathbf{k}}\,(\boldsymbol{\alpha}\cdot\boldsymbol{\epsilon}_1)}{E_{\mathbf{p}+\mathbf{k}} - E_{\mathbf{p}} - \omega} + \frac{(\boldsymbol{\alpha}\cdot\boldsymbol{\epsilon}_1)\,\Lambda^+_{\mathbf{p}-\mathbf{k}}\,(\boldsymbol{\alpha}\cdot\boldsymbol{\epsilon}_2)}{E_{\mathbf{p}-\mathbf{k}} - E_{\mathbf{p}} + \omega} \right] U, \\ T_- &= e^2 U^+ \left[\frac{(\boldsymbol{\alpha}\cdot\boldsymbol{\epsilon}_2)\,\Lambda^-_{\mathbf{p}+\mathbf{k}}\,(\boldsymbol{\alpha}\cdot\boldsymbol{\epsilon}_1)}{-E_{\mathbf{p}+\mathbf{k}} - E_{\mathbf{p}} - \omega} + \frac{(\boldsymbol{\alpha}\cdot\boldsymbol{\epsilon}_1)\,\Lambda^-_{\mathbf{p}-\mathbf{k}}\,(\boldsymbol{\alpha}\cdot\boldsymbol{\epsilon}_2)}{-E_{\mathbf{p}-\mathbf{k}} - E_{\mathbf{p}} + \omega} \right] U, \end{aligned} \tag{4.33}$$

where U is the Dirac spinor ($U^+U = 1$) and $\Lambda^\pm_{\mathbf{p}}$ are the projectors onto the positive and negative energy states:

$$\Lambda^\pm_{\mathbf{p}} = \frac{1}{2}\left(1 \pm \frac{\boldsymbol{\alpha}\cdot\mathbf{p} + \beta M}{E_{\mathbf{p}}}\right), \quad E_{\mathbf{p}} = \sqrt{M^2 + \mathbf{p}^2}. \tag{4.34}$$

Keeping only the spin-independent part of the amplitude and the leading relativistic correction with respect to $1/M$, we find in the semirelativistic case of $p \ll M$, $\omega \ll M$:

$$\begin{aligned} T_+ &= \frac{e^2}{M}(\boldsymbol{\epsilon}_1\cdot\boldsymbol{\epsilon}_2)\left(-\frac{\omega^2}{4M^2}\right) - \frac{e^2}{M^3}(\boldsymbol{\epsilon}_1\cdot\mathbf{p})\,(\boldsymbol{\epsilon}_2\cdot\mathbf{p}), \\ T_- &= \frac{e^2}{M}(\boldsymbol{\epsilon}_1\cdot\boldsymbol{\epsilon}_2)\left(-1 + \frac{p^2}{2M^2} + \frac{V_s}{M} + \frac{\omega^2}{4M^2}\right) + \frac{e^2}{M^3}(\boldsymbol{\epsilon}_1\cdot\mathbf{p})\,(\boldsymbol{\epsilon}_2\cdot\mathbf{p}), \end{aligned} \tag{4.35}$$

where we have explicitly restored the Lorentz-scalar potential V_s hidden in the particle mass M. Terms with ω^2 in Eq. (4.35) are quantum corrections $\sim \hbar^2$ which are specific for the spin 1/2 particle having a magnetic moment $e\hbar/2M$; they are absent in the spinless case (see section 10.3). Moreover, the ω^2 terms cancel in the sum $T = T_+ + T_-$ and therefore do not appear in the resonance amplitude (4.31). The term with the energy $V_s + p^2/(2M)$ in T_- describes a physical effect, which is a modification of the high-energy behavior of the total amplitude T, in exact accordance with the findings of Goldberger and Low [187, 195]:

$$T(\omega, 0) = -(\boldsymbol{\epsilon}_1\cdot\boldsymbol{\epsilon}_2)\left[\frac{e^2}{E_{\mathbf{p}}}\right]_{M\to M+V_s} \simeq \frac{e^2}{M}(\boldsymbol{\epsilon}_1\cdot\boldsymbol{\epsilon}_2)\left(-1 + \frac{p^2}{2M^2} + \frac{V_s}{M}\right). \tag{4.36}$$

Using Eq. (4.36) for the evaluation of $T(\omega_m, 0)$ and Eq. (4.35) for the evaluation of $T_-(0,0)$, we find that the difference (4.32) of the resonance amplitudes and therefore the difference of the GGT and TRK integrals is determined solely by the term with $(\boldsymbol{\epsilon}_1\cdot\mathbf{p})\,(\boldsymbol{\epsilon}_2\cdot\mathbf{p})$ in T_-, Eq, (4.35). Specifically,

$$\Delta R^{Gerasimov}(0,\theta) = \frac{e^2}{M^3}(\boldsymbol{\epsilon}_1\cdot\mathbf{p})\,(\boldsymbol{\epsilon}_2\cdot\mathbf{p}). \tag{4.37}$$

This perfectly agrees with a direct evaluation of the GGT integral done by Friar and Fallieros [187]. See section 10 and, in particular, Eq. (10.47) for an alternative derivation of the $(\boldsymbol{\epsilon}_1\cdot\mathbf{p})\,(\boldsymbol{\epsilon}_2\cdot\mathbf{p})$ component of T_-.

Applying these results to nucleons in the nucleus, taking a sum over Z protons, averaging over nucleon momenta $\mathbf{p}$ and subtracting the center-of-mass contribution (which is assumably unaffected by relativistic corrections), we conclude that the GGT sum rule including relativistic effects but not including meson exchange currents is given by

$$\frac{1}{2\pi^2}\int_0^{\omega_m}\sigma(\omega)\,d\omega = \frac{Ze^2}{M}\left(1 - \frac{1}{M}\left\langle\frac{p^2}{2M} + V_s\right\rangle\right) - \frac{Z^2e^2}{M_A}, \tag{4.38}$$

where $M_A \simeq AM$ is the mass of the nucleus. The relativistic correction arising in the r.h.s. of (4.38) cannot be found without further assumptions about a splitting of the mean-field potential into the

Lorentz-scalar and Lorentz-vector parts V_s and V_v, respectively. We suggest that the net result might be very similar to that contained in the last term in (4.38). That is, it might be roughly equivalent to the replacement of the free nucleon mass $M = 938.9$ MeV by the mass $\overline{M} = M_A/A \simeq 931.2$ MeV (as found for ^{12}C). If so, this would have only a tiny effect of about 0.8% on the sum rule and would give a small negative contribution -0.008 to the extracted value of κ^{GR} and $\overset{\circ}{\kappa}{}^{GDR}$.

Similarly, the difference of the GGT and TRK sum rules including relativistic effects but not including meson exchange currents is given by

$$\frac{1}{2\pi^2}\int_0^{\omega_m}\Big(\sigma(\omega)-\overset{\circ}{\sigma}_{E1}(\omega)\Big)\,d\omega=\frac{Ze^2}{M}\left\langle\frac{p^2}{3M^2}\right\rangle. \tag{4.39}$$

This equation may suggest that the value of the unretarded enhancement parameter $\overset{\circ}{\kappa}$ has to be smaller than the value of the retarded one, κ, by

$$\overset{\circ}{\kappa}-\kappa\simeq-\frac{A}{N}\langle\frac{p^2}{3M^2}\rangle\sim-0.05. \tag{4.40}$$

Here the Fermi-gas estimate of the nucleon average momentum squared was used at the standard nuclear density $\rho_0 = 0.17$ fm^{-3} and A/N was set to be 2. Such a large difference between $\overset{\circ}{\kappa}$ and κ would, of course, be important. However, within the simple potential model used it is not clear whether such an expected difference is concentrated in the giant resonance region or in the quasi-deuteron one. As we will see, the retardation model developed in the previous sections, leads to a close agreement between the enhancement parameters $\overset{\circ}{\kappa}{}^{GDR}$ and κ^{GR} relevant to the giant resonances.

4.5 The effects of enhancement and retardation in electric multipole sum rules

The general phenomenology of giant resonances gives the possibility to predict the integrated strengths of electric giant multipoles including the effects of retardation and enhancement. As each multipole component in the photoabsorption cross section may in principle consist of several Lorentzians, it is convenient for the further discussion to introduce a quantity $\overline{(F^2)^{(\lambda L)}}$ which is the squared retardation form factor at resonance energy averaged over the different multipole components:

$$\overline{(F^2)^{(\lambda L)}}=\left(\sum_\nu\frac{\overset{\circ}{\sigma}{}^{\lambda L}_\nu\Gamma^{\lambda L}_\nu}{(E^{\lambda L}_\nu)^{2L-2}}\,F^2_{(ret)}(E^{\lambda L}_\nu)\right)\left(\sum_\nu\frac{\overset{\circ}{\sigma}{}^{\lambda L}_\nu\Gamma^{\lambda L}_\nu}{(E^{\lambda L}_\nu)^{2L-2}}\right)^{-1}. \tag{4.41}$$

In case of only one Lorentzian line contributing to the multipole λL Eq. (4.41) reduces to $\overline{(F^2)^{(\lambda L)}} = F^2_{(ret)}(E^{\lambda L}_\nu)$ which will be used in the following applications. In principle it could be necessary to distinguish between isoscalar and isovector averages of the retardation form factor. As in the case of the retardation form factor itself we will neglect such differences.

From Eqs. (4.6), (4.11) and (4.18), together with Eq. (4.41) it follows that the relevant sum rule for the giant-dipole resonance (GDR) is given by

$$\begin{aligned}\int_0^\infty\sigma^{GDR}(\omega)\,d\omega &= \frac{\pi}{2}\sum_\nu\sigma^{E1}_\nu\Gamma^{E1}_\nu=\frac{\pi}{2}\sum_\nu\overset{\circ}{\sigma}{}^{E1}_\nu\Gamma^{E1}_\nu\,F^2_{(ret)}(E^{E1}_\nu)\\ &= 2\pi^2\frac{NZ}{A}\frac{e^2}{M}(1+\overset{\circ}{\kappa}{}^{GDR})\,\overline{(F^2)^{(E1)}}.\end{aligned} \tag{4.42}$$

In (4.42) $\sigma^{GDR}(\omega)$ is the giant-dipole resonance component of the experimental (retarded) photoabsorption cross section and σ^{E1}_ν, Γ^{E1}_ν and E^{E1}_ν are the Lorentz parameters of the νth component of the

giant-dipole resonance, denoting the peak cross section, the width and the peak position, respectively. The quantity $\overline{(F^2)^{(E1)}}$ on the r.h.s. of Eq. (4.42) characterizes the modification of the Thomas-Reiche-Kuhn (TRK) sum rule due to the effect of retardation.

In the same way one obtains sum rules for the electric giant-quadrupole resonances, following from Eqs. (4.7), (4.13) and (4.14):

$$\int_0^\infty \frac{\sigma_{E2}^{(is)}(\omega)}{\omega^2} d\omega = \frac{\pi}{2} \sum_\nu {}^{(is)} \frac{\sigma_\nu^{E2} \Gamma_\nu^{E2}}{(E_\nu^{\lambda L})^2} = \frac{\pi^2}{3} \frac{Z^2}{A} \frac{e^2}{M} \left\langle r^2 \right\rangle_1 \overline{(F^2)^{(E2)}} \tag{4.43}$$

$$\int_0^\infty \frac{\sigma_{E2}^{(iv)}(\omega)}{\omega^2} d\omega = \frac{\pi}{2} \sum_\nu {}^{(iv)} \frac{\sigma_\nu^{E2} \Gamma_\nu^{E2}}{(E_\nu^{\lambda L})^2} = \frac{\pi^2}{3} \frac{NZ}{A} \frac{e^2}{M} \left(\left\langle r^2 \right\rangle_1 + \mathring{\kappa}^{GDR} \left\langle r^2 \right\rangle_2^{GR} \right) \overline{(F^2)^{(E2)}}, \tag{4.44}$$

which differ from the similar relations (4.13) and (4.14) by the fact that here retardation has been taken into account explicitly by the averaged form factor appearing on the r.h.s.

From Eqs. (4.42)–(4.44) it is possible to make predictions for the properties of the three most important giant resonances, the giant-dipole resonance (GDR), the isovector (IVGQR) and isoscalar (ISGQR) giant-quadrupole resonances, if we also take into account experimental results, as far as they are known. In order to clarify the quantitative influence of mesonic currents, retardation and the relative strength of the different multipoles, it appears useful to introduce the following quantity:

$$\gamma^{\lambda L} = \left(\int_0^\infty \sigma_{\lambda L}(\omega)\, d\omega \right) \left(2\pi^2 \frac{NZ}{A} \frac{e^2}{M} \right)^{-1}, \tag{4.45}$$

which is the total multipole absorption strength given in units of the (unmodified) TRK sum rule. The cross section $\sigma_{\lambda L}(\omega)$ in Eq. (4.45) includes the effects of enhancement and retardation and may in principle be the result of an experiment. In the case, where only one Lorentzian contributes, Eq. (4.45) can be written for the three lowest electric multipoles, i.e. GDR, IVGQR and ISGQR, in the form

$$\begin{aligned}
\gamma^{E1} &= \left(1 + \mathring{\kappa}^{GDR}\right) F_{(ret)}^2(E_{E1}) \\
\gamma_{(iv)}^{E2} &= \frac{1}{6} (E_{(iv)}^{E2})^2 \left(\left\langle r^2 \right\rangle_1 + \mathring{\kappa}^{GDR} \left\langle r^2 \right\rangle_2^{GR} \right) F_{(ret)}^2(E_{(iv)}^{E2}) \\
\gamma_{(is)}^{E2} &= \frac{Z}{6N} (E_{(is)}^{E2})^2 \left\langle r^2 \right\rangle_1 F_{(ret)}^2(E_{(is)}^{E2}).
\end{aligned} \tag{4.46}$$

Replacing in Eq. (4.46) the form factor by 1 and $\mathring{\kappa}^{GDR}$ by 0 one obtains expressions for the integrated multipole cross sections $\gamma_0^{\lambda L}$ without any effects of mesonic currents (enhancement) and retardation. These quantities will be called the unmodified integrated cross sections which are theoretical quantities to be obtained from sum rules not containing enhancement and retardation effects. The inclusion of the form factor corresponds to taking into account retardation , while $\mathring{\kappa}^{GDR}$ is responsible for mesonic contributions (enhancement). For the case of ^{208}Pb these and other quantities are listed in Table 4.1. The widths and peak positions of the giant resonances are taken from the following references: GDR [198], IVGQR [25] and ISGQR [199]. The unmodified and the modified integrated cross sections are related to each other through the relation

$$\gamma^{\lambda L} = \gamma_0^{\lambda L} \times \mathrm{MEF} \times F_{(ret)}^2(E_{\lambda L}), \tag{4.47}$$

where MEF depends on λL and means a meson enhancement factor (any MEF = 1 when $\mathring{\kappa}^{GDR} = 0$). Using this equation and the definitions of $\gamma^{\lambda L}$ and $\gamma_0^{\lambda L}$, the quantities MEF may easily be obtained

from Eqs. (4.46). For the calculation of $F^2(E_{\lambda L})$ the same prescriptions have been used as in our previous paper [95]. For the one-body radius $\langle r^2 \rangle_1^{1/2}$ the charge radius as determined by electron scattering has been used, i.e. for ^{208}Pb $\langle r^2 \rangle_1^{1/2}$= 5.51 fm. For a big nucleus like ^{208}Pb this quantity should be a good measure for the square-averaged radius defined through the distribution of (pointlike) protons, *viz.* $\langle r^2 \rangle_p^{1/2}$ and, therefore, also for the isoscalar radius, but differences may be expected [95] for the isovector radius $(\langle r^2 \rangle_1 + \mathring{\kappa}^{GDR} \langle r^2 \rangle_2^{GR})/(1 + \mathring{\kappa}^{GDR})$. The two-body radius entering into this latter quantity was determined [95] through experimental and theoretical arguments and a numerical value of $\left(\langle r^2 \rangle_2^{GR}\right)^{1/2} \equiv \langle r^2 \rangle_{pn}^{1/2} = (4.3 \pm 0.8)$ fm has been obtained. The value of $\mathring{\kappa}^{GDR}$ has been chosen in such a way that the experimental integrated GDR cross section of ^{208}Pb, γ^{E1}=1.38, is reproduced. This number has been obtained through photo-neutron experiments [198] on ^{208}Pb. Exactly the same result is obtained as an average over a larger number of nuclei in the ^{208}Pb mass range, where the peak cross sections have partly been redetermined through precise Compton scattering experiments. This will be described in section 4.6. The importance of the content of Table 4.1 lies in the fact, that a prediction for the "experimental" enhancement, i.e. the combination of retardation and enhancement is obtained for the IVGQR which is an unknown quantity otherwise. The mesonic enhancement factor of MEF = 1.28 calculated from $\mathring{\kappa}^{GDR}$ and the radii $\langle r^2 \rangle_1$ and $\langle r^2 \rangle_2^{GR}$ combines with the retardation factor $F^2_{(ret)}(E^{E2}_{(iv)}) = 0.88$ to give an "experimental" enhancement of MEF $\times F^2_{(ret)}(E^{E2}_{(iv)}) = 1.13$. This result of 13% is the only information we have on the "experimental" enhancement because experiments are by far not precise enough to measure this quantity. Details will be given in section 4.7.

Table 4.1: *Giant multipoles in ^{208}Pb: Peak energy $E_{\lambda L}$, width Γ, unmodified integrated cross section $\gamma_0^{\lambda L}$ in units of the (unmodified) TRK sum rule, retardation factor $F^2(E_{\lambda L})$, mesonic enhancement factor MEF and experimental or modified integrated cross section $\gamma^{\lambda L}$.*

Parameter	GDR	IVGQR	ISGQR
$E_{\lambda L}$	13.42 MeV	22.5 MeV	10.6 MeV
Γ	4.1 MeV	9.0 MeV	3.0 MeV
$\gamma_0^{\lambda L}$	1	0.066	0.007
$F^2_{(ret)}(E_{\lambda L})$	0.945	0.88	0.98
MEF	1.46	1.28	1
$\gamma^{\lambda L}$	1.38	0.074	0.007

It is interesting to note that the numbers contained in Table 4.1 are in line with the predictions of Gerasimov's argument. The sum of the integrated strengths of the three multipoles is $1 + \kappa^{GR} = 1.38 + 0.074 + 0.007 = 1.46$ whereas the corresponding non-retarded dipole strength is $1 + \mathring{\kappa}^{GDR} = 1.46$ in units of the unmodified TRK sum rule. This certainly is an important confirmation of Gerasimov's argument since the two numbers compared here are (almost) completely independent of each other.

4.6 Scaling of giant resonance parameters via Compton scattering

The quantity we wish to determine is the unretarded enhancement constant for the giant-dipole resonance, *viz.* $\mathring{\kappa}^{GDR}$, which is the *universal parameter* of giant resonance enhancement phenomena. In principle this quantity can be determined from photoabsorption experiments. In a first place these are photoneutron experiments [150, 151, 200] for heavy nuclei and total photoabsorption experiments [84] for light nuclei. The reason for this difference in methods is that for heavy nuclei the photoneutron channel largely dominates the photoproton channel and total photoabsorption measurements are inaccurate because of the $e^+ e^-$ pair production cross section which is much larger than the nuclear

photoabsorption cross section. On the other hand, at low mass numbers the photoproton and the photoneutron channels are about equal in strength. Since low-energy protons are difficult to detect, especially for solid targets the total photoabsorption cross section measurements are preferable.

In case of photoneutron experiments there may be one or more neutrons in the final state per photoabsorption process. Furthermore, the neutrons may be emitted after a fission process. This means that photoneutron experiments require a precise counting technique for neutrons and a method to determine the neutron multiplicity. These experiments, therefore, gave an excellent overview of the properties of giant resonances [150, 151, 200], but suffer from systematic uncertainties because of the fact that the intensity of the photon beam and the detection efficiency of the neutron detector have to be known on an absolute scale. As a consequence, the integrated cross sections measured in different laboratories showed large deviations from each other [150, 151]. On the other hand, the relative cross sections measured in one experiment for different photon energies, i.e. the shape of the cross-section curve, turned out to be much more reliable. Therefore, general scaling factors of the cross sections were required in order to improve on the integrated cross sections.

The amplitude for forward-angle Compton scattering is related to the total photoabsorption cross section via optical theorem and dispersion relation. Therefore, the total photoabsorption cross section may also be determined via Compton scattering provided the angular distribution of Compton scattered photons is well enough known so that an extrapolation to zero angle becomes possible and provided there is enough information to carry out the dispersion integral. Given these premises, Compton scattering provides a rather precise information because there are no principal difficulties in arriving at absolute numbers. The reason for this is that the projectiles and the reaction products are photons of (almost) the same energy. This makes it possible to measure the rates of incident photons and scattered photons with the same detector and thus to avoid the determination of detection efficiencies on an absolute scale. A further advantage of Compton scattering is that it is possible to very largely reduce the effects of $e^+ e^-$ pair production. This latter process enters into the Compton scattering amplitude via Delbrück [5] scattering. Since Delbrück scattering takes place in the Coulomb field surrounding the nucleus this process is much more peaked to the forward direction than nuclear Compton scattering and, therefore, can be avoided except for small scattering angles or photon energies below 10 MeV where sizable contributions of Delbrück scattering are also observed at large angles [5]. As a result the determination of the Compton differential cross section only depends on the relative rates of incoming and scattered photons and makes this method a favorable tool to scale the photon-neutron data. One experiment of this type has been carried for ^{209}Bi [63], being an immediate neighbor of ^{208}Pb. The advantage of investigating ^{209}Bi instead of ^{208}Pb is, that because of the much higher level density the cross section is a smooth function of energy whereas that of ^{208}Pb is rather fragmented [64]. Furthermore, information on magnetic moments to compare with when studying the Fujita-Hirata relation (see section 7) is most clear-cut for ^{209}Bi which has one valence nucleon out side a closed core. The enhancement constant obtained in this way was rather large, amounting to $\gamma^{E1} = 1.46 \pm 0.05$. Later on it was realized that in spite of the smoothness of the cross section the exact value for $\overset{\circ}{\kappa}^{GDR}$ depends on very fine details of the shape of the measured cross sections [65, 66, 201] so that from one single experiment alone the desired systematic precision can hardly be achieved. This point has been investigated by Fuhrberg et al. [66], showing that in spite of precise scaling through a Compton scattering experiment minor differences in available photoneutron cross sections lead to sizable differences in γ^{E1}. Details of this investigation are shown in Figs. 4.2–4.4. The results of the two different Compton scattering experiments [63, 201] are shown in Fig. 4.2. The data points at 9.0, 11.4 and 17.74 MeV depicted by closed circles have been measured using photons from nuclear reactions [63], the other data points by tagged photons [201]. It is interesting to note that the data from the two experiments coincide on a percent level of pecision at the high-energy side of the spectrum at 17.4 Mev and that there are no data from tagged photons below 12.5 MeV. There are two different photoabsorption experiments shown in Figs. 4.3 and 4.4. The photoabsorption data

of Fig. 4.3 are in agreement with the solid curve after applying a scaling factor of 1.35 whereas the data of Fig. 4.4 are partly in favour of the solid curve and partly in favour of the dashed curve after multiplying with a scaling factor of 1.09. As a whole the solid curve appears to be more justified than the dashed curve but on the other hand the difference — at least at a first sight — appears to be not dramatic. But nevertheless, when drawing conclusions with repsect to the retarded enhancement constant $\kappa^{GDR} = \gamma^{E1} - 1$ the difference between curves become essential. For the solid curve we get $\kappa^{GDR} = 0.46 \pm 0.05$ whereas for the dashed curve $\kappa^{GDR} = 0.29 \pm 0.05$. Summarizing we can say that two different Compton scattering experiments lead to the same large scaling factors for the available photoabsrption data. In spite of this, a slight difference in the shapes of the photoabsorption cross sections on the low-energy sides leads to a sizable (3σ) difference in κ^{GDR}. In view of the rather precise Compton cross sections shown in Fig. 4.2 at 9.0. and 11.4 MeV the larger of the two κ^{GDR} results appears more likely to be true.

Figure 4.2: *Differential cross sections for Compton scattering by ^{209}Bi. Scattering angle θ = 135°. Data points at 9.0, 11.4 and 17.74 MeV are measured by [63]. Other data points are measured by [201]. Solid curve: calculated using the GDR parameters of [63]. Dashed curve: calculated using the GDR parameters of [201].*

Figure 4.3: *Photoabsorption cross sections for ^{209}Bi measured by [202] multiplied by a scaling factor of 1.35. Solid curve: calculated using the GDR parameters of [63]. Dashed curve: calculated using the GDR parameters of [201].*

Figure 4.4: *Photoabsorption cross sections for ^{209}Bi measured by [203] multiplied by a scaling factor of 1.09. Solid curve: calculated using the GDR parameters of [63]. Dashed curve: calculated using the GDR parameters of [201].*

The conclusion from the foregoing is, that it has advantages to rely on averages over a larger number of nuclei rather than on the result obtained for one single nucleus. On the theoretical side it was realized [95] that instead of the *experimental* quantity $(\gamma^{E1} - 1) = \kappa^{GDR}$ the *unretarded* quantity $\overset{\circ}{\kappa}{}^{GDR}$ is of interest for a comparison with models, as outlined in the previous section.

An extensive investigation of Compton scattering in the giant resonance region in addition to total photoabsortion measurements has been summarized in our previous paper [95]. The result of this investigation is contained in Table 4.2. For nuclei in the spherical region around ^{208}Pb, i.e. for mass numbers A = 197–209, the average integrated cross section amounted to $\gamma^{E1} = 1.38 \pm 0.05$ leading to

$$\overset{\circ}{\kappa}{}^{GDR} = 0.46 \pm 0.05 \tag{4.48}$$

as a best value for the *unretarded* GDR enhancement constant in the ^{208}Pb range [95]. By change this number coincides with the one given in our original experiment [63] as documented in Figs. 4.2–4.4. For the neighbouring mass regions of deformed nuclei the quantities γ^{E1} proved to be smaller than for the spherical region as also shown in Table 4.2. This observation is rather interesting and will be interpreted in connection with the effective mass M^* of the Fermi liquid theory (*cf.* section 7) quoted in column 4 of Table 4.2.

In case of the total photoabsorption measurements which are the favorable method at low and intermediate mass numbers there are also two major difficulties and, thus, require a rescaling through Compton scattering. The first is that the measurement of the total photoabsorption cross section can only be done as a measurement of the target-in target-out difference. The second is that even for light nuclei $e^+ e^-$ pair production is the dominating process so that this process has to be calculated

Table 4.2: *Average experimental (retarded) integrated cross section γ^{E1} in units of the (unmodified) TRK value, average unretarded enhancement constant $\overset{\circ}{\kappa}^{GDR}$ and effective mass M^* with $M^*/M = 1/(1 + 3\overset{\circ}{\kappa}^{GDR}/4)$ following from Fermi liquid theory (cf. section 7, Eq. (7.30)) for three different nuclear mass ranges.*

A	γ^{E1}	$\overset{\circ}{\kappa}^{GDR}$	M^*/M
181	1.27	0.34	0.80
197–209	1.38	0.46	0.75
232–238	1.27	0.34	0.80

precisely and subtracted from the data. The precise calculation of the $e^+ e^-$ pair production cross section is by far not without problems because of quantum-electrodynamic corrections entering into the calculation. Therefore, also in this case a scaling via Compton scattering leads to improvements on the photoabsorption cross section in general and to tests on the structure of the photoabsorption cross section [42, 48].

4.7 The isovector giant-quadrupole resonance and higher multipoles

Giant multipole resonances other than the giant-dipole resonance are an important subject of photonuclear physics. In the previous sections we have mainly covered the theoretical aspects of these investigations. An overview over the status of research both experimental and theoretical up to the late 1970s is given in a conference proceedings edited by Bertrand [204].

The isoscalar and isovector magnetic-dipole resonances have been identified below particle emission threshold as isolated levels or sequences of isolated levels [205, 206]. The favorable tool for these investigations is nuclear resonance fluorescence.

The isoscalar electric giant-quadrupole resonance has been discovered [207] by electron scattering experiments at energies below the peak of the giant-dipole resonance and investigated through different nuclear reactions [208]. Because of this location at the low energy side of the giant dipole resonance and because of the small strength located in this resonance is not possible to observe the isoscalar quadrupole excitation through Compton scattering. Most of the information regarding the location of the corresponding isovector excitation has also been obtained from inelastic electron scattering experiments [209], which show a concentration of quadrupole strength at an excitation energy of $\sim 130 \times A^{-(1/3)}$ MeV. However, the interpretation of the results in terms of excitation strength remains uncertain. Other methods of determining location and strength mainly rely on the interference of the quadrupole resonance with the predominant electric dipole resonance, leading to for-aft asymmetries. Among these are photon-nucleon reactions, the radiative capture of nucleons and Compton scattering experiments.

The IVGQR in ^{208}Pb has been investigated via Compton scattering of unpolarized [25] and polarized [33] photons where in the latter case linear polarization has been produced through off-axis tagging. These experiments confirm that at least one isovector quadrupole sum rule is exhausted by these resonances though the experimental errors forbid precise conclusions on the overfulfilment of the sum rule. One example of Compton scattering experiments identifying the IVGQR is discussed in Fig. 4.5. The quadrupole strength shows up as an interference of $E2$ and $E1$ resonance amplitudes. A further property of the IVGQR of ^{208}Pb which only can be seen through Compton scattering at high energy-resolution by using photons from nuclear reactions and Ge(Li) detectors [64] is its partial fragmentation. This experiment [64] showed that there is E2 strength located at about 17.6 MeV.

Figure 4.5: *Cross-section ration $\sigma(\theta = 150^\circ)/\sigma(\theta = 60^\circ)$ for Compton scattering of unpolarized photons by ^{208}Pb [25]. Solid line: Calculated including the IVGQR. Dashed line: Calculated not including the IVGQR. The IVGQR shows up as interference of the $E2$ amplitude with the predominant $E1$ amplitude from the GDR.*

Studies of (n, γ) reactions have provided valuable data on the IVGQR in nuclei ranging from ^{40}Ca to ^{208}Pb [210–213]. However, neutron capture experiments are limited by the difficulty of producing a sufficiently intense flux of high-energy monochromatic neutrons.

Data on the isovector quadrupole resonance of ^{40}Ca have been obtained via the photo-neutron reaction (γ, n) and the (n, γ) neutron capture reaction [214]. Data analysis in terms of models estimate the isovector quadrupole resonance to be at an energy of 31.0 MeV with a width of 16.0 MeV, and exhausting most of the energy weighted IVGQR sum rule.

A study of Compton scattering by ^{12}C and ^{40}Ca carried out by Wright et al. [18, 19] did not lead to the identification of localized IVGQR strength.

4.8 The electromagnetic polarizabilities of the nucleus

After first estimates of the electric polarizabilities of nuclei due to Migdal [215] (see also [216]), the electromagnetic polarizabilities of the nucleus were addressed by Ericson and Hüfner [175] for the case of no enhancement of the giant multipole strength and by Friar [69] on a more general ground. In this section we want to use our formalism to include the effects of enhancement and to give a transparent formulation of the retardation effects. For this purpose we start from the amplitude for Compton scattering by giant resonances, *viz.*

$$T_{GR}(\omega, \theta) = B(\omega, \theta) + S_{GR}(\omega, \theta) + R_{GR}(\omega, \theta) \tag{4.49}$$

where $B(\omega, \theta)$ is the kinetic seagull amplitude, $S_{GR}(\omega, \theta)$ is the GR part of the mesonic seagull amplitude, which does not contain any energy dependence except of the form factor, as introduced before, and $R_{GR}(\omega, \theta)$ is the resonance amplitude. The electromagnetic polarizabilities are obtained by expanding the scattering amplitude up to the quadratic order of ω, i.e. at small ω the amplitude T_{GR} can be written as

$$T_{GR}(\omega, \theta) = -\frac{Z^2 e^2}{AM}\, \boldsymbol{\epsilon}_1 \cdot \boldsymbol{\epsilon}_2 + \omega^2 \left(\bar{\alpha}_{GR}\, \boldsymbol{\epsilon}_1 \cdot \boldsymbol{\epsilon}_2 + \bar{\beta}_{GR}\, \mathbf{s}_1 \cdot \mathbf{s}_2 \right). \tag{4.50}$$

This expansion is first given for the forward direction, making use of the optical theorem and the once-subtracted dispersion relation (*cf.* Eq. (3.21)). One obtains a form valid for ω much below giant resonance energies:

$$\mathrm{Re}T_{GR}(\omega, 0) = -\frac{Z^2 e^2}{AM} + \frac{\omega^2}{2\pi^2} \int_0^\infty \frac{\sigma^{GR}(\omega')}{\omega'^2} d\omega' + \mathcal{O}(\omega^4). \tag{4.51}$$

From (4.51) we read off the Baldin–Lapidus sum rule [217] for the sum of electric and magnetic polarizabilities due to giant resonance excitations in the form

$$\bar{\alpha}_{GR} + \bar{\beta}_{GR} = \frac{1}{2\pi^2} \int_0^\infty \frac{\sigma^{GR}(\omega)}{\omega^2} d\omega = \frac{1}{4\pi} \sum_{\lambda L,\, \nu} \frac{\sigma_\nu^{\lambda L} \Gamma_\nu^{\lambda L}}{(E_\nu^{\lambda L})^2}. \tag{4.52}$$

In order to arrive at the electromagnetic polarizabilities of the nucleus we have to take into account that in addition to giant resonances the quasideuteron and nucleon-internal degrees of freedom lead

to contributions. Applying the Baldin–Lapidus sum rule to all three contributions we arrive at the relation

$$\bar{\alpha}_{tot} + \bar{\beta}_{tot} = (\bar{\alpha}_{GR} + \bar{\beta}_{GR}) + (\bar{\alpha}_{QD} + \bar{\beta}_{QD}) + A(\tilde{\alpha}_N + \tilde{\beta}_N), \tag{4.53}$$

where $\bar{\alpha}_{QD}$ and $\bar{\beta}_{QD}$ are the QD electric and magnetic polarizabilities, while again $\tilde{\alpha}_N$ and $\tilde{\beta}_N$ are the in-medium electromagnetic polarizabilities of the nucleon. A rough estimate shows that the main contribution to electromagnetic polarizabilities of the nucleus stems from the giant resonances with the QD degree of freedom contributing additional 3 per cent and the nucleon internal excitations giving 0.3 per cent. Therefore, our present discussion can be restricted to the GR degree of freedom.

The Baldin–Lapidus sum rule cannot simply be separated into an electric part and a magnetic part. In order to nevertheless obtain explicit expressions for $\bar{\alpha}_{GR}$ and $\bar{\beta}_{GR}$ one can either make use of dispersion sum rules written separately for the electric and magnetic polarizabilities (see [99, 226] and section 8) or make use of second-order perturbation theory. The latter procedure is as follows: We expand the representation (3.56) of the giant resonance amplitude R_{GR} with respect to ω, as well as the corresponding seagull amplitude $B + S_{GR}$ and take into account the fact that the resonant E2 contribution proportional to ω^2 cancels explicitly with the part coming from the seagull amplitude. As a result we get

$$\bar{\alpha}_{GR} = \alpha_0 + \Delta\alpha\ , \quad \bar{\beta}_{GR} = \beta_{para} + \beta_{dia}, \tag{4.54}$$

where

$$\alpha_0 = \frac{2}{3}\sum_{n\neq 0}\frac{|\,\langle 0|\mathbf{D}|n\rangle\,|^2}{E_n - E_0}\ , \quad \beta_{para} = \frac{2}{3}\sum_{n\neq 0}\frac{|\,\langle 0|\mathbf{M}|n\rangle\,|^2}{E_n - E_0}, \tag{4.55}$$

are the so-called "proper" electric and paramagnetic polarizabilities, respectively. The sums in Eq. (4.55) are taken over all intermediate states corresponding to an internal excitation and $\mathbf{M}$ is the magnetic dipole operator. The quantity $\Delta\alpha$ is the retardation correction of the electric polarizability and β_{dia} the diamagnetic polarizability. For giant resonances these quantities are given by

$$\Delta\alpha = \frac{1}{3}\frac{Z^2e^2}{AM}\left\langle r^2\right\rangle_1\ , \quad \beta_{dia} = -\frac{1}{6}\frac{Ze^2}{M}\left(\left\langle r^2\right\rangle_1 + \mathring{\kappa}^{GDR}\frac{N}{A}\left\langle r^2\right\rangle_2^{GR}\right) - \frac{\langle\mathbf{D}^2\rangle}{2AM}\,. \tag{4.56}$$

The contribution α_0 is obtained from the part of Θ_ν^{E1} in Eq. (3.57) containing the electric dipole moment operator. The retardation correction $\Delta\alpha$ has two contributions, one from the expansion of the form factor in the seagull amplitude and the other from the expansion of the difference

$$|\langle\nu|\,Q_{E1}\,|0\rangle|^2 - \left|\langle\nu|\,\mathring{Q}_{E1}\,|0\rangle\right|^2$$

in Eq. (3.57). Similarly, β_{para} corresponds to the contribution of Θ_ν^{M1} in the resonance amplitude, Eq. (3.56). The first term in Eq. (4.56) for β_{dia} as in the case of $\Delta\alpha$ is due to the expansion of the form factors in the seagull amplitude, but in contrast to the expression for $\Delta\alpha$ the mesonic contribution (proportional to $\mathring{\kappa}^{GDR}$) appears explicitly. The second part of β_{dia} is a recoil correction, which is small as it contains an additional factor $1/A$ in comparison to the first term. In our review we do not consider any recoil corrections, but write this term only for the sake of completeness. The two quantities $\Delta\alpha$ and β_{dia} are common ingredients to all quantum mechanical treatments of the electromagnetic polarizabilities, either of atoms [218] or of nuclei [69, 175] and hadrons [99, 103, 197]. An extensive investigation of the two quantities in the framework of a nonrelativistic theory is given by L'vov and Schumacher [103]. According to all these investigations the quantity $\Delta\alpha$ has its origin in the form factor squared of the charged composite object at the momentum of the incoming or outgoing photon. The formula (4.56) for $\Delta\alpha$, first established by Petrun'kin (see in [99, 197]), is independent of the model used to describe the hadron or nucleus and also valid in the relativistic case, what was recently re-emphasized in [219].

A discussion of the electromagnetic polarizabilities of the nucleus including the effects of enhancement has been given in [95] in the framework of the phenomenology outlined in section 3. These polarizabilities have two contributions, one from the expansion of the form factors in the seagull amplitude $B + S_{GR}$, the other from the resonance amplitude R_{GR}. Using Eqs. (3.70), (3.71) and (4.16) we arrive at the multipole decompositions

$$
\begin{aligned}
(B+S_{GR})^{(E1)} &= -\frac{Ze^2}{M}\left[\left(1+\frac{N}{A}\mathring{\kappa}^{GDR}\right)-\frac{\omega^2}{3}\left(\left\langle r^2\right\rangle_1+\frac{N}{A}\mathring{\kappa}^{GDR}\left\langle r^2\right\rangle_2^{GR}\right)\right]g^{E1}(\theta)\\
(B+S_{GR})^{(M1)} &= -\frac{Ze^2}{M}\frac{\omega^2}{6}\left(\left\langle r^2\right\rangle_1+\frac{N}{A}\mathring{\kappa}^{GDR}\left\langle r^2\right\rangle_2^{GR}\right)g^{M1}(\theta)\\
(B+S_{GR})^{(E2)} &= -\frac{Ze^2}{M}\frac{\omega^2}{6}\left(\left\langle r^2\right\rangle_1+\frac{N}{A}\mathring{\kappa}^{GDR}\left\langle r^2\right\rangle_2^{GR}\right)g^{E2}(\theta)\\
\hat{R}_{GR} &= \frac{NZ}{A}\frac{e^2}{M}\left[\left(1+\mathring{\kappa}^{GDR}\right)-\frac{\omega^2}{3}\left(\left\langle r^2\right\rangle_1+\mathring{\kappa}^{GDR}\left\langle r^2\right\rangle_2^{GR}\right)\right]g^{E1}(\theta)\\
&\quad+\frac{\omega^2}{4\pi}\sum_{E1,M1,E2,\,\nu}\frac{\sigma_\nu^{\lambda L}}{F_{(ret)}^2(E_\nu^{\lambda L})}\frac{\Gamma_\nu^{\lambda L}}{(E_\nu^{\lambda L})^2}g^{\lambda L}(\theta),
\end{aligned}
\tag{4.57}
$$

where the sum for the resonance amplitude is written with taking into account only the first three multipoles ($E1$, $M1$ and $E2$), as in the order ω^2 higher multipoles do not contribute. Here we used the retarded form $\hat{R}_{GR}$ of the resonance amplitude, as it is most appropriate at energies below the resonance region. In addition, we took into account the fact that different retardation form factors should appear for the one-nucleon and the two-nucleon contribution. Inserting Eq. (4.57) into the definitions, Eq. (4.55), we find

$$
\begin{aligned}
\alpha_0 &= \frac{1}{2\pi^2}\int_0^\infty\frac{\mathring{\sigma}^{E1}(\omega)}{\omega^2}d\omega=\frac{1}{4\pi}\sum_\nu\frac{\sigma_\nu^{E1}}{F_{(ret)}^2(E_\nu^{E1})}\frac{\Gamma_\nu^{E1}}{(E_\nu^{E1})^2}\\
\beta_{para} &= \frac{1}{2\pi^2}\int_0^\infty\frac{\mathring{\sigma}^{M1}(\omega)}{\omega^2}d\omega=\frac{1}{4\pi}\sum_\nu\frac{\sigma_\nu^{M1}}{F_{(ret)}^2(E_\nu^{M1})}\frac{\Gamma_\nu^{M1}}{(E_\nu^{M1})^2}.
\end{aligned}
\tag{4.58}
$$

In the same way we may also obtain expressions for $\Delta\alpha$ and β_{para} from Eq. (4.57), together with (4.56). The quantity $\Delta\alpha$ has two terms, $\Delta\alpha_s$ and $\Delta\alpha_r$ stemming from the seagull amplitude $(B+S_{GR})^{(E1)}$ and from the $E1$ part of the resonance amplitude $\hat{R}_{GR}$, respectively, whereas β_{para} has only one term coming from $(B+S_{GR})^{(M1)}$. These terms are

$$
\begin{aligned}
\Delta\alpha_s &= \frac{1}{3}\frac{Ze^2}{M}\left(\left\langle r^2\right\rangle_1+\frac{N}{A}\mathring{\kappa}^{GDR}\left\langle r^2\right\rangle_2^{GR}\right)\\
\Delta\alpha_r &= -\frac{1}{3}\frac{e^2}{M}\frac{NZ}{A}\left(\left\langle r^2\right\rangle_1+\mathring{\kappa}^{GDR}\left\langle r^2\right\rangle_2^{GR}\right)\\
\Delta\alpha &= \Delta\alpha_s+\Delta\alpha_r=\frac{1}{3}\frac{Z^2e^2}{AM}\left\langle r^2\right\rangle_1\\
\beta_{dia} &= -\frac{1}{6}\frac{Ze^2}{M}\left(\left\langle r^2\right\rangle_1+\frac{N}{A}\mathring{\kappa}^{GDR}\left\langle r^2\right\rangle_2^{GR}\right).
\end{aligned}
\tag{4.59}
$$

It is seen that a sizable dependence of the diamagnetic polarizability β_{dia} on the enhancement constant $\mathring{\kappa}^{GDR}$ exists.

The main assumption in putting together these expressions is the following: In Eq. (4.57) the retarded resonance amplitude $\hat{R}_{GR}$ has been used. Clearly, the influence of the function ΔR introduced in section 4.4 should be small in the low-energy expansion. Nevertheless, it may be useful to understand

what contributions are coming from this correction. The angular dependence in Eq. (4.20) shows that the function ΔR only influences the electric polarizability, but not the magnetic one. Substituting the definitions of $\tilde{R}_{GR}$ and R_{GR} in Eq. (4.20) and extracting the term proportional to ω^2 we obtain an expression for the ΔR-contribution $\alpha(\Delta R)$ to the electric polarizability:

$$\alpha(\Delta R) = \frac{1}{4\pi} \sum_{\lambda L,\,\nu} \frac{\sigma_\nu^{\lambda L} \Gamma_\nu^{\lambda L}}{(E_\nu^{\lambda L})^2} - \frac{1}{4\pi} \sum_{E1, M1, E2,\,\nu} \frac{\mathring{\sigma}_\nu^{\lambda L} \Gamma_\nu^{\lambda L}}{(E_\nu^{\lambda L})^2} + \frac{1}{3} \frac{NZ}{A} \frac{e^2}{M} \left(\left\langle r^2 \right\rangle_1 + \mathring{\kappa}^{GDR} \left\langle r^2 \right\rangle_2^{GR} \right). \quad (4.60)$$

Making use of the relation (4.18) and noting again that

$$F^2_{(ret)}(\omega) \approx 1 - \frac{1}{3} \frac{\left\langle r^2 \right\rangle_1 + \mathring{\kappa}^{GDR} \left\langle r^2 \right\rangle_2^{GR}}{1 + \mathring{\kappa}^{GDR}} \omega^2,$$

we find a simple expression for $\alpha(\Delta R)$:

$$\alpha(\Delta R) = \frac{1}{4\pi} \sum_{M2, E3, \ldots} \frac{\mathring{\sigma}_\nu^{\lambda L} \Gamma_\nu^{\lambda L}}{(E_\nu^{\lambda L})^2}. \quad (4.61)$$

The most important property of Eq. (4.61) is the fact that only multipoles higher than the electric quadrupole contribute to the correction $\alpha(\Delta R)$. This statement can independently be confirmed via the Baldin–Lapidus sum rule, Eq. (4.52). Subtracting all polarizability contributions, Eqs. (4.58) and (4.59), from this relation, one easily comes to the same conclusion. Evidently, $\alpha(\Delta R)$ is highly suppressed. Similar effects will be discussed on the basis of fixed-t dispersion relations in section 8.

Table 4.3: *Electromagnetic polarizabilities of the nucleus ^{208}Pb and nucleon in units of $10^{-4} fm^3$. The nuclear polarizabilities are devided by the number A of nucleons in the nucleus. The nucleon polarizabilities are proton-neutron averages $\bar{\alpha}_N = \frac{1}{2}(\bar{\alpha}_p + \bar{\alpha}_n)$ and $\bar{\beta}_N = \frac{1}{2}(\bar{\beta}_p + \bar{\beta}_n)$ of the free nucleons.*

α_0/A	1202
$\Delta\alpha_s$/A	68
$\Delta\alpha_r$/A	-54
$\bar{\alpha}_{GR}$/A	1216
β_{dia}/A	-36
$\bar{\alpha}_N$	11.3 ± 1.5
$\bar{\beta}_N$	3.7 ∓ 1.5

For the nucleus ^{208}Pb numerical values for the electromagnetic polarizabilities are obtained using the parameters given in section 4.5. The results are given in Table 4.3 together with the proton-neutron averages of the free-nucleon, the latter taken from section 5.3. For the magnetic polarizability of the nucleus we only quote the diamagnetic component because the paramagnetic component is expected to be considerably smaller. A fraction of 85% of the nuclear diamagnetism is due to kinetic currents and the remaining 15% due to exchange currents.

5 Compton scattering in the quasideuteron range

In framework of our concept to describe nuclear Compton scattering in terms of three different degrees of freedom, *viz.* giant-resonance (GR), quasi-deuteron (QD) and nucleon-internal (N), we now consider the second of these contributions, i.e. the amplitude $T_{QD}(\omega,\theta)$. We may write the total nuclear scattering amplitude in the from

$$T_{tot}(\omega,\theta) = T_{GR}(\omega,\theta) + T_{QD}(\omega,\theta) + T_N(\omega,\theta) = T_A(\omega,\theta) + T_N(\omega,\theta) \tag{5.1}$$

where $T_A(\omega,\theta)$ collects the two amplitudes, $T_{GR}(\omega,\theta)$ and $T_{QD}(\omega,\theta)$, which are related to the external degrees of freedom of the nucleon. In the QD energy region we observe a superposition of contributions from all three degrees of freedom with the QD part being the least important one. The reason for this surprising property may be understood as follows. In the QD range the scattering amplitude $T_{tot}(\omega,\theta)$ consists of contributions from the imaginary part of $T_{QD}(\omega,\theta)$ and the superposition of the real parts of all three amplitudes. The real part of the QD amplitude is suppressed in middle of the QD range because of its sign change at the peak of the QD cross section. As a consequence the resulting scattering amplitude is mainly due to the high-energy tail of the GR amplitude, $T_{GR}(\omega,\theta)$, and the low-energy tail of the amplitude $T_N(\omega,\theta)$ which is related to the in-medium electromagnetic polarizabilities $\tilde{\alpha}_N$ and $\tilde{\beta}_N$ of the nucleons. The most interesting topic of Compton scattering experiments in the QD range is the experimental determination of the in-medium polarizabilities and their comparison with the values for the free nucleon.

In spite of the small size of the QD contribution to the Compton differential cross sections we have to discuss this amplitude with care in order to take it into account with the highest possible precision. This will be done in the following.

5.1 The quasideuteron amplitudes

The quasideuteron amplitude has two parts, *viz.*

$$T_{QD}(\omega,\theta) = S_{QD}(\omega,\theta) + R_{QD}(\omega,\theta). \tag{5.2}$$

The seagull amplitude $S_{QD}(\omega,\theta)$ has a static part $\tilde{S}_{QD}(\omega,\theta)$ which is energy-independent in the forward direction and a dynamic, energy-dependent part which can be parameterized in terms of mesonic corrections $\delta\alpha$ and $\delta\beta$ to the in-medium electromagnetic polarizabilities $\tilde{\alpha}_N$ and $\tilde{\beta}_N$ of the nucleon. By definition the quantities $\tilde{\alpha}_N$ and $\tilde{\beta}_N$ are one-body effects which are related to the nucleon internal coordinates only, whereas the quantities $\delta\alpha$ and $\delta\beta$ are related to two-body effects. The important field of our current research concerning two-body effects will be discussed in section 9. The static part of the mesonic seagull amplitude is of the same structure as the corresponding GR part. This is

$$\tilde{S}_{QD}(\omega,\theta) = -\frac{NZ}{A}\frac{e^2}{M}\kappa^{QD} g^{E1}(\theta) F_2(q) \tag{5.3}$$

where again κ^{QD} is the quasideuteron part of the enhancement constant $\kappa = \kappa^{GR} + \kappa^{QD}$ and $F_2(q)$ the two-body form factor. In principle the exact form factor $F_2^{(QD)}(q)$ for the quasideuteron contribution to the static mesonic seagull-amplitude differs from the (total) two-body form factor $F_2(q)$ introduced in section 3.2 and the following relation holds: $\kappa^{GR}F_2^{(GR)}(q) + \kappa^{QD}F_2^{(QD)}(q) = \kappa F_2(q)$, where the function $F_2^{(GR)}(q)$ appears in the GR part of the seagull amplitude as discussed in sections 4 and 9 and in appendix B. However, the difference between $F_2^{(QD)}(q)$ and $F_2(q)$ is much smaller than between $F_2^{(GR)}(q)$ and $F_2(q)$ and may be neglected, as will be shown in section 9. In the following

discussion we will not distinguish between $F_2^{(QD)}(q)$ and $F_2(q)$. The meson exchange corrections of the electromagnetic polarizabilities enter into the scattering amplitude in the form

$$S_{QD}(\omega,\theta) - \tilde{S}_{QD}(\omega,\theta) = \omega^2\, A\, (\delta\alpha\, \boldsymbol{\epsilon}_1 \cdot \boldsymbol{\epsilon}_2 + \delta\beta\, \mathbf{s}_1 \cdot \mathbf{s}_2)\, F_2(q) + \mathcal{O}(\omega^4). \tag{5.4}$$

Recently it was found [193] that the form factor $F_2(q)$ in Eq. (5.4) is not identical with the two-body form factor of Eq. (5.3). This difference, which is not negligible in the case of relatively light nuclei, is due to the complicated structure of the two-nucleon correlation function and will be discussed in section 9 within a modified Fermi gas model, together with the polarizability modifications $\delta\alpha$ and $\delta\beta$. For convenience all such energy dependences of the (total) mesonic seagull amplitude $S(\omega,\theta)$ is put into $S_{QD}(\omega,\theta)$, so that $S_{GR}(\omega,\theta)$ only consists of the term proportional to κ^{GR}. This is possible, because any model investigation within the Fermi gas model may only address the total mesonic seagull amplitude $S(\omega,\theta)$ with no strict possibility to separate it into the GR and QD parts. The reason for this is that the Fermi gas model does not take into account the specific differences between GR and QD excitations. Therefore, this separation into GR and QD parts can only be understood in the discussion of properties of the two resonance amplitudes $R_{GR}(\omega,\theta)$ and $R_{QD}(\omega,\theta)$ if we go beyond the Fermi gas model, by explicitly taking into account the different nuclear excitation mechanisms corresponding to the two processes. A possibility to extend the distinction between the GR and QD parts to the mesonic seagull amplitude is provided by the Fermi liquid theory as discussed in section 7.

If we suggest that the resonance part of the quasi-deuteron contribution does not involve the nucleus as a whole, but rather is connected with deuteron-like subsystems, its dependence on momentum transfer should be given by the form factor $F_2(q)$, which is in contrast to the giant resonance case, where no such form factor appears. The energy dependence may be represented in a Lorentzian form, which leads to

$$R_{QD}(\omega,\theta) = \boldsymbol{\epsilon}_1 \cdot \boldsymbol{\epsilon}_2 F_2(q) \Big\{ \frac{NZ}{A}\frac{e^2}{M}\kappa^{QD} + \frac{\omega^2}{4\pi}\sigma_{QD}\Gamma_{QD}\frac{E_{QD}^2 - \omega^2 + i\omega\Gamma_{QD}}{(E_{QD}^2-\omega^2)^2 + \omega^2\Gamma_{QD}^2} \Big\}. \tag{5.5}$$

Equation (5.5) expresses our supposition that the scattering amplitude of each of the contributing quasideuterons follows an electric-dipole characteristic which should be the case. For the energy independent term the factor $F_2(q)$ is necessary to ensure vanishing of the resonance amplitude $R_{QD}(\omega,\theta)$ in the high-energy limit for all angles. The assumption that the amplitude $R_{QD}(\omega,\theta)$ vanishes in the high-energy limit leads again to the sum rule (3.42) for the integral over the absorption cross section σ_{QD}. By explicitly using the Lorentzian form for σ_{QD} one finds

$$\frac{1}{4\pi}\sigma_{QD}\Gamma_{QD} = \frac{NZ}{A}\,\frac{e^2}{M}\,\kappa^{QD}$$

which is a useful relation between Lorentzian parameters and enhancement constant κ^{QD} . It is interesting to note that as a result the seagull amplitude $\tilde{S}_{QD}(\omega,\theta)$ and the energy-independent term of the resonance amplitude $R_{QD}(\omega,\theta)$ cancel exactly.

In photon-nucleon investigations another phenomenological description other than a purely Lorentzian form exists for $\sigma_{QD}(\omega)$. It is known as the Levinger representation ([220], see also [221]) and has the following form:

$$\sigma_{QD}(\omega) = L\frac{NZ}{A}\,\sigma_D(\omega)\,\exp(-D/\omega) \tag{5.6}$$

where L and D are some parameters and σ_D is the experimental photoabsorption cross section for the deuteron. The exponential function takes into account that due to Pauli blocking not the total deuteron absorption strength should appear in σ_{QD}. However, for the analysis of Compton scattering data it is convenient and sufficient to use Lorentzian fits to the expression given in (5.6).

5.2 The single-nucleon contribution to Compton scattering up to quadratic order in the photon energy

We now want to introduce the amplitude $T_N(\omega,\theta)$, which is connected with the third degree of freedom, i.e. with the contribution from individual nucleons to the nuclear Compton scattering amplitude. Our consideration starts from the spin-independent part of the scattering amplitudes T_p and T_n for the free proton and neutron, respectively, [99] in the laboratory system,

$$\begin{aligned} T_p &= \frac{e^2}{M}\Bigg(-\boldsymbol{\epsilon}_1\cdot\boldsymbol{\epsilon}_2 + \omega_1\omega_2\frac{2\kappa_p+{\kappa_p}^2}{4M^2}\boldsymbol{\epsilon}_1\cdot\boldsymbol{\epsilon}_2 \\ &\quad - \omega_1\omega_2\frac{(1+\kappa_p)^2}{4M^2}\mathbf{s}_1\cdot\mathbf{s}_2\,\hat{\mathbf{k}}_1\cdot\hat{\mathbf{k}}_2 + \omega_1\omega_2\frac{1}{4M^2}\mathbf{s}_1\cdot\mathbf{s}_2\Bigg) \\ &\quad + \omega_1\omega_2\bar{\alpha}_p\,\boldsymbol{\epsilon}_1\cdot\boldsymbol{\epsilon}_2 + \omega_1\omega_2\bar{\beta}_p\,\mathbf{s}_1\cdot\mathbf{s}_2 + \mathcal{O}(\omega^4), \end{aligned} \tag{5.7}$$

$$\begin{aligned} T_n &= \frac{e^2}{M}\left(\omega_1\omega_2\frac{{\kappa_n}^2}{4M^2}\boldsymbol{\epsilon}_1\cdot\boldsymbol{\epsilon}_2 - \omega_1\omega_2\frac{{\kappa_n}^2}{4M^2}\mathbf{s}_1\cdot\mathbf{s}_2\,\hat{\mathbf{k}}_1\cdot\hat{\mathbf{k}}_2\right) \\ &\quad + \omega_1\omega_2\bar{\alpha}_n\,\boldsymbol{\epsilon}_1\cdot\boldsymbol{\epsilon}_2 + \omega_1\omega_2\bar{\beta}_n\,\mathbf{s}_1\cdot\mathbf{s}_2 + \mathcal{O}(\omega^4), \end{aligned} \tag{5.8}$$

The quantities κ_p and κ_n are the anomalous magnetic moments of the proton and neutron, respectively, and $\bar{\alpha}_p$, $\bar{\beta}_p$, $\bar{\alpha}_n$ and $\bar{\beta}_n$ are the electromagnetic polarizabilities of the free proton and neutron, respectively. Both amplitudes, Eqs. (5.7) and (5.8), can be divided into a non-Born part (containing the electromagnetic polarizabilities) and a Born part (containing all other terms). When the nucleons are embedded in a nucleus, recoil effects may be disregarded so that $\omega_2=\omega_1$ to a good approximation. Furthermore, form factors have to be introduced in order to take into account the spatial distributions of nucleons in a nucleus. Clearly, it is also necessary to account for the Fermi motion of the nucleons. In the energy region considered here this contribution is of the same order as relativistic corrections and may thus be skipped for our present purpose.

The only problem in considering these single-nucleon contributions is to avoid any double-counting with respect to the other parts of the nuclear scattering amplitude. It can directly be seen that (i) the non-Born contributions have not yet been included in any other part of the amplitude T_{tot} and (ii) the first term in Eq. (5.7) is evidently related to the kinetic seagull amplitude $B(\omega,\theta)$. The remaining terms in Eqs. (5.7) and (5.8) are corrections proportional to ω^2 and depend on the anomalous magnetic moments of the nucleons. If one compares the values of $\bar{\alpha}_N$ and $\bar{\beta}_N$ given in section 5.3 with the coefficients at ω^2 in the nucleon Born terms one can see that the latter are essentially smaller (of the order of 0.4×10^{-4} fm^3) and, therefore, may be neglected. Moreover, the contribution of the magnetic moment is partly included into the resonance amplitudes R_{GR} and R_{QD}. Thus, we have to keep only the nucleon non-Born contributions to the nuclear Compton amplitude which read

$$\begin{aligned} T^{non-Born}(\omega,\theta) &= \omega^2\Big[Z\Big(\bar{\alpha}_p\,\boldsymbol{\epsilon}_1\cdot\boldsymbol{\epsilon}_2 + \bar{\beta}_p\,\mathbf{s}_1\cdot\mathbf{s}_2\Big) \\ &\quad + N\Big(\bar{\alpha}_n\,\boldsymbol{\epsilon}_1\cdot\boldsymbol{\epsilon}_2 + \bar{\beta}_n\,\mathbf{s}_1\cdot\mathbf{s}_2\Big) + \mathcal{O}(\omega^4)\Big]F_1(q). \end{aligned} \tag{5.9}$$

In this representation, Eq. (5.9), use has been made of the assumption that protons and neutrons follow the same one-body form factor $F_1(q)$. From $T^{non-Born}(\omega,\theta)$ of Eq. (5.9) we may construct the amplitude $T_N(\omega,\theta)$ of (5.1) by introducing the in-medium electromagnetic polarizabilities of the nucleon $\tilde{\alpha}_N$ and $\tilde{\beta}_N$ leading to

$$T_N(\omega,\theta) = \omega^2\,A\,\left[\Big(\tilde{\alpha}_N\,\boldsymbol{\epsilon}_1\cdot\boldsymbol{\epsilon}_2 + \tilde{\beta}_N\,\mathbf{s}_1\cdot\mathbf{s}_2\Big) + \mathcal{O}(\omega^4)\right]F_1(q). \tag{5.10}$$

For the special case of no modification of the electromagnetic polarizabilities in the nuclear medium we have

$$\tilde{\alpha}_N \equiv \bar{\alpha}_N = \frac{Z}{A}\bar{\alpha}_p + \frac{N}{A}\bar{\alpha}_n \qquad\qquad \tilde{\beta}_N \equiv \bar{\beta}_N = \frac{Z}{A}\bar{\beta}_p + \frac{N}{A}\bar{\beta}_n. \tag{5.11}$$

5.3 Status of the free polarizabilities of the nucleon

Though electromagnetic polarizabilities of hadrons have been discussed already for a long time, some clarifying remarks concerning these quantities are advisable at the beginning. The electromagnetic polarizabilities $\bar{\alpha}_p$ and $\bar{\beta}_p$ of the free proton appearing in the Baldin-Lapidus sum rule or in the differential cross section for proton Compton scattering of real photons (RCS) [99] are most natural characteristics of the second-order proton response to external electromagnetic fields. Details of this view are discussed below. The often used expressions like $\bar{\alpha} = \alpha_0 + \Delta\alpha$ and $\bar{\beta} = \beta_{para} + \beta_{dia}$ introduce quantities (they are normally termed the static electric polarizabilty α_0, the retardation correction of the electric polarizability $\Delta\alpha$, the paramagnetic polarizability β_{para} and the diamagnetic polarizability β_{dia}) which have only a theoretical significance but cannot be measured in real (or even gedanken) experiments.

There is a persisting prejudice that $\bar{\alpha}$ has not its own fundamental sense and rather appears in Compton scattering as an artificial combination of the genuine polarizability α_0 and the retardation correction $\Delta\alpha$. The latter is thought to be caused by non-static effects pertinent to real photons. They think that the static polarizability α_0 determines a coupling of the particle to a static electric field and therefore α_0 alone is measured under static conditions which allow to expell the retardation effects. Such a view point is wrong, what is easily demonstrated by a general consideration based on effective Lagrangians [100].

A rigorous theorem, which, for the sake of simplicity, we formulate here for a *spinless* composed hadron or nucleus of a known mass m and electric charge e, is the following. Whenever the particle stays or slowly moves in the region outside external electromagnetic charges or currents $j_\mu^{ext}(\mathbf{r},t)$ which create the probing electric $\mathbf{E}$ (or magnetic $\mathbf{H}$) field, the internal structure of the particle and its low-energy long-wavelength response to the field is characterized by the only additional parameter $\bar{\alpha}$ through an effective potential $-\frac{1}{2}\bar{\alpha}\mathbf{E}^2$ (or by $\bar{\beta}$ through $-\frac{1}{2}\bar{\beta}\mathbf{H}^2$, respectively) [100]. This implies that the so-called static polarizability is irrelevant whenever the particle has a charge and an internal size $\langle r^2\rangle \neq 0$, thus leading to $\bar{\alpha} = \alpha_0 + e^2\langle r^2\rangle/(3m) \neq \alpha_0$. This theorem signifies that all standard tools considered in textbooks as methods for measuring the electric polarizability (like placing the particle into the field of an electric capacitor and looking at its energy shift or at an induced dipole moment) give $\bar{\alpha}$ rather than α_0 [222]. There is no way to measure α_0 instead of $\bar{\alpha}$ but putting the probing external charges $j_0^{ext}(\mathbf{r},t)$ *inside* the particle, *e.g.* in an electron scattering experiment with observation of a secondary real or virtual photon. In an experiment like this one could simultaneously measure $e^2\langle r^2\rangle$ and $\bar{\alpha}$ and, therefore, determine α_0. This means that the polarizabilities $\bar{\alpha}$ and $\bar{\beta}$ introduced in Compton scattering studies are structure parameters which have a more general sense than sometimes assumed. In essense, nothing changes when spin of the particle is included.

Since we are dealing here with Compton scattering itself, the relevance of the free-nucleon polarizabilities $\bar{\alpha}_N$ and $\bar{\beta}_N$ needs no further explanations. However we have to explain how the in-medium polarizabilities of the nucleon, $\tilde{\alpha}_N$ and $\tilde{\beta}_N$, enter to nuclear Compton scattering. For a clear-cut definition of the in-medium polarizabilities [80,166] we have to distinguish between (i) effects of rebuiding the internal (*e.g.*, quark) structure of the nucleon entering into $\tilde{\alpha}_N$ and $\tilde{\beta}_N$ as one-body quantities and (ii) two-body effects of meson exchange currents between pn pairs which may be denoted by $\delta\alpha$ and $\delta\beta$. From a phenomenological point of view developed in sections 3 and 4 these latter quantities are not part of the in-medium electromagnetic polarizabilities but are rather used to parametrize that part of the "mesonic seagull amplitude" (Thomson scattering by correlated pn pairs) which is energy

dependent in the forward direction (*cf.* Eq. (5.4); for more details see section 9). In a first step of the analysis of experimental data the convolution of the true in-medium electromagnetic polarizabilities and the meson exchange corrections are determined. This leads to the effective in-medium electromagnetic polarizabilities

$$\tilde{\alpha}_N^{eff} = \tilde{\alpha}_N + \delta\alpha, \quad \tilde{\beta}_N^{eff} = \tilde{\beta}_N + \delta\beta. \tag{5.12}$$

The quantities $\delta\alpha$ and $\delta\beta$ have to be calculated and, therefore, introduce some model dependence into the determination of $\tilde{\alpha}_N$ and $\tilde{\beta}_N$. However, as will be shown later, the respective model dependent uncertainties are not large.

We have to repeat our words said in the beginning of section 3 that it would be also possible to accept the effective quantities (5.12) as an alternative (and different) definition of the in-medium polarizabilities. Since the free-nucleon polarizabilities (at least, the electric one) are essentially determined by the pion cloud of the nucleon [223,224], the in-medium modifications of the pion contribution to $\bar{\alpha}_N$ and $\bar{\beta}_N$ like a Pauli blocking [82, 104] have also a right to be attributed to the in-medium polarizabilities of the nucleon. However, in no way such effects should be added to the mesonic seagull contribution because this leads to the double counting. Considering in the following the in-medium polarizabilities we always mean the quantities $\tilde{\alpha}_N$ and $\tilde{\beta}_N$ which are free from the mesonic seagull correction.

In nuclei with $Z = N$ which are investigated in the following the arithmetic averages of the proton and neutron electromagnetic polarizabilities are observed. From the Baldin-Lapidus sum rule applied to experimental photoabsorption cross sections the sum $(\bar{\alpha} + \bar{\beta})_N = 14.5 \pm 0.5$ (in units of 10^{-4} fm^3) is very well known [225–228], where later estimates [227, 228] give values by a few per cent lower that the older ones [225, 226]. Among the reasons for that is that experiments on Compton scattering by the proton in the Δ-resonance range [229] and photoproduction experiments (like [146]) carried out at MAMI (Mainz) lead to a more precise determination of the resonant M_{1+} amplitude of the Δ photoexcitation. Now [230, 231] this amplitude is by about 3% lower than it was assumed a few years ago in the SAID (SM95) parametrization of photo-meson amplitudes [232].

Though, apparently there is some room for discussion, the overall precision of $(\bar{\alpha} + \bar{\beta})_N$ is by far good enough for the purpose of our present data analysis. Furthermore, adjustments in the predicted differential cross sections are possible at small angles within the limits given by the errors of the nuclear photoabsorption cross sections (*cf.* Fig. 5.2), making small differences in $(\bar{\alpha} + \bar{\beta})_N$ unobservable. Note that the free parameter of our data analysis is the difference of in-medium polarizabilities $(\tilde{\alpha} - \tilde{\beta})_N$ which has no influence on the differential cross section at zero angle.

Separately, polarizabilities of the free proton have been measured in proton Compton scattering experiments performed at photon energies below photo-meson threshold [233–237]. Their results are partly summarized in the review paper [99] and in the Review of Particle Physics 1998 [238] (in fact, the latter reference relies on a "global average" over experiments of 90's derived in [237] on the base of the Baldin–Lapidus sum rule and experimental data on the differential cross section of proton Compton scattering). It was found that $\bar{\alpha}_p = 12.1 \pm 0.8$ (stat + syst) ± 0.5 (theor) and $\bar{\beta}_p = 2.1 \pm 0.8$ (stat + syst) ± 0.5 (theor).

The knowledge of polarizabilities of the neutron is less certain. Using model-dependent dispersion relations at fixed t, the differences $\bar{\alpha}_p - \bar{\alpha}_n \simeq -1.4$ and $\bar{\beta}_p - \bar{\beta}_n \simeq 0.1$ are theoretically expected [226,228]. On the experimental side the first meaningful number for the electric polarizability of the neutron was measured by Rose et al. [239] through quasifree Compton scattering on neutrons bound in the deuteron. The precision of this experiment was surpassed by an experiment on scattering of neutrons in the Coulomb field of Pb nuclei, enriched in ^{208}Pb [240]. The reported number[5] $\bar{\alpha}_n = 12.6 \pm$

[5] We give that number and a similar number below with a small correction of 0.62 added which takes care of relativistic effects lost in the fully nonrelativistic treatment of the Coulomb scattering experiments [100, 222, 241].

1.5 (stat) $\pm$ 2.0 (syst) perfectly agrees with the above theoretical expectation. However, more recently a new experiment on Coulomb scattering of the neutron [242] gave a rather different polarizability $\bar{\alpha}_n = 0.6 \pm 5$. It was also claimed that the high accuracy of the former Coulomb scattering result [240] may possibly be grossly overestimated [243]. A detailed discussion of these points and a possible experimental way out of this problem has recently been addressed by Wissmann et al. [244].

Given the experimental results for proton polarizabilities and the theoretical evaluations of the proton–neutron differences, the works on nuclear Compton scattering discussed below use the following values for averaged free-nucleon polarizabilities: $\bar{\alpha}_N = 11.3 \pm 1.5$ and $\bar{\beta}_N = 3.7 \mp 1.5$. These numbers should be compared with what is inferred from nuclear Compton scattering experiments themselves. The free-nucleon value of the sum is slightly shifted down in the nuclear medium to about $(\tilde{\alpha} + \tilde{\beta})_N = 14.0$ [34]. This observation of an approximately constant sum of electromagnetic polarizabilities does not exclude that the relative sizes of the in-medium electric $\tilde{\alpha}_N$ and magnetic $\tilde{\beta}_N$ polarizabilities may be considerably different from the corresponding free-nucleon values due to meson exchange-currents and/or modifications of the internal structure of the nucleon. In this connection it is of interest that in-medium shifts as large as $\Delta\alpha^{eff}_{exp} = -8$ and $\Delta\beta^{eff}_{exp} = +8$ have been reported on the basis of analyses of Compton scattering experiments on ^{16}O [43].

5.4 Meson exchange currents

In complex nuclei meson exchange currents are a consequence of the interaction between proton-neutron pairs (quasideuterons). Following the notation of our previvous work [39] and the discussion of section 5.1, the corresponding modification of the nuclear scattering amplitude up to the order ω^4 may be written in the form

$$S(\omega,\theta) - \tilde{S}(\omega,\theta) = \Big(\delta\alpha\, g_{E1}(\theta) + \delta\beta\, g_{M1}(\theta)\Big)\omega^2 F_2(q). \tag{5.13}$$

The r.h.s. of (5.13) takes care of the fact that the meson exchange corrections $\delta\alpha$ and $\delta\beta$ are related to a two-body effect and, therefore, go along with the formfactor $F_2(q)$. The approximative definition in the following Eq. (5.14) is more convenient, because in this case $\delta\alpha$ and $\delta\beta$ can be directly compared with the electromagnetic polarizabilities of the free nucleon.

$$S(\omega,\theta) - \tilde{S}(\omega,\theta) \approx \Big(\delta\alpha^{(1)}\, g_{E1}(\theta) + \delta\beta^{(1)}\, g_{M1}(\theta)\Big)\, \omega^2 F_1(q). \tag{5.14}$$

A calculation of $\delta\alpha$ and $\delta\beta$ has been carried out by Hütt and Milstein [168] for nuclear matter. The result is $\delta\alpha^{(1)}(A=\infty) = -3.4$ and $\delta\beta^{(1)}(A=\infty) = +2.4$ (*cf.* Table 5.1). For finite nuclei the same authors [193] find the results also listed in Table 5.1. We see that the meson exchange corrections of the electromagnetic polarizabilities become smaller with decreasing mass number. The reason for this is that the possibility for two-body or — even more — three-body effects to take place becomes smaller for decreasing mass number. Three-body effects are essential because they enter into the process through correlations. In ^{4}He the possibility for two-body effects is largely reduced and that for three-body effects almost absent.

5.5 Experiments on the bound-nucleon electromagnetic polarizabilities

Figure 5.1 shows a typical experimental arrangement as used at the MAX laboratory of the university of Lund (Sweden) [51, 52]. The photon beam having an energy of about 100 MeV hits a thin metal foil serving as a bremsstrahlung radiator. Quasi monochromatic photons are obtained through a coincidence condition between an event in one of the NaI(Tl) detectors (A, B, C) and an event in the tagger. The tagger consists of a magnetic spectrometer which directs the unused electrons into

Table 5.1: *Meson exchange corrections of the in-medium electromagnetic polarizabilities in units of* $10^{-4} fm^3$

A	$\delta\alpha^{(1)}$	$\delta\beta^{(1)}$
∞	-3.4	$+2.4$
40	-2.4	$+2.1$
16	-1.3	$+1.0$
4	≈ 0	≈ 0

the beam dump, and electrons which have lost energy through bremsstrahlung production on an array of plastic scintillators. These plastic scintillators provide energy channels for the coincident bremsstrahlung photons.

Figure 5.1: *Typical experimental arrangement as used at the MAX laboratory of the university of Lund (Sweden) [51, 52]. The photon beam having an energy of about 100 MeV hits a thin metal foil serving as a bremsstrahlung radiator. Quasi monochromatic photons are produced through a coincidence condition between an event in one of the NaI(Tl) detectors (A, B, C) and an event in the tagger.*

For the data interpretation the resonance amplitude $R(\omega,\theta)$ and the static part of the mesonic seagull amplitude $\tilde{S}(\omega,\theta)$ have to be calculated in addition to the kinetic seagull amplitude $B(\omega,\theta)$. This is possible with very good precision for nuclei where the total photoabsorption cross section is known. To illustrate this, the total photoabsorption cross sections of ^{16}O and ^{40}Ca measured by Ziegler et al. [84] are shown in Fig. 5.2. The experimental photoabsorption cross section as fitted by the solid line is partitioned into Lorentzian lines. Except for the sum of all these Lorentzian lines, the only constraint is that the QD cross section as given by the dotted line resembles the Levinger representation of Eq. (5.6) as close as possible. All the other Lorentzian lines may be interpreted in terms of GR components. The experiments carried out to measure the in-medium electromagnetic polarizabilities use photons of 50 to 80 MeV. At these energies only the tails of the GR components are of relevance since the real part of the QD amplitude has a zero crossing in this energy range. This makes the determination of the amplitude $R(\omega,\theta)$ quite unambiguous. For the determination of the static part of the mesonic seagull amplitude $\tilde{S}(\omega,\theta)$ only the integrated GR and QD cross sections have to be known in order to determine κ^{GR} and κ^{QD}. The formfactor $F_2(q)$ is taken from model calculations (*cf.* section 9).

On the basis of the prerequisites discussed in the preceding paragraph, we now discuss the present status of our knowledge about in-medium electromagnetic polarizabilities based on recent results [48] obtained for ^{40}Ca and ^{16}O. Throughout this section we will calculate the predictions for different "effective" in-medium electromagnetic polarizabilities $\tilde{\alpha}_N^{eff}$ and $\tilde{\beta}_N^{eff}$. These quantities are introduced such that they may be inserted into Eq. (5.10) in order to take care of different tentative choices for the in-medium electromagnetic polarizabilities including the effects of meson-exchange currents and of modifications of the internal structure of the nucleon, while simultaneously the mesonic seagull-amplitude $S(\omega,\theta)$ is represented through its static approximation $\tilde{S}(\omega,\theta)$. These choices are
(i) the free-nucleon electromagnetic polarizabilities,
(ii) the free-nucleon electromagnetic polarizabilities supplemented by meson exchange corrections predicted for the finite nucleus,
(iii) the free-nucleon electromagnetic polarizabilities supplemented by meson exchange corrections predicted for nuclear matter.

^{40}Ca: Figure 5.3 shows the energy distributions of the differential cross sections obtained in recent

Figure 5.2: *Total photoabsorption cross sections [84] for ^{40}Ca (upper figure) and ^{16}O (lower figure) partitioned into components having Lorentzian shapes. Dashed curves: GR components. Dotted curves: QD components.*

experiments [42, 47, 48] together with predictions. The nuclear part of the amplitudes, i.e. $B(\omega,\theta) + \tilde{S}(E,\theta)+R(E,\theta)$, is fixed through the experimental total photoabsorption cross section so that the only parameters are the effective electromagnetic polarizabilities $\tilde{\alpha}_N^{eff}$ and $\tilde{\beta}_N^{eff}$. All three curves are in good agreement with each other and with the data points at $\theta = 45°$. This shows that the nuclear part of the scattering amplitudes has been calculated with sufficient precision, so that the angular dependence of the differential cross section may be interpreted in terms of properties of the effective electromagnetic polarizabilities. The only remaining precaution is concerned with the isovector giant-quadrupole resonance (IVGQR) which also has an effect on the angular distribution of the differential cross section. After taking the IVGQR into account using experimental photoabsorption data [212, 214], the uncertainty of the strength and location of the IVGQR leads to modifications of the angular distribution, being essentially smaller than the differences between the lower (dashed) curves and the (solid) curves in the middle and, thus, is irrelevant for our conclusion that there is no noticeable modification of the in-medium electromagnetic polarizabilities compared to the free ones. Indeed, there is apparent preference of the experimental data for the solid curves i.e. the predictions including the free-nucleon electromagnetic polarizabilities supplemented by the meson-exchange corrections $\delta\alpha^{(1)}$ and $\delta\beta^{(1)}$ predicted for the finite nucleus. However, for ^{40}Ca it apparently makes no major difference whether we make use of the nuclear matter (A = ∞, dotted curves) predictions or the predictions for the finite nucleus (A = 40, solid curves). In the next paragraph we will see that such differences become visible for the smaller nucleus ^{16}O.

Figure 5.3: *Experimental elastic differential cross sections [42, 47, 48] for ^{40}Ca versus scattering angle compared with predictions. E_γ = 58 MeV (upper Figure), E_γ = 75 MeV (lower Figure). The curves are calculated for (i) the free-nucleon electromagnetic polarizabilities (dashed), (ii) the free-nucleon electromagnetic polarizabilities supplemented by meson exchange corrections predicted for the finite nucleus (solid), and (iii) the free-nucleon electromagnetic polarizabilities supplemented by meson exchange corrections predicted for nuclear matter (dotted).*

^{16}O: Figure 5.4 shows data obtained for ^{16}O versus scattering angle. For this smaller nucleus the meson exchange corrections $\delta\alpha^{(1)}$ and $\delta\beta^{(1)}$ of the electromagnetic polarizabilities predicted for the finite nucleus (A = ∞, solid curve) shows a sizable difference from the corresponding prediction for nuclear matter (A = 16, dotted curve). The lower curves (dashed) have been calculated with the meson-exchange corrections set to zero. It is apparent that the solid curves provide the optimum fit to the majority of the experimental data — if we tentatively exclude the two data points for E_γ = 75 MeV and about $\theta = 60°$ from the present consideration. This finding leads to the conclusion that the predicted meson-exchange corrections are in line with our experiments and that there are no indications of an additional in-medium modification of the electromagnetic polarizabilities.

Figure 5.4: *Differential cross sections [39, 47, 48] for Compton scattering by ^{16}O versus scattering angle compared with predictions. E_γ = 58 MeV (upper figure); E_γ = 75 MeV (lower figure). The curves are calculated for (i) the free-nucleon electromagnetic polarizabilities (dashed), (ii) the free-nucleon electromagnetic polarizabilities supplemented by meson exchange corrections predicted for the finite nucleus (solid), and (iii) the free-nucleon electromagnetic polarizabilities supplemented by meson exchange corrections predicted for nuclear matter (dotted).*

5.6 Summary and Conclusions

The data presented above have led to a satisfactory consistency in our conclusion concerning the in-medium electromagnetic polarizabilities. This conclusion is that the proton-neutron averages of in-medium electromagnetic polarizabilities $\tilde{\alpha}_N$ and $\tilde{\beta}_N$ are the same as the corresponding quantities $\bar{\alpha}_N$ and $\bar{\beta}_N$ for the free nucleon within a precision of the order of $\pm 2.5 \times 10^{-4}$ fm^3, if we do not put too much weight on some points discussed in the next paragraph. Furthermore, there are strong indications that the data obtained for ^{40}Ca and ^{16}O are in favour of the predicted [193] meson-exchange corrections $\delta\alpha$ and $\delta\beta$ of the electromagnetic polarizabilities. It was known before that the sum of electromagnetic polarizabilities $\bar{\alpha}_N + \bar{\beta}_N$ is not modified through binding. The essential additional message of our result is that the difference of electromagnetic polarizabilities $\bar{\alpha}_N - \bar{\beta}_N$ also remains the same. In the dispersion theory of nucleon Compton scattering [101] the difference $\bar{\alpha}_N - \bar{\beta}_N$ is an independent input parameter which may be related to the exchange of the scalar σ meson in the t-channel. On the other hand the scalar σ meson is believed to be responsible for the largest part of the binding potential between nucleons in a complex nucleus. This observation suggests that there might be a relation between the quantity $\tilde{\alpha}_N - \tilde{\beta}_N$ measured in nuclear Compton scattering and the nucleon binding potential. The tentative conclusion from our experimental result, therefore, may be that the role the σ meson plays for the structure of the nucleon is not modified when the nucleons are imbedded in nuclear matter.

The conclusions drawn in the foregoing section are weakened to some extent by some unsolved problems which should be cleared up in further studies: (i) The free-nucleon polarizabilities of the neutron are not known with the desirable reliability. (ii) The angular distribution of Compton-scattering differential cross-sections for ^{12}C and ^{16}O at an energy of 75 MeV deviates from the predictions at $\theta = 60^\circ$ by 20–30 % [39]. These deviations have not been removed by the recent theoretical studies of Hütt and Milstein [168, 193].

6 Compton scattering above π meson threshold

Nuclear Compton scattering above π meson threshold has three regions of current interest where experimental work has been carried out:
(i) Compton scattering in resonance range where the experiments were restricted to the energy region of the Δ resonance.
(ii) Compton scattering in the asymptotic range at small transverse momenta p_T, where shadowing and vector-meson dominance phenomena may be studied (see *e.g.* [128]).
(iii) Compton scattering in the asymptotic range at large transverse momenta p_T, where the direct coupling of photons to valence quarks may be studied. These experiments are of interest because the wave function of quarks in the nucleon may be investigated. Data are available only for the proton (see *e.g.* Kroll et al. [138, 139]).

In principle there is also a fourth type of Compton scattering experiments at high p_T, *viz.* the deep inelastic scattering of photons by quarks [245]. These deep inelastic Compton processes are not coherent-elastic with respect to the nucleon or nucleus but resemble Compton scattering by single quarks with subsequent hadronization. As a consequence a jet of hadrons is leaving the nucleon after Compton scattering has taken place.

Our discussion here is rather brief and restricted to the Δ-resonance region of nuclei, i.e. to case (i). The latter choice is made because this is the only region where recent experimental data are available and because the theoretical ideas which are tested through the experiments have a large overlap with those considered in the rest of the present paper.

6.1 Pioneering work on Compton scattering in the resonance range

The study of nuclear Compton scattering above π meson threshold started on the experimental side with the work of Hayward and Ziegler [17]. The experiment has been carried out with a low-duty factor linear accelerator then available in Mainz and with a comparatively small (25 cm$\oslash$ $\times$ 36 cm) NaI(Tl) detector positioned at one scattering angle of $\theta = 115^\circ$ and in an energy range from 180 to 375 MeV. One difficulty in these experiments was the separation of elastic from inelastic photon scattering processes. Therefore, the main interest in subsequent theoretical work [246, 247] was directed to this problem. These investigations were based on Δ-hole model approaches [105, 107, 248, 249] including inelastic processes and led to some agreement with the experimental data. These first investigations showed that the proper experimental separation of elastic and inelastic components is essential for this type of experiments. This was one of the major motivations for purchasing the large Mainz 48 cm$\oslash$ $\times$ 64 cm NaI(Tl) detector [37].

6.2 Compton scattering by ^{12}C in the Δ range

In a first application of the large Mainz 48 cm$\oslash$ $\times$ 64 cm NaI(Tl) detector elastic and inelastic photon scattering from ^{12}C was investigated [37] at $\theta_{LAB} = 40^\circ$ using the tagged-photon beam at the 855 MeV microtron MAMI (Mainz). With a width of tagger intervals of ΔE= 2 MeV and an energy resolution of the NaI(Tl) detector of 1.5 % the separation of the elastic and the inelastic lines was sufficient to obtain elastic (Compton) and inelastic differential cross sections in an energy interval from 200 MeV to 500 MeV. The differential cross sections for Compton scattering were compared with calculations carried out in the Δ-hole model [108] leading to a remarkably good agreement between theory and experiment at photon energies above 250 MeV and a drastic disagreement at photon energies below 250 MeV. The occurance of this discrepancy was very surprising because $\theta_{LAB} = 40^\circ$ is close enough to the forward direction so that any theory which reproduces the photoabsorption cross section and has a

correct low-energy limit should also reproduce the Compton scattering differential cross section. It is interesting to note that the same observation was made in first interpretations of Compton differential cross sections measured for ^{4}He at the same angle $\theta_{LAB} = 40^\circ$ [44, 109] This observation seemed to suggest that some omission should be in the Δ-hole approach as formulated in Refs. [107,108]. In the meantime this omission was identified to be the neglect of the seagull amplitudes $B(\omega,\theta) + \tilde{S}(\omega,\theta)$ which were discussed in section 3. Indeed after including the seagull amplitudes $B(\omega,\theta) + \tilde{S}(\omega,\theta)$ the agreement between theory and the $\theta_{LAB} = 40^\circ$ data for ^{12}C and ^{4}He became much better, as is further discussed below.

6.3 Compton scattering by ^{4}He in the Δ range

Among the nuclei to be studied by Compton scattering ^{4}He is of special interest, because this nucleus combines the well-known structure of a few-body system with the binding energy of a complex nucleus. Furthermore, the first excited state is at 20 MeV, thus making the separation of elastic and inelastic processes easy. Previous experiments on Compton scattering by ^{4}He in the Δ range [20, 23, 29, 35, 40] were carried out using the bremsstrahlung method and, therefore, may have suffered from the well-known systematic errors contained in that method. In spite of that, the use of large NaI(Tl) detectors made it possible to get good data on the elastic reaction at energies close to the end points of the bremsstrahlung beams.

The first fully high-resolution Compton scattering experiments on ^{4}He were carried out only recently with a remarkable progress. At LEGS (BNL) [45], the first data were obtained with a polarized and tagged photon beam ($\Delta E \approx 5$ MeV) produced by backscattering of laser light on 2.5 GeV electrons. Photons were detected with a 48 cm$\oslash \times$48 cm NaI(Tl) detector. Measurements were performed at six angles between 31° and 130° which produced angular dependences of the differential cross sections and beam asymmetries at 5 energies between 206 and 310 MeV. At MAMI (Mainz), for the first time Selke et al. [44] performed measurements at a scattering angle of $\theta_{LAB} = 37^\circ$ through the whole Δ region from 120 to 510 MeV. The tagged-photon beam with $\Delta E \approx 2$ MeV and the large Mainz 48 cm$\oslash \times$ 64 cm NaI(Tl) detector were used in that experiment. The latter data were supplemented by Kraus et al. [46] leading to additional data at $\theta_{LAB} = 37^\circ$ taken with 48 cm$\oslash \times$ 64 cm NaI(Tl) detector and to additional data at energies between 150 and 300 MeV for the two angles of $\theta_{LAB} = 93^\circ$ and $\theta_{LAB} = 137^\circ$ covered by smaller 25.4 cm$\oslash \times$ 35.6 cm NaI(Tl) detectors. In this work also the beam asymmetry was determined between 230 and 270 MeV using linear polarization produced by the coherent bremsstrahlung in a diamond crystal.

The results of the recent Mainz experiments [44, 46] for the differential cross section are shown in Fig. 6.1 together with theoretical predictions to be discussed below. Not shown in that Figure are the LEGS data [45] which, for example, lie in between the data points of Mainz [46] and Saskatoon [29] at 90° and agree with both, the Mainz and Saskatoon data, at 130°. A sample of the LEGS data can be seen in Fig. 6.3 below. As was already found in the very first measurements at Bates (MIT) [20, 23], any version of the Δ-hole model — the original version of Ref. [107], a simplified version [109] based on a local-density approximation, and a version [108] corrected [46] for the seagull contributions to the elementary γN scattering amplitude — fails to explain the large size of the differential cross section observed at angles $\theta_{LAB} \gtrsim 90^\circ$. This is in contrast to the fact that a nice agreement exists between the experimental data and the modern predictions [46] at a small scattering angle of $\theta_{LAB} = 37^\circ$. Therefore, something fundamental must be wrong with our present understanding of Compton scattering in the Δ range.

Figure 6.1: *Differential cross sections $(d\sigma/d\Omega)_{LAB}$ for Compton scattering by ^4He [46] compared with predictions. The full circles are calculated within the Δ-hole model including the seagull amplitudes [46]. The results of the schematic model (dashed) and the extended schematic model (solid) are also shown [46].*

6.4 Calculations of Compton scattering in the Δ range

The discrepancies found between the experimental ^{4}He data and the theory at large angles demonstrate the necessity of comparing the main components of the existing different approaches with each other and to search for possible lines of developments which may solve the problems, apparently existing in all them. We will not discuss here whether the solution of these problems may be possible in a genuine isobar-meson model or whether it might be necessary to introduce different degrees of freedom like those of constituent quarks. Some ideas going into the latter direction have been published in recent literature [250].

The schematic model:
A zero-order approach to a theoretical interpretation of Compton scattering in the Δ range has been attempted through the "schematic model". It is based on the suppositions (i) that the absorption and emission of photons takes place locally on one nucleon, (ii) that different nucleons contribute equally and coherently, thus introducing into the nuclear Compton scattering amplitude $T_{tot}(\omega,\theta)$ the one-body nuclear form factor, and (iii) that the local spin-averaged γN scattering amplitude has a pure magnetic dipole, $M1$, characteristic (or optionally $E1$ but not both). In the schematic model the energy dependence is not taken from the elementary γN scattering amplitude but rather from the full nuclear amplitude at zero angle, $T_{tot}(\omega,0)$. The latter quantity can be derived from the total photoabsorption cross section $\sigma_{tot}(\omega)$ through the optical theorem and the GGT dispersion relation, thus giving the dispersion-theoretical differential cross section $d\sigma_{GGT}/d\Omega$. One then arrives at the simple formula [17, 46] usually used in the CM frame:

$$\frac{d\sigma}{d\Omega}(\omega,\theta) = \frac{d\sigma_{GGT}}{d\Omega}(\omega,0)\,|F_1(q)|^2\;\frac{1+\cos^2\theta}{2}. \tag{6.1}$$

Here q is the momentum transfer and $F_1(q)$ the one-body formfactor. It is not expected that the schematic model (6.1) makes a very realistic prediction except for very forward directions, because *e.g.* of the neglect of any multipolarity except for $M1$, which is an oversimplification for the Δ energy-range.

The extended schematic model:
The nuclear scattering amplitude in the "extended schematic model" [46] is given by a combination of several pieces which are results of different reaction mechanisms. In close analogy with the considerations given in sections 3 to 5, we write

$$\begin{aligned} T_{tot}(\omega,\theta) &= T_A(\omega,\theta) + T_N(\omega,\theta), \\ T_N(\omega,\theta) &= T^{E1}(\omega,0)\,F_1(q)\,g^{E1}(\theta) + T^{nm}_{\Delta}(\omega,0)\,F_2(q)\,g^{M1}(\theta) \\ &\quad + T^{m}_{\Delta}(\omega,0)\,F_1(q)\,g^{M1}(\theta). \end{aligned} \tag{6.2}$$

In (6.2) the amplitude $T_A(\omega,\theta)$ contains all the relevant nuclear contributions as there are the kinetic and mesonic seagull amplitudes and some high-energy tail from the positive-energy part of the quasideuteron amplitude. These pieces were discussed in sections 3 and 5. The amplitude $T_N(\omega,\theta)$ is related to nucleon excitations including the πN continuum. It contains one term of electric-dipole ($E1$) multipolarity and two terms of magnetic-dipole ($M1$) multipolarity. The term $T^{E1}(\omega,0)$ is calculated via optical theorem and dispersion relation from the total photoabsorption cross section of

the nucleon excluding the Δ-resonance contribution. This is justified because the nonresonant one-pion channel and the $D_{13}(1520)$ resonance are of $E1$ multipolarity and also the nonresonant two-pion channel is predominantly of $E1$ multipolarity. At low energies, a large part of T^{E1} comes from the so-called Kroll-Ruderman mechanism of pion photoproduction. The Δ-resonance itself appears in two terms, $T_\Delta^{nm}(\omega,0)$ and $T_\Delta^{m}(\omega,0)$, corresponding to the nonmesonic (nm) and the mesonic (m) photoabsorption cross section of the nuclear Δ resonance (see Fig. 2.6). Of the three terms on the r.h.s. of (6.2) the nonmesonic Δ term goes along with the formfactor $F_2(q)$ because this term corresponds to a two-body process. At forward angle the total amplitude (6.2) necessarily coincides with the dispersion-theoretical amplitude $T_{GGT}(\omega,0)$ provided the sum of partial cross-sections used to calculate the different pieces in (6.2) give $\sigma_{tot}(\omega)$, i.e. the total photoabsorption cross section of the nucleus. Therefore, it is not surprising that the nuclear Compton scattering data at small angles find an explanation in the framework of such a model. Really important is that by making use of both multipolarities, $M1$ and $E1$, and by including the seagull contributions improvements at large angles are obtained.

The Δ-hole model:
Recent calculations of Compton scattering in the Δ-hole approach [46, 108, 109] originate from the treatment of the problem given by Koch, Moniz and Ohtsuka [107]. Due to simplifications introduced by the local density approximation, which was used in the later works, many parallels with the two models described above become transparent. The scattering amplitude schematically reads

$$T_{tot}(\omega,\theta) = AT_\Delta^\gamma(\omega) g^{M1}(\theta) F_\Delta(q) + \Big(ZT_T^\gamma(\omega) + AT_{KR}^\gamma(\omega)\Big) g^{E1}(\theta) F_1(q). \tag{6.3}$$

Here the first term gives the Δ-resonance part of the scattering amplitude. It appears from the model as local and has a pure $M1$ multipolarity. However, the form factor $F_\Delta(q)$ it is accompanied with is not identical with the one-body form factor $F_1(q)$, because $F_\Delta(q)$ counts both, the nucleon distribution in the nucleus and a nuclear-density dependence of elementary Compton scattering on elements of the nuclear volume through the Δ-hole excitation, which appears due to the density-dependent width and self-energy of the dressed Δ in the nuclear medium. The second term is of $E1$ multipolarity. It represents the Thomson part of the γp scattering amplitude (which was omitted in [107, 108]) and the Kroll-Ruderman part which appears due to an intermediate isovector excitation of the nucleon to the s-wave πN state. It is assumed that the $E1$ part is not density dependent and, therefore, is accompanied with the one-body form factor $F_1(q)$.

Most recently such an approach was used in Ref. [109], in which the Δ resonance amplitude takes the form[6]

$$AT_\Delta^\gamma(\omega) F_\Delta(q) = \frac{4}{9}\frac{f_\gamma^2}{m_\pi^2}\omega_c^2 \int d\mathbf{r}\, \rho(\mathbf{r})\, e^{i\mathbf{q}\cdot\mathbf{r}} \Big[G_{\Delta h}(\rho(\mathbf{r}), s_+) + G_{\Delta h}(\rho(\mathbf{r}), s_-)\Big]. \tag{6.4}$$

Here f_γ is the $\gamma N\Delta$ coupling, $\rho(\mathbf{r})$ the nuclear density, ω_c the photon energy in the rest frame of the produced Δ , and $G_{\Delta h}$ the local density approximation to the Δ-hole Green function:

$$G_{\Delta h}(\rho, s) = \Big[\sqrt{s} - M_\Delta + \frac{i}{2}\tilde{\Gamma}(\rho, s) - \Sigma_\Delta(\rho, s)\Big]^{-1}, \tag{6.5}$$

where $\tilde{\Gamma}$ and Σ_Δ are the Pauli-blocked width and self-energy of the Δ in the nuclear matter [107, 251, 252]. The effective energies $s_\pm$ in the s- and u-channels of the Δ-hole excitation include small shifts caused by Fermi motion of the nucleons and read in the Fermi gas approximation:

$$s_\pm = M^2 \pm 2\omega\Big(M + \frac{3}{5}\frac{k_F^2}{2M}\Big), \tag{6.6}$$

[6] Strictly speaking, the form factor $F_\Delta(q)$ in Eq. (6.4) depends on both, the momentum transfer q and the photon energy ω.

where k_F is the (local) Fermi momentum, $k_F^3 = \frac{3}{2}\pi^2\rho$.

In the microscopic calculations of the Δ-hole model the constraint of the GGT dispersion relation is not used. Therefore, an agreement of the calculated differential cross section with the experimental data at small angles supports the validity of the model for nuclear Compton scattering. The agreement at energies below 350 MeV is largly improved when the kinetic (Thomson) seagull contribution is included [46, 109]. At energies above the Δ peak the results of different implementations [46, 109] of the Δ-hole model are different. A nice agreement with the experimental small-angle data [44] was found in Ref. [46], in which the Δ contribution was calculated with the parameters borrowed from [108, 253].

Missing effects at large angles – nonlocality:
However, all the considered models fail to correctly describe the experimental results at large angles, where the ^{4}He data [20, 23, 29, 45, 46] largely exceed the predictions. Comparing the different calculations, one may conclude that the density-dependent self-energy of the Δ which results in a shift and broadening of the Δ peak is not the only effect which has to be taken into account to explain nuclear Compton scattering in the Δ range. At high momentum transfers the self-energy cannot be considered as a local operator and therefore nonlocal effects should be taken into account. Nonlocal two- or many-body $E1$ contributions might be important as well. This view was supported by a calculation done by L'vov and Petrun'kin [129], in which large two-body $E1$ contibutions were obtained as a result of effective contact interactions arising in a gauge-invariant description of Compton scattering on a bound nucleon — see [133] for a more detailed motivation and derivation of such an approach and its relation with the standard language. In spite of a phenomenological success of the proposed scheme [45, 129], it cannot be fully applicable in the Δ range, because *e.g.* the contact $E1$ contributions arise there as purely real, what cannot be true at energies exceeding the pion threshold.

The following simple model provides strong evidence that nonlocal effects missing in the relations (6.3) and (6.4) may be responsible for the long-standing discrepancy between the Δ-hole model and the ^{4}He Compton scattering data at large angles. The model we consider includes only one- and two-body mechanisms of photon scattering by ^{4}He mediated by one-pion exchange. They are shown in Fig. 6.2. We disregard the ρ-meson exchange. Pion absorption or rescattering by intermediate nucleons is disregarded too what makes this model inapplicable close to the Δ-resonance peak where the absorption is very strong. In spite of all these oversimplifications, the model is not fully unreasonable at energies like 200 MeV, *i.e.* well below the Δ peak.

Diagram *a* in Fig. 6.2 gives the impulse approximation. The corresponding amplitude is equal to

$$T_{IA}(\omega,\theta) = A\,F_1(q)\,\langle\, T_{\gamma N}(\omega_{eff},\theta)\,\rangle \tag{6.7}$$

and is given by the spin-isospin average of the elementary γN scattering amplitude on the free nucleon. The effective energy in Eq. (6.7),

$$\omega_{eff} = \omega + \frac{q^2}{8M}\Big(1 - \frac{1}{A}\Big), \tag{6.8}$$

is obtained by assuming that the active nucleon has the momentum

$$\mathbf{p}_{eff} = -\frac{\mathbf{q}}{2}\Big(1 - \frac{1}{A}\Big) \tag{6.9}$$

in the Lab frame and that the rest of the nucleus is on shell (see *e.g.* [254]). The elementary γN scattering amplitude could easily be approximated by the Δ-pole diagram plus a Thomson and Kroll-Ruderman-like background as this was done *e.g.* in Refs. [107,109]. However, in the present context we use instead numerical results obtained in the framework of the dispersion theory [101]. The differential cross section for Compton scattering by ^{4}He obtained within the impulse approximation (6.7) at the energy $\omega = 206$ MeV is compared with predictions of the Δ-hole model [109] and with available

data [45, 46] in Fig. 6.3. Though the Δ-hole model includes the density-dependent modification of the Δ-resonance contribution, this modification is numerically not a big effect at 206 MeV and the predictions of the IA and the Δ-hole model are quite close to each other. The only exception is the region of large angles where the difference is big. However, this difference is not related with the IA or the Δ-hole model itself and is mostly caused by our choice for the effective energy (6.8) which includes a q-dependent correction absent in the Ansatz (6.6).

Figure 6.2: *One- and two-body contributions to nuclear Compton scattering. Diagram a is the impulse approximation. Diagram b describes real pion production followed by pion absorption. Diagrams c are required by the gauge invariance; in particular, the last diagram contains the contact $\gamma\pi N\Delta$ vertex.*

Figure 6.3: *Differential cross sections $(d\sigma/d\Omega)_{CM}$ for Compton scattering by ^{4}He at $E_\gamma = 206$ MeV. Data are from [45] (solid circles) and from [46] (open circles). Shown are predictions of the Δ-hole model in the local-density approximation [109], impulse approximation, Eq. (6.7), and the total contribution including the two-body MEC, Eq. (6.13).*

The two-body contributions are given by diagrams b and c in Fig. 6.2. Diagram b is determined by amplitudes of pion photoproduction which we take in the tree approximation with fixed nucleons, *i.e.* including the Kroll-Ruderman $\gamma\pi NN$ vertex, the pion-in-flight current, and Δ excitations in the direct and crossed channels. In the diagram b the intermediate pion has the energy ω and, therefore, can be real (not only virtual). Accordingly, even without Δ contributions the diagram b contributes to the imaginary part of the nuclear Compton scattering amplitude. In contrast to this, the diagrams c do not contain real-pion propagators. Actually, the diagrams c do not represent a self-dependent contribution but they rather ensure the gauge invariance of the total two-body amplitude. In particular, the last of the diagrams c contains the contact $\gamma\pi N\Delta$ vertex which is labeled as the Δ–Kroll–Ruderman vertex in Fig. 6.2. Explicit formulas for the kernel amplitude $\langle\, T_{b+c}(\mathbf{k}_1, \mathbf{k}_2, \mathbf{Q})\,\rangle$ which corresponds to the diagrams b and c with omitted wave functions of external photons and nucleons and spin-isospin averaged over nucleons in the nucleus are very similar to those given in Ref. [168] (see also section 9, Eqs. (9.3) and (9.21)). The kernel amplitude depends on the photon momenta $\mathbf{k}_1$, $\mathbf{k}_2$ and on the internal momentum $\mathbf{Q}$ which defines the sharing of the total momentum transfer $\mathbf{q}$ between the momenta $\frac{1}{2}\mathbf{q} - \mathbf{Q}$, $\frac{1}{2}\mathbf{q} + \mathbf{Q}$ transferred to each of the two interacting nucleons. Assuming oscillator wave function for ^{4}He,

$$\Psi(\mathbf{p}_1, \ldots \mathbf{p}_A) = \text{const} \times \exp\Big\{ -\frac{C_p}{2}\Big(\mathbf{p}_1^2 + \ldots + \mathbf{p}_A^2 - \frac{1}{A}\mathbf{P}^2\Big)\Big\}, \quad \mathbf{P} = \mathbf{p}_1 + \ldots + \mathbf{p}_A, \tag{6.10}$$

we fix the oscillator parameter C_p through the one-body formfactor:

$$F_1(q) = \exp\Big(-\frac{C_p}{4}\,\frac{A-1}{A}\,q^2\Big) = \exp\Big(-\frac{q^2}{4\alpha^2}\Big), \tag{6.11}$$

where $\alpha = 165$ MeV is determined from the electric radius of ^{4}He and that of the proton.Then the two-body form factor is equal to[7]

$$F_2(q) = \exp\Big(-\frac{C_p}{8}\,\frac{A-2}{A}\,q^2\Big). \tag{6.12}$$

For $A = 4$ we have $F_2(q) = [F_1(q)]^{1/3}$. Then the total MEC amplitude corresponding to diagrams b and c reads

$$T_{MEC}(\omega, \theta) = A(A-1)\,F_2(q) \int \frac{d\mathbf{Q}}{(2\pi)^3} \exp\Big(-\frac{C_p}{2}\mathbf{Q}^2\Big)\,\langle\, T_{b+c}(\mathbf{k}_1, \mathbf{k}_2, \mathbf{Q})\,\rangle. \tag{6.13}$$

[7]Note that we use the oscillator wave function only in order to evaluate the two-body form factor. Finding the amplitude (6.7), we use a more accurate form factor found through experimental data on electron scattering by ^{4}He [256].

In the limit $\omega = 0$ the mesonic amplitude (6.13) determines the (unretarded) enhancement parameter $\mathring{\kappa}$ (see section 9 for more detail). Actually the value of $\mathring{\kappa}$ obtained through the two-body diagrams of the lowest order in the πNN coupling is rather small [168], so that $\mathring{\kappa}$ is dominated by two-pion exchanges and three-body interactions. In the chiral limit of $m_\pi \to 0$ the amplitude (6.13) vanishes at $\omega = 0$ due to the exact compensation between the diagrams b and c. However, when the energy ω becomes higher than the pion threshold, such compensation is destroyed. In particular, the diagram b gets an imaginary part at $\omega > m_\pi$, whereas the diagram c without Δ contributions remains real. At energies above pion threshold the amplitude (6.13) is not suppressed any more by the small pion mass and is numerically large. Adding the meson-exchange amplitude T_{MEC} to the amplitude of the impulse approximation T_{IA}, we find a strong enhancement in the differential cross section at backward angles shown in Fig. 6.3 at the energy 206 MeV which brings the predictions of the model into a qualitative agreement with the data. At the energy 253 MeV the agreement with available data [45, 46] is almost perfect but this may be accidental because the model is not expected to work well close to the Δ peak. On the other hand, the IA and the Δ-hole model grossly underestimate the differential cross section at backward angles at these energies.

The increase obtained at backward angles is caused by mainly three reasons. First, the two-body formfactor does not suppress the MEC contribution as much as the one-body formfactor does the IA contribution; for instance, $F_2(q)/F_1(q) \simeq 2.5$ at 206 MeV and backward angles. Second, the medium correction to photon scattering through $E1$ photoproduction which is described by diagrams b and c with only electric couplings (these are diagrams without Δ) is quite large and predominately imaginary. It explains about 50% of the obtained enhancement (in the amplitude) at 206 MeV and backward angles. Such a correction was not included into the Δ-hole calculations of nuclear Compton scattering. Third, equally large and also predominately imaginary is the nonlocal correction due to propagation of the Δ-excitation from one nucleon to an other one through intermediate pion propagation.

The model considered here clearly is too simple to provide a perfect description of the ^{4}He Compton-scattering data, especially close to the Δ peak where multiple processes including pion absorption and rescattering are very important. In addition to pion exchange, ρ-meson exchange has also to be included. Moreover, nucleons should not to be considered fixed and also couplings to NN continuum-states should be incorporated; in the Δ-hole model these couplings are a large part of the so-called spreading potential of the Δ-hole states. It might also be important to calculate two-body contributions with a more accurate wave function of ^{4}He including the D-wave. Despite all these omissions, we believe that we can conclude that realistic calculations of nuclear Compton scattering at high momentum transfers should properly take into account the nonlocal effects.

7 Fermi liquid theory and nuclear Compton scattering

An appropriate method to describe enhancement phenomena of the giant dipole resonance is within Landau's Fermi liquid theory [255,257] of finite systems as first applied by Migdal [86,258]. The Fermi liquid theory is concerned with strongly interacting particles, which are replaced by weakly interacting quasiparticles analogous to particles in an ideal Fermi gas with a residual interaction.

In a finite system, the problem has to be treated in close analogy to the nuclear shell model, with the main difference that particle-hole excitations are replaced by quasiparticle-quasihole excitations. Giant-dipole excitations involve transitions between neighboring oscillator shells from below the Fermi energy-level to above it. In case of particle-hole excitations these transitions exhaust exactly one TRK sum rule so that the transition to the quasiparticle picture should contain the overfulfilment of the TRK sum rule as represented by $\overset{\circ}{\kappa}{}^{GDR}$. This will be shown in this section.

The spectrum of collective excitations (*e.g.* sound and spin waves of giant resonances) and the response of the system to an external (electromagnetic) field are determined by the quasi-particle scattering amplitude near the Fermi surface for zero scattering angle. This amplitude is a function of the angle between the initial quasi-particle momenta and is satisfactorily described by the first two Legendre polynomials. The coefficients of these polynomials are the constants introduced into the theory and are the main parameters of Landau's theory of Fermi liquids [255].

In the Fermi liquid theory the system of particles with the spin 1/2 is replaced by a system of quasiparticles with the same spin. This theory is aimed at the description of low-lying excitations. Each quasiparticle is characterized by the momentum $\mathbf{p}$ and the quasiparticle number $n(\mathbf{p})$. Strictly speaking, this quasiparticle number is a matrix $\hat{n}(\mathbf{p}) \equiv n_{\alpha\,\beta}(\mathbf{p})$ in spin and isospin spaces (for the sake of simplicity we assume that each index simultaneously corresponds to spin and isospin variables). The total number of particles N is equal to the total number of quasiparticles:

$$\mathrm{Tr} \int \hat{n}(\mathbf{p})\, d\tau = \frac{N}{V}\,, \quad d\tau = \frac{d\mathbf{p}}{(2\pi)^3}\,, \tag{7.1}$$

where V is the volume of system. In the ground state one has $n^{(0)}_{\alpha\,\beta}(\mathbf{p}) = \delta_{\alpha\,\beta}\theta(p_F - p)$ as in a Fermi gas. Due to the interaction between quasiparticles, the total energy of the system is not the sum of quasiparticle energies. The energy matrix $\hat{\epsilon} \equiv \epsilon_{\alpha\,\beta}(\mathbf{p})$ of the (individual) quasiparticle is defined as a variational derivative of the total energy E :

$$\frac{\delta E}{V} = \mathrm{Tr} \int \hat{\epsilon}(\mathbf{p}) \delta\hat{n}(\mathbf{p})\, d\tau \quad . \tag{7.2}$$

In the ground state $\epsilon_{\alpha\,\beta}(\mathbf{p}) = \epsilon^{(0)}(p)\delta_{\alpha\,\beta}$ and

$$\epsilon_F = \epsilon^{(0)}(p_F) \quad , \quad \left.\frac{\partial\epsilon^{(0)}(p)}{\partial p}\right|_{p=p_F} = v_F = \frac{p_F}{M^*} \quad , \tag{7.3}$$

where M^* is the effective mass of the quasiparticle. Giant-dipole excitations involve transitions between neighboring oscillator shells from below the Fermi energy to above it. Therefore, the relevant nucleons have momenta close to the Fermi momentum. Near the Fermi surface $\epsilon^{(0)}(p) = \epsilon_F + v_F(p - p_F)$. Including quasiparticle excitations the energy matrix $\epsilon_{\alpha\,\beta}(\mathbf{p})$ depends on the quasiparticle numbers $n_{\alpha\,\beta}(\mathbf{p})$:

$$\epsilon_{\alpha\,\beta}(\mathbf{p}) = \epsilon^{(0)}(p)\delta_{\alpha\,\beta} + \int f_{\alpha\gamma,\beta\delta}(\mathbf{p},\mathbf{p}')\delta n_{\delta\,\gamma}(\mathbf{p}')d\tau'\,, \tag{7.4}$$

where $\delta n_{\delta\,\gamma}(\mathbf{p})$ is the difference between $n_{\delta\,\gamma}(\mathbf{p})$ and $n^{(0)}_{\delta\,\gamma}(\mathbf{p})$ and $f_{\alpha\gamma,\beta\delta}(\mathbf{p},\mathbf{p}')$ describes the quasiparticle-quasiparticle interaction. In this function one can put $p = p' = p_F$. Therefore, it depends only on the

directions of the vectors $\mathbf{p}$ and $\mathbf{p}'$. In matrix notations one can write Eq. (7.4) as

$$\hat{\epsilon}(\mathbf{p}) = \hat{\epsilon}^{(0)}(\mathbf{p}) + \mathrm{Tr}' \int \hat{f}(\mathbf{p},\mathbf{p}')\delta\hat{n}(\mathbf{p}')d\tau' \quad , \tag{7.5}$$

where Tr' denote the trace with respect to indices corresponding to momentum $\mathbf{p}'$. Using (7.2) and (7.5) one can write an expression for the excitation energy:

$$\frac{\delta E}{V} = \mathrm{Tr} \int \hat{\epsilon}^{(0)}(\mathbf{p})\delta\hat{n}(\mathbf{p})\, d\tau + \frac{1}{2}\mathrm{Tr}\,\mathrm{Tr}' \int\int \hat{f}(\mathbf{p},\mathbf{p}')\delta\hat{n}(\mathbf{p}')\delta\hat{n}(\mathbf{p})d\tau d\tau' \quad . \tag{7.6}$$

Usually the following representation is used for the operator $\hat{f}(\mathbf{p},\mathbf{p}')$ of the interaction between quasiparticles:

$$N_0\hat{f}(\mathbf{p},\mathbf{p}') = F + \boldsymbol{\tau}\cdot\boldsymbol{\tau}'\, F' + \boldsymbol{\sigma}\cdot\boldsymbol{\sigma}'\, G + \boldsymbol{\tau}\cdot\boldsymbol{\tau}'\boldsymbol{\sigma}\cdot\boldsymbol{\sigma}'\, G' \,. \tag{7.7}$$

Here

$$N_0 = 4\int \delta(\epsilon^{(0)}(p) - \epsilon_F)\, d\tau = \frac{2p_F M^*}{\pi^2} \tag{7.8}$$

is the density of states on the Fermi surface (the factor four corresponds to two possible states in both, spin space and isospin space), $\boldsymbol{\tau}$ and $\boldsymbol{\sigma}$ are Pauli matrices for isospin and spin, respectively. The functions F, F', G and G' depend on the angle θ between $\mathbf{p}$ and $\mathbf{p}'$ and can be expanded with respect to Legendre polynomials:

$$F = \sum F_l P_l(\cos\theta) \quad , \tag{7.9}$$

and the same for the other functions. The coefficients in this series are some phenomenological constants which should be extracted from experiment. Usually only the zeroth and first harmonics are essential. It possible to describe a big variety of processes inside the nucleus with only a few coefficients F_l, F_l', G_l and G_l' (see [258]).

It follows from Galilei invariance that the momentum density is equal to the density of mass flow. Since the number of particles is equal to the number of quasiparticles, one has

$$\mathrm{Tr} \int \mathbf{p}\, \hat{n}(\mathbf{p})\, d\tau = M\,\mathrm{Tr} \int \frac{\partial\hat{\epsilon}}{\partial\mathbf{p}}\hat{n}(\mathbf{p})\, d\tau \,, \tag{7.10}$$

where M is the nucleon mass. Substituting $\hat{n}(\mathbf{p}) = \hat{n}^{(0)}(\mathbf{p}) + \delta\hat{n}(\mathbf{p})$ and using (7.5), we get for the isoscalar current:

$$\mathbf{j}_0 = \mathrm{Tr} \int \frac{\mathbf{p}}{M}\,\delta\hat{n}(\mathbf{p})\, d\tau = \mathrm{Tr} \int \left[\frac{\partial\epsilon^{(0)}}{\partial\mathbf{p}} - \mathrm{Tr}' \int \frac{\partial n^{(0)}(\mathbf{p}')}{\partial\mathbf{p}'}\hat{f}(\mathbf{p}',\mathbf{p})d\tau'\right]\delta\hat{n}(\mathbf{p})d\tau \quad . \tag{7.11}$$

Taking into account the relation

$$\frac{\partial n^{(0)}(\mathbf{p})}{\partial\mathbf{p}} = -\delta(\epsilon^{(0)}(p) - \epsilon_F)\frac{\partial\epsilon^{(0)}(p)}{\partial\mathbf{p}} \tag{7.12}$$

and also the representation (7.7), we finally obtain

$$\mathbf{j}_0 = \mathrm{Tr} \int \frac{\mathbf{p}}{M}\,\delta\hat{n}(\mathbf{p})\, d\tau = \mathrm{Tr} \int \frac{\partial\epsilon^{(0)}}{\partial\mathbf{p}}\left[1 + \frac{F_1}{3}\right]\delta\hat{n}(\mathbf{p})d\tau \quad , \tag{7.13}$$

where $F_1 = (F_1^{pp} + F_1^{pn})/2$ with $F_1^{pp} = F_1^{nn} \neq F_1^{pn} = F_1^{np}$ being the coefficients at $l = 1$ for the interaction of pp, nn and np quasiparticles (see Eqs. (7.7) and (7.9)). It is seen that due to the interaction between quasiparticles any motion of particles is accompanied by a backflow of quasiparticles

(corresponding to the term proportional to F_1). From Eqs. (7.3) and(7.13) it follows that the effective mass M^* is equal to:

$$M^* = M\left[1 + \frac{F_1}{3}\right]. \tag{7.14}$$

For the isovector current $\mathbf{j}_1$ one obtains in the same way:

$$\mathbf{j}_1 = \mathrm{Tr}\int \frac{\partial\hat{\epsilon}}{\partial\mathbf{p}}\tau_3\hat{n}(\mathbf{p})\,d\tau \;= \mathrm{Tr}\int \frac{\mathbf{p}}{M}\frac{1+F_1'/3}{1+F_1/3}\tau_3\,\delta\hat{n}(\mathbf{p})d\tau \quad . \tag{7.15}$$

The electromagnetic current is given by $\mathbf{j}_{em} = (e/2)(\mathbf{j}_0 + \mathbf{j}_1)$. Therefore,

$$\mathbf{j}_{em} = \frac{e}{2}\mathrm{Tr}\int \frac{\mathbf{p}}{M}\left[1 + \tau_3 + \frac{1}{3}\,\frac{F_1' - F_1}{1+F_1/3}\,\tau_3\right]\delta\hat{n}(\mathbf{p})d\tau \quad . \tag{7.16}$$

Note that $F_1' = (F_1^{pp} - F_1^{pn})/2$. The application of a relativistic approach [88, 259, 260]leads to some modification of the mentioned results. A review of the numerous articles devoted to this subject can be found in [88].

In order to obtain an information on the parameters of Fermi liquid theory for nuclei it is possible to start from a pion-exchange and ρ-meson-exchange interaction in the Born approximation. Then one can apply the Brueckner approach to take into account higher orders of perturbation theory with respect to the interaction between particles (see [87, 261–263] and the review [264]). The operator for the one-pion-exchange potential is of the form

$$V_\pi(\mathbf{p}) = -\frac{f^2}{m_\pi^2(m_\pi^2+p^2)}\,(\boldsymbol{\sigma}\cdot\mathbf{p})(\boldsymbol{\sigma}'\cdot\mathbf{p})\boldsymbol{\tau}\cdot\boldsymbol{\tau}' = \tag{7.17}$$
$$-\frac{f^2}{m_\pi^2}\left[\frac{S_T}{m_\pi^2+p^2} + \frac{1}{3}\boldsymbol{\sigma}\cdot\boldsymbol{\sigma}' - \frac{m_\pi^2}{3\,(m_\pi^2+p^2)}\,\boldsymbol{\sigma}\cdot\boldsymbol{\sigma}'\right]\boldsymbol{\tau}\cdot\boldsymbol{\tau}',$$

where $S_T = (\boldsymbol{\sigma}\cdot\mathbf{p})(\boldsymbol{\sigma}'\cdot\mathbf{p}) - (\boldsymbol{\sigma}\cdot\boldsymbol{\sigma}')\,p^2/3$. The potential arising from ρ-exchange is

$$V_\rho(\mathbf{p}) = -\frac{f_\rho^2}{m_\rho^2(m_\rho^2+p^2)}\,[\boldsymbol{\sigma}\cdot\boldsymbol{\sigma}'\,p^2 - (\boldsymbol{\sigma}\cdot\mathbf{p})(\boldsymbol{\sigma}'\cdot\mathbf{p})]\,\boldsymbol{\tau}\cdot\boldsymbol{\tau}' = \tag{7.18}$$
$$-\frac{f_\rho^2}{m_\rho^2}\left[-\frac{S_T}{m_\rho^2+p^2} + \frac{2}{3}\boldsymbol{\sigma}\cdot\boldsymbol{\sigma}' - \frac{2m_\rho^2}{3\,(m_\rho^2+p^2)}\,\boldsymbol{\sigma}\cdot\boldsymbol{\sigma}'\right]\boldsymbol{\tau}\cdot\boldsymbol{\tau}'.$$

Taking into account ω- and σ-exchange potentials one is lead to replacing f_ρ^2 in (7.18) by $\tilde{f}_\rho^2 = 0.4\,f_\rho^2$ [87]. Equations (7.17) and (7.18) correspond to the contributions to the nuclear exchange potential given in Eq. (3.12), except that here a separation into central and tensor parts is given.

Brown and Rho [87] arrived at a quantitative derivation of the effective mass M^* making use of such a model, where the isospin dependent interactions between nucleons consist of π and ρ exchanges. The effective mass M^* is obtained by evaluating the self energy stemming from the Fock term. The results of this investigation are summarized in the following. Writing $\epsilon(p)$ as

$$\epsilon(p) = \frac{p^2}{M} + \Sigma(p, \epsilon(p))\,, \tag{7.19}$$

where $\Sigma(p, \epsilon(p))$ is the quasiparticle self-energy. Then using the definition of the effective mass (7.3) one has [87]:

$$\frac{1}{M^*} = \frac{1}{M} + \frac{1}{p_F}\,\frac{\partial\Sigma(p,\epsilon(p)}{\partial p}\Big|_{p=p_F} \tag{7.20}$$

Substituting this relation into (7.14) and calculating the one-pion-exchange contribution to the self-energy, one obtains an expression for the pion contribution to F_1 [87]:

$$F_{1\,\pi} = -\frac{9f^2M^*}{8\pi^2 p_F}\left[\frac{m_\pi^2+2p_F^2}{2p_F^2}\ln\frac{m_\pi^2+4p_F^2}{m_\pi^2}-2\right] = -0.46\frac{M^*}{M}\,. \tag{7.21}$$

The contribution of ρ-exchange to F_1 reads [87]:

$$F_{1\,\rho} = -0.56\frac{M^*}{M}\,. \tag{7.22}$$

Taking a sum of (7.21) and (7.22) and then using (7.14) one has:

$$\frac{M^*}{M} = 0.75 \quad , \quad F_1 = -0.76 \quad . \tag{7.23}$$

The numerical value for M^*/M is in a good agreement with the experimental value given in Table 4.2 for the mass region $A = 197$–209 of spherical nuclei. It is interesting to note that the A-dependence of the effective mass M^* also finds a satisfactory explanation in the work of Brown and Rho [87]. The explanation which can be extracted from that work is as follows. First of all we have to realize that the excellent agreement between theory and experiment found in (7.23) and the $A = 197$–209 mass range discussed in Table (4.2), respectively, partly comes as a surprise because in its theoretical derivation it was assumed [87] that most of the difference $M - M^*$ comes from the Fock terms for $\pi-$ and $\rho-$ exchange, whereas it was discussed in that paper that quasiparticle-phonon couplings also have an effect on the difference $M - M^*$ but with the opposite sign. The mathematical procedure of treating the two effects is very much the same. The only difference is that the pion propagator has to be replaced by the appropriate energy denominator for the intermediate state involving quasiparticle plus vibration. The essential point is that the contributions from couplings to vibrations leads to effects close to the nuclear surface only. High-l orbitals are confined by the centrifugal barrier more to the interior of nuclei than those of low-l ones [87]. Since states with high angular momentum dominate at the ^{208}Pb shell closures this property is exactly what we need to understand the A-dependence of M^*/M with a minimum in the ^{208}Pb mass range.

The operators of the pion-exchange and ρ-exchange potentials are proportional to

$$\boldsymbol{\tau}\cdot\boldsymbol{\tau}' = 2(\tau_+\tau'_- + \tau_-\tau'_+) + \tau_3\tau'_3 \quad ,$$

where τ_+ and τ_- are isospin raising and lowering operators, respectively. Therefore, the following relation between F_1^{pp} and F_1^{pn} is obtained [87]:

$$F_1^{pn} = 2F_1^{pp} \tag{7.24}$$

Starting from Eqs. (7.17) and (7.18) one can obtain the contributions of pion-exchange and ρ-exchange to the quasiparticle-quasiparticle interaction (7.7). For this purpose one can calculate the forward scattering amplitude of a quasiparticle with $p > p_F$ and a hole with momentum $p < p_F$. After the Fourier transform to configuration space the momentum independent terms in (7.17) and (7.18) are proportional to $\delta(\mathbf{r})$. Due to the strong short-range repulsion from the ω-meson, the wave function vanishes at zero distance between the nucleons. Therefore, the momentum-independent terms in (7.17) and (7.18) can be omitted. Neglecting also the tensor part of the interaction (proportional to S_T), we have [264] :

$$\hat{f}_\pi(\mathbf{p},\mathbf{p}') = \boldsymbol{\sigma}\cdot\boldsymbol{\sigma}'\boldsymbol{\tau}\cdot\boldsymbol{\tau}'\,\frac{f^2}{3\,m_\pi^2} + \tag{7.25}$$

$$(-9 + 3\boldsymbol{\sigma}\cdot\boldsymbol{\sigma}' + 3\boldsymbol{\tau}\cdot\boldsymbol{\tau}' - \boldsymbol{\sigma}\cdot\boldsymbol{\sigma}'\boldsymbol{\tau}\cdot\boldsymbol{\tau}')\,\frac{f^2}{12\,(m_\pi^2+(\mathbf{p}-\mathbf{p}')^2)}\,.$$

Here the first term corresponds to particle-hole annihilation and the second one to particle-hole exchange. In the last case the following identities have been used:

$$\boldsymbol{\sigma}_{\alpha\beta}\boldsymbol{\sigma}_{\delta\gamma} = \frac{3}{2}\delta_{\alpha\gamma}\delta_{\delta\beta} - \frac{1}{2}\boldsymbol{\sigma}_{\alpha\gamma}\boldsymbol{\sigma}_{\delta\beta}$$

and the same for isospin matrices. The contribution of ρ-exchange has the form:

$$\hat{f}_\rho(\mathbf{p},\mathbf{p}') = \boldsymbol{\sigma}\cdot\boldsymbol{\sigma}'\boldsymbol{\tau}\cdot\boldsymbol{\tau}'\,\frac{2\tilde{f}_\rho^2}{3\,m_\rho^2} + \tag{7.26}$$

$$(-9 + 3\boldsymbol{\sigma}\cdot\boldsymbol{\sigma}' + 3\boldsymbol{\tau}\cdot\boldsymbol{\tau}' - \boldsymbol{\sigma}\cdot\boldsymbol{\sigma}'\boldsymbol{\tau}\cdot\boldsymbol{\tau}')\,\frac{\tilde{f}_\rho^2}{6\,(m_\rho^2 + (\mathbf{p}-\mathbf{p}')^2)}\,.$$

Multiplying both sides of (7.25) by $P_1(x) = x = \mathbf{p}\cdot\mathbf{p}'/p^2$ and taking the integral over x from minus one to one, we obtain expressions for the Landau parameters at $l = 1$. As it should be, the result for $F_{1\,\pi}$ agrees with (7.21). It is clear from (7.25) and (7.26) that

$$F_1' = G_1 = -\frac{1}{3}\,F_1 = 0.25 \quad , \quad G_1' = \frac{1}{9}\,F_1 = -0.08 \quad . \tag{7.27}$$

Even though F_1' is not known with great precision, a 10–20 per cent uncertainty in it [96] only has a 1–2 per cent effect in the quantities of interest here. The discussion of the Landau parameters at $l = 0$ as well as the contribution of tensor interaction can be found in the review [264].

Let us now pass to the consideration of the enhancement constant $\overset{\circ}{\kappa}{}^{GDR}$ and its connection with the parameters of the Fermi liquid. It was shown in [86] that without taking into account tensor correlations the following relation is valid for the modified TRK sum rule:

$$\int_0^\infty \overset{\circ}{\sigma}{}^{GDR}(\omega)\,d\omega = 2\pi^2\frac{e^2}{M}\,\frac{NZ}{A}(1 + \overset{\circ}{\kappa}{}^{GDR}) =$$

$$2\pi^2\frac{e^2}{M^*}\,\frac{NZ}{A}\left(1 + \frac{1}{3}F_1'\right) = 2\pi^2\frac{e^2}{M}\,\frac{NZ}{A}\frac{\left(1+\frac{1}{3}F_1'\right)}{\left(1+\frac{1}{3}F_1\right)} \quad , \tag{7.28}$$

where $\overset{\circ}{\sigma}{}^{GDR}(\omega)$ is the unretarded electric giant-dipole cross section for nuclear photoabsorption and $\overset{\circ}{\kappa}{}^{GDR}$ is the unretarded enhancement constant. It is seen from (7.28) that $\overset{\circ}{\kappa}{}^{GDR}$ is related not only to the effective mass M^* but also to the constant F_1'. Besides, if $F_1^{pn} = 0$ then $\overset{\circ}{\kappa}{}^{GDR} = 0$ (in this case $F_1' = F_1$). Equation (7.28) gives a relation for $\overset{\circ}{\kappa}{}^{GDR}$ in the form:

$$\overset{\circ}{\kappa}{}^{GDR} = \frac{\frac{1}{3}F_1' - \frac{1}{3}F_1}{1 + \frac{1}{3}F_1} \quad . \tag{7.29}$$

Alternatively, one may also express the ratio M^*/M of the effective mass and the free mass via $\overset{\circ}{\kappa}{}^{GDR}$. Using Eqs. (7.14), (7.24) and (7.29) one obtains

$$\frac{M^*}{M} = \left(1 + \frac{3}{4}\overset{\circ}{\kappa}{}^{GDR}\right)^{-1} \quad . \tag{7.30}$$

Using the relations given above it is easy to see that the theoretical results for M^*/M, F_1 and F_1' are nicely consistent with the experimental quantity $\overset{\circ}{\kappa}{}^{GDR} = 0.46$ (see also Table 4.2).

We now return to tensor correlations. The calculation of the total enhancement constant κ with the use of its representation as a double commutator [172] gives $\kappa \sim 1$, if the tensor correlations in

the ground state are taken into account. In this paper [172] it was noted that the total enhancement constant κ consists of two pieces, $\kappa = \kappa' + \Delta\kappa$, where only κ' has a relation to the Sachs magnetic moment. Therefore, we have to conclude that the quantities $\overset{\circ}{\kappa}{}^{GDR}$ and κ' may be identified with each other. One consequence of this identification is that the short-range tensor correlations giving rise to $\Delta\kappa$ are not important for giant resonances as anticipated above. In fact short-range tensor correlations give the main contribution to the quasi-deuteron part of the total enhancement constant (see [172]).

We present here a simple derivation of (7.28). The cross section $\overset{\circ}{\sigma}{}^{GDR}$ is of the form:

$$\overset{\circ}{\sigma}{}^{GDR}(\omega) = \frac{4\pi^2}{3}\omega \sum_n |\langle n|\ \mathbf{d}\ |0\rangle|^2\, \delta(E_0 + \omega - E_n)\,, \tag{7.31}$$

where $\mathbf{d}$ is the dipole moment operator with respect to the center of mass of the nucleus,

$$\mathbf{d} = e\frac{N}{A}\sum_i \mathbf{r}_{ip} - e\frac{Z}{A}\sum_i \mathbf{r}_{in}\,. \tag{7.32}$$

The additional indices p and n indicate that in that term the sum is taken over only protons and only neutrons, respectively. Using the relation $\mathbf{j}_{em} = i[H, \mathbf{d}]$, we get

$$\int_0^\infty \overset{\circ}{\sigma}{}^{GDR}(\omega)\, d\omega = \frac{2\pi^2}{3i}\,\langle 0|\,[\mathbf{d}, \mathbf{j}_{em}]\,|0\rangle \quad . \tag{7.33}$$

It follows from (7.16) that in the c.m. frame the electromagnetic current is given by

$$\begin{aligned}\mathbf{j}_{em} &= \frac{e}{2M}\left[(2 + \overset{\circ}{\kappa}{}^{GDR})\sum_i\left(\mathbf{p}_{ip} - \sum_j \frac{\mathbf{p}_{jp} + \mathbf{p}_{jn}}{A}\right) - \overset{\circ}{\kappa}{}^{GDR}\sum_i\left(\mathbf{p}_{in} - \sum_j \frac{\mathbf{p}_{jp} + \mathbf{p}_{jn}}{A}\right)\right] \\ &= \frac{e(1 + \overset{\circ}{\kappa}{}^{GDR})}{M}\left[\frac{N}{A}\sum_i \mathbf{p}_{ip} - \frac{Z}{A}\sum_i \mathbf{p}_{in}\right] \quad .\end{aligned} \tag{7.34}$$

Substituting (7.32) and (7.34) into (7.33) and evaluating the commutator, we get (7.28).

Next we discuss the low-energy limit of the Compton scattering amplitude. Within the framework of second-order perturbation theory the resonance amplitude in the long-wavelength approximation is given by:

$$R(\omega, \theta) = -\sum_\nu \left\{\frac{\langle f|\,\mathbf{j}_{em}\cdot\boldsymbol{\epsilon}_2\,|\nu\rangle\,\langle\nu|\,\mathbf{j}_{em}\cdot\boldsymbol{\epsilon}_1\,|i\rangle}{E_0 - E_\nu + \omega} + \frac{\langle f|\,\mathbf{j}_{em}\cdot\boldsymbol{\epsilon}_1\,|\nu\rangle\,\langle\nu|\,\mathbf{j}_{em}\cdot\boldsymbol{\epsilon}_2\,|i\rangle}{E_0 - E_\nu - \omega}\right\} \tag{7.35}$$

Again expressing the current via the commutator of the electric dipole moment with the Hamiltonian it is easy to extract the low-energy limit of the resonance amplitude:

$$R(0, \theta) = \frac{1}{2i}\left\{\langle 0|\,[\boldsymbol{\epsilon}_1\cdot\mathbf{d}, \boldsymbol{\epsilon}_2\cdot\mathbf{j}_{em}]\,|0\rangle + \langle 0|\,[\boldsymbol{\epsilon}_2\cdot\mathbf{d}, \boldsymbol{\epsilon}_1\cdot\mathbf{j}_{em}]\,|0\rangle\right\} \quad . \tag{7.36}$$

Then it follows from (7.32) and (7.34) that

$$R(0, \theta) = \boldsymbol{\epsilon}_1\cdot\boldsymbol{\epsilon}_2\frac{e^2}{M}\frac{ZN}{A}(1 + \overset{\circ}{\kappa}{}^{GDR})\,. \tag{7.37}$$

Using the low-energy theorem we may also obtain the low-energy limit of the relevant seagull amplitude

$$B(0, \theta) + S_{GR}(0, \theta) = -\boldsymbol{\epsilon}_1\cdot\boldsymbol{\epsilon}_2\frac{Z^2e^2}{MA} - R(0, \theta) = -\boldsymbol{\epsilon}_1\cdot\boldsymbol{\epsilon}_2\frac{Ze^2}{M}\left(1 + \frac{N}{A}\overset{\circ}{\kappa}{}^{GDR}\right)\,. \tag{7.38}$$

It is possible to derive Eq. (7.38) directly, when the explicit expression, Eq. (3.61), for the total seagull amplitude is translated into the language of Fermi liquid theory. One has

$$B(0,\theta)+S_{GR}(0,\theta)=\frac{i}{2}\left\{\langle f|\left[\boldsymbol{\epsilon}_1\cdot\mathbf{D}\,,\ \boldsymbol{\epsilon}_2\cdot\mathbf{J}\right]+\left[\boldsymbol{\epsilon}_2\cdot\mathbf{D}\,,\ \boldsymbol{\epsilon}_1\cdot\mathbf{J}\right]|i\rangle\right\} \tag{7.39}$$

with

$$\mathbf{D}=\mathbf{d}+\frac{eZ}{A}\sum_i\left(\mathbf{r}_{ip}+\mathbf{r}_{in}\right),\quad \mathbf{J}=\mathbf{j}_{em}+\frac{eZ}{AM}\sum_i\left(\mathbf{p}_{ip}+\mathbf{p}_{in}\right). \tag{7.40}$$

Calculating the commutator we obtain again Eq. (7.38).

When nucleons inside a nucleus have an angular momentum l they also produce an angular (Sachs) magnetic moment. Meson exchange currents modify this angular magnetic moment and it is easy to derive from Eq. (7.34) that for the proton this modification is given by

$$\delta g_l^{meson}(p)=\frac{N}{A}\mathring{\kappa}^{GDR}. \tag{7.41}$$

For the neutron one has

$$\delta g_l^{meson}(n)=-\frac{Z}{A}\mathring{\kappa}^{GDR}. \tag{7.42}$$

As a result, we obtain that the isovector part of the angular momentum correction is given by

$$\delta g_l^{(iv)}=\frac{1}{2}\left(\delta g_l^{meson}(p)-\delta g_l^{meson}(n)\right)=\frac{1}{2}\mathring{\kappa}^{GDR}. \tag{7.43}$$

This relations between $\delta g_l^{(iv)}$ and $\mathring{\kappa}^{GDR}$ is known as the Fujita-Hirata relation [87, 172, 173, 265–267]. A detailed investigation of it has been performed in [172] with special attention on the role of tensor correlations.

The Fujita-Hirata relation opens the possibility to compare different measurable quantities related to meson exchange currents with each other as there are the strength of the giant-dipole resonance and the magnetic moments of nucleons in a nucleus. Taking the result for nuclei with a ^{208}Pb double-magic core, (*cf.* (4.48)) $\mathring{\kappa}^{GDR}=0.46\pm0.05$, we arrive at

$$\delta g_l^{meson}(p)=0.28\pm0.02,\qquad \delta g_l^{meson}(n)=-0.18\pm0.02 \tag{7.44}$$

corresponding to

$$\delta g_l^{(iv)}=0.23\pm0.03. \tag{7.45}$$

Given the validity of the Fujita-Hirata relation we may consider these quantities in (7.44) and (7.45) as experimental results which may be compared with predictions. We find good agreement with the prediction of Brown and Rho [87], *viz.*

$$\delta g_l^{meson}(p)=0.27,\qquad \delta g_l^{meson}(n)=-0.17 \tag{7.46}$$

and with the prediction of Hyuga et al. [268], *viz.*

$$\delta g_l^{meson}(p)=0.27,\qquad \delta g_l^{meson}(n)=-0.14. \tag{7.47}$$

The quantities δg_l^{meson} are not directly observable in measurements of magnetic moments because of the effects of higher-order configuration mixing. For a certain fraction of time protons and neutrons are correlated to each other producing an additional angular momentum, and related to this a correction δg_l^{high} to the orbital g-factor. An analysis of mesonic effects on nuclear magnetic moments has

been carried out by Yamazaki [269]. After correcting for first-order configuration mixing he arrives at anomalous orbital g-factors of

$$\delta g_l^{obs}(p) = 0.15 \pm 0.02, \qquad \delta g_l^{obs}(n) = -0.05 \pm 0.02, \tag{7.48}$$

consistent for all measured g-factors of nuclear states having a ^{208}Pb core. Comparing these quantities with our results of (7.44) we find

$$\delta g_l^{obs} - \delta g_l^{meson} = -(0.13 \pm 0.03)\,\tau_3, \tag{7.49}$$

[$\tau_3(p) = +1$, $\tau_3(n) = -1$]. This result (7.49) may be compared with the predicted [268, 270] effects of higher-order configuration mixing, *viz.*,

$$\delta g_l^{high}(p) = -0.15, \qquad \delta g_l^{high}(n) = +0.10. \tag{7.50}$$

We notice that the "experimental" result (7.49) is purely isovector, whereas the predictions (7.50) suggests some isoscalar component. However, in view of the error given (7.49) it is not possible to draw any conclusion from this difference.

A summary of these results is given in Fig. 7.1. The first column shows the result of the measurement of magnetic moments carried out by Yamazaki [269]. The second column shows the quantities δ_l^{meson} obtained from the experimental $\mathring{\kappa}^{GDR}$ on the basis of the Fijita-Hirata relation together with higher-order correction δg_l^{high} obtained as a difference of δ_l^{meson} in column II and δg_l^{obs} in column I. Column III shows the predictions of Hyuga et al. [268] and column 4 the prediction of Brown and Rho [87].

Figure 7.1: *Summary of results on the Fujita-Hirata relation. Column I: Experimental result of Yamazaki [269]. Column II: δg_L^{meson} calculated from the experimental $\mathring{\kappa}^{GDR}$ and δg_L^{high} obtained as a difference between δ_l^{meson} of column II and δg_L^{obs} of column I. Column III: Predictions of Hyuga et al. [268]. Column IV: Predictions of Brown and Rho [87].*

The quasiparticle aspect of nucleons in a nucleus may be discussed in different forms. Instead of considering the dynamics of nucleon interactions explicitly, as done in Landau's Fermi liquid theory and its interpretation by Brown and Rho [87] there are attempts to view the role of the nuclear environment as a modification of the vacuum [271]. The advantages of this approach are that it is possible to make use of different models like the chiral mean field and the Walecka model of nuclear matter [272] and to arrive at new predictions which are not that easy to obtain within the framework of the original Fermi liquid theory. One disadvantage is that these new vacua are less familiar than the building blocks of Fermi liquid theory, thus making it desirable to build bridges between these different aspects of nuclear matter. The most recent works going into this direction are those of G.E. Brown [96], Friman and Rho [97], Brown and Rho [98] and Rho [273].

In [96] essentially the same effective mass M^*, which is related to the Migdal parameter F_1 as in Eq. (7.14), is also related to a (negative) scalar mean field Φ of the Walecka type [272] via

$$M^* = M + g_{\sigma NN}\Phi. \tag{7.51}$$

In terms of (7.51) the primary process is the lowering of the mass from M to M^*. The physical reason for this lowering of the mass is that the scalar mean field with the coupling constant $g_{\sigma NN}$ gives an attractive scalar potential. Both descriptions, *viz.* the velocity dependence of quasi-particle interactions in the Fermi liquid and the lowering of the *in-medium* mass lead to the same increase of the quasiparticle velocity $v = p/M^*$ as compared to p/M and these two interpretations are equivalent.

This equivalence is seen in a relativistic formulation, where Lorentz invariance provides a connection between the two interpretations. These matters are reviewed in Brown et al. [88].

A further aspect of the in-medium modification of the nucleon-nucleon interaction has been investigated Brown and Rho in [91]. They discuss the enhancement of the ρ meson tensor coupling to the nucleon. The ρ-meson is assumed to acquire an effective mass inside the nuclear medium with

$$\frac{m_\rho^*}{m_\rho} \simeq \frac{M^*}{M} \simeq \frac{3}{4} \tag{7.52}$$

as suggested by the general concept of Brown and Rho scaling [92] and by the Fermi liquid theory together with the experimental value of $\overset{\circ}{\kappa}{}^{GDR} = 0.46$. It is shown [91] that this implies that in the nuclear medium the ρ-meson tensor force is enhanced by a factor 16/9.

8 Dispersion relations at fixed momentum transfer for nuclear Compton scattering

In the previous sections phenomenological approaches have been applied in order to obtain the angular dependence of the Compton scattering amplitude. One of the main guidelines has been the fulfilment of a dispersion relation in forward direction, together with the requirement that the resonance parts of the amplitude should vanish in the high-energy limit at arbitrary scattering angle. Another ingredient in this construction of the Compton amplitude has been the correct low-energy behaviour of each (electric and magnetic) multipole. In this section we investigate the angular dependence of the nuclear Compton amplitude within a different approach based on a dispersion theory for the invariant amplitudes at fixed momentum transfer. This approach gives a correct form of dispersion relations for the resonance and partial-wave amplitudes which sometimes are written too naively.

8.1 General structure of the Compton amplitude

In the case of spin-0 nuclei, which are considered in this review, the general form (see *e.g.* [99]) of the Compton scattering amplitude T is

$$T(\omega,t) = \omega^2 \left\{ \Big(A_1(\omega,t) + A_2(\omega,t) \Big)\, \boldsymbol{\epsilon}_1 \cdot \boldsymbol{\epsilon}_2 + \Big(A_1(\omega,t) - A_2(\omega,t) \Big)\, \mathbf{s}_1 \cdot \mathbf{s}_2 \right\}, \tag{8.1}$$

where $A_1(\omega,t)$ and $A_2(\omega,t)$ are invariant amplitudes and

$$t = -\mathbf{q}^2 = -2\omega^2(1-\cos\theta) \tag{8.2}$$

is the square of momentum transfer. Here all recoil corrections are neglected. The form (8.1) for the amplitude is most convenient, when a discussion of low-energy properties, such as sum rules and the behaviour of multipole amplitude below resonance energies, is intended. The invariant amplitudes A_i, which appear in a Lorentz-invariant form of the Compton amplitude as soon as unphysical (kinematical) singularities and zeroes are eliminated, are related to the helicity non-flip amplitude $T_{1,1}$ and the helicity flip amplitude $T_{1,-1}$ for a circularly polarized photon via

$$A_1 = \frac{T_{1,1}(\omega,t)}{\omega^2(1+\cos\theta)} = 2\frac{T_{1,1}(\omega,t)}{(4\omega^2+t)}\,, \quad A_2 = \frac{T_{1,-1}(\omega,t)}{\omega^2(1-\cos\theta)} = -2\frac{T_{1,-1}(\omega,t)}{t}. \tag{8.3}$$

Due to the conservation of angular momentum only $T_{1,1}$ differs from zero in forward direction. For linearly polarized photons the two non-vanishing amplitudes are

$$T_{||} = T_{1,1} - T_{1,-1}\,, \quad T_{\perp} = T_{1,1} + T_{1,-1}\,, \tag{8.4}$$

where $T_{||}$ ($T_{\perp}$) corresponds to the polarization of both photons being parallel (perpendicular) to the scattering plane.

Furthermore, we will apply the usual partial wave expansion of the helicity amplitudes (see *e.g.* [274, 275]),

$$T_{1,\pm1}(\omega,\theta) = \sum_{j=1}^{\infty} T^j_{1,\pm1}(\omega)\; d^j_{1,\pm1}(\theta), \tag{8.5}$$

where the d-functions are given by the formulae [275, 276]

$$\begin{aligned} d^j_{1,1}(\theta) &= \cos^2\frac{\theta}{2}\, F(-j+1, j+2, 1, \sin^2\frac{\theta}{2}), \\ d^j_{1,-1}(\theta) &= \frac{j(j+1)}{2}\sin^2\frac{\theta}{2}\, F(-j+1, j+2, 3, \sin^2\frac{\theta}{2}). \end{aligned} \tag{8.6}$$

Here $F(a,b,c,x) = 1 + (ab/c)(x/1!) + \ldots$ is the hypergeometric function. Equations (8.6) can be rewritten as

$$\begin{aligned} d^j_{1,\pm1}(\theta) &= \frac{1 \pm z}{j(j+1)}\Big(P'_j(z) + (z \mp 1)P''_j(z)\Big) \\ &= \pm P_j(z) + \frac{1 \mp z}{j(j+1)}\, P'_j(z), \quad z = \cos\theta, \\ d^j_{1,-1}(\theta) &= (-1)^{j-1} d^j_{1,+1}(\pi - \theta). \end{aligned} \tag{8.7}$$

The functions $d^j_{\lambda\lambda'}$ satisfy an orthogonality relation:

$$\int_{-1}^{1} d^j_{\lambda\lambda'}(\theta) d^{j'}_{\lambda\lambda'}(\theta)\, d(\cos\theta) = \frac{2}{2j+1}\delta_{jj'}. \tag{8.8}$$

The partial waves $T^j_{1,\pm1}(\omega)$ contain electric (T^{Ej}) and magnetic (T^{Mj}) multipoles:

$$T^j_{1,\pm1}(\omega) = T^{Ej} \pm T^{Mj}, \tag{8.9}$$

what can be easily inferred from (3.45). Due to the optical theorem the imaginary parts of the partial amplitudes T^{Ej} and T^{Mj} give rise to partial absorption cross sections σ^{Ej} and σ^{Mj} via

$$\frac{\omega}{4\pi}\,\sigma^{\lambda j}(\omega) = \mathrm{Im}\; T^{\lambda j}(\omega), \tag{8.10}$$

where $\lambda = E, M$.

In order to obtain a definite multipole amplitude, let us start from a dispersion relation at fixed momentum transfer t for the invariant amplitudes A_i. From Eq. (8.3) one can expect that at fixed t the amplitude A_1 tends to zero as ω tends to infinity and hence satisfies an ordinary unsubtracted dispersion relation. At the same time the amplitude A_2 does not generally tend to zero and therefore a dispersion relation for A_2 should include either a subtraction or a safe regularization. The regularization can be implemented by cutting the dispersion integral at some high maximal energy $\omega_{\max}$ and by adding an asymptotic contribution $a(t)$ which is energy independent (but is momentum-transfer dependent) at low and medium energies $\omega^2 \ll \omega^2_{\max}$ — see a parallel discussion of the nucleon case in [99, 101]. For the sake of simplicity we disregard here such a regularization which can be easily restored. Since the asymptotic piece $a(t)$ does not depend on the energy, it does not affect the resonance part $R(\omega,t)$ of the Compton scattering amplitude and enters only into the seagull $S(\omega,t)$, to its helicity-flip energy-dependent part.

So, we write the dispersion relation for either amplitude A_i in the same form with the dispersion integral taken up to infinity and without the explicit addition $a(t)$ to the amplitude A_2:

$$A_i(\omega,t) = -\frac{Z^2e^2}{2AM\omega^2} + \frac{2}{\pi}\int\limits_0^\infty \mathrm{Im}A_i(\omega',t)\,\frac{\omega'\,d\omega'}{\omega'^2 - \omega^2 - i0}. \tag{8.11}$$

Here the pole contribution (*viz.* the first term on the r.h.s.) ensures the Thomson limit for the total amplitude $T(\omega,t)$.

In the following we apply the partial-wave expansion (8.5) and write the imaginary parts of A_i through the partial absorption cross sections σ^{Ej} and σ^{Mj}. Such a procedure may be invalid at high $|t|$ exceeding a binding threshold for disintegrating the nucleus into separate parts. In this case we consider the resulting formulas in the sense of an analytical continuation. Nevertheless, this procedure allows us to investigate the deviation of the exact partial scattering amplitudes from the naive assumption of a purely Lorentzian form for its resonance part.

The use of Eq. (8.3) leads to dispersion relations for the helicity amplitudes. With the help of Eq. (8.5) and Eq. (8.10) for the r.h.s. of Eq. (8.11), one obtains

$$T_{1,\pm1}(\omega,\theta) = (1\pm\cos\theta)\left\{-\frac{Z^2e^2}{2AM} + \frac{\omega^2}{2\pi^2}\sum_{j=1}^{\infty}\int_0^{\infty}\frac{d^j_{1,\pm1}(\theta')}{1\pm\cos\theta'}\,\frac{\sigma^{Ej}(\omega')\pm\sigma^{Mj}(\omega')}{\omega'^2-\omega^2-i0}\,d\omega'\right\} \tag{8.12}$$

where θ' is a function of θ, ω and ω', due to the condition that the square of the momentum transfer $q^2=-t$ is fixed,

$$\omega'^2\,(1-\cos\theta') = \omega^2\,(1-\cos\theta) = -\frac{t}{2}. \tag{8.13}$$

Here the θ'-dependent factors in the braces of Eq. (8.12) are polynomials in $\cos\theta'$ and hence polynomials in $x=\omega^2/\omega'^2$.

Let us multiply both sides of Eq. (8.12) by $d^J_{\lambda,\lambda'}$ and take the integral with respect to θ using Eqs. (8.5) and (8.8). As a result we obtain

$$T^{EJ}(\omega)\pm T^{MJ}(\omega) = -\frac{Z^2e^2}{AM}\,\delta_{J,1} + \frac{\omega^2}{2\pi^2}\sum_{L=1}^{\infty}\int_0^{\infty}\Phi^{(\pm)}_{JL}(\omega,\omega')\,\frac{\sigma^{EL}(\omega')\pm\sigma^{ML}(\omega')}{\omega'^2-\omega^2-i0}\,d\omega'. \tag{8.14}$$

The function $\Phi^{(\pm)}_{JL}$ has the following integral representation:

$$\Phi^{(\pm)}_{JL}(\omega,\omega') = \frac{2J+1}{2}\int_{-1}^{1}\frac{1\pm\cos\theta}{1\pm\cos\theta'}\,d^J_{1,\pm1}(\theta)d^L_{1,\pm1}(\theta')\,d(\cos\theta). \tag{8.15}$$

In all cases the function $\Phi^{(\pm)}_{JL}$ is a polynomial in x, whoes properties follows from the orthogonality relation (8.8) and can be summarized in the following way:

$$\Phi^{(\pm)}_{JL}(\omega,\omega') = \begin{cases} 0, & J>L,\\ x^{J-1}, & J=L,\\ x^{J-1}(1-x)\tilde\Phi^{(\pm)}_{JL}(x), & J<L,\end{cases} \tag{8.16}$$

where $\tilde\Phi^{(\pm)}_{JL}(x)$ is a polynomial of the $(L-J-1)$th power in x. By applying Eq. (8.16) to the dispersion relation (8.14) via (8.15) we obtain dispersion representations for the multipole amplitudes of nuclear Compton scattering:

$$T^{EJ}(\omega) = -\frac{(Ze)^2}{AM}\delta_{J1} + \frac{1}{2\pi^2}\int_0^{\infty}\left(\frac{\omega}{\omega'}\right)^{2J}\left\{\frac{\omega'^2\sigma^{EJ}(\omega')}{\omega'^2-\omega^2-i0} + \sum_{L>J}\left[\sigma^{EL}(\omega')A_{JL}(x)+\sigma^{ML}(\omega')B_{JL}(x)\right]\right\}d\omega', \tag{8.17}$$

and

$$T^{MJ}(\omega) = \frac{1}{2\pi^2}\int_0^{\infty}\left(\frac{\omega}{\omega'}\right)^{2J}\left\{\frac{\omega'^2\sigma^{MJ}(\omega')}{\omega'^2-\omega^2-i0} + \sum_{L>J}\left[\sigma^{ML}(\omega')A_{JL}(x)+\sigma^{EL}(\omega')B_{JL}(x)\right]\right\}d\omega'. \tag{8.18}$$

Here $A_{JL}(x)$ and $B_{JL}(x)$ are polynomials of $(L-J-1)$th power in x, with $x=(\omega/\omega')^2$:

$$A_{JL}(x) = \frac{1}{2}[\tilde\Phi^{(+)}_{JL}(x)+\tilde\Phi^{(-)}_{JL}(x)],\quad B_{JL}(x) = \frac{1}{2}[\tilde\Phi^{(+)}_{JL}(x)-\tilde\Phi^{(-)}_{JL}(x)]. \tag{8.19}$$

The first few of them are given by

$$
\begin{aligned}
&A_{12}(x) = 2, && B_{12}(x) = -1,\\
&A_{13}(x) = \tfrac{7}{2} - \tfrac{21}{4}x, && B_{13}(x) = -\tfrac{5}{2} + \tfrac{15}{4}x,\\
&A_{14}(x) = \tfrac{11}{2} - \tfrac{77}{4}x + \tfrac{77}{5}x^2, && B_{14}(x) = -\tfrac{9}{2} + \tfrac{63}{4}x - \tfrac{63}{5}x^2,\\
&A_{23}(x) = \tfrac{15}{4}, && B_{23}(x) = -\tfrac{5}{4},\\
&A_{24}(x) = \tfrac{39}{4} - 13x, && B_{24}(x) = -\tfrac{21}{4} + 7x,\\
&A_{34}(x) = \tfrac{28}{5}, && B_{34}(x) = -\tfrac{7}{5}.
\end{aligned}
\tag{8.20}
$$

Since each partial absorption cross section is nonzero only above an energy threshold corresponding to the first excitation level of the nucleus, no divergence at $\omega' = 0$ appears in Eqs. (8.17) and (8.18). Similar multipole dispersion relations are used in the analysis of pion photoproduction data [277]. The partial-wave series in (8.17), (8.18) may become divergent at high ω and should be understand in the sense of an analytical continuation in such a case.

One can see from the relations (8.17) and (8.18) that at $\omega \to 0$ the partial photoabsorption cross sections σ^{EJ} and σ^{MJ} give contributions to the partial amplitudes T^{EJ} and T^{MJ}, which are proportional to ω^{2J}. The asymptotic contribution $a(t)$ which is disregarded in the above consideration and which makes equal but opposite additions to T^{EJ} and T^{MJ} does not change this threshold behavior. The nonzero contributions of $\sigma^{\lambda' L}$ to $T^{\lambda J}$ with $L > J$ is another important property of the partial scattering amplitudes, which follows from (8.17) and (8.18). These properties may be used as a starting point to investigate the deviation of multipole amplitudes from a purely Lorentzian form.

8.2 Resonance and seagull amplitudes at fixed momentum transfer

In the previous section we obtained a representation for the total Compton scattering amplitude in non-forward direction, Eq. (8.12). Starting from this expression we now want to construct the t-dependence of the giant resonance, the quasi-deuteron and the seagull parts, which enter into the Compton amplitude T_A. The additional contribution T_N, which contains the electromagnetic polarizabilities of the nucleon, is not considered here. This decomposition should be consistent with the definitions (3.21), (3.22) and (3.29) given for the case of forward direction. Here our dispersion-theoretical method (as opposed to the operator-based techniques found *e.g.* in [70, 121, 278]) can be efficiently used to reconstruct these contributions to the Compton amplitude on the base of an experimental information. The t-dependence can consistently be constructed due to the use of dispersion relations at fixed momentum transfer.

Let us define the contributions of each of the three parts to the total (nuclear) helicity amplitudes $T^A_{1,\pm1}$ by

$$
T^A_{1,\pm1}(\omega, t) = R^{GR}_{1,\pm1}(\omega, t) + R^{QD}_{1,\pm1}(\omega, t) + S^{tot}_{1,\pm1}(\omega, t). \tag{8.21}
$$

The representations of the two resonant parts should fulfill certain requirements. In the dispersion integral contributing to the amplitude $R^{GR}_{1,\pm1}(\omega, t)$ instead of the full partial wave cross section $\sigma^{\lambda j}$ only $\sigma^{\lambda j}_{GR}$ should appear. In all other aspects it has the same form as the one in Eq. (8.12). Furthermore, some function of t, which does not depend on ω and ensures vanishing R^{GR} at high ω, has to be added. The amplitude $R^{QD}_{1,\pm1}(\omega, t)$ should have similar properties. It also is represented as a sum of a dispersion integral containing $\sigma^{\lambda j}_{QD}$ and some function of t. As for the seagull amplitude $S^{tot}_{1,\pm1}(\omega, t)$, the integration in the dispersion contribution should start from pion mass m_π with the integrand depending on the difference $\sigma^{\lambda j} - \sigma^{\lambda j}_{QD}$. The seagull amplitude has no resonance structure and corresponds to

the scattering by an object of small size in comparison with the nuclear radius R. More specifically, it can be argued (see *e.g.* [68, 72] and the discussion in sections 3.1 and 3.2) that two distinct processes contribute to S_{tot}, namely the Thomson scattering by individual nucleons (kinetic seagull) and the scattering by correlated nucleon pairs (mesonic seagull). For the latter, the characteristic size is of the order of $1/m_\pi$. The comparison of the nuclear radius R with the relevant interaction range for the processes contributing to the seagull amplitude leads to the conclusion that the t-dependence of the total seagull amplitude is similar to the nuclear form factor. We will investigate this point in more detail in section 9. Finally, using Eq. (3.43) and taking the above-mentioned properties into account, we get

$$S_{1,\pm1}(\omega,\theta) = (1\pm\cos\theta)\left\{ \; -\frac{Ze^2}{2M}\left(F_1(t)+\kappa\frac{N}{A}\,F_2(t)\right)+ \right. \tag{8.22}$$
$$\left. \frac{\omega^2}{2\pi^2}\sum_{j=1}^{\infty}\int\limits_{m_\pi}^{\infty}\frac{d^j_{1,\pm1}(\theta')}{1\pm\cos\theta'}\;\frac{\Delta\sigma^{Ej}(\omega')\pm\Delta\sigma^{Mj}(\omega')}{\omega'^2-\omega^2}\,d\omega' \;\right\},$$

with $\Delta\sigma(\omega)=\sigma_{tot}(\omega)-\sigma_{QD}(\omega)-A\sigma_N^{bound}(\omega)$, the function $F_1(t)$ being the nuclear one-body form factor and $F_2(t)$ corresponding also to a nuclear form factor but taking into account the finite size of a correlated nucleon pair (*cf.* sections 3.5 and 9).

Let us discuss the behaviour of Eq. (8.22) in the case $\omega \ll m_\pi$. Then $(-t) \ll m_\pi^2$ due to (8.13). Since the integral with respect to ω' starts from m_π, the same relation shows that also $\theta' \ll 1$. We can omit ω^2 in the denominator of the integrand in Eq. (8.22). However, it is not possible also to neglect θ', which would correspond to $t=0$, because as described above the t-dependence of any contribution to the seagull amplitude should approximately be given by a nuclear form factor. Since quasi-deuteron production occures from small regions of size $\sim 1/m_\pi \ll R$ scattered over the whole volume of the nucleus, many multipoles contribute to the integrand in (8.22), thus making the partial-wave expansion almost useless. It is physically clear, however, that the t-dependence of the integrand reflects a distribution of participating pn pairs in the nucleus, so that the integral is proportional to the two-body form factor $F_2(t)$. The coefficient of the proportionality can be identified with modifications of the electric and magnetic polarizabilities of the nucleon, $\delta\alpha$ and $\delta\beta$, caused by the mesonic seagull amplitude:

$$S_{1,\pm1}(\omega,\theta)=\frac{(1\pm\cos\theta)}{2}\left\{-\frac{Ze^2}{M}\left(F_1(t)+\kappa\frac{N}{A}\,F_2(t)\right)+A\omega^2\;(\delta\alpha\pm\delta\beta)\;F_2(t)\right\}. \tag{8.23}$$

The important quantities $\delta\alpha$ and $\delta\beta$ will be discussed in section 9 within a specific model, where it will also be shown that form factors accompaning κ, $\delta\alpha$ and $\delta\beta$ in (8.22) are actually not identical, as a consequence of a different configuration size of the correlated pn pairs determining these values. In this section, however, we disregard this nontrivial feature and use the same form factor $F_2(t)$ everywhere. It is also possible to discuss this particular form (8.23) of the seagull amplitude on the level of nuclear matrix elements, as was done in section 3.

Now, taking into account Eqs. (3.35), (3.41) and (8.22), we obtain an explicit representation of the resonance amplitudes from Eq. (8.12). For $R^{GR}_{1,\pm1}(\omega,t)$ we have

$$R^{GR}_{1,\pm1}(\omega,\theta)=\frac{(1\pm\cos\theta)}{2}\left\{\;\frac{Ze^2}{M}\left(-\frac{Z}{A}+F_1(t)+\kappa^{GR}\,\frac{N}{A}\,F_2(t)\right)+\right. \tag{8.24}$$
$$\left.\frac{\omega^2}{\pi^2}\sum_{j=1}^{\infty}\int\limits_{0}^{\infty}\frac{d^j_{1,\pm1}(\theta')}{1\pm\cos\theta'}\;\frac{\sigma^{Ej}_{GR}(\omega')\pm\sigma^{Mj}_{GR}(\omega')}{\omega'^2-\omega^2-i0}\;d\omega'\right\}.$$

This representation of the giant resonance amplitude, in which form factors appear explicitly, is convenient, as in the dispersive part each multipole contains the correct ω-dependence at low energies.

Similarly, for $R^{QD}_{1,\pm1}(\omega,t)$ one has

$$R^{QD}_{1,\pm1}(\omega,\theta) = \frac{(1\pm\cos\theta)}{2}\left\{\ \kappa^{QD}\,\frac{e^2}{M}\frac{ZN}{A}\,F_2(t) + \right. \tag{8.25}$$
$$\left.\frac{\omega^2}{\pi^2}\,\sum_{j=1}^{\infty}\int_0^{\infty}\frac{d^j_{1,\pm1}(\theta')}{1\pm\cos\theta'}\,\frac{\sigma^{Ej}_{QD}(\omega')\pm\sigma^{Mj}_{QD}(\omega')}{\omega'^2-\omega^2-i0}\,d\omega'\right\}.$$

In contrast to (8.24), the integral here involves many multipoles and therefore is less useful. It's physically clear again that the t-dependence of the integral mainly follows the two-body form factor F_2.

Now we should fulfill the requirement that the resonance amplitudes tend to zero at high ω and fixed t. Since in both amplitudes $R^{GR}_{1,-1}$ and $R^{QD}_{1,-1}$ the external factor $(1-\cos\theta)/2 = -t/(4\omega^2)$ tends to zero in this limit, they vanish independently of the explicit shape of the form factors. Moreover, the asymptotic piece $a(t)$ can also affect the helicity-flip amplitudes. Therefore, model-independent restrictions appear only from the asymptotic behaviour of $R^{GR}_{1,1}$ and $R^{QD}_{1,1}$. In the limit $\omega\to\infty$ the requirement of vanishing $R^{GR}_{1,1}$ leads to

$$\frac{Ze^2}{M}\left(-\frac{Z}{A}+F_1(t)+\kappa^{GR}\,\frac{N}{A}\,F_2(t)\right) = \frac{1}{\pi^2}\,\sum_{j=1}^{\infty}\int_0^{\infty}\frac{d^j_{1,1}(\theta')}{1+\cos\theta'}\,[\sigma^{Ej}_{GR}(\omega')+\sigma^{Mj}_{GR}(\omega')]\,d\omega'\,, \tag{8.26}$$

while the same condition for $R^{QD}_{1,1}$ gives

$$\kappa^{QD}\,\frac{e^2}{M}\,\frac{NZ}{A}\,F_2(t) = \frac{1}{\pi^2}\,\sum_{j=1}^{\infty}\int_0^{\infty}\frac{d^j_{1,1}(\theta')}{1+\cos\theta'}\,[\sigma^{Ej}_{QD}(\omega')+\sigma^{Mj}_{QD}(\omega')]\,d\omega'\,. \tag{8.27}$$

Using Eq. (8.26) we can express the giant resonance amplitude $R^{GR}_{1,\pm1}$ of Eq. (8.24) via the absorption cross sections $\sigma^{\lambda j}_{GR}$ only, without the explicit appearance of form factors. Putting t equal to zero in Eqs. (8.26) and (8.27) we obtain again the sum rules (3.36) and (3.42), since

$$\sigma_{GR}(\omega) = \sum_{j=1}^{\infty}\left(\sigma^{Ej}_{GR}(\omega)+\sigma^{Mj}_{GR}(\omega)\right)\,,\quad \sigma_{QD}(\omega) = \sum_{j=1}^{\infty}\left(\sigma^{Ej}_{QD}(\omega)+\sigma^{Mj}_{QD}(\omega)\right).$$

Expanding both sides of (8.26) with respect to t and comparing the coefficients, we obtain additional sum rules

$$\frac{Ze^2}{M}\,\frac{\pi^2(n!)^2 2^{2n+1}}{(2n+1)!}\,\left[\left\langle r^{2n}\right\rangle_1+\kappa^{GR}\,\frac{N}{A}\left\langle r^{2n}\right\rangle_2\right] = \tag{8.28}$$
$$\sum_{j=n+1}^{\infty}\frac{(j+n+1)!}{j(j+1)(j-n-1)!}\int_0^{\infty}\frac{d\omega}{\omega^{2n}}\left(\sigma^{Ej}_{GR}(\omega)+\sigma^{Mj}_{GR}(\omega)\right),\quad ,n>0$$

where the ordinary definition of the average values of r^{2n} is used. In the particular case of $n=1$ Eq. (8.28) gives

$$\frac{Ze^2}{M}\,\frac{4\pi^2}{3}\,\left[\left\langle r^2\right\rangle_1+\kappa^{GR}\,\frac{N}{A}\left\langle r^2\right\rangle_2\right] = \sum_{j=2}^{\infty}(j+2)(j-1)\int_0^{\infty}\frac{d\omega}{\omega^2}\left(\sigma^{Ej}_{GR}(\omega)+\sigma^{Mj}_{GR}(\omega)\right). \tag{8.29}$$

Restricting ourselves to the lowest electric multipole on the r.h.s. of Eq. (8.28) we reclaim the usual energy-weighted sum rules [279, 280]. In reality, only the lowest multipoles $E1$,$M1$,$E2$ are experimentally observed and taken into account in the analysis of scattering data [19, 32, 39]. For this case Eq.

(8.24) is of the following form:

$$R^{GR}_{1,\pm1}(\omega,\theta) = \frac{(1\pm\cos\theta)}{2}\left\{ \frac{Ze^2}{M}\left(-\frac{Z}{A}+F_1(t)+\kappa^{GR}\frac{N}{A}F_2^{GR}(t)\right)+ \right. \tag{8.30}$$
$$\left. \frac{\omega^2}{2\pi^2}\int\limits_0^\infty \frac{d\omega'}{\omega'^2-\omega^2-i0}\left[\sigma^{E1}_{GR}(\omega')\pm\sigma^{M1}_{GR}(\omega')+\sigma^{E2}_{GR}(\omega')\left(2-\frac{2\omega^2}{\omega'^2}(1-\cos\theta)\mp1\right)\right]\right.$$

At very low energies it agrees with the standard formalism, as is discussed below. However, this approximation fails at high energies where higher multipoles are not negligible — see section 10.

If as before we assume that the quasi-deuteron contribution $R^{QD}_{1,\pm1}$ to the resonance amplitude corresponds to the scattering by correlated nucleon pairs, its dependence on t is described by the form factor $F_2(t)$. From Eq. (8.25), together with (3.42), one has approximately

$$R^{QD}_{1,\pm1} = \frac{1\pm\cos\theta}{2}F_2(t)\frac{1}{2\pi^2}\int\limits_0^\infty \frac{\omega'^2\,d\omega'\,\sigma_{QD}(\omega')}{\omega'^2-\omega^2-i0} \tag{8.31}$$

For practical purposes the absorption cross section $\sigma_{QD}(\omega)$ may then be expressed using a phenomenological description as discussed in section 5. It is also possible to represent σ_{QD} as a Lorentzian with a very big width [25, 34].

A straightforward application of the fixed-t dispersion relations discussed in this section is the dispersion representation of the nuclear polarizabilities $\bar\alpha_A$ and $\bar\beta_A$. Expanding the amplitudes T^{E1} and T^{M1} from Eqs. (8.17) and (8.18) with respect to ω up to the order ω^2 we obtain [99, 226]

$$\begin{aligned}
\bar\alpha_A &= \frac{1}{2\pi^2}\int_0^\infty\frac{d\omega}{\omega^2}\left\{\sigma^{E1}(\omega)+\frac{1}{2}\sum_{L>1}\left[\sigma^{EL}(\omega)\left(1+\frac{L(L+1)}{2}\right)\right.\right.\\
&\quad\left.\left.+\sigma^{ML}(\omega)\left(1-\frac{L(L+1)}{2}\right)\right]\right\},\\
\bar\beta_A &= \frac{1}{2\pi^2}\int_0^\infty\frac{d\omega}{\omega^2}\left\{\sigma^{M1}(\omega)+\frac{1}{2}\sum_{L>1}\left[\sigma^{EL}(\omega)\left(1-\frac{L(L+1)}{2}\right)\right.\right.\\
&\quad\left.\left.+\sigma^{ML}(\omega)\left(1+\frac{L(L+1)}{2}\right)\right]\right\}.
\end{aligned} \tag{8.32}$$

One can see that not only σ^{E1} and σ^{M1} give a contribution to the electromagnetic polarizabilities, but also higher multipoles of the photoabsorption cross section. In general, the asymptotic piece $a(t)$ also contributes and gives equal but opposite additions $\pm a(0)$ to $\bar\alpha_A$ and $\bar\beta_A$, respectively. There are also recoil corrections $\sim 1/AM$ [99, 226] which are again equal but opposite for $\bar\alpha_A$ and $\bar\beta_A$. When in Eq. (8.32) the sum $\bar\alpha_A+\bar\beta_A$ is taken, one recovers the usual Baldin-Lapidus sum rule. If only the lowest three multipoles are taken into account, one has

$$\begin{aligned}
\bar\alpha_A &= \frac{1}{2\pi^2}\int_0^\infty\frac{d\omega}{\omega^2}\left(\sigma^{E1}(\omega)+2\sigma^{E2}(\omega)+\frac{\omega}{AM}\sigma^{E1}(\omega)\right)+a(0),\\
\bar\beta_A &= \frac{1}{2\pi^2}\int_0^\infty\frac{d\omega}{\omega^2}\left(\sigma^{M1}(\omega)-\sigma^{E2}(\omega)-\frac{\omega}{AM}\sigma^{E1}(\omega)\right)-a(0),
\end{aligned} \tag{8.33}$$

where the asymptotic contributions and recoil corrections are explicitly written for the sake of completeness though the latter are negligible for nuclei with $A\gg1$. Evaluating these formulas with a nonrelativistic sum rules technique and using a closure, one can reproduce known answers for the polarizabilities of nonrelativistic systems [100, 281]. Clearly, when in Eqs. (8.32) and (8.33) one passes

from the total cross sections $\sigma^{\lambda J}$ to the giant resonance contributions $\sigma^{\lambda J}_{GR}$ the quantities $\bar{\alpha}_{GR}$ and $\bar{\beta}_{GR}$ are obtained. In particular, the diamagnetic correction (4.56) is derived using the sum rule (8.29).

Furthermore, it is instructive to have a closer look at the interplay of the seagull and resonance parts in the total amplitude. To this end we again restrict ourselves to the lowest three multipoles. We make use of the previously defined quantities $\tilde{R}^{\lambda j}$ (see Eqs. (4.2) and (4.4)), i.e.

$$\tilde{R}^{\lambda j}(\omega,\theta) = \frac{\omega^2}{2\pi^2} \int\limits_0^\infty \frac{\sigma^{\lambda j}(\omega')\, d\omega'}{\omega'^2 - \omega^2 - i0}\, g^{\lambda j}(\theta) \tag{8.34}$$

to express the giant resonance amplitude for this special case. From Eqs. (8.30) and (8.26) we obtain

$$\begin{aligned} R_{GR}(\omega,\theta) &= \tilde{R}^{E1}(\omega,\theta) + \tilde{R}^{E2}(\omega,\theta) + \tilde{R}^{M1}(\omega,\theta) \\ &\quad + \frac{1}{2\pi^2} \int\limits_0^\infty d\omega' \, \Big(\sigma^{E1}_{GR}(\omega') + \sigma^{M1}_{GR}(\omega') + \sigma^{E2}_{GR}(\omega') \Big)\, g^{E1}(\theta). \end{aligned} \tag{8.35}$$

Similarly, the seagull amplitude has the form

$$\begin{aligned} &B(\omega,\theta) + S_{GR}(\omega,\theta) = \\ &\quad - g^{E1}(\theta) \left[\frac{Z^2 e^2}{AM} + \frac{1}{2\pi^2} \int\limits_0^\infty d\omega' \, \Big(\sigma^{E1}_{GR}(\omega') + \sigma^{M1}_{GR}(\omega') + \sigma^{E2}_{GR}(\omega') \Big) \right] \\ &\quad + \frac{\omega^2}{2\pi^2} \int\limits_0^\infty \frac{d\omega'}{\omega'^2}\, \sigma^{E2}_{GR}(\omega') \Big(2g^{E1}(\theta) - g^{M1}(\theta) - g^{E2}(\theta) \Big). \end{aligned} \tag{8.36}$$

If one takes into account the modified TRK sum rule, Eq. (3.36), for the last term on the r.h.s. of Eq. (8.35), this expression is in agreement with the formulation of the giant resonance amplitude given in Eq. (4.2). As before, when considered at fixed momentum transfer, the amplitude $R_{GR}(\omega,\theta)$ vanishes in the high-energy limit. However, the individual multipole contributions from $E2$ and $M1$ do not vanish in this limit. Note that the applicability of fixed-t dispersion relations is restricted to small momentum transfer, since due to the relation (8.13) for some ω' the angle θ' becomes imaginary at high $-t$ and the cosine $\cos\theta'$ runs away the range of convergence of partial-wave series (*viz.* the Lehmann ellipse). Thus, for large ω and t, but fixed θ the sum with respect to j in Eq. (8.12) is not necessarily convergent. Unfortunately, this is precisely the regime, where the effects of retardation as discussed in section 4.4 become important. Therefore, at this point one has to get back to the phenomenological discussion of retardation given in section 4.4.

9 The mesonic seagull amplitude

It was pointed out above that the seagull amplitude has no imaginary part below pion threshold. It contains contributions from two fundamentally different physical sources, Thomson scattering on individual nucleons inside the nucleus and the scattering by correlated nucleon pairs. Such correlations occur as a result of the nucleon-nucleon interaction, which can be described in terms of mesonic exchange between the nucleons. As discussed before, the amplitude for the first process contains the form factor $F_1(t)$, while the second contribution is proportional to $F_2(t)$. Since the correlation radius is of the order $1/m_\pi$, i.e. much smaller than the nuclear radius R, one can expect that the form factor F_2 does not differ tremendously from F_1. Nevertheless, this difference produces an observable effect. We will confirm this statement within a model calculation. The same model will be used to investigate the different contributions to the enhancement constant κ, as well as the energy-dependence of the mesonic seagull amplitude, which is expressed in terms of polarizability modifications $\delta\alpha$ and $\delta\beta$ and the influence of the finite nuclear size on all these quantities.

9.1 Construction of the mesonic seagull amplitude for nuclear matter

In this section the contribution of correlated nucleon pairs to the seagull amplitude, Eq. (8.23), will be discussed on the basis of the results obtained in [168]. There the contribution of mesonic exchange currents to the nuclear Compton scattering amplitude was investigated within the framework of a (modified) Fermi gas model of nuclear matter in the non-relativistic limit. Such an approach was suggested in [70, 282] and for the case of forward direction used in [80, 83]. There it was also shown that the nuclear degrees of freedom can be taken into account by representing the amplitude S as a convolution of a two-body spin-isospin correlation function with matrix elements corresponding to the amputated irreducible Feynman diagrams for meson exchange. Such a correlation function consists of a central and a tensor part. In a pure Fermi gas model the tensor correlator is zero, but the importance of tensor correlations was pointed out in [83, 87, 172]. In its effect on the enhancement constant κ, for example, the central correlator makes a comparatively small contribution due to the strong compensation between the different Feynman diagrams taken into account. In [83] the results of numerical calculations for the correlators in nuclear matter were used and compared to a similar calculation based on the variational principle [283].

In [168] corrections to the pure Fermi gas wave function were calculated up to first order in a non-covariant perturbation theory. As a result of this model calculation the values of the enhancement constant κ and the polarizability modifications $\delta\alpha$ and $\delta\beta$ were obtained and the central and tensor part of the correlation function due to pion exchange between the nucleons were represented in an analytical form. In section 9.3 we will use this representation as a starting point to investigate the difference between the form factors F_1 and F_2. In the case of the present section, for the nuclear radius tending to infinity, the correlation function is proportional to F_1. Since in [168] a Fermi gas model has been used, these results are only applicable for heavy nuclei, where it can be expected that the quasi-classical approximation is valid. The effects of a finite nuclear size as well as of a realistic nuclear density have been investigated in [193] and will also be discussed in section 9.3.

Let us start our discussion from the static Hamiltonian for the interaction of the nucleon with the pion field $\boldsymbol{\phi}$ (see *e.g.* [173]),

$$H_{\pi NN} = -\frac{f}{m_\pi} \left(\boldsymbol{\sigma} \cdot \boldsymbol{\nabla}\right) \left(\boldsymbol{\tau} \cdot \boldsymbol{\phi}\right), \tag{9.1}$$

together with a minimal coupling to the photon field. For all coupling constants we use the same notation and values as given in [173], in particular $f^2/(4\pi)$=0.08. The mesonic seagull amplitude S

can be written in the following form [70, 80, 83, 168]:

$$S = \int \frac{d\mathbf{Q}}{(2\pi)^3}\, \mathcal{F}^{ij}(\mathbf{Q})\, T_{ij}(\mathbf{Q}). \tag{9.2}$$

The contribution $\mathcal{T}^{ij}_{(\pi)}$ of π-meson exchange to $\mathcal{T}_{ij}$, corresponding to the diagrams shown in Fig. 9.1, is given by:

$$\begin{aligned}\mathcal{T}^{ij}_{(\pi)} &= \frac{2e^2 f^2}{m_\pi^2}\left\{ \frac{\epsilon_1^i \epsilon_2^j}{D_1} - 2\,\frac{\epsilon_1^i Q_2^j\, \boldsymbol{\epsilon}_2\cdot\mathbf{Q}_2}{D_1 d_2} - 2\,\frac{\epsilon_2^i Q_2^j\, \boldsymbol{\epsilon}_1\cdot\mathbf{Q}_2}{D_2 d_2}\right.\\ &+ \left. 4\,\frac{Q_2^j Q_1^i\, \boldsymbol{\epsilon}_1\cdot\mathbf{Q}_1\, \boldsymbol{\epsilon}_2\cdot\mathbf{Q}_2}{D_1 d_1 d_2} - \frac{Q_2^j Q_1^i\, \boldsymbol{\epsilon}_1\cdot\boldsymbol{\epsilon}_2}{d_1 d_2} + \begin{pmatrix} i\leftrightarrow j \\ \mathbf{Q}\leftrightarrow -\mathbf{Q}\end{pmatrix}\right\},\end{aligned} \tag{9.3}$$

where the following abbreviations have been used:

$$D_{1,2} = (\mathbf{Q}\pm\mathbf{K})^2 + m_\pi^2 - \omega^2\,, \quad \mathbf{Q}_{1,2} = \mathbf{Q}\pm\frac{\mathbf{q}}{2}\,, \quad d_i = \mathbf{Q}_i^2 + m_\pi^2\,, \quad \mathbf{K} = (\mathbf{k}_1+\mathbf{k}_2)/2.$$

The correlator $\mathcal{F}^{ij}$ entering Eq. (9.2) has the following general form:

$$\mathcal{F}^{ij} = \sum_{a\neq b} \langle 0|\, \tau_a^{(-)}\tau_b^{(+)}\sigma_a^i\sigma_b^j\; e^{i\,\mathbf{Q}\cdot(\mathbf{x}_b-\mathbf{x}_a)}\; e^{-i\,\mathbf{q}\cdot(\mathbf{x}_a+\mathbf{x}_b)/2}\,|0\rangle\,. \tag{9.4}$$

Here the summation with respect to a and b is performed over all nucleons, $\tau_a^{(\pm)} = (\tau_a^1 \pm i\tau_a^2)/2$ are the isospin raising and lowering operators, while $\sigma_a^i/2$ denotes the i-th component of the spin operator for the a-th nucleon.

Figure 9.1: *Typical diagrams contributing to $\mathcal{T}^{ij}_{(\pi)}$. The wavy lines denote photons and dashed lines denote pions. The amputation indicates that T^{ij} contains only the nucleon vertices, but not its wave functions.*

For the simplest case of a pure Fermi gas model the correlator (9.4) only has a central part: $\mathcal{F}^{ij} = \mathcal{F}_C\delta^{ij}$, where

$$\mathcal{F}_C = -2\int \frac{d\mathbf{p}_1 d\mathbf{p}_2}{(2\pi)^6}\int d\mathbf{x}_1 d\mathbf{x}_2\, e^{-i(\mathbf{x}_1+\mathbf{x}_2)\mathbf{q}/2}\, e^{i(\mathbf{x}_1-\mathbf{x}_2)((\mathbf{p}_1-\mathbf{Q}-\mathbf{p}_2)}. \tag{9.5}$$

The ranges of integration for the nucleon momenta $\mathbf{p}_1$ and $\mathbf{p}_2$ are the proton and neutron Fermi spheres, with the radii

$$p_F^{(p)} = 2.27\, m_\pi \left(\frac{Z}{A}\right)^{1/3}\,, \quad p_F^{(n)} = 2.27\, m_\pi \left(\frac{N}{A}\right)^{1/3}\,, \quad A = N+Z.$$

This form is easily obtained in a usual Fermi gas model, where the proton ($i=p$) and neutron ($i=n$) densities are written as

$$\rho^{(i)} = 2\int \frac{d\mathbf{p}}{(2\pi)^3}\, n^{(i)}(\mathbf{p})\,, \quad n^{(i)}(\mathbf{p}) = \theta(p_F^{(i)} - |\mathbf{p}|)\,, \;\text{ i.e. }\quad \rho^{(i)} = \frac{\left(p_F^{(i)}\right)^3}{3\pi^2}.$$

Here $\theta(x)$ is the step function. Together with the assumption of a homogeneous distribution of protons and neutrons inside the nuclear volume one has

$$\frac{4\left(p_F^{(p)}R\right)^3}{9\pi} = Z\,, \quad \frac{4\left(p_F^{(n)}R\right)^3}{9\pi} = N.$$

Finally, by writing $R = 1.2\ A^{1/3}$ fm one finds the above relations for $p_F^{(i)}$. In Eq. (9.5) the integrations with respect to $\mathbf{x}_i$ are taken over a sphere with the radius R.

The dependence of the correlation function (9.5) on the nuclear radius R, on N and Z and on the momentum transfer $\mathbf{q}$ were investigated in [168]. In the following we will put $N = Z = A/2$. Let us pass in Eq. (9.5) to the variables $\mathbf{X} = (\mathbf{x}_1 + \mathbf{x}_2)/2$ and $\mathbf{r} = \mathbf{x}_1 - \mathbf{x}_2$, which denote the c.m. of the nucleon pair and the relative distance between the two nucleons, respectively. Taking the integral with respect to $\mathbf{X}$ over the region $|\mathbf{X}| < R$ and with respect to $\mathbf{r}$ over an infinite range, one obtains as a first approximation for the correlator

$$\mathcal{F}_C = \mathcal{F}_C^{(0)}(q)\, F_1(t), \tag{9.6}$$

where $q = Q/p_F$, $p_F = p_F^{(p)} = p_F^{(n)} = 1.8\, m_\pi$ and

$$\mathcal{F}_C^{(0)}(q) = -\frac{A}{2}\left(1 - \frac{q}{2}\right)^2 \left(1 + \frac{q}{4}\right)\ \theta(2-q), \tag{9.7}$$

which is a well-known result (see *e.g.* [126]) of the Fermi model. In the model under consideration the form factor $F_1(q)$ is equal to $F(Rq)$, where

$$F(x) = \frac{3}{x^2}\left(\frac{\sin x}{x} - \cos x\right). \tag{9.8}$$

Thus, the use of the approximate result (9.6) for the correlator leads to a proportionality of the mesonic seagull amplitude (9.2) to a form factor $F_1(q)$.

Although this conclusion was obtained for the pure Fermi gas model, where only the central part of the correlator contributes, the same is valid for the general case, if one integrates in Eq. (9.4) with respect to $\mathbf{x}_b - \mathbf{x}_a$ over an infinite range. It is important to understand the difference between the mesonic seagull amplitude arising from the approximate correlator and the exact amplitude, which is obtained by integrating in (9.4) over a finite volume with respect to both, $\mathbf{x}_a$ and $\mathbf{x}_b$. In the amplitude this difference manifests itself as a difference between the form factors $F_1(q)$ and $F_2(q)$. At low energies the dependence of the amplitude S on momentum transfer $\mathbf{q}$ is determined by the distribution of nucleon pairs inside the nucleus. In the case of heavy nuclei the scale of nucleon correlations is essentially smaller than the nuclear radius R. Thus, one can expect that the $\mathbf{q}$-dependence of S is similar to the nuclear charge form factor $F_1(q)$. However, experimental data clearly indicate [25,32,95] that this $\mathbf{q}$-dependence cannot fully be identified with the form factor F_1 In [71, 72] it was suggested to use for the amplitude S another form factor F_2 instead of F_1. It has been proposed to apply $F_2(q) = F_1^2(q/2)$, which corresponds to the distribution of uncorrelated nucleon pairs [19,174]. A first attempt to quantitatively discuss the function F_2 within a model calculation has been made in [75]. As a first step, we will consider this effect calculating the q-dependence of the term in S proportional to the enhancement constant κ (*cf.* Eq. (8.23)). Putting $\mathbf{K}$ and $\mathbf{q}$ equal to zero in Eq. (9.3), substituting (9.5) into (9.2) and integrating first with respect to $\mathbf{Q}$ and then with respect to the variables $\mathbf{p}_i$ and $\mathbf{x}_i$ we get the following representation of F_2:

$$F_2(q) = \frac{J(Rq)}{J(0)}, \tag{9.9}$$

where

$$J(\zeta) = \int\limits_0^2 dx\, x^3 \exp(-m_\pi R\, x)\, F^2(p_F R\, x) \times \tag{9.10}$$

$$\left[\frac{1}{3}\left(1 - \frac{x}{2}\right)^3 F(\zeta(1 - x/2)) + \frac{1}{\zeta x}\int\limits_{1-\frac{x}{2}}^{\sqrt{1-\frac{x^2}{4}}} dy\ \sin(\zeta y)\left(1 - y^2 - \frac{x^2}{4}\right)\right]$$

and $F(x)$ is given in Eq. (9.8). The integral with respect to y in (9.10) can easily be taken analytically, but we represent the result in the form (9.10) for the sake of brevity. In Fig. 9.2 the two form factors $F_1(q)$ and $F_2(q)$ as given in Eqs. (9.8) and (9.9), respectively, are compared for A=40. As expected, the difference is not very big. In Fig. 9.2 we also show the widely used approximation $F_1^2(q/2)$. As one sees, this approximation is not valid. Note that in Fig. 9.2 the form factor $F(x)$ is not the experimental (charge) form factor. For the general discussion of exchange form factors here this difference is not important. However, experimental form factors F_1 will be used as a reference in section 9.3 and appendix B, where exchange form factors will be discussed in a more quantitative form.

Figure 9.2: *Comparison of the form factors from Eqs. (9.8) (dotted curve) and (9.9) (full curve) for the case of ^{40}Ca. The approximation $F_1^2(q/2)$ is shown as a dashed curve.*

A statement better suited for practical purposes than the analytical result (9.10) is obtained by considering the slope of the form factor. We represent the form factors F_i at small momentum transfer in the form:

$$F_i(q) = 1 + \frac{q^2}{6} \left\langle r^2 \right\rangle_i . \tag{9.11}$$

As known, $\langle r^2 \rangle_1 = (3/5)\, R^2$. In order to get the value of $\langle r^2 \rangle_2$, it is necessary to expand the r.h.s. of Eq. (9.10) up to the order $(Rq)^2$. The resulting ratio $\chi(A) = \langle r^2 \rangle_2 / \langle r^2 \rangle_1$ is shown in Fig. 9.3. We checked numerically that a good approximation for the function F_2 in a wide range of t is given by $F_2(q) \approx F_1(\chi t)$. In a range for A between 4 and 200 the relation

$$\chi \approx \left(1 - \frac{0.32\,\mathrm{fm}}{\sqrt{\langle r^2 \rangle_1}} \right)^2 \tag{9.12}$$

accounts for the dependence of χ on A within a few percent. This corresponds to a finite shift of the mean charge radius:

$$\sqrt{\langle r^2 \rangle_2} \approx \sqrt{\langle r^2 \rangle_1} - 0.32\,\mathrm{fm}. \tag{9.13}$$

In the following section it will become evident that tensor correlations influence mostly the short-range behavior of the correlation function. We can therefore expect that the difference between F_1 and F_2 is mainly governed by central correlations. The more refined discussion in the next section will confirm this.

Figure 9.3: *Ratio $\chi(A) = \langle r^2 \rangle_2 / \langle r^2 \rangle_1$ as a function of the nuclear mass number A*

9.2 Corrections to the correlation function

In order to obtain the correct behavior of the mesonic seagull amplitude, it is necessary to take into account not only the central part of the correlator, but also its tensor part. To this end the correction to the nuclear wave function has been calculated in [168] using perturbation theory with respect to π- and ρ-meson exchange. These corrections are important, because they determine an essential part of the nuclear correlation functions. In [168] all diagrams up to the order f^4 have been taken into account, where f is the meson-nucleon coupling constant. In the course of that calculation it has been realized that three-body corrections to the correlator are as important as two-body corrections. A word of caution is necessary concerning the gauge invariance of the amplitude obtained in such a model. In [168] it was shown that the modifications of electromagnetic polarizabilities are, indeed, gauge invariant quantities. However, in higher order with respect to ω^2 terms violating gauge invariance

appear, which by definition have to cancel with some corresponding terms in the resonance part of the amplitude. Such cancellations either can be incorporated implicitly in the phenomenology of the resonance amplitude or may give rise to additional photonuclear sum rules.

As pointed out in the last section all dependence of the correlator on the momentum transfer is given by the form factor $F_2(q)$. So, putting $\mathbf{q} = 0$ in Eq. (9.4) we represent without change of notation the correlator $\mathcal{F}^{ij}$ in the following form:

$$\mathcal{F}^{ij} = \mathcal{F}_C\, \delta^{ij} + \mathcal{F}_T\, t^{ij}\,, \quad t^{ij} = \frac{3Q^iQ^j}{Q^2} - \delta^{ij}. \tag{9.14}$$

The diagrams, which correspond to the two-body part of the correlator correction, are shown in Fig. 9.4. Explicit evaluation of these diagrams leads to the following result:

$$\begin{aligned}\mathcal{F}^{ij}_{(1)} &= -\frac{4Mf^2}{m_\pi^2} V \int \frac{d\mathbf{p}_1 d\mathbf{p}_2}{(2\pi)^6} \left\{ \frac{4Q^iQ^j}{\mathbf{Q}^2 + m_\pi^2} + \frac{2r^ir^j - \mathbf{r}^{\,2}\delta^{ij}}{\mathbf{r}^{\,2} + m_\pi^2} \right\} \times \\ &\quad \frac{n(\mathbf{p}_1)n(\mathbf{p}_2)\,[1 - n(\mathbf{p}_2 + \mathbf{Q})]\,[1 - n(\mathbf{p}_1 - \mathbf{Q})]}{\mathbf{Q}\cdot\mathbf{r}},\end{aligned} \tag{9.15}$$

where $\mathbf{r} = \mathbf{p}_1 - \mathbf{p}_2 - \mathbf{Q}$ and V is the nuclear volume. The function $n(\mathbf{p}) = \theta(p_F - |\mathbf{p}\,|)$ is the occupation number in the Fermi gas model.

Figure 9.4: *Set of diagrams, from which the two-body correction to the correlator is extracted. Here the same symbolic abbreviation is used as in Fig. 9.1. The nucleon spin projections are denoted by λ_i.*

Figure 9.5: *Three-body diagrams yielding an additional correction to the correlator, which is of the same order in f/m_π as the two-body diagrams shown in Fig. 9.4. The notations are the same as in Fig. 9.1 and Fig. 9.4.*

It is interesting to note that the three-body diagrams displayed in Fig. 9.5 also give a significant contribution. The corresponding general expression for the three-body contribution to the correlator reads

$$\begin{aligned}\mathcal{F}^{ij}_{(2)} &= \frac{16Mf^2}{m_\pi^2} V \int \frac{d\mathbf{p}_1 d\mathbf{p}_2}{(2\pi)^6} \left\{ \frac{2Q^iQ^j}{\mathbf{Q}^2 + m_\pi^2} + \frac{2r^ir^j - \mathbf{r}^{\,2}\delta^{ij}}{\mathbf{r}^{\,2} + m_\pi^2} \right\} \times \\ &\quad \frac{n(\mathbf{p}_1)n(\mathbf{p}_2)n(\mathbf{p}_1 + \mathbf{Q})}{\mathbf{Q}\cdot\mathbf{r}}.\end{aligned} \tag{9.16}$$

The result of the explicit analytical integration for Eqs. (9.16) and (9.15) can be found in [168]. As before, the correction (9.16) contributes to the central part of the correlator, as well as to its tensor part. Thus, at this stage of our discussion the correlation function $\mathcal{F}^{ij}$ has the following form:

$$\mathcal{F}^{ij} = \mathcal{F}^{(0)}_C \delta^{ij} + \mathcal{F}^{ij}_{(1)} + \mathcal{F}^{ij}_{(2)}. \tag{9.17}$$

Note that central and tensor parts of the corrections can be extracted by using the definitions in (9.14). In Fig. 9.6 the full central part of the correlator as a function of Q/p_F is shown, together with the zeroth order approximation $\mathcal{F}^{(0)}_C$ and the one, where only two-body correlations have been taken into account. It can be seen that almost over the whole range of Q the asymptotic form of the central correlator is modified, although the overall shape remains the same. Figure 9.7 shows the tensor correlator with and without three-body effects. Here a strong modification due to three-body correlations occurs at comparatively low Q, where we found a strong damping that is in fact essential

for obtaining reasonable physical results. One can see from Fig. 9.7 that the contribution of the high-Q region is not negligible. It is known that taking into account only the one-pion exchange leads to a wrong behavior in the tensor part of the nucleon-nucleon potential at small distances (i.e. at large Q) (see *e.g.* [173]). Thus, it is necessary to include ρ-meson exchange in the calculation of the tensor part of the correlator. This can be done [87, 284] by replacing $\mathcal{F}_T$ by:

$$\tilde{\mathcal{F}}_T = \mathcal{F}_T \left[1 - 2\,\frac{q^2 + m_\pi^2/p_F^2}{q^2 + m_\rho^2/p_F^2}\right], \tag{9.18}$$

where m_ρ is the ρ-meson mass. This inclusion of ρ-meson exchange improves essentially the behaviour of the correlator at $Q \sim p_F$ and higher (*cf.* Fig. 9.8).

Figure 9.6: *Central part of the correlator with three-body corrections (full curve), without three-body corrections (dotted curve) and Fermi correlator without any corrections (dashed curve).*

Figure 9.7: *Tensor part of the correlator with three-body corrections (full curve) and without three-body corrections (dashed curve).*

Figure 9.8: *Comparison of the tensor part of the correlator with (full curve) and without (dashed curve) the ρ-meson contribution.*

Even below pion threshold the contribution of a virtual Δ-isobar excitation to the mesonic part of the seagull amplitude is not negligible. General properties of such an effect were discussed in [74]. In [168] this contribution was investigated quantitatively using the same diagrammatic approach as for the amplitude $T^{ij}_{(\pi)}$. In the static limit the corresponding Hamiltonians, which determine the interaction, are of the form (see *e.g.* [173])

$$H_{\gamma N\Delta} = -\frac{e f_{\gamma N\Delta}}{m_\pi}\,\mathbf{S}^+ \cdot (\boldsymbol{\nabla} \times \mathbf{A})\; T_3^+ \tag{9.19}$$

and

$$H_{\pi N\Delta} = -\frac{f_\Delta}{m_\pi}\,(\mathbf{S}^+ \cdot \boldsymbol{\nabla})(\mathbf{T}^+ \cdot \boldsymbol{\phi}), \tag{9.20}$$

with the hermitian conjugate to be added in both cases. Here $\mathbf{S}$ and $\mathbf{T}$ are the 1/2-to-3/2 transition operators in spin space and isospin space, respectively. Evaluating the corresponding diagrams on this basis, one obtains the following expression for the isobar contribution to the tensor T^{ij} entering into Eq. (9.2):

$$T^{ij}_{(\Delta)} = \eta \left[\frac{h_1^i l_2^j + l_1^i h_2^j}{D_1} + \frac{Q_1^i}{d_1}\;[\boldsymbol{\epsilon}_1 \times (\mathbf{k}_2 \times \boldsymbol{\epsilon}_2) - \boldsymbol{\epsilon}_2 \times (\mathbf{k}_1 \times \boldsymbol{\epsilon}_1)]^j\right], \tag{9.21}$$

with

$$\mathbf{h}_a = \boldsymbol{\epsilon}_a - \frac{2(\mathbf{Q}_a \cdot \boldsymbol{\epsilon}_a)\mathbf{Q}_a}{d_a}\,, \quad \mathbf{l}_a = (\mathbf{Q} + \mathbf{K}) \times (\mathbf{k}_a \times \boldsymbol{\epsilon}_a)$$

and the coefficient

$$\eta = -\frac{8\Omega e^2 f_\Delta f_{\gamma N\Delta} f}{9(\omega^2 - \Omega^2) m_\pi^3}.$$

In (9.21) the same abbreviations have been used as in Eq. (9.3) and, in addition, $\Omega = M_\Delta - M$ is the mass difference between the Δ-isobar and the nucleon. Also, the symmetry with respect to the substitution $\mathbf{Q} \to -\mathbf{Q}$, which is due to the integration in Eq. (9.2), has been used to bring $T^{ij}_{(\Delta)}$ into the form (9.21). Comparison of this mesonic seagull amplitude for nuclear matter with Eq. (8.23) allows us to give the numerical results in terms of explicit values for κ, $\delta\alpha$ and $\delta\beta$. These numerical values are given in appendix A.

9.3 The mesonic seagull amplitude in finite nuclei

In order to discuss the properties of the mesonic seagull amplitude for the case of specific nuclei rather than for nuclear matter, it is convenient to consider the Fourier transform of the correlation function discussed in section 9.2. Then the function $\mathcal{F}^{ij}$ can be written as

$$\mathcal{F}^{ij} = \int d\mathbf{x}_1 d\mathbf{x}_2 \, e^{-i\mathbf{q}\cdot(\mathbf{x}_1+\mathbf{x}_2)/2} e^{-i\mathbf{Q}\cdot(\mathbf{x}_1-\mathbf{x}_2)} \times \\ \Big[g_C(\mathbf{x}_1-\mathbf{x}_2)\ \delta^{ij} + g_T(\mathbf{x}_1-\mathbf{x}_2)\, t^{ij} \Big] , \tag{9.22}$$

with t^{ij} from (9.14). In Eq. (9.22) the functions g_C and g_T describe the central and tensor correlations of two nucleons, while the exponential function depending on $\mathbf{q}$ is responsible for the distribution of such nucleon pairs inside the nucleus. The functions g_C and g_T are related to the momentum space correlation functions $\mathcal{F}_C$ and $\mathcal{F}_T$ via

$$g_{C,T}(\rho) = \frac{1}{V} \int \frac{d\mathbf{Q}}{(2\pi)^3} \, \mathcal{F}_{C,T}(Q) \, e^{i\,\boldsymbol{\rho}\cdot\mathbf{Q}} . \tag{9.23}$$

Note that in the functions $\mathcal{F}_C$ and $\mathcal{F}_T$ the contribution from ρ-meson exchange has been taken into account. In the case of a pure Fermi gas model we have

$$g_C^{(0)}(\rho) = -2 \left(\frac{p_F^3}{6\pi^3} \right)^2 F^2(p_F\rho) \ , \quad g_T^{(0)}(\rho) = 0 \tag{9.24}$$

with the function F from Eq. (9.8). Next, we expand $T_{(\pi)}^{ij}$ in Eq. (9.2) with respect to $\mathbf{k}_1$ and $\mathbf{k}_2$ up to $O(\omega^2)$, pass to the variables $\boldsymbol{\rho} = \mathbf{x}_2 - \mathbf{x}_1$ and $\boldsymbol{\xi} = (\mathbf{x}_1 + \mathbf{x}_2)/2$. Then, taking the integral with respect to $\mathbf{Q}$ and the angles of $\boldsymbol{\rho}$ and $\boldsymbol{\xi}$ we obtain the contribution of $T_{(\pi)}^{ij}$ to the mesonic seagull amplitude:

$$\begin{aligned} S_{(\pi)} \ &= \ \frac{Ae^2}{4M} \Big\{ \ \Phi_1(q)\, \boldsymbol{\epsilon}_1 \cdot \boldsymbol{\epsilon}_2 + \frac{\omega^2}{m_\pi^2} \Phi_2(q)\, \boldsymbol{\epsilon}_1 \cdot \boldsymbol{\epsilon}_2 + \\ &\quad \frac{1}{m_\pi^2} \Phi_3(q)\, (\boldsymbol{\epsilon}_1 \times \mathbf{k}_1) \cdot (\boldsymbol{\epsilon}_2 \times \mathbf{k}_2) \ \Big\} , \end{aligned} \tag{9.25}$$

where

$$\Phi_i = \frac{2Mf^2}{3m_\pi \pi^2} (2Rp_F)^3 \int_0^1 dx \ \Big[G_i^C(\rho_1)\, \tilde{g}_C(\rho_2) + \ G_i^T(\rho_1)\, \tilde{g}_T(\rho_2) \Big] \times \\ x^2 e^{-\rho_1} \left(\int_0^{1-x} d\xi \ \xi \, \frac{\sin \xi Rq}{Rq} + \int_{1-x}^{\sqrt{1-x^2}} d\xi \ \frac{\sin \xi Rq}{Rq} \ \frac{1-x^2-\xi^2}{2x} \right) . \tag{9.26}$$

In Eq. (9.26) the following abbreviations have been used:

$$\tilde{g}_{C,T}(\rho_2) = \frac{1}{2} \left(\frac{6\pi^2}{p_F^3} \right)^2 g_{C,T}(\rho_2/p_F) \ , \quad \rho_1 = 2Rm_\pi x \ , \quad \rho_2 = 2Rp_F x \quad .$$

The functions $G_i^{C,T}$ are of the form

$$G_1^C(\rho_1) = \rho_1 \ , \quad G_1^T(\rho_1) = \frac{2\rho_1^2 - 12}{\rho_1} \ , \\ G_2^C(\rho_1) = \frac{150 + 30\rho_1 - \rho_1^3}{60} \ , \quad G_2^T(\rho_1) = \frac{24 + 12\rho_1 - \rho_1^3}{30} \\ G_3^C(\rho_1) = \frac{3 - 21\rho_1 + 2\rho_1^2}{12} \ , \quad G_3^T(\rho_1) = \frac{2\rho_1^2 - 3\rho_1 - 15}{6}$$

The integral with respect to ξ in (9.26) can easily be taken analytically, but we represent the result in this form for the sake of brevity. By comparing Eq. (9.25) with the corresponding terms in Eq. (8.23) one sees that the parameters appearing in the mesonic seagull amplitude are given by the functions $\Phi_i(q)$ at q=0:

$$\kappa = -\Phi_1(0)\ , \quad \delta\alpha = \frac{e^2}{4Mm_\pi^2}\Phi_2(0)\ , \quad \delta\beta = \frac{e^2}{4Mm_\pi^2}\Phi_3(0). \tag{9.27}$$

It is evident from Eq. (9.26) that three different form factors

$$F_2^{(i)}(q) = \frac{\Phi_i(q)}{\Phi_i(0)} \tag{9.28}$$

appear instead of only F_2.

In order to account for the contribution of ρ-meson exchange to T^{ij} one may follow the prescription of [87] and make the substitution $f^2 \to 2\tilde{f}_\rho^2$ for the central part of each quantity and $f^2 \to -\tilde{f}_\rho^2$ for the tensor part. The pion mass m is substituted in all cases by the ρ-meson mass m_ρ.

In the case of the magnetic polarizability $\delta\beta$ the contribution of the Δ-isobar excitation to the mesonic seagull amplitude should also be taken into account [74,168]. In our notation this corresponds to an additional contribution to the function Φ_3, which is of the following form:

$$\delta\Phi_3 = \frac{8Mf_\Delta f_{\gamma N\Delta} f (2Rp_F)^3}{81(M_\Delta - M)\pi^2} \int\limits_0^1 dx\ \Big[G_\Delta^C(\rho_1)\,\tilde{g}_C(\rho_2) + \ G_\Delta^T(\rho_1)\,\tilde{g}_T(\rho_2)\Big]\ \times$$
$$x^2 e^{-\rho_1}\left(\int\limits_0^{1-x} d\xi\ \xi\,\frac{\sin\xi Rq}{Rq} + \int\limits_{1-x}^{\sqrt{1-x^2}} d\xi\ \frac{\sin\xi Rq}{Rq}\ \frac{1-x^2-\xi^2}{2x}\right), \tag{9.29}$$

where again M_Δ is the Δ-isobar mass and

$$G_\Delta^C(\rho_1) = \frac{6-12\rho_1}{\rho_1}\ , \quad G_\Delta^T(\rho_1) = \frac{12-6\rho_1}{\rho_1}.$$

The coupling constants appearing in Eq. (9.29) are taken to be $f_\Delta = 2f$ and $f_{\gamma N\Delta} = 0.35$.

Up to now we have considered a constant nucleon density $n_0 = p_F^3/3\pi^2$ inside the nucleus, which is normalized as $n_0 V = Z$. Using a local-density approximation we will extend our consideration to realistic nuclear densities $n(r)$. With the help of the usual plane-wave expansion via Legendre polynomials $P_l(x)$ we obtain the realistic-density (rd) form

$$\Phi_i^{(rd)} = \frac{64\pi M f^2}{3m_\pi Z} \int\limits_0^\infty dx\, x^2 e^{-2m_\pi x} \int\limits_x^\infty dr\, r^2 n^2(r)\ \times \tag{9.30}$$
$$\Big[G_i^C(2xm_\pi)\,\tilde{g}_C(2xp(r)) + G_i^T(2xm_\pi)\,\tilde{g}_T(2xp(r))\Big]\ \times$$
$$\sum_{l=0}^\infty j_l(r\Delta)\,j_l(x\Delta)\,(P_{l-1}(x/r) - P_{l+1}(x/r)),$$

where $p(r) = (3\pi^2 n(r))^{1/3}$ is the local Fermi momentum. In numerical calculations a three-parameter Fermi parameterization of the densities $n(r)$ has been used with values for the different nuclei taken from [256].

Equations (9.25)–(9.30) form the starting point of our numerical investigation of the mesonic seagull amplitude. Note that due to the use of either the Fermi gas model or a local density approximation the accuracy of our results decreases with decreasing Z.

First we discuss the numerical results for the different contributions to the enhancement constant κ. Note that, as it was argued in [172] and is also discussed in [173], the main contribution to κ^{GR} comes from central correlations, while κ^{QD} is mainly determined by tensor correlations. Obviously, it is impossible to give a precise separation of κ into a GR part and a QD part, but this approximation seems reasonable, as the GR contribution should be associated with a small momentum transfer between the two nucleons in comparison with the QD part. In the pure Fermi gas model, where $g_C = g_C^{(0)}$ and g_T=0, the contribution to κ from pion exchange κ^π is approximately equal to the ρ-meson contribution κ^ρ. For nuclear matter (infinite nuclear radius) one has $\kappa^\pi = \kappa^\rho$=0.2, which is in agreement with a variety of model calculations, *e.g.* [87, 171, 172]. For finite nuclei, again in the pure Fermi gas, the value for κ^π decreases slightly with decreasing Z, whereas κ^ρ remains the same. With inclusion of the full correlation functions g_C and g_T the situation for κ changes drastically. Now the main contribution to κ comes from tensor correlations related to pion exchange. The pionic central contribution is still of the same order as before, while κ_C^ρ becomes negligible. The only significant contribution from ρ-meson exchange is now due to tensor correlations and has a negative value. All these relations between the different ingredients to κ remain valid, when realistic nuclear densities are considered. In Fig. 9.9 the different contributions to κ are shown as a function of Z for the modified Fermi gas model. In addition, the realistic-density result $\kappa^{(rd)}$, which is obtained from Eq. (9.30), is shown in the same figure.

Figure 9.9: *Dependence of enhancement constant κ on proton number Z. The dashed curve corresponds to the pionic tensor contribution κ_T^π, the dash-dotted curve includes also the central contribution κ_C^π and the dotted curve gives the total κ, including the contribution from ρ-meson exchange. The realistic-density result $\kappa^{(rd)}$ for the full enhancement constant (cf. Eq. (9.30)) is shown as a full curve.*

In the case of electric and magnetic polarizabilities $\delta\alpha$ and $\delta\beta$ the contributions from ρ-meson exchange are suppressed by a factor of m_π^2/m_ρ^2 in comparison with the pion contributions and, therefore, are negligible. The values of $\delta\alpha$ and $\delta\beta$ are determined mainly by pionic central correlations, as can be seen in Figs. 9.10 and 9.11. In the case of $\delta\beta$ the inclusion of the Δ-isobar intermediate state produces a noticeable effect (*cf.* Fig. 9.11). In this contribution the values due to central and tensor correlations are of the same order. Note that κ, $\delta\alpha$ and $\delta\beta$ get close to their asymptotic (nuclear matter) values calculated in [168] only at extremely high Z. The size of both, $\delta\alpha$ and $\delta\beta$ becomes noticeably smaller, when a realistic density is taken into account. This effect gains importance with decreasing Z. The ratio of central and tensor contributions to $\delta\alpha$ is approximately the same for a realistic density as in a modified Fermi gas model. For $\delta\beta$ the influence of tensor correlations in the realistic-density case is slightly stronger than for homogeneous nuclear density.

We consider now the dependence of the mesonic seagull amplitude S on momentum transfer q, which is determined by the form factors $F_2^{(i)}(q)$ (*cf.* Eq. (9.28)). Here these form factors are given for ^{40}Ca. A wider range in A is covered in Appendix B, where explicit results are given for ^{208}Pb, ^{16}O and ^{12}C. The results from [193] indicate that $F_2^{(2)}$ for the term proportional to $\delta\alpha$ and $F_2^{(3)}$ (for $\delta\beta$) are equal with high accuracy, but differ significantly from the form factor $F_2^{(1)}$ for the term containing κ. All three functions $F_2^{(i)}$ differ noticeably from F_1. Figure 9.12 shows the corresponding curves for ^{40}Ca, for the case of a realistic density. One can see that the frequently used phenomenological approximation $F_2(q) = F_1^2(q/2)$, which is also shown in Fig. 9.12, is not in agreement with the q-dependence of the amplitude S obtained here. For very small q it is convenient to represent the form factors as $F_2^{(i)} = 1 - q^2 r_i^2/6$. Then for calcium we find r_1=3.0 fm and r_2=2.5 fm. For other nuclei the corresponding numbers are given in Appendix B. In the case of ^{208}Pb, the result from [75] coincides within good accuracy with the corresponding form factor $F_2^{(2)}$ from [193].

Figure 9.10: *Pion-exchange contribution to electric polarizability $\delta\alpha$ as a function of Z. The dashed curve corresponds to the central contribution $\delta\alpha_C$ and the dotted curve gives the total $\delta\alpha = \delta\alpha_C + \delta\alpha_T$. The use of a realistic density leads to the full curve.*

Figure 9.11: *Pion-exchange contribution to magnetic polarizability $\delta\beta$ as a function of Z. The dashed curve corresponds to the central contribution $\delta\beta_C$ and the dash-dotted curve gives the sum $\delta\beta_C + \delta\beta_T$. Adding the contribution of the Δ-isobar excitation as given in Eq. (9.29) leads to the total value of $\delta\beta$ given as the dotted curve. The use of a realistic density leads to the full curve.*

Figure 9.12: *Form factors $F_2^{(i)}(\Delta)$ for ^{40}Ca. The dashed curve is $F_2^{(1)}$ and the full curve is $F_2^{(2)}$. For comparison the (experimental) charge form factor F_1 is also shown (dash-dotted curve), as well as the function $F_1^2(\Delta/2)$ (dotted curve).*

10 Retardation effects in Compton scattering. A model study with a relativistic oscillator

10.1 Motivation and aims

In many earlier works [16,19,127,166], a simple ansatz for the Compton scattering amplitude through the GR region was widely used. It is formulated in terms of the lowest partial-wave amplitudes,

$$R_{GR}(\omega,\theta) = \sum_{\lambda L = E1, M1, E2} R^{\lambda L}_{GR}(\omega) g^{\lambda L}(\theta), \tag{10.1}$$

whose imaginary parts, $\mathrm{Im}R^{\lambda L}_{GR}(\omega) = (\omega/4\pi)\sigma^{\lambda L}_{GR}(\omega)$, exhaust photoabsorption in the GR region. The real parts of these partial amplitudes are assumed to be given by the dispersion integrals

$$\mathrm{Re}R^{\lambda L}_{GR}(\omega) = R^{E1}_{GR}(0)\delta_{\lambda L,\,E1} + \frac{\omega^2}{2\pi^2}\mathcal{P}\int_0^\infty \frac{\sigma^{\lambda L}_{GR}(\omega')\,d\omega'}{\omega'^2-\omega^2}, \tag{10.2}$$

where

$$R^{E1}_{GR}(0) = \frac{1}{2\pi^2}\int_0^\infty \sigma_{GR}(\omega)\,d\omega. \tag{10.3}$$

This ansatz was constructed in a way that ensured the fulfillment of the Gell-Mann–Goldberger–Thirring dispersion relation in forward direction, when all $g^{\lambda L} = 1$:

$$R_{GR}(\omega,0) = \frac{1}{2\pi^2}\int_0^\infty \frac{\omega'^2}{\omega'^2-\omega^2-i0}\sigma_{GR}(\omega')\,d\omega'. \tag{10.4}$$

In particular, when $\omega \to \infty$, the amplitude $R_{GR}(\omega,0)$ vanishes, and the total Compton scattering amplitude T_{GR} is determined by the seagull contribution S^{GR}.

This nice feature is destroyed by the $E2$ and $M1$ contributions when the scattering angle θ is not zero. For example, when $\theta = \pi$, the asymptotically nonvanishing part of the resonance amplitude reads

$$R_{GR}(\infty,\pi) = \frac{1}{\pi^2}\int \left(\sigma^{E2}_{GR}(\omega) + \sigma^{M1}_{GR}(\omega)\right)\,d\omega \neq 0. \tag{10.5}$$

However, the vanishing of R_{GR} for $\omega = \infty$ and for all angles is physically necessary. Such a vanishing was used in section 8.2 to analyze the seagull contribution emerging from the fixed-t dispersion relations and to derive a set of related sum rules.

Phenomenologically, the dispersion relations (10.2) for the partial amplitudes could be corrected through introducing special ω-dependent form factors $F(\omega)$ [95,176] which erase the unphysical asymptotic pieces. Though well motivated by retardation effects calculated in the frame of nuclear models [176], such a procedure may however need a further theoretical justification because the form factors $F(\omega)$ generally destroy the asymptotic behavior of the amplitude at high complex energies and violate the validity of dispersion relations. Only taken consistently by taking into account the contributions of higher multipoles and relativistic corrections, they lead to a correct result. Accordingly, the present section is aimed to illustrate an interplay between the retardation effects, higher multipoles, relativistic corrections, asymptotic behavior and the dispersion relations by using a model which contains the Compton scattering amplitude with all correct analytical properties. Such a model has to be relativistic, and therefore we consider a relativistic harmonic oscillator, which allows an analytical treatment of this problem. In addition to its theoretical transparency, this model has the advantage of having a very close relation to the physical problem we are considering here, *i.e.* to giant resonances. The $1\hbar\omega_0$ transition from the ground state to the $n = 1$ oscillator state corresponds to the electric giant-dipole resonance, the $2\hbar\omega_0$ transition to the d-component of the $n = 2$ oscillator states corresponds to the

electric giant-quadrupole resonance, *etc.* This interpretation shows that each electric giant-multipole resonance is accompanied by higher harmonics which are closely related to the retardation problem. Magnetic giant resonances are not taken into consideration.

In the following subsections we explicitly formulate the model. We find an analytical representation of the Compton scattering amplitude[8] $T = S + R$, study the high-energy behavior of T and show that the amplitude satisfies the fixed-t dispersion relation. We discuss why relativistic effects are important for the validity of the dispersion relation. Finally, we study the retardation effects on the amplitude at low and high energies and on the $E1$ and $E2$ sum rules and discuss how the retardation form factors can appear in the Compton scattering amplitude and in the dispersion relations.

10.2 Basics of the model. The seagull and resonance amplitudes

We consider a scalar particle with the electric charge e described by the Klein-Gordan equation with an oscillator Lorentz-scalar potential,

$$\Big[\Big(i\frac{\partial}{\partial t} - eA_0\Big)^2 - (i\boldsymbol{\nabla} + e\mathbf{A})^2 - (\mu^2 + \gamma^4 r^2)\Big]\psi(\mathbf{r}, t) = 0. \tag{10.6}$$

When the electromagnetic potential A_μ is absent, the normalized solutions $\psi^{\pm}_{n\alpha}$ of the above Klein-Gordan equation with positive and negative energies read

$$\psi^{\pm}_{n\alpha}(\mathbf{r}, t) = \frac{1}{\sqrt{2E_n}} \exp(\mp iE_n t)\phi_{n\alpha}(\mathbf{r}), \tag{10.7}$$

where $n = 2n_r + j$ is the quantum number which determines the energies $\pm E_n$ of degenerated levels with different radial quantum numbers n_r and angular momenta j, and the generic parameter $\alpha = (jm)$ describing the angular momentum j and its projection m. The eigen functions $\phi_{n\alpha}$ satisfy the equation

$$-\boldsymbol{\nabla}^2\phi_{n\alpha}(\mathbf{r}) + \gamma^4 r^2\phi_{n\alpha}(\mathbf{r}) = (E_n^2 - \mu^2)\phi_{n\alpha}(\mathbf{r}), \qquad \int |\phi_{n\alpha}(\mathbf{r})|^2 d\mathbf{r} = 1, \tag{10.8}$$

and the eigen energies E_n are

$$E_n = \sqrt{\mu^2 + (2n+3)\gamma^2} = \sqrt{E_0^2 + 2n\gamma^2}, \quad n = 0, 1, 2, \ldots. \tag{10.9}$$

The wave functions and the energy spectrum are characterized by two parameters, γ and E_0. The parameter γ determines the scale for the wave function of the ground state,

$$\phi_0(r) = N_0 \exp\left(-\frac{1}{2}\gamma^2 r^2\right), \quad |N_0|^2 = \gamma^3\pi^{-3/2}, \tag{10.10}$$

the corresponding r.m.s. electric radius, $\langle r_E^2\rangle^{1/2} = \sqrt{\frac{3}{2}}\gamma^{-1}$, and the form factor of the charge distribution in the ground state,

$$F(q) = \int \exp(i\mathbf{q}\cdot\mathbf{r})\,|\phi_0(\mathbf{r})|^2 d\mathbf{r} = \exp\left(-\frac{q^2}{4\gamma^2}\right). \tag{10.11}$$

The parameter $2E_0$ determines the energy gap between positive and negative parts of the spectrum. In the nonrelativistic limit, E_0 becomes the mass of the particle, and the quantity

$$\omega_0 \equiv \frac{\gamma^2}{E_0} \tag{10.12}$$

[8] We drop here and in the following the subscript GR

becomes the oscillator frequency. The scale of relativistic effects is determined by the dimensionless ratio

$$\eta = \frac{\gamma^2}{E_0^2} = \frac{\omega_0}{E_0} = \frac{\omega_0^2}{\gamma^2}, \quad 0 < \eta < \infty. \tag{10.13}$$

In the nonrelativistic regime, $\eta \ll 1$. When $\eta \gtrsim 1$, the energies which are necessary to excite the oscillator or create a particle-antiparticle pair become of the same order.

Figure 10.1: *Diagrams of Compton scattering off the relativistic oscillator (crossed terms are not shown)*

The total amplitude of photon scattering on the particle confined in the potential wall consists of two parts. The first one, T_D, is the so-called Delbrück scattering amplitude which describes scattering by the empty potential wall via virtual particle-antiparticle pairs (see the recent review [5] and references therein). It is usually small except for a region of near-forward scattering angles. For the case of the oscillator potential, the Delbrück amplitude was calculated in [285]. The second part T, which solely will be discussed in the following, is the amplitude for Compton scattering by the particle itself. It is given by diagrams of the noncovariant perturbation theory which are shown in Fig. 10.1. There, the diagram a gives the seagull contribution S, and the diagrams b and c correspond to the resonance part R of the amplitude $T = S + R$. The seagull contribution reads

$$S = -\frac{e^2}{E_0}(\boldsymbol{\epsilon}_1 \cdot \boldsymbol{\epsilon}_2)\langle\phi_0|\exp(i\mathbf{q}\cdot\mathbf{r})|\phi_0\rangle = -\frac{e^2}{E_0}(\boldsymbol{\epsilon}_1 \cdot \boldsymbol{\epsilon}_2)F(q) \tag{10.14}$$

with $\mathbf{q} = \mathbf{k}_1 - \mathbf{k}_2$, whereas the resonance amplitude R has the form

$$\begin{aligned} R &= \sum_{n\alpha} \frac{e^2}{E_0 E_n} \frac{\langle\phi_0|(\boldsymbol{\epsilon}_2\cdot\mathbf{p})\exp(-i\mathbf{k}_2\cdot\mathbf{r})|\phi_{n\alpha}\rangle\langle\phi_{n\alpha}|(\boldsymbol{\epsilon}_1\cdot\mathbf{p})\exp(i\mathbf{k}_1\cdot\mathbf{r})|\phi_0\rangle}{E_n - \omega - E_0 - i0} + \\ &\sum_{n\alpha} \frac{e^2}{E_0 E_n} \frac{\langle\phi_0|(\boldsymbol{\epsilon}_2\cdot\mathbf{p})\exp(-i\mathbf{k}_2\cdot\mathbf{r})|\phi_{n\alpha}\rangle\langle\phi_{n\alpha}|(\boldsymbol{\epsilon}_1\cdot\mathbf{p})\exp(i\mathbf{k}_1\cdot\mathbf{r})|\phi_0\rangle}{E_n + \omega + E_0 - i0} + \\ &(\omega \to -\omega,\ \mathbf{k}_1 \leftrightarrow -\mathbf{k}_2,\ \boldsymbol{\epsilon}_1 \leftrightarrow \boldsymbol{\epsilon}_2). \end{aligned} \tag{10.15}$$

The factors $1/E_0$ in (10.14) and $1/E_0E_n$ in (10.15) are related with the proper normalization of the wave functions, *cf.* Eq. (10.7). The first sum in (10.15) corresponds to the contribution of positive-energy intermediate states (the diagram b), whereas the second one accounts for negative-energy states, or virtual pair production (the diagram c).[9] Taken together, they give the resonance amplitude in the Feynman approach with the Feynman propagator $(E_n^2 - (\omega + E_0)^2 - i0)^{-1}$. The crossed term has a similar structure and interpretation. The k-dependent exponents in (10.15) describe the retardation effects. Keeping in the operators $(\boldsymbol{\epsilon}\cdot\mathbf{p})\exp(\pm i\mathbf{k}\cdot\mathbf{r})$ the leading-in-k terms of a given total angular momentum j (*cf.* section 3.4), we can obtain unretarded contributions to different multipole amplitudes $R^{\lambda j}$. The unretarded amplitudes can also be extracted from leading terms in an expansion of the total amplitude (10.15) in powers of photon momenta, k_1 and k_2, considered at arbitrary absolute values of $k_1 \neq \omega$ and $k_2 \neq \omega$. The momenta are still assumed to be orthogonal to the photon polarizations,

[9] In terms of physical states having positive energies and consisting of particles and antiparticles (i.e. p and $\bar{p}$), the two sums in (10.15) have a different meaning. The first sum is related with transitions of the particle p from the ground state to an excited state ($p_0 \leftrightarrow p_{n\alpha}$). The second sum is related with pair production from the vacuum. Most of the pair production is included through the Delbrück scattering amplitude T_D which takes into account all possible transitions $vac \leftrightarrow p_i\bar{p}_j$. However, due to Bose correlations, the presence of the particle p_0 in the initial state doubles the probability of pair production to the occupied state $i = 0$. Respectively, the second sum in Eq. (10.15) takes into account these additional transitions $vac \leftrightarrow p_0\bar{p}_j$ caused by the initial particle p_0. Note that in the case of a spin-1/2 particle the second sum would change its sign. It would describe Fermi correlations with p_0, i.e. Pauli blocking of pair production to the occupied state p_0.

$\boldsymbol{\epsilon}_1 \cdot \mathbf{k}_1 = \boldsymbol{\epsilon}_2 \cdot \mathbf{k}_2 = 0$. Since it is equally easy, in our simple model, to calculate the amplitude R for such a general case of arbitrary k_1 and k_2, we follow this way to make the retardation effects manifestly evident. In other words, we calculate the amplitude of virtual Compton scattering with transversely polarized photons.

A powerful tool to calculate the resonance amplitude (10.15) is provided by the Greens function which is explicitly known for the oscillator potential. Introducing

$$G(\mathbf{r}_2, \mathbf{r}_1|E) = \sum_{n\alpha} \frac{\langle \mathbf{r}_2|\phi_{n\alpha}\rangle\langle\phi_{n\alpha}|\mathbf{r}_1\rangle}{E^2 - E_n^2 + i0}, \tag{10.16}$$

we rewrite the resonance amplitude like

$$R = -\frac{2e^2}{E_0} \int \exp(i\mathbf{k}_1 \cdot \mathbf{r}_1 - i\mathbf{k}_2 \cdot \mathbf{r}_2) \Big(\boldsymbol{\epsilon}_2 \cdot \boldsymbol{\nabla}\phi_0(\mathbf{r}_2)\Big)^* G(\mathbf{r}_2, \mathbf{r}_1|\omega + E_0) \times \Big(\boldsymbol{\epsilon}_1 \cdot \boldsymbol{\nabla}\phi_0(\mathbf{r}_1)\Big)\, d\mathbf{r}_1\, d\mathbf{r}_2 + \text{crossed term}. \tag{10.17}$$

Substituting the Greens function for the relativistic oscillator [285, 286],

$$G(\mathbf{r}_2, \mathbf{r}_1|E) = -\frac{i\gamma}{2} \int_0^\infty \frac{ds}{(2\pi i \sin s)^{3/2}} \times \exp\left\{ \frac{is}{2\gamma^2}(E^2 - \mu^2 + i0) + \frac{i\gamma^2}{2\sin s}\Big[(r_1^2 + r_2^2)\cos s - 2\mathbf{r}_1 \cdot \mathbf{r}_2\Big] \right\} \tag{10.18}$$

and taking simple Gaussian integrals with respect to $\mathbf{r}_1$ and $\mathbf{r}_2$, we finally get

$$R = \frac{e^2\, F(q)}{2E_0} \left\{ g(a, x)(\boldsymbol{\epsilon}_1 \cdot \boldsymbol{\epsilon}_2) + g(a-1, x)\frac{(\boldsymbol{\epsilon}_1 \cdot \mathbf{k}_2)(\boldsymbol{\epsilon}_2 \cdot \mathbf{k}_1)}{2\gamma^2} \right\} + (\omega \to -\omega). \tag{10.19}$$

Here the function g, a close relative of the standard incomplete gamma-function, reads

$$g(a, x) = \frac{i}{e^{-2\pi i a} - 1} \int_0^{2\pi} \exp\Big(-ias + x(e^{is} - 1)\Big)\, ds, \tag{10.20}$$

and the quantities x and a are defined as

$$x = \frac{\mathbf{k}_1 \cdot \mathbf{k}_2}{2\gamma^2}, \qquad a = \frac{\omega^2 + 2\omega E_0}{2\gamma^2} - 1 + i0. \tag{10.21}$$

In this form, Eqs. (10.14) and (10.19) for the seagull and the resonance amplitude, respectively, are valid for any k_1 and k_2. We have to set $k_1 = k_2 = \omega$ whenever we consider Compton scattering with real photons, including the retardation effects.

For further references note that

$$g(a, x) = e^{-x} \sum_{n=0}^{\infty} \frac{x^n}{n!(n-a)} = -\sum_{n=0}^{\infty} \frac{x^n}{a(a-1)\ldots(a-n)} \tag{10.22}$$

and

$$xg(a-1, x) = ag(a, x) + 1. \tag{10.23}$$

It is seen that $g(a, x)$ is a regular function of x and a except for simple poles at $a = 0, 1, 2, \ldots$. Asymptotic expansions of g at low energies (when $x \ll a \approx -1$) or at "nonrelativistically high energies" (*i.e.* when $\omega \sim \gamma \gg \omega_0$ and $\omega \ll E_0$, or, in other words, when $a \gg x \sim 1$; such a regime is possible, provided $\eta \ll 1$) directly follow from Eq. (10.22). The important case of $a \approx x \sim (a - x)^2 \to \infty$,

which arises for real Compton scattering at ultra-relativistic energies, is described by the saddle-point asymptotics

$$g(a,x) = -\sqrt{\frac{\pi}{2x}}\exp\Big(-\frac{(a-x)^2}{2x}\Big)\,\mathrm{ctg}\,(\pi a) + \frac{i}{\sqrt{x}}\int_0^\infty \sin\Big(\frac{a-x}{\sqrt{x}}s\Big)\,e^{-s^2/2}\,ds + O(\frac{1}{x}). \tag{10.24}$$

Here the sign of $\sqrt{x}$ must be chosen in such a way that $\mathrm{Re}\sqrt{x} > 0$.

Given (10.22), the amplitude R is recast to the form[10]

$$R = \frac{e^2}{2E_0}\sum_{n=1}^{\infty}\frac{\omega_0\,F(k_1)\,F(k_2)}{n\omega_0 - \omega - \omega^2/2E_0 - i0}\times \left\{\frac{x^{n-1}}{(n-1)!}(\boldsymbol{\epsilon}_1\cdot\boldsymbol{\epsilon}_2) + \frac{x^{n-2}}{(n-2)!}\frac{(\boldsymbol{\epsilon}_1\cdot\mathbf{k}_2)(\boldsymbol{\epsilon}_2\cdot\mathbf{k}_1)}{2\gamma^2}\right\} + (\omega\to-\omega), \tag{10.25}$$

which is useful to single out the individual contributions of different intermediate states. In particular, from (10.25) one can directly read off individual contributions of oscillator excitations and pair production to the amplitude (10.15). These contributions correspond to the pole parts of the ω-dependent propagator in (10.25),

$$\frac{\omega_0/E_0}{n\omega_0 - \omega - \omega^2/2E_0} = \frac{\gamma^2}{E_0E_n}\left(\frac{1}{E_n - E_0 - \omega} + \frac{1}{E_n + E_0 + \omega}\right). \tag{10.26}$$

The sum over n in (10.25) starts from $n = 1$ because the matrix elements in (10.15) vanish at $n = 0$. Also, in (10.25) it should be taken into account that $(-1)! = \infty$. For a weakly relativistic oscillator (i.e. $\eta \ll 1$) and low energies $\omega \sim \omega_0$, the resonance amplitude R is dominated by the dipole term ($n = 1$), whereas the higher-level corrections are generally suppressed as η^{n-1}.

Equation (10.25) is convenient for obtaining the multipole structure of the resonance amplitudes. All the angular dependence of R is contained in the x-dependent braces in (10.25), where $x \propto \cos\theta \equiv z$. Applying the same technique of helicity amplitudes as was used in section 8.1, we find the partial Ej-components of the resonance amplitude as a sum over radial excitations,[11]

$$R^{Ej} = \frac{e^2}{2E_0}\sum_{n=j,j+2,j+4,\ldots}\frac{\omega_0\,F(k_1)\,F(k_2)}{n\omega_0 - \omega - \omega^2/2E_0 - i0}\left(\frac{k_1k_2}{2\gamma^2}\right)^{n-1}\frac{C_{jn}}{(n-1)!} + (\omega\to-\omega). \tag{10.27}$$

Here the coefficients C_{jn} determine the multipole expansion of the braces in (10.25),

$$z^{n-1}(\boldsymbol{\epsilon}_1\cdot\boldsymbol{\epsilon}_2) + (n-1)z^{n-2}(\boldsymbol{\epsilon}_1\cdot\hat{\mathbf{k}}_2)(\boldsymbol{\epsilon}_2\cdot\hat{\mathbf{k}}_1) = \sum_j C_{jn}\,g_{Ej}. \tag{10.28}$$

They are normalized as $\sum_j C_{jn} = 1$ and are equal to

$$C_{jn} = \frac{2j+1}{4}\int_{-1}^{1}\Big(nz^{n-1} - (n-1)z^{n-2}\Big)(1+z)\,d^j_{1,1}(\theta)\,dz = \frac{1}{4}\Big(1 + (-1)^{n-j}\Big)\,\frac{j(j+1)(2j+1)}{(n+j+1)(n+j-1)}\prod_{i=1}^{[(j-1)/2]}\frac{n-j+2i}{n+j-2i-1}\,, \tag{10.29}$$

[10] This form can be easily derived from (10.15) by using, instead of the Greens function method, the well-known technique of the creation and annihilation operators for the harmonic oscillator.

[11] The partial amplitudes here are normalized as $R(\omega,\theta) = \sum_j R^{Ej}(\omega)\,g^{Ej}(\theta)$.

provided $n \geq j$ (otherwise $C_{jn} = 0$). In particular,

$$C_{1n} = \frac{3}{n(n+2)}, \quad C_{2n} = \frac{15}{(n+1)(n+3)}, \quad \textit{etc.} \qquad (\text{for} \quad n-j = \text{even}). \tag{10.30}$$

The (magnetic) Mj-components of R are identically zero in our model due to parity conservation.

Keeping in (10.27) the leading-in-k term, i.e. omitting the form factors $F(k_1)$ and $F(k_2)$ and retaining only the lowest $n = j$ contribution, we obtain the unretarded multipoles,

$$\mathring{R}^{Ej} = \frac{e^2}{E_0} \frac{\omega_0 \, (j\omega_0 - \omega^2/2E_0)}{(j\omega_0 - \omega^2/2E_0)^2 - \omega^2 - i0} \left(\frac{k_1 k_2}{2\gamma^2}\right)^{j-1} \frac{C_{jj}}{(j-1)!} \; . \tag{10.31}$$

For a weakly relativistic oscillator ($\eta \ll 1$), the main difference between the unretarded and retarded multipoles R^{Ej} at low energies $\omega \lesssim j\omega_0$ is described by the k-dependent form factor squared of the ground state. Also, the form factor damps the amplitude at the resonance peak, *e.g.* to the amount of $F^2(\omega_0) = e^{-\eta/2}$ in the case of the $E1$-multipole at $\omega \simeq \omega_0$.

In order to understand what happens at somewhat higher energies ω (but still a few ω_0), note that all the coefficients C_{jn} are positive. They determine relative contributions of different radial excitations to R^{Ej} and are proportional to the matrix element squared of the transition operator $(\boldsymbol{\epsilon}_1 \cdot \mathbf{p}) \exp(i\mathbf{k}_1 \cdot \mathbf{r})$ between the ground state $|\phi_0\rangle$ and a state $|\phi_{n(jm)}\rangle$ of the energy E_n and the angular momentum j. So, this feature does not depend on a specific shape of the potential. Then, in the region between the energies ω_0 and $3\omega_0$, the positive contributions $O(\eta^2)$ of the radial excitations to R^{E1} tend to cancel the leading negative contribution from the first level $n = 1$ and thus slightly intensify the damping effect $O(\eta)$ caused by the k-dependent form factors alone. Similar small local strengthening of the damping effects just above the first peak holds for higher multipoles as well.

At even higher energies, $\omega \sim \gamma \gg \omega_0$, which we would call intermediate energies, when the k-dependent form factors produce essential damping of individual transitions, the contributions of radial excitations are not negligible at all. They are enhanced by powers of the same parameter $k_1 k_2/2\gamma^2$ which determines the magnitude of the form factors. As a result, many multipoles R^{Ej} become as large as R^{E1}, which dominates at low energies. They act coherently at small angles and tend to compensate the effect of the form factors. Below we explicitly demonstrate this important feature.

10.3 Asymptotic behavior and fixed-t dispersion relations

The resonance amplitude (10.25) at $k_1 = k_2 = \omega$ is given by a convergent series in $x = (2\omega^2 - q^2)/4\gamma^2$ and has no singularities at finite energies ω and momentum transfer $q^2 = -t$, except for the poles at $\omega = \omega_n^{\pm}$ and $\omega = -\omega_n^{\pm}$, where the quantities

$$\omega_n^{\pm} = E_n \mp E_0 \tag{10.32}$$

describe the energies of the oscillator excitation and pair production, respectively. Moreover, the seagull amplitude (10.14), considered as a function of the energy, is a (t-dependent) constant. Therefore, the validity of the fixed-t dispersion relation for the Compton scattering amplitude T and for the appropriate invariant amplitudes depends on whether or not they vanish at high complex ω.

Using (10.14) and (10.19), we find coefficients of the structures $(\boldsymbol{\epsilon}_1 \cdot \boldsymbol{\epsilon}_2)$ and $(\mathbf{s}_1 \cdot \mathbf{s}_2)$ in the total amplitude T and then obtain the invariant amplitudes $A_{1,2}(\omega, t)$. They read

$$\omega^2 \, (A_1 + A_2) \;\; = \;\; \frac{e^2}{2E_0} F(q) \Big\{ (1+a) g(a,x) + (\omega \to -\omega) \Big\}, \tag{10.33}$$

$$(A_1 - A_2) \;\; = \;\; -\frac{e^2}{4\gamma^2 E_0} F(q) \Big\{ g(a-1,x) + (\omega \to -\omega) \Big\}. \tag{10.34}$$

Note that, at low energies $\omega \to 0$ and fixed t, the parameter $a \to -1$ and $x \to t/4\gamma^2$. In this limit, the r.h.s. of Eq. (10.33) vanishes. Respectively, both the amplitudes $A_{1,2}(\omega, t)$ are finite at $\omega = 0$ and thus are free from the $1/\omega^2$ pole. This perfectly agrees with the low-energy theorem, since the system of "the particle plus the potential wall" has an infinite mass and, therefore, its Thomson amplitude has to vanish.

At high energies, $\omega \to \infty$, and fixed t, both a and x go to infinity like ω^2, and $(a-x)^2 = O(\omega^2)$ as well. Using Eq. (10.24), we find that both amplitudes $A_{1,2}(\omega, t)$ vanish like $O(1/\omega)$ in the complex plane of ω and, therefore, satisfy unsubtracted fixed-t dispersion relations (8.17). The ultra-relativistic asymptotics of the resonance amplitude reads

$$R \simeq -\frac{e^2}{2E_0} F(q)\, e^{-1/\eta} \sqrt{\frac{\pi}{2x}} \Big(\mathrm{ctg}\,(\pi a) + (\omega \to -\omega) \Big) \left\{ (\boldsymbol{\epsilon}_1 \cdot \boldsymbol{\epsilon}_2) + \frac{(\boldsymbol{\epsilon}_1 \cdot \mathbf{k}_2)(\boldsymbol{\epsilon}_2 \cdot \mathbf{k}_1)}{2\gamma^2} \right\}, \tag{10.35}$$

where $\mathrm{Re}\sqrt{x} > 0$, like in (10.24). Beyond the real axis of ω, the amplitude R is predominately imaginary,

$$R \simeq i\,\mathrm{sign}(\mathrm{Im}\,\omega)\, \frac{e^2}{\omega} F(q) \sqrt{\pi\eta}\, e^{-1/\eta} \left\{ (\boldsymbol{\epsilon}_1 \cdot \boldsymbol{\epsilon}_2) + \frac{(\boldsymbol{\epsilon}_1 \cdot \mathbf{k}_2)(\boldsymbol{\epsilon}_2 \cdot \mathbf{k}_1)}{2\gamma^2} \right\}. \tag{10.36}$$

When the relativistic parameter η is small, the coefficient of the leading $1/\omega$ term in this asymptotics is exponentially suppressed. Then the asymptotic regime (10.36) holds only at extremely high energies, whereas at intermediate energies of $\omega \sim \gamma \gg \omega_0$ the resonance amplitude is predominately real and follows the $1/\omega^2$ dependence,

$$R \simeq -\frac{e^2}{E_0}\, \frac{\omega_0^2}{\omega^2} F(q) \left\{ \Big(1 - \frac{q^2}{4\gamma^2}\Big)(\boldsymbol{\epsilon}_1 \cdot \boldsymbol{\epsilon}_2) + \Big(2 - \frac{q^2}{4\gamma^2}\Big) \frac{(\boldsymbol{\epsilon}_1 \cdot \mathbf{k}_2)(\boldsymbol{\epsilon}_2 \cdot \mathbf{k}_1)}{2\gamma^2} \right\}. \tag{10.37}$$

The remarkable feature of these asymptotics is that the retardation k-dependent form factors $F(k_1)$ and $F(k_2)$, which accompany all individual contributions of the transitions $|0\rangle \to |n\alpha\rangle$ and exponentially grow at high complex energies, are canceled when many transitions come into play. In the asymptotic regime, the resulting amplitude depends on the form factor only through the momentum transfer q rather than the energy ω and, therefore, is free from the exponential growth at $\omega \to i\infty$. This is why the fixed-t dispersion relation holds.

As an important particular case, note that the asymptotics (10.37) of the exact amplitude R at $\theta = 0$ and at intermediate energies behaves like the asymptotics of the naive unretarded electric dipole amplitude

$$\overset{\circ}{R}{}^{E1,\mathrm{naive}} = \frac{e^2}{E_0}\, \frac{\omega_0^2}{\omega_0^2 - \omega^2 - i0}\ . \tag{10.38}$$

This feature is connected with a validity of the dispersion relation and its consequence, the $E1$-sum rule, is discussed in the next subsection.

It is instructive to compare the high-energy behavior of the Compton scattering amplitude off the relativistic and nonrelativistic (nonrel) oscillator and to see where a difference comes from. The nonrelativistic oscillator has the energy spectrum

$$E_n^{\mathrm{nonrel}} = E_0^{\mathrm{nonrel}} + n\omega_0 \tag{10.39}$$

(only with positive energies) and is described by the same eigen functions $\phi_{n\alpha}$ as in (10.8), with the substitution $E_n^2 - \mu^2 \to (2n+3)\gamma^2$. The nonrelativistic oscillator frequency $\omega_0 = \gamma^2/M$ is determined by the size of the charge distribution in the ground state, $1/\gamma$, and the mass of the particle, M. The nonrelativistic resonance amplitude R^{nonrel} is given by expressions similar to (10.15) and (10.25),

$$R^{\mathrm{nonrel}} \quad = \quad \sum_{n\alpha} \frac{e^2}{M^2} \frac{\langle\phi_0|(\boldsymbol{\epsilon}_2 \cdot \mathbf{p}) \exp(-i\mathbf{k}_2 \cdot \mathbf{r})|\phi_{n\alpha}\rangle\langle\phi_{n\alpha}|(\boldsymbol{\epsilon}_1 \cdot \mathbf{p}) \exp(i\mathbf{k}_1 \cdot \mathbf{r})|\phi_0\rangle}{E_n - \omega - E_0 - i0}$$

$$+ (\omega \to -\omega,\ \mathbf{k}_1 \leftrightarrow -\mathbf{k}_2,\ \boldsymbol{\epsilon}_1 \leftrightarrow \boldsymbol{\epsilon}_2) \tag{10.40}$$

$$= \sum_{n=1}^{\infty} \frac{e^2\gamma^2\, F(k_1)\, F(k_2)}{2M^2(n\omega_0 - \omega - i0)} \left\{ \frac{x^{n-1}}{(n-1)!}(\boldsymbol{\epsilon}_1 \cdot \boldsymbol{\epsilon}_2) + \frac{x^{n-2}}{(n-2)!} \frac{(\boldsymbol{\epsilon}_1 \cdot \mathbf{k}_2)(\boldsymbol{\epsilon}_2 \cdot \mathbf{k}_1)}{2\gamma^2} \right\}$$
$$+ (\omega \to -\omega) \tag{10.41}$$

$$= \frac{e^2\, F(q)}{2M} \left\{ g(a_0, x)(\boldsymbol{\epsilon}_1 \cdot \boldsymbol{\epsilon}_2) + g(a_0 - 1, x) \frac{(\boldsymbol{\epsilon}_1 \cdot \mathbf{k}_2)(\boldsymbol{\epsilon}_2 \cdot \mathbf{k}_1)}{2\gamma^2} \right\}$$
$$+ (\omega \to -\omega), \qquad a_0 = \omega/\omega_0 - 1 + i0. \tag{10.42}$$

The absence of ω^2-pieces in the denominator in (10.41) and in a_0 drastically changes the behavior of the amplitude $R^{\rm nonrel}$ at very high complex energies. When $\omega \to i\infty$, the function $g(a_0, x)$ grows exponentially like e^{-x} with x given by Eq. (10.21).. Respectively, the resonance amplitude $R^{\rm nonrel}$ grows like the retardation form factors $F^2(\omega)$ and does not obey the fixed-t dispersion relation.[12]

A difference between the asymptotics of the relativistic and nonrelativistic amplitudes appears not only at extremely high energies. The retardation corrections become essential already at intermediate energies, $\omega \sim \gamma$, and the amplitude $R^{\rm nonrel}$ behaves like

$$R^{\rm nonrel} \simeq -\frac{e^2}{M} \frac{\omega_0^2}{\omega^2} F(q) \left\{ (1 + x)(\boldsymbol{\epsilon}_1 \cdot \boldsymbol{\epsilon}_2) + (2 + x) \frac{(\boldsymbol{\epsilon}_1 \cdot \mathbf{k}_2)(\boldsymbol{\epsilon}_2 \cdot \mathbf{k}_1)}{2\gamma^2} \right\} \tag{10.43}$$

at such ω, with $x = (-q^2 + 2\omega^2)/4\gamma^2$. Therefore, it shows no tendency to decrease, in contrast to (10.37).

It is again instructive to obtain the nonrelativistic asymptotics (10.43) directly from Eq. (10.40) and to trace a difference with the relativistic consideration. Since the sum in (10.40) is saturated by intermediate states with the typical momentum $\sim k$ and, hence, with the excitation energies $E_n - E_0 \sim k^2/(2M) \ll \omega$, the denominator in (10.40) can be expanded in the inverse powers of ω,

$$\frac{1}{E_n - E_0 - \omega} = -\frac{1}{\omega} - \frac{E_n - E_0}{\omega^2} - \cdots. \tag{10.44}$$

Here the leading term is odd and is canceled by the crossed term. The asymptotics is determined by the next term. Using closure, one can recast the result in terms of the double commutator of the electromagnetic currents and the nonrelativistic Hamiltonian $H = p^2/(2M) + M\omega_0^2 r^2/2$,

$$R^{\rm nonrel} \simeq -\frac{1}{\omega^2} \langle \phi_0 | \, [j_2, [H, j_1]] \, | \phi_0 \rangle. \tag{10.45}$$

Here $j_1 = (e/M)(\boldsymbol{\epsilon}_1 \cdot \mathbf{p}) \exp(i\mathbf{k}_1 \cdot \mathbf{r})$ and $j_2 = (e/M)(\boldsymbol{\epsilon}_2 \cdot \mathbf{p}) \exp(-i\mathbf{k}_2 \cdot \mathbf{r})$. Calculating the above matrix element, we arrive at Eq. (10.43). The derivatives of the k-dependent exponents in the operators j_1 and j_2, coming from the commutator with the kinetic energy, lead to the ω^2-terms in the braces of (10.43). With similar steps for the relativistic oscillator, we would get a difference due to the negative-energy intermediate states which results in an ω^2-correction in the energy denominator. So, instead of Eq. (10.44), we get the terms

$$\frac{1}{E_n - E_0 - \omega - \omega^2/(2M)} = -\frac{1}{\omega} - \frac{E_n - E_0 - \omega^2/(2M)}{\omega^2} - \cdots \tag{10.46}$$

[12]The violation of the dispersion relation for the nonrelativistic Compton scattering amplitude was discussed in Ref. [186–188] where it was connected with additional poles or cuts at $\omega \simeq 2M$. In the nonrelativistic oscillator model such singularities are absent, but the exponential growth at $\omega \to i\infty$ does make standard dispersion relations inapplicable. It is still possible to write a "practical" dispersion relation with a Cauchy loop of a finite size $\omega_{\rm max}$ with $\gamma \ll \omega_{\rm max} \ll M$ and use the asymptotics discussed in the text for allowing for high-ω contributions.

in this case. Here, the relativistic correction $\omega^2/(2M)$ is of the same order of magnitude as $E_n - E_0$ itself . It gives an additional ω-independent contribution to the asymptotic resonance amplitude,

$$R_- = \frac{1}{2M}\langle\phi_0|j_1 j_2 + j_2 j_1|\phi_0\rangle. \tag{10.47}$$

This R_-, which is the contribution of negative energies, compensates the ω-independent term, which appears in (10.43) through the terms containing x, and results in a relativistic $1/\omega^2$-asymptotics, Eq. (10.37), consistent with the fixed-t dispersion relation.

10.4 Retarded and unretarded sum rules

Since the amplitude R vanishes at $\omega \to \infty$ and fixed t, it obeys the unsubtracted dispersion relation. That means that both the coefficients of $(\boldsymbol{\epsilon}_1 \cdot \boldsymbol{\epsilon}_2)$ and $(\boldsymbol{\epsilon}_1 \cdot \mathbf{k}_2)(\boldsymbol{\epsilon}_2 \cdot \mathbf{k}_1)$ obey the relation:

$$\begin{aligned} R(\omega,t) &= \frac{2}{\pi}\int_0^\infty \mathrm{Im}\, R(\omega',t)\,\frac{\omega' d\omega'}{\omega'^2 - \omega^2 - i0} \\ &= \sum_{\pm}\sum_{n=1}^{\infty} \frac{e^2}{E_0 E_n}\,\frac{\gamma^2 \omega_n^{\pm} F^2(\omega_n^{\pm})}{(\omega_n^{\pm})^2 - \omega^2 - i0} \times \\ &\qquad \left\{ \frac{(x_n^{\pm})^{n-1}}{(n-1)!}(\boldsymbol{\epsilon}_1 \cdot \boldsymbol{\epsilon}_2) + \frac{(x_n^{\pm})^{n-2}}{(n-2)!}\,\frac{(\boldsymbol{\epsilon}_1 \cdot \mathbf{k}_2)(\boldsymbol{\epsilon}_2 \cdot \mathbf{k}_1)}{2\gamma^2} \right\}. \end{aligned} \tag{10.48}$$

Here the sign of $\pm$ refers to the contributions of positive and negative energies, and $x_n^{\pm} = (2(\omega_n^{\pm})^2 + t)/4\gamma^2$. Matching the r.h.s. of Eq. (10.48) with the relation

$$R(0,t) = -S(t) = \frac{e^2}{E_0}(\boldsymbol{\epsilon}_1 \cdot \boldsymbol{\epsilon}_2)F(t), \tag{10.49}$$

which strictly follows from the low-energy theorem for the total amplitude, which reads $T(\omega = 0, t) = 0$ in our case, we arrive at the series of sum rules as discussed in section 8.2. In the following we consider two of them which are closely related with the $E1$ and $E2$ photoabsorption, respectively.

(i) The first one, the Gell-Mann–Goldberger–Thirring (GGT) sum rule, corresponds to the particular case of $t = 0$ in (10.48). It reads

$$\Sigma \equiv \int_0^\infty \sigma(\omega)\, d\omega = 2\pi^2 R(0,0) = \frac{2\pi^2 e^2}{E_0}, \tag{10.50}$$

where

$$\sigma(\omega) = \frac{4\pi}{\omega}\,\mathrm{Im}\, R(\omega, 0) \tag{10.51}$$

is the total photoabsorption cross section. In accordance with Eqs. (10.25) and (10.48), this cross section consists of the contribution of particle excitation, σ_+, and that of pair production, σ_-,

$$\sigma = \sigma_+ + \sigma_-, \qquad \sigma_\pm(\omega) = \sum_{n=1}^{\infty} \frac{2\pi^2 e^2 \gamma^2}{\omega E_0 E_n} e^{-A}\frac{A^{n-1}}{(n-1)!}\delta(\omega - E_n \pm E_0), \quad A = \frac{\omega^2}{2\gamma^2}. \tag{10.52}$$

Respectively, the integral in (10.50) consists of two parts as well,

$$\Sigma = \Sigma_+ + \Sigma_-, \quad \Sigma_\pm = \sum_{n=1}^{\infty} \frac{2\pi^2 e^2 \gamma^2}{\omega_n^{\pm} E_0 E_n}\,\frac{(A_n^{\pm})^{n-1}}{(n-1)!}\exp(-A_n^{\pm}), \qquad A_n^{\pm} = \frac{(\omega_n^{\pm})^2}{2\gamma^2}. \tag{10.53}$$

Both of them are needed to strictly fulfil the GGT sum rule. However, in the weakly relativistic case, the pair contribution is exponentially suppressed by the retardation form factors, $\Sigma_- \propto \exp(-1/\eta)$,

and the sum rule is saturated with the positive-energy contribution Σ_+. Even when $\eta = 1$, Σ_- contributes still only 5% to the total magnitude of Σ. Only in the extreme case of $\eta \gg 1$ both parts of Σ become compatible. $\Sigma_- = \Sigma_+ = \frac{1}{2}\Sigma$ in this limit.

When the retardation in Eq. (10.50) is switched off, i.e. when k_1 and k_2 are set to zero, we find the unretarded $E1$-amplitude,

$$\overset{\circ}{R}{}^{E1}(\omega) = \frac{e^2\gamma^2}{E_0}\frac{1}{2\gamma^2 - \omega^2 - 2\omega E_0} + (\omega \to -\omega). \tag{10.54}$$

It also satisfies the unsubtracted dispersion relation, and, being matched with the low-energy theorem (10.49), gives the unretarded partner of the GGT sum rule, which is the Thomas–Reiche–Kuhn (TRK) sum rule:

$$\overset{\circ}{\Sigma} \equiv \int_{\omega_{\rm thr}}^{\infty} \overset{\circ}{\sigma}{}^{E1}(\omega)\, d\omega = 2\pi^2 \overset{\circ}{R}{}^{E1}(0) = \frac{2\pi^2 e^2}{E_0}. \tag{10.55}$$

Here the unretarded photoabsorption cross section, $\overset{\circ}{\sigma}{}^{E1} = (4\pi/\omega){\rm Im}\overset{\circ}{R}{}^{E1}$, also consists of the contributions of excitation and pair production,

$$\overset{\circ}{\sigma}{}^{E1} = \overset{\circ}{\sigma}{}^{E1,+} + \overset{\circ}{\sigma}{}^{E1,-}, \qquad \overset{\circ}{\sigma}{}^{E1,\pm} = \frac{2\pi^2 e^2\gamma^2}{\omega E_0 E_1}\delta(\omega - E_1 \pm E_0). \tag{10.56}$$

Corresponding parts of $\overset{\circ}{\Sigma}$ read

$$\overset{\circ}{\Sigma}_{\pm} = \frac{2\pi^2 e^2\gamma^2}{\omega_1^{\pm} E_0 E_1}, \tag{10.57}$$

and their sum, $\overset{\circ}{\Sigma} = \overset{\circ}{\Sigma}_+ + \overset{\circ}{\Sigma}_-$, coincides with the retarded integral in Eq. (10.50),

$$\overset{\circ}{\Sigma} = \Sigma. \tag{10.58}$$

The last equation was discussed in literature many times after S. Gerasimov [95, 185–190]. It strictly holds in our model. Moreover, as is seen from the above derivation, it is valid in a more general case, with a general form of the current operators or the energy spectrum, provided the unsubtracted dispersion relation is valid for the retarded amplitude $R(\omega, 0)$. Other ingredients of the derivation, which are the unsubtracted dispersion relation for $\overset{\circ}{R}{}^{E1}(\omega)$ and the identity $R(0,0) = \overset{\circ}{R}{}^{E1}(0)$, are model independent.[13]

However, Gerasimov's relation (10.58) is valid only when both positive- and negative-energy parts are included. It is not valid for each of these parts separately. For a weakly relativistic oscillator, the contribution of pair production is exponentially small, $\Sigma_- \propto \exp(-1/\eta)$, whereas it is of order $\mathcal{O}(\eta)$ for the unretarded counterpart. Respectively,

$$\overset{\circ}{\Sigma}_+ - \Sigma_+ = -(\overset{\circ}{\Sigma}_- - \Sigma_-) \simeq -\overset{\circ}{\Sigma}_- \simeq -\frac{1}{2}\eta\Sigma \tag{10.59}$$

in this case. In other words, the positive-energy TRK sum rule differs from the GGT sum rule. Saturation of the full TRK sum rule needs the consideration of relativistically high energies, whereas such energies are irrelevant for the GGT sum rule. When the GGT and TRK integrals are truncated below the pair production threshold (that is what is usually done in most nuclear applications), they become different in order $\mathcal{O}(\eta)$. Such a "practical" violation of the Gerasimov's relation was studied and exemplified in [186–188, 190]. As was said, another reason for the violation of Eq. (10.58) can be

[13] These requirements are not fulfilled for a Dirac particle, for which the seagull contribution is absent and $R(\infty, 0) = T(\infty, 0) \neq 0$. In that case a sensical comparison of the GGT and TRK sum rule needs a consideration of positive-energy components [121, 287].

caused by a nonvanishing amplitude R at high real or complex energies, which makes the *unsubtracted* dispersion relation inapplicable for R (see an example in [189]).

Note that the retardation form factor in Σ_+ reduces the dominating $E1$ contribution by $F^2(\omega_1) \simeq 1-\frac{1}{2}\eta$. Since the $E2$ contribution also increases Σ_+ by η, the resulting GGT magnitude is bigger than the nonrelativistic TRK by $\frac{1}{2}\eta$. Only after adding the negative-energy part of TRK, $\mathring{\Sigma}_- \simeq \frac{1}{2}\eta\Sigma$, the balance between GGT and TRK is achieved.[14] Equation (10.59) perfectly agrees with the evaluation of the difference between positive-energy GGT and TRK sum rules for a bound particle done by Friar and Fallieros [187] who showed that this difference is equal to $-2\pi^2 e^2\langle p^2/3M^3\rangle$ (note that for the oscillator model $\langle p^2\rangle = \frac{3}{2}\gamma^2$). The origin of the difference (10.59) can be traced to the asymptotic behavior of the unretarded amplitude (10.54) at intermediate energies $\omega_0 \ll \omega \ll M$. This asymptotics is determined by the energy-independent contribution $\mathring{R}_-^{E1}$ of negative-energy states (see Eq. (10.47), in which one has to use $j_{1,2}$ with $\mathbf{k}_{1,2}=0$) and reads

$$\mathring{R}^{E1}(\omega) \simeq \mathring{R}_-^{E1} \simeq \frac{e^2\gamma^2}{2M^3} = \frac{e^2\langle p^2\rangle}{3M^3}. \tag{10.60}$$

Accordingly, the dispersion integral (10.55) truncated at an intermediate energy ω_m becomes

$$\mathring{\Sigma}(\omega_m) \equiv \int_{\omega_{\rm thr}}^{\omega_m} \mathring{\sigma}^{E1}(\omega)\,d\omega = 2\pi^2\Big(\mathring{R}^{E1}(0) - \mathring{R}^{E1}(\omega_m)\Big) \simeq \Big(1-\frac{\gamma^2}{2M^2}\Big)\,\Sigma, \tag{10.61}$$

from which Eq. (10.59) follows.

Usually in low-energy applications, all contributions of negative-energy states which do not depend on the energy ω and thus survive at high ω are included into an effective seagull amplitude. Doing so, we conclude from Eq. (10.60) that the effective (i.e. vanishing at high ω) unretarded resonance amplitude is exactly the positive-energy contribution $\mathring{R}_+^{E1}(\omega)$. Due to $\mathring{R}_-^{E1} \neq 0$, it is *different* from the retarded (i.e. dispersion) amplitude $R(\omega,0)$ at zero energy, and, correspondingly, the effective unretarded seagull $\mathring{S}(\omega,\theta) = S(\omega,\theta) + \mathring{R}_-^{E1} g^{E1}(\theta)$ is different from the retarded seagull $S(\omega,\theta)$ as well.

Considering unretarded and retarded amplitudes which vanish at intermediate energies, we find a difference in that these vanishing amplitudes are exactly the positive-energy part $\mathring{R}_+^{E1}$ and the total amplitude $R = R_+ + R_-$, respectively. The latter includes both positive- and negative-energy states, because the positive-energy part R_+ alone does not vanish, as was discussed in section 10.3. Therefore, using dispersion relations with an intermediate-energy cut ω_m, we obtain through the retarded cross section $\sigma(\omega)$ the amplitude R which includes *both* positive- and negative-energy states. At the same time, the dispersion integral of the unretarded cross section $\mathring{\sigma}^{E1}(\omega)$ gives *only* the positive-energy part of $\mathring{R}^{E1}$. That is why the obtained amplitudes are not exactly the same at zero energy and that is why Gerasimov's argument, which is a combination of the (retarded) dispersion relation and of the equation $R(0,0) = \mathring{R}^{E1}(0)$, Eq. (3.39), has a flaw when applied to photonuclear reactions at intermediate energies.

(ii) The second sum rule, which is briefly discussed below along the same line, appears as a derivative d/dt of the relation (10.48) taken at the point $t=0$. More specifically, (i) we consider the case of equal photon helicities, $\lambda_1 = \lambda_2$, so that $(\boldsymbol{\epsilon}_1\cdot\mathbf{k}_2)(\boldsymbol{\epsilon}_2\cdot\mathbf{k}_1) = (t/2)(\boldsymbol{\epsilon}_1\cdot\boldsymbol{\epsilon}_2)$, and (ii) we do not apply the derivative to the product $(\boldsymbol{\epsilon}_1\cdot\boldsymbol{\epsilon}_2)$.[15] We therefore have

$$\Sigma_t \equiv \int_0^\infty \sigma_t(\omega)\,d\omega = 2\pi^2\frac{\partial}{\partial t}R_1(0,0) = \frac{2\pi^2e^2}{E_0}\frac{1}{6}\langle r_E^2\rangle = \frac{\pi^2e^2}{2\gamma^2E_0}, \tag{10.62}$$

[14] Since the relativistic corrections affect the energy E_0 of the bound state, they change also the high energy limit of the Compton scattering amplitude T and the magnitude of the GGT and TRK sum rule, *cf.* [187,195]. However, this in itself does not destroy Gerasimov's theorem (10.58). What does is a projection to positive-energy states.

[15] In other words, we consider the t-derivative of the invariant amplitude A_1. *Cf.* Eq. (8.29).

where $R_1(\omega,t)=R(\omega,t;\ \lambda_1=\lambda_2,\ \boldsymbol{\epsilon}_1\cdot\boldsymbol{\epsilon}_2=1)$ and the integrand

$$\sigma_t(\omega)=\frac{4\pi}{\omega}\frac{\partial}{\partial t}\mathrm{Im}R_1(\omega,0) \tag{10.63}$$

is generally determined by the partial Ej and Mj cross sections,

$$\sigma_t=\sum_{j=2}^{\infty}\frac{(j+2)(j-1)}{4\omega^2}(\sigma^{Ej}+\sigma^{Mj})=\frac{1}{\omega^2}(\sigma^{E2}+\sigma^{M2})+\text{higher } j. \tag{10.64}$$

(In fact, the magnetic cross sections are absent in our model.) The derivative cross section σ_t consists of contributions of the excitation and the pair production,

$$\sigma_t=\sigma_{t,+}+\sigma_{t,-},\qquad \sigma_{t,\pm}(\omega)=\sum_{n=2}^{\infty}\frac{\pi^2e^2}{\omega E_0E_n}e^{-A}\frac{A^{n-2}}{(n-2)!}\delta(\omega-E_n\pm E_0),\quad A=\frac{\omega^2}{2\gamma^2}, \tag{10.65}$$

and so does the corresponding integral,

$$\Sigma_t=\Sigma_{t,+}+\Sigma_{t,-},\quad \Sigma_{t,\pm}=\sum_{n=2}^{\infty}\frac{\pi^2e^2}{\omega_n^{\pm}E_0E_n}\frac{(A_n^{\pm})^{n-2}}{(n-2)!}\exp(-A_n^{\pm}),\qquad A_n^{\pm}=\frac{(\omega_n^{\pm})^2}{2\gamma^2}. \tag{10.66}$$

With the relativistic parameter $\eta\ll 1$, the pair contribution is exponentially suppressed, $\Sigma_{t,-}\propto\exp(-1/\eta)$.

Again, we can consider the unretarded analogue of the sum rule (10.62) which involves the unretarded t-derivative of the amplitude $R(\omega,t)$,

$$\overset{\circ}{R}_t(\omega)=\frac{1}{\omega^2}\overset{\circ}{R}^{E2}=\frac{e^2}{2E_0}\,\frac{1}{4\gamma^2-\omega^2-2\omega E_0}+(\omega\to-\omega), \tag{10.67}$$

and the unretarded cross section $\overset{\circ}{\sigma}_t=(1/\omega^2)\overset{\circ}{\sigma}^{E2}$. Its positive- and negative-energy components read

$$\overset{\circ}{\sigma}^{E2}=\overset{\circ}{\sigma}_+^{E2}+\overset{\circ}{\sigma}_-^{E2},\qquad \overset{\circ}{\sigma}_{\pm}^{E2}=\frac{\pi^2e^2\omega}{E_0E_2}\delta(\omega-E_2\pm E_0). \tag{10.68}$$

The corresponding integral

$$\overset{\circ}{\Sigma}_t=\int_0^{\infty}\overset{\circ}{\sigma}^{E2}(\omega)\frac{d\omega}{\omega^2}=\overset{\circ}{\Sigma}_{t,+}+\overset{\circ}{\Sigma}_{t,-},\qquad \overset{\circ}{\Sigma}_{t,\pm}=\frac{\pi^2e^2}{\omega_2^{\pm}E_0E_2} \tag{10.69}$$

exactly satisfies the Gerasimov-like relation

$$\Sigma_t=\overset{\circ}{\Sigma}_t. \tag{10.70}$$

Again, this relation does not hold separately for the $+$ and $-$ components. In essence, the relation (10.70) is based only on the assumption that the amplitude $R_t(\omega)$ satisfies an unsubtracted dispersion relation. Other ingredients of the derivation, *viz.* an unsubtracted dispersion relation for $\overset{\circ}{R}_t(\omega)$ and the identity $R_t(0)=\overset{\circ}{R}_t(0)$ are model independent.

Since $\overset{\circ}{\Sigma}_{t,-}\simeq\eta\Sigma_t$, when η is small, the "practical" violation of the Gerasimov $E2$-theorem (10.70) happens in first order in η whenever the integrals are truncated at nonrelativistic energies $\omega\ll E_0$. Details of the balance between the retarded and full unretarded sum rules are as follows. The retardation form factor reduces the dominating $E2$ contribution to Σ_t by $F^2(\omega_2)\simeq 1-2\eta$, but the $E3$

contribution (additional $+3\eta\Sigma_t$) increases Σ_t with respect to $\overset{\circ}{\Sigma}_{t,+}$ by $\eta\Sigma_t$. After taking into account $\overset{\circ}{\Sigma}_{t,-}$ the balance is restored.

The important conclusion, which holds in a more general situation than the oscillator model suggests, is that relativistic corrections to the TRK-like sum rules are of the same scale as the retardation effects and effects of higher multipoles in the GGT-like sum rules. Taken together, they lead to an exact balance between retarded and unretarded sum rules. Incomplete saturation of the unretarded sum rules with nonrelativistically low energies results in an error of the same scale as the relativistic and retardation corrections themselves.

Relativistic TRK sum rule matches the GGT sum rule, nonrelativistic TRK does not.

10.5 Comparison with the phenomenological approach

The amplitude $R \equiv R_{\rm osc}$ suggested by our oscillator model is too simple to include all details of nuclear Compton scattering in the giant-resonance region. For example, it cannot describe the ensemble of isoscalar giant resonances which begins with the quadrupole excitation. (The dipole isoscalar mode is a translation.) The oscillator model better works for the isovector modes, for which the $E2/E1$ ratio of excitation energies and widths is close to the oscillator value of 2. (We can include the widths into the oscillator model by using a complex parameter ω_0, although this gives an imaginary part to a few other parameters such as the oscillator radius or the ground-state energy E_0.) An other restriction of the oscillator model, which is caused by a shape of the oscillator potential, is that it keeps a firm relation between the nuclear form factor and the quadrupole photoabsorption strength which may not work well for all nuclei. In terms of the oscillator frequency ω_0 and of the small relativistic parameter η, this relation reads

$$F^2(\omega_0) \simeq 1 - \frac{\eta}{2}, \quad F^2(2\omega_0) \simeq 1 - 2\eta, \quad \int_0^\infty \sigma^{E2}(\omega)\, d\omega \simeq \eta \times \int_0^\infty \sigma^{E1}(\omega)\, d\omega. \tag{10.71}$$

So, we cannot directly use the oscillator-model amplitude for the comparison with or the interpretation of experimental data on Compton scattering. But we observe that the phenomenological amplitude R_{GR} from Eq. (4.20), which is used for practical data analyses, indeed incorporates some gross features of the amplitude $R_{\rm osc}$ at energies in the GR region. These include (i) the fulfillment of the GGT sum rule, (ii) retardation form factors accompanying the lowest resonance peaks, and (iii) the asymptotic tail $\mathcal{O}(\omega^{-2})$. One difference which does exist between these two amplitudes is that the asymptotics of $R_{\rm osc}$ contains a q-dependent form factor which erases the amplitude at large angles. This feature is absent in the phenomenological amplitude R_{GR} where the vanishing in the high-energy limit and at all angles is caused by an exact cancellation of the high-energy limit of the ω-dependent part of R_{GR} and the ω-independent subtraction.

We can check how the prescription (4.20), being applied to the oscillator-model cross sections, matches the amplitude $R_{\rm osc}$ which is known exactly. For a numerical illustration we take the parameters ω_0 and η as determined by the isovector giant dipole and quadrupole resonances in ^{208}Pb [95] (see Table 4.1):

$$\omega_0 = (13.4 - 2.1i)\ \text{MeV}, \quad \eta = 0.06\,. \tag{10.72}$$

With these parameters, the r.m.s. radius of the oscillator is $\langle r^2\rangle^{1/2} = \omega_0^{-1}\sqrt{\frac{3}{2}\eta} \simeq 4.4$ fm. The energy region of our interest will be $\omega \leq 100$ MeV, that is well below the threshold of pair production $2E_0 = 2\omega_0/\eta \simeq 450$ MeV.

Applying the prescription (4.20), we act in line with the phenomenological procedure and keep in the dispersion integrals (10.2) only the lowest $E1$ and $E2$ peaks. Thus, we omit radial excitations,

which give corrections of order $\mathcal{O}(\eta^2)$, and the pair contribution. Then we get

$$R_{GR}(\omega,\theta) = g^{E1}(\theta) R_{GR}(\omega,\theta=0) + (g^{E2}(\theta) - g^{E1}(\theta)) \hat{R}^{E2}_{GR}(\omega)\,, \tag{10.73}$$

where

$$R_{GR}(\omega,\theta=0) = \frac{e^2\gamma^2}{E_0} \left\{ \frac{\omega_1^+ F^2(\omega_1^+)}{((\omega_1^+)^2-\omega^2)E_1} + \frac{\omega_2^+ F^2(\omega_2^+)}{((\omega_2^+)^2-\omega^2)E_2} \frac{(\omega_2^+)^2}{2\gamma^2} \right\} \tag{10.74}$$

and

$$\hat{R}^{E2}_{GR}(\omega) = \frac{e^2\gamma^2}{E_0 E_2} \frac{\omega_2^+ F^2(\omega)}{(\omega_2^+)^2-\omega^2} \frac{\omega^2}{2\gamma^2}. \tag{10.75}$$

By construction, $R_{\rm osc}$ and the amplitudes from (10.73) are very close at zero energy (the difference there is $\mathcal{O}(\eta^2)$, see the previous discussion of the GGT sum rule), near the $E1$ and $E2$ peaks, and at forward angle. They remain very close at other energies and angles, see Fig. 10.2.

This would not be the case if the retardation form factors were removed in Eqs. (4.20), (10.74), (10.75). Then, in particular, the backward scattering amplitude $R_{GR}(\omega, 180^\circ)$ at energies above the GR region would behave as $R_{GR}(\infty, 180^\circ) \simeq 2\eta e^2/E_0$ and would show a wrong asymptotic tail $2\eta = 0.12$ in Fig. 10.2.

Thus, the oscillator model suggests that the phenomenological prescription (4.20) provides a very good approximation to the exact amplitude.

Figure 10.2: *Phenomenological, Eq. (10.73), (dashed lines) and exact (solid lines) amplitudes R_{GR} in the relativistic oscillator model at $\omega_0 = (13.4 - 2.1i)$ MeV and $\eta = 0.06$. Units are e^2/E_0.*

A Parameters of the mesonic seagull amplitude for different nuclei

In section 9 the parameters κ, $\delta\alpha$ and $\delta\beta$, which constitute the mesonic seagull amplitude, are shown as a function of the proton number Z. In this appendix the corresponding numerical values are given, including all values for the various contributions to each of these parameters. In the following tables this has been done for both, a pure Fermi gas model and a realistic nuclear density based upon the parameterizations in [256]. The results for the mesonic seagull amplitude in nuclear matter, which has been discussed in sections 9.1 and 9.2 are also included in the tables (denoted "$A \to \infty$"), as well as the case of an asymptotic correlation function $\mathcal{F}_0^{ij}$ as in section 9.1 (superscript "0"). The polarizability modifications $\delta\alpha$ and $\delta\beta$ are given in the usual units 10^{-4}fm^3.

Table A.1: *Numerical values for the various contributions to the enhancement constant κ shown for nuclear matter ($A \to \infty$) and different finite nuclei. The quantities κ_π^C and κ_ρ^C denote the pion and ρ-meson contributions due to central correlations, respectively, while κ_π^T and κ_ρ^T denote the contributions due to tensor correlations. When only the asymptotic correlation function has been used, the contributions are termed κ_π^0 and κ_ρ^0. The right-hand half of the table shows the values for realistic nuclear densities based on the Fermi parameterizations from [256].*

	constant density				realistic density			
	$A \to \infty$	^{208}Pb	^{40}Ca	^{12}C	^{208}Pb	^{40}Ca	^{12}C	^{4}He
κ_π^0	0.19	0.16	0.13	0.11	0.15	0.11	0.09	0.05
κ_π^C	0.15	0.13	0.11	0.09	0.12	0.09	0.07	0.03
κ_π^T	0.86	0.85	0.84	0.83	0.79	0.68	0.67	0.60
κ_ρ^0	0.19	0.17	0.16	0.15	0.16	0.11	0.10	0.08
κ_ρ^C	0.01	0	0	0	-0.03	-0.01	-0.01	-0.18
κ_ρ^T	-0.11	-0.11	-0.11	-0.10	-0.06	-0.07	-0.07	-0.07
κ	0.91	0.87	0.84	0.84	0.82	0.69	0.66	0.52

Table A.2: *Same as Table A.1, but for the electric polarizability modification $\delta\alpha$. The ρ contribution is negligible in comparison with the π contribution.*

	constant density				realistic density			
	$A \to \infty$	^{208}Pb	^{40}Ca	^{12}C	^{208}Pb	^{40}Ca	^{12}C	^{4}He
$\delta\alpha^0$	-4.17	-3.58	-3.11	-2.59	-3.26	-2.44	-1.94	-1.22
$\delta\alpha^C$	-2.87	-2.42	-2.05	-1.62	-2.21	-1.51	-1.07	-0.41
$\delta\alpha^T$	-0.15	-0.09	-0.04	-0.02	-0.06	0.02	0.08	0.13
$\delta\alpha$	-3.02	-2.51	-2.09	-1.64	-2.27	-1.49	-0.99	-0.28

Table A.3: *Same as Table A.1, but for the magnetic polarizability modification $\delta\beta$. The ρ contribution is negligible in comparison with the π contribution. The subscript Δ denotes contributions to $\delta\beta$ from diagrams with a Δ-isobar as an intermediate state.*

	constant density				realistic density			
	$A \to \infty$	^{208}Pb	^{40}Ca	^{12}C	^{208}Pb	^{40}Ca	^{12}C	^{4}He
$\delta\beta^0$	1.86	1.55	1.30	1.03	1.42	1.10	0.83	0.47
$\delta\beta^C$	1.54	1.31	1.13	0.91	1.25	0.93	0.69	0.30
$\delta\beta^T$	0.11	0	-0.10	-0.20	-0.06	-0.21	-0.30	-0.38
$\delta\beta^0_\Delta$	0.29	0.24	0.19	0.19	0.22	0.17	0.12	0.05
$\delta\beta^C_\Delta$	0.38	0.33	0.29	0.29	0.30	0.22	0.17	0.09
$\delta\beta^T_\Delta$	0.30	0.29	0.28	0.28	0.27	0.22	0.21	0.18
$\delta\beta$	2.33	1.93	1.60	1.28	1.76	1.16	0.77	0.19

B Exchange form factors

At low energies the dependence of the mesonic seagull amplitude on momentum transfer is given by exchange form factors. In this appendix the numerical results for such form factors are presented on the basis of the model calculation discussed in section 9. Notations for the different types of exchange form factors are given in Table B.1.

Table B.1: *Notations for the different form factors and their formulation within a specific model.*

notation	**description**	**model realization**
F_1	one-nucleon form factor	taken from ref. [256]
$F_2^{(1)}$	exchange form factor for the static part of the mesonic seagull amplitude	$F_2^{(1)}(q) = \Phi_1(q)/\Phi_1(0)$
$F_2^{(2)}$	same as $F_2^{(1)}$, but for the energy-dependent part	$F_2^{(2)}(q) = \Phi_2(q)/\Phi_2(0)$
$F_2^{(GR)}$	same as $F_2^{(1)}$, but for the giant resonance contribution only	$F_2^{(GR)}(q) = (\Phi_1(q)/\Phi_1(0))\vert_{g_T=0}$
$F_2^{(QD)}$	same as $F_2^{(1)}$, but for the quasideuteron contribution only	$F_2^{(QD)}(q) = (\Phi_1(q)/\Phi_1(0))\vert_{g_C=0}$

Figure B.1 (for ^{208}Pb) and Fig. B.2 (for ^{12}C) show the form factors in comparison with both, the nuclear charge form factor and the form factor for uncorrelated nucleon pairs. Furthermore, our model prediction for the giant resonance and quasideuteron exchange form factors are shown for for ^{40}Ca (Fig. B.3) and ^{12}C (Fig. B.4). Again in these two figures the nuclear charge form factor and the approximation of uncorrelated nucleon pairs is shown for the sake of comparison.

Table B.2 gives the radii corresponding to the exchange form factors shown in Figs. B.1, B.2 and 9.12, which are obtained by representing the functions $F_2^{(i)}$ in the form $F_2^{(i)} = 1 - q^2 r_i^2/6$.

Table B.2: *Numerical values for the radii appearing in the expansion of the exchange form factors from Figs. (B.1), (B.2) and (9.12).*

A	r_1 [fm]	r_2 [fm]
208	5.0	4.7
40	3.0	2.5
12	1.9	1.4

Figure B.1: *Exchange form factors $F_2^{(i)}(q)$ for the case of ^{208}Pb. The dashed curve represents $F_2^{(1)}$, while the full curve corresponds to $F_2^{(2)}$. For comparison the (experimental) charge form factor F_1 (dash-dotted curve) and the function $F_1^2(q/2)$ (dotted curve) are also shown. The parameters for the form factor F_1 were taken from ref. [256].*

Figure B.2: *Same as Fig. B.1, but for ^{12}C.*

Figure B.3: *Form factors $F_2^{(GR)}(\Delta)$ and $F_2^{(QD)}(\Delta)$for ^{40}Ca. The dashed curve is $F_2^{(QD)}$ and the full curve is $F_2^{(GR)}$. In addition, the (experimental) charge form factor F_1 (dash-dotted curve) and the function $F_1^2(\Delta/2)$ (dotted curve) are shown for the sake of comparison.*

Figure B.4: *Same as Fig. B.3, but for ^{12}C.*

C Multipole angular distribution functions

Here the partial-wave expansion of the seagull amplitude (3.67) given in Section 3 in terms of the functions $g^{\lambda L}$ is derived. When both photons have definite helicities $\lambda_1, \lambda_2 = \pm 1$ and the scattering plane is xz, these functions read

$$g^{El}(\theta) = d^l_{\lambda_1,\lambda_2}(\theta), \quad g^{Ml}(\theta) = \lambda_1\lambda_2\, d^l_{\lambda_1,\lambda_2}(\theta).$$

To expand the product $\boldsymbol{\epsilon}_1 \cdot \boldsymbol{\epsilon}_2^*\, P_l(\cos\theta)$, we use $\boldsymbol{\epsilon}_1 \cdot \boldsymbol{\epsilon}_2^* = (1 + \lambda_1\lambda_2 \cos\theta)/2 = d^1_{\lambda_1,\lambda_2}(\theta)$ and $P_l(\cos\theta) = d^l_{0,0}(\theta)$ and apply the general rule of adding angular momenta for the d-functions:

$$d^{j_1}_{m_1,n_1}(\theta)\, d^{j_2}_{m_2,n_2}(\theta) = \sum_{jmn} C^{jm}_{j_1m_1,j_2m_2} C^{jn}_{j_1n_1,j_2n_2} d^j_{m,n}(\theta).$$

Using specific values for the Clebsch-Gordan coefficients $C^{j\lambda}_{1\lambda,l0}$ with $\lambda = \pm 1$, we get

$$d^1_{\lambda_1,\lambda_2}(\theta)\, d^l_{0,0}(\theta) = \frac{l+2}{2(2l+1)} d^{l+1}_{\lambda_1,\lambda_2}(\theta) + \frac{\lambda_1\lambda_2}{2} d^l_{\lambda_1,\lambda_2}(\theta) + \frac{l-1}{2(2l+1)} d^{l-1}_{\lambda_1,\lambda_2}(\theta).$$

Coming back to the functions $g^{\lambda L}$, we find

$$G_l(\theta) \equiv (2l+1)\boldsymbol{\epsilon}_1 \cdot \boldsymbol{\epsilon}_2^*\, P_l(\cos\theta) = \frac{l+2}{2} g^{E(l+1)}(\theta) + \frac{2l+1}{2} g^{Ml}(\theta) + \frac{l-1}{2} g^{E(l-1)}(\theta)$$

which is Eq. (3.69).

Acknowledgements

The authors are indebted to Prof. G.E. Brown for his continuing interest to this work. They thank Deutsche Forschungsgemeinschaft for support of several visits of A.I.M. and A.I.L. in Göttingen and Deutscher Akademischer Austauschdienst for support of visits of M.T.H. in Novosibirsk. One of us (M.S.) thanks B. Schröder (MAX–LAB, Lund) and B. Ziegler, J. Ahrens and Th. Walcher (MAMI, Mainz) for fruitful cooperations during the experiments and Deutsche Forschungsgemeinschaft for the support of the experimental work.

[1] A.H. Compton, Phys. Rev. 21 (1923) 484

[2] P.P. Kane, L. Kissel, R.H. Pratt, S.C. Roy, Phys. Rep. 140 (1986) 75

[3] P.P. Kane, Phys. Rep. 218 (1992) 67

[4] P. Papatzacos and K. Mork, Phys. Rep. 21 (1975) 81

[5] A.I. Milstein, M. Schumacher, Phys. Rep. 243 (1994) 183

[6] E.R. Gaerttner, G.L. Yeater, Phys. Rev. 76 (1949) 363

[7] R. Dressel, M. Goldhaber, A.O. Hanson, Phys. Rev. 77 (1950) 754

[8] M. Goldhaber and E. Teller, Phys. Rev. 74 (1948) 1046

[9] M.B. Stearns, Phys. Rev. 87 (1952) 706

[10] E.G. Fuller, E. Hayward, Phys. Rev. 94 (1954) 732; 95 (1954) 1106

[11] E.G. Fuller, E. Hayward, Phys. Rev. 101 (1956) 692

[12] E. Hayward, W.C. Barber, J. Sazama, Phys. Rev. C 8 (1973) 1065

[13] W.R. Dodge, E. Hayward, R.G. Leicht, B.H. Patrick, R. Starr, Phys. Rev. Lett. 44 (1980) 1040

[14] E. Hayward, R.G. Leicht, Annals of the New York Academy of Sciences 40 (1980) 99

[15] R. Leicht, M. Hammen, K.P. Schelhaas, B. Ziegler, Nucl. Phys. A 326 (1981) 111

[16] W.R. Dodge, E. Hayward, R.G. Leicht, M. McCord, R. Starr, Phys. Rev. C 28 (1983) 8

[17] E. Hayward, B. Ziegler, Nucl. Phys. A 414 (1984) 333

[18] D.H. Wright, A.M. Nathan, L.J. Morford, P.T. Debevec, Phys. Rev. Lett. 52 (1984) 244

[19] D.H. Wright, P.T. Debevec, L.J. Morford, A.M. Nathan, Phys. Rev. C 32 (1985) 1174

[20] E.J. Austin, E.C. Booth, E.K. McIntyre, J.P. Miller, B.L. Roberts, D.A. Whitehouse, G. Dodson, Phys. Rev. Lett. 57 (1986) 972

[21] A.M. Nathan, P.L. Cole, P.T. Debevec, S.D. Hoblit, S.F. LeBrun, D.H. Wright, Phys. Rev. C 34 (1986) 480

[22] S.F. LeBrun, A.M. Nathan, S.D. Hoblit, Phys. Rev. C 35 (1987) 2005

[23] E.J. Austin, E.C. Booth, D. Delli Carpini, K.P. Gall, E.K. McIntyre, J.P. Miller, D. Warner, D.A. Whitehouse, G. Dodson, Phys. Rev. Lett. 61 (1988) 1922

[24] A. Baumann, P. Rullhusen, K.W. Rose, M. Schumacher, J.M. Henneberg, N. Wieloch-Laufenberg, B. Ziegler, Phys. Rev. C 38 (1988) 1940

[25] K.P. Schelhaas, J. Ahrens, J.M. Henneberg, M. Sanzone-Arenhövel, N. Wieloch-Laufenberg, U. Zurmühl, B. Ziegler, M. Schumacher, F. Wolf, Nucl. Phys. 489 (1988) 189

[26] K.P. Schelhaas, J.M. Henneberg, N. Wieloch-Laufenberg, U. Zurmühl, B. Ziegler, M. Schumacher, F. Wolf, Nucl. Phys. A 506 (1990) 307

[27] B. Ziegler, Phys. Lett. B 237 (1990) 334

[28] D.P. Wells, Doctoral Thesis, University of Illinois at Urbana-Champaign, 1990 (unpublished)

[29] D. Delli Carpini, E.C. Booth, J.P. Miller, R. Igarashi, J. Bergstrom, H. Caplan, M. Doss, E. Hallin, C. Rangacharyulu, D. Skopic, M.A. Lucas, A.M. Nathan, D.P. Wells, Phys. Rev. C 43 (1991) 1525

[30] K.P. Schelhaas, J.M. Henneberg, N. Wieloch-Laufenberg, U. Zurmühl, B. Ziegler, M. Schumacher, F. Wolf, Nucl. Phys. A 528 (1991) 189

[31] A. Baumann, P. Rullhusen, K.W. Rose, M. Ludwig, M. Schumacher, A.I. Milstein, J.M. Henneberg, N. Wieloch-Laufenberg, B. Ziegler, Nucl. Phys. A 536 (1992) 87

[32] K. Fuhrberg, G. Martin, D. Häger, M. Ludwig, M. Schumacher, B.-E. Andersson, K.I. Blomqvist, H. Ruijter, B. Sondell, E. Hayward, L. Nilsson, B. Schröder and R. Zorro, Nucl. Phys. A548 (1992) 579

[33] D.S. Dale, R.M. Laszewski, R. Alarcon, Phys. Rev. Lett. 68 (1992) 3507

[34] M. Ludwig, B.-E. Andersson, A. Baumann, K.I. Blomqvist, K. Fuhrberg, E. Hayward, G. Müller, D. Nilsson, A. Sandell, B. Schröder, M. Schumacher, Phys. Lett. B 274 (1992) 275

[35] J.P. Miller, E.J. Austin, J. Bergstrom, E.C. Booth, H. Caplan, D. Delli Carpini, G. Dodson, M. Doss, K.P. Gall, E. Hallin, R. Igarashi, M.A. Lucas, E.K. McIntyre, A.M. Nathan, C. Rangacharyulu, D. Skopic, D. Warner, D.P. Wells, D.A. Whitehouse, Nucl. Phys. A 546 (1992) 199c

[36] D.P. Wells, D.S. Dale, R.A. Eisenstein, F.J. Federspiel, M.A. Lucas, K.E. Mellendorf, A.M. Nathan, A.E. O'Neill, Phys. Rev. C 46 (1992) 449

[37] F. Wissmann, J. Peise, M. Schmitz, M. Schneider, J. Ahrens, I. Antony, R. Beck, B. Dolbilkin, S.J. Hall, S. Herdade, J. Herrmann, A. Hünger, P. Jennewein, J.D. Kellie, R. Kondratjev, H.-P. Krahn, K.-H. Krause, V. Kusnezov, V. Lisin, G.J. Miller, A. Polonski, M. Schumacher, J. Sobolewski, Th. Walcher, A. Zabrodin, Phys. Lett. B 335 (1994) 119

[38] K. Fuhrberg, D. Häger, T. Glebe, B.-E. Andersson, K. Hansen, M. Hütt, B. Nilsson, L. Nilsson, D. Ryckbosch, B. Schröder, M. Schumacher, R. Van de Vyver, Nucl. Phys. A 591 (1995) 1

[39] D. Häger, K. Fuhrberg, T. Glebe, M. Hütt, M. , M. Schumacher, B.E. Andersson, K. Hansen, B. Nilsson, B. Schröder, L. Nilsson, H. Freiesleben, E. Kuhlmann, Nucl. Phys. A 595 (1995) 287

[40] R. Igarashi, J.C. Bergstrom, H.S. Caplan, K.G.E. Doss, E.L. Hallin, D.M. Skopik, D. Delli Carpini, E.C. Booth, E.K. McIntyre, J.P. Miller, M.A. Lucas, B.R. MacGibbon, A.M. Nathan, D. Wells, Phys. Rev. C 52 (1995) 755

[41] T. Glebe, Doctoral Thesis, University of Göttingen 1996 (unpublished)

[42] C. Pöch, Doctoral Thesis, University of Göttingen 1996 (unpublished)

[43] G. Feldman, M.E. Mellendorf, R.A. Eisenstein, F.J. Federspiel, G. Garino, R. Igarashi, N. R. Kolb, M.A. Lucas, B.E. MacGibbon, W.K. Mize, A.M. Nathan, R. E. Pywell, D.P. Wells, Phys. Rev. C 54 (1996) R2124

[44] O. Selke, A. Hünger, A. Kraus, M. Schumacher, R. Wichmann, J. Ahrens, H.J. Arends, R. Beck, J. Peise, M. Schneider, F. Wissmann, Phys. Lett. B 369 (1996) 207

[45] D. Moricciani, V. Bellini, M. Capogni, A. Caracappa, L. Casano, R.M. Chasteler, A. D'Angelo, F. Ghio, B. Girolami, S. Hoblit, L. Hu, M. Khandaker, O.C. Kistner, L.H. Kramer, C.M. Laymon, A.I. L'vov, B. Marks, L. Micele, V.A. Petrun'kin, B.J. Rice, A.M. Sandorfi, C. Schaerf, C.E. Thorn, D.E. Tilley, H.R. Weller, Few Body Systems Suppl. 9 (1995) 349

[46] A. Kraus, O. Selke, F. Wissmann, J. Ahrens, H.-J. Arends, R. Beck, G. Galler, M.-Th. Hütt, B. Körfgen, J. Peise, M. Schumacher, F. Smend, R. Wichmann, Phys. Lett. B 432 (1998) 45

[47] S. Proff, Doctoral Thesis, University of Göttingen 1998 (unpublished)

[48] S. Proff, C. Pöch, T. Glebe, J.-O. Adler, K. Fissum, K. Hansen, M.-Th. Hütt, O. Kaltschmidt, M. Lundin, B. Nilsson, B. Schröder, M. Schumacher, D. Sims, F. Smend, F. Wissmann, Nucl. Phys. A (in press)

[49] T.J. Bowles, R.J. Holt, H.E. Jackson, R.M. Laszewski, A.M. Nathan, J.R. Specht, R. Starr, Phys. Rev. Lett. 41 (1978) 1095

[50] C.E. Thorn, G. Giordano, O.C. Kistner, G. Matone, A.M. Sandorfi, C. Schaerf, C.S. Whisnant, Nucl. Instr. Meth. A 285 (1989) 447

[51] J.-O. Adler, B.-E. Andersson, K.I. Blomqvist, B. Forkman, K. Hansen, L. Isaksson, K. Lindgren, D. Nilsson, A. Sandell, B. Schröder, K. Ziakas, Nucl. Instr. Meth. A 294 (1990) 15

[52] J.-O. Adler, B.-E. Andersson, K.I. Blomqvist, K.G. Fissum, K. Hansen, L. Isaksson, B. Nilsson, H. Ruijter, A. Sandell, B. Schröder, D.A. Sims, Nucl. Instr. Meth. A 388 (1997) 17

[53] I. Anthony, J.D. Kellie, S.J. Hall, G.J. Miller, J. Ahrens, Nucl. Instr. Meth. A 301 (1991) 230

[54] S.J. Hall, G.J. Miller, R. Beck, P. Jennewein, Nucl. Instr. Meth. A 368 (1996) 698

[55] J.M. Vogt, R.E. Pywell, D.M. Skopic, E.L. Hallin, J.C. Bergstrom, H.S. Caplan, K.I. Blomqvist, W. Del Bianco, J.W. Juri, Nucl. Instr. Meth. A 324 (1993) 198

[56] D. Lohmann, J. Peise, J. Ahrens, I. Anthony, H.J. Arends, R. Beck, R. Crawford, A. Hünger, K.H. Kaiser, J.D. Kellie, Ch. Klümper, H.-P. Krahn, A. Kraus, U. Ludwig, M. Schumacher, O. Selke, M. Schmitz, M. Schneider, F. Wissmann, S. Wolf
Nucl. Instr. Meth A 343 (1994) 494

[57] A. Kraus, O. Selke, F. Rambo, G. Galler, M. Schumacher, F. Smend, R. Wichmann, F. Wissmann, J. Ahrens, H.-J. Arends, R. Beck, J. Peise,
Phys. Rev. Lett. 17 (1997) 3834

[58] F. Rambo, G. Galler, A. Kraus, M. Schumacher, F. Smend, F. Wissmann, S. Wolf,J. Ahrens, H.-J. Arends, R. Beck, H.-P. Krahn, J. Peise, Phys. Rev. C 58 (1998) 489

[59] K.-H. Krause, J. Sobolewski, D. Hauff, J.M. Henneberg, N. Wieloch-Laufenberg, J. Ahrens, H. Gimm, A. Zieger, B. Ziegler, Nucl. Instr. Meth. A 310 (1991) 577

[60] S. Kahane, R. Moreh, Phys. Rev. C 9 (1974) 2384

[61] M. Schumacher, F. Smend, W. Mückenheim, P. Rullhusen, Z. Physik A 300 (1981) 193

[62] P. Rullhusen, U. Zurmühl, F. Smend, M. Schumacher, H.G. Börner, S.A. Kerr, Phys. Rec. C 27 (1983) 559

[63] R. Nolte, A. Baumann, K.W. Rose, M. Schumacher, Phys. Lett. B 173 (1986) 388

[64] K. Fuhrberg, G. Mondry, D. Novotny, H.-J. Brinkmann, M. Ludwig, G. Müller, W. Scharfe, M. Schumacher, Europhys. Lett. 9 (1989) 427

[65] R. Nolte, F. Schröder, A. Baumann, K.W. Rose, K. Fuhrberg, M. Schumacher, P. Fettweis, R. Carchon, Phys. Rev. C 40 (1989) 1175

[66] K. Fuhrberg, R. Nolte, A. Baumann, P. Rullhusen, M. Schumacher, Phys. Rev. C 40 (1989) 2394

[67] J.S. Levinger and H.A. Bethe, Phys. Rev. 78 (1950) 115

[68] P. Christillin and M. Rosa-Clot, Phys. Lett. B51 (1974) 125

[69] J.L. Friar, Ann. Phys. 95 (1975) 170

[70] J.L. Friar, Phys. Rev. Lett. 36 (1976) 510

[71] P. Christillin and M. Rosa-Clot, Nuovo Cimento 28A (1975) 29

[72] P. Christillin and M. Rosa-Clot, Nuovo Cimento 43A (1978) 172

[73] P. Christillin, in: Proceedings of the Workshop "Intermediate Energy Nuclear Physics with Monochromatic and Polarized Photons" (Frascati 1980)

[74] H. Arenhövel, Z. Phys. A 297 (1980) 129

[75] W.A. Alberico and A. Molinari, Z. Phys. A 309 (1982) 143

[76] M. Ericson and M. Rosa-Clot, Nuovo Cim. 76A (1983) 180

[77] P. Christillin, J. Phys. G: Nucl. Phys. 10 (1984) L65

[78] M. Weyrauch, H. Arenhövel, Phys. Lett. 134B (1984) 21

[79] P. Christillin, J. Phys. G: Nucl. Phys. 11 (1985) 795

[80] M. Rosa-Clot, M. Ericson, Z. Phys. A 320 (1985) 675

[81] P. Christillin, J. Phys. G: Nucl. Phys. 12 (1986) 837

[82] M. Ericson and M. Rosa-Clot, Z. Phys. A 324 (1986) 373

[83] M. Ericson, M. Rosa-Clot, Phys. Lett. B 188 (1987) 11

[84] J. Ahrens, H. Borchert, K.H. Czok, H.B. Eppler, H. Gimm, H. Gundrum, M. Kröning, P. Riehn, G. Sita Ram, A. Zieger, B. Ziegler, Nucl. Phys. A251 (1975) 479

[85] A.J.F. Siegert, Phys. Rev. 52 (1937) 787

[86] A.B.Migdal, A.A.Lushnikov and D.F.Zaretsky, Nucl. Phys. 66 (1965) 193.

[87] G.E. Brown and M. Rho, Nucl. Phys. A338 (1980) 269

[88] G.E. Brown, W. Weise, G. Baym, J. Speth, Comments Nucl. Part. Phys. 17 (1987) 39

[89] G.E. Brown, M. Rho, Phys. Lett. B 222 (1989) 324

[90] G.E. Brown, H. Müther, M. Prakash, Nucl. Phys. A 506 (1990) 565

[91] G.E. Brown, M. Rho, Phys. Lett. B237 (1990) 3

[92] G.E. Brown, M. Rho, Phys. Rev. Lett. 66 (1991) 2720

[93] W. Weise, Nucl. Phys. A 553 (1993) 59c

[94] G.E. Brown, M. Rho, M. Soyeur, Nucl. Phys. A 553 (1993) 705c

[95] M. Schumacher,A.I. Milstein, H. Falkenberg, K. Fuhrberg, T. Glebe, D. Häger, M.-Th. Hütt, Nucl. Phys. A 576 (1994) 603

[96] "Chiral Symmetry and Changes of Properties in Nuclei" G.E. Brown, in:"Symmetries and fundamental interactions in nuclei" E. Henley and W. Haxton Eds., World Scientific 1995

[97] B. Friman, M. Rho, Nucl.Phys. A 606 (1996) 303

[98] G.E. Brown, M. Rho, Nucl. Phys. A 596 (1996) 503

[99] V.A. Petrunkin, Sov. J. Part. Nucl. 12 (1981) 278

[100] A.I. L'vov, Int. J. Mod. Phys. A 8 (1993) 5267

[101] A.I. L'vov, V.A. Petrun'kin, M. Schumacher, Phys. Rev. C 55 (1997) 359

[102] D. Drechsel, A. Russo, Phys. Lett. 137 B (1984) 294

[103] A.I. Lvov, M. Schumacher, Nucl. Phys. A 548 (1992) 613

[104] G.G. Bunatian, Sov. J. Nucl. Phys. 55 (1992) 1781

[105] E. Oset, W. Weise, Nucl. Phys. A 319 (1979) 477

[106] E. Oset, W. Weise, Nucl. Phys. A 368 (1981) 375

[107] J.H. Koch, E.J. Moniz, N. Ohtsuka, Ann. Phys. 154 (1984) 99

[108] B. Körfgen, F. Osterfeld, T. Udagawa, Phys. Rev. C 50 (1994) 1637

[109] B. Pasquini, S. Boffi, Nucl. Phys. A 598 (1996) 485

[110] T. Bar-Noy, R. Moreh, Nucl. Phys. A 229 (1974) 417

[111] T. Bar-Noy, R. Moreh, Nucl. Phys. A 275 (1977) 151

[112] A.M. Nathan, R. Moreh, Phys. Lett. 91B (1980) 38

[113] T.J. Bowles, R.J. Holt, H.E. Jackson, R.M. Laszewski, R.D. McKeon, A.M. Nathan, J.R. Specht, Phys. Rev. C 24 (1981) 1940

[114] R. Alarcon, A.M. Nathan, S.F. LeBrun, S.D. Hoblit, Phys. Rev. C 39 (1989) 324

[115] G. Mondry, F. Wissmann, G. Müller, F. Schröder, P. Rullhusen, F. Smend, M. Schumacher, P. Fettweis, R. Carchon, Nucl. Phys. A 531 (1991) 237

[116] U. Fano, Natl. Bureau of Standards Technical Note 83 (1960) 1

[117] H. Arenhövel, H.J. Weber, Nucl. Phys. A 91 (1967) 145

[118] H. Arenhövel, M. Danos, W. Greiner, Phys. Rev. 157 (1967) 1109

[119] H. Arenhövel, W. Greiner, Progr. Nucl. Phys. 10 (1969) 167

[120] H. Arenhövel, in: International Conf. Photonuclear Reactions and Applications, Asilomar 1973, B.L. Berman Ed., Oak Ridge, Tennessee (1973)

[121] H. Arenhövel, in: New Vistas in Electro-Nuclear Physics, E.L. Tomusiak, H.S. Caplan and E.T. Dressler Eds., NATO ASI Series B 142, Plenum Press, New York and London (1985) 251

[122] H. Arenhövel, M. Weirauch, Nucl. Phys. A457 (1986) 573

[123] U. Kneissl, Prog. Part. Nucl. Phys. 24 (1990) 41, *ibid.* 28 (1992) 331

[124] E.G. Fuller,E. Hayward,in: Photonuclear Reactions II, P.M. Endt, P.B. Smith Eds., North. Holland (1962) 113

[125] E. Hayward, in: Photonuclear Reactions I, S. Costa and C. Schaerf Eds., Lecture Notes in Physics 61, Springer, Heidelberg, (1977) 342

[126] A. Molinari, Phys. Rep. 64 (1980) 283

[127] B. Ziegler, in: New Vistas in Electro-Nuclear Physics, E.L. Tomusiak, H.S. Caplan and E.T. Dressler Eds., NATO ASI Series B 142, Plenum Press, New York and London (1985) 293

[128] P. Rullhusen, in: Perspectives on Photon Interactions with Hadrons and Nuclei, M. Schumacher and G. Tamas Eds., Lecture Notes in Physics, Springer, Heidelberg, (1990) 23

[129] A.I. L'vov and V.A. Petrun'kin, in: Perspectives on Photon Interactions with Hadrons and Nuclei, M. Schumacher and G. Tamas Eds., Lecture Notes in Physics, Springer, Heidelberg, (1990) 123

[130] P. Christillin, Phys. Rep. C 190 (1990) 63

[131] M.A. Lucas, PhD Thesis, Univ. Illinois at Urbana-Champaign 1994.

[132] T. Wilbois, P. Wilhelm and H. Arenhövel, Few-Body Syst. Suppl. 9 (1995) 263.

[133] M.I. Levchuk and A.I. L'vov, Few-Body Syst. Suppl. 9 (1995) 439

[134] M.I. Levchuk and A.I. L'vov, Proc. 7th Conf. Mesons and Light Nuclei, Prague 1998 (World Scientific, eds. J. Adam et al.); nucl-th/9809034
M.I. Levchuk and A.I. L'vov (submitted).

[135] J.-W. Chen, H. Grießhammer, M.J. Savage and R.P. Springer, Nucl. Phys. A 644 (1998) 245; J.-W. Chen (submitted), nucl-th/9810021.

[136] J.J. Karakowski, PhD thesis, Univ. of Washington (1998), nucl-th/9901011
J.J. Karakowski and G.A. Miller (submitted), nucl-th/9901018.

[137] T.H. Bauer, R.D. Spital and D.R. Yennie, Rev. Mod. Phys. 50 (1978) 261

[138] P. Kroll, W. Schweiger, M. Schürmann, Int. Jour. of Mod. Physics, A6 (1991) 4107

[139] P. Kroll, M. Schürmann, P. Guichon, Nucl. Phys. A 598 (1996) 435

[140] X. Ji, Phys. Rev. D 55 (1997) 7114

[141] A.V. Radyushkin, Phys. Rev. D 56 (1997) 5524

[142] T.A. Armstrong, W.R. Hogg, G.M. Lewis, A.W. Robertson, G.R. Brookes, A.S. Clough, J.H. Freeland, W. Galbraith, A.F. King, W.R. Rawlinson, N.R.S. Tait, J.C. Thompson, D.W.L. Tolfree, Phys. Rev. D 5 (1972) 1640; Nucl. Phys. B 41 (1972) 445.

[143] Lecture Notes in Physics 365, M. Schumacher, G. Tamas Eds., Springer, Berlin (1990)

[144] M. Schumacher, J. Phys. G: 14 Suppl. (1988) S235

[145] U. Zurmühl, P. Rullhusen, F. Smend, M. Schumacher, H.G. Börner, S.A. Kerr, Z. Phys. A 314 (1983) 171

[146] M. MacCormic, J. Habermann, J. Ahrens, G, Audit, R. Beck, A. Braghieri, G. Galler, N. d' Hose, V. Isbert, P. Pedroni, T. Pinelli, G. Tamas, S. Wartenberg, A. Zabrodin, Phys. Rev. C55 (1997) 1033.

[147] J. Ahrens, private communication

[148] J. Ahrens, Nucl. Phys. A 446 (1985) 229c

[149] H. Steinwedel und J.H.D. Jensen, Z. Naturforsch 5a (1950) 413

[150] B.L. Berman, ATOMIC DATA AND NUCLEAR DATA TABLES 15 (1975) 319

[151] S.S. Dietrich, B.L. Berman, ATOMIC DATA AND NUCLEAR DATA TABLES 38 (1988) 199

[152] A. Leprêtre, H. Beil, R. Bergère, P. Carlos, J. Fagot, A. Veyssière, J. Ahrens, P. Axel, U. Kneissl, Phys. Lett. 79B (1978) 43

[153] M. Schumacher, U. Zurmühl, F. Smend, R. Nolte, Nucl. Phys. A 438 (1985) 493

[154] J.S. Levinger, Phys. Rev. 84 (1951) 43

[155] K. Gottfried, Nucl. Phys. 5 (1958) 557

[156] J. M. Laget, Lecture Notes in Physics 137 (1981) 148

[157] M.-Th. Hütt, A.I. Milstein, M. Schumacher, Nucl. Phys. A 618 (1997) 483

[158] R. Wichmann,J. Ahrens, H.-J. Arends, R. Beck, G. Galler, A. Hünger, A. Kraus, I.J.D. MacGregor, J. Peise, B. Seitz, M. Schmitz, M. Schneider, O. Selke, M. Schumacher, F. Wissmann, Z. Physik A 355 (1996) 169

[159] M. Wakamatsu and K. Matsumoto, Nucl. Phys. A392 (1983) 323

[160] R.C. Carrasco and E. Oset, Nucl. Phys. A536 (1992) 445

[161] J. Ryckebusch, M. Vanderhaeghen, L. Machenil, M. Waroquier, Nucl. Phys. A568 (1994) 828

[162] M. Vanderhaeghen, K. Heyde, J. Ryckebusch, M. Waroquier, Nucl. Phys. A595 (1995) 219

[163] J. Ryckebusch, L. Machenil, M. Vanderhaeghen, V. Van der Sluys and M. Waroquier, Phys. Rev. C49 (1994) 2704

[164] J. Ryckebusch, L. Machenil, M. Vanderhaeghen, V. Van der Sluys and M. Waroquier, Phys. Lett. B291 (1992) 213

[165] M. Gell-Mann, M.L. Goldberger, W. Thirring, Phys. Rev. 95 (1954) 1612

[166] M. Schumacher, P. Rullhusen and A. Baumann, Nuovo Cim. 100A (1988) 339

[167] D. Kurath, Phys. Rev. 130 (1963) 1525

[168] M.-Th. Hütt and A.I. Milstein, Nucl. Phys. A 609 (1996) 391

[169] E. Hayward, Radiat. Phys. Chem. 41 (1993) 739

[170] H. Falkenberg, K. Fuhrberg, T. Glebe, D. Häger, A. Hünger, M. Hütt, A. Kraus, M. Schumacher and O. Selke, in: "Mesons and Nuclei at Intermediate Energies", Dubna, Russia,1994, Mikhail Kh. Khankhasayev and Zh.B. Kurmanov Eds., World Scientific 1995

[171] W.T. Weng, T.T.S. Kuo and G.E. Brown, Phys. Lett. 46B (1973) 329

[172] A. Arima, G.E. Brown, J. Hyuga, M. Ichimura, Nucl. Phys. A 205 (1973) 27

[173] "Pions and Nuclei", T. Ericson and W. Weise, Clarendon Press, Oxford 1988

[174] D.O. Riska, Phys. Rep. 181 (1989) 207

[175] T.E.O. Ericson and J. Hüfner, Nucl. Phys. B 57 (1973) 604

[176] N. Baron, G. Baur, M. Schumacher, Nucl. Phys. A 530 (1991) 267

[177] W. Franz, Z. Physik 98 (1935) 314

[178] G.E. Brown and D.F. Mayers, Proc. Roy. Soc. 242 (1957) 89 and references therein

[179] M. Schumacher, Phys. Rev. 182 (1969) 7

[180] W. Weise, Phys. Rev. Lett. 31 (1973) 773

[181] W. Weise, Phys. Reports 13 (1974) 53

[182] J. Ahrens, L.S. Ferreira, W. Weise, Nucl. Phys. A 485 (1988) 621

[183] R. Silbar, C. Werntz and H. Überall, Nucl. Phys. A107 (1968) 655

[184] W. Thirring, Phil. Mag. 41 (1950) 1193

[185] S.B. Gerasimov, Phys. Lett. 13 (1964) 240

[186] T. Matsuura and K. Yazaki, Phys. Lett. B46 (1973) 17

[187] J.L. Friar and S. Fallieros, Phys. Rev. C 11 (1975) 274; *ibid.* p. 277

[188] H.P. Schröder and H. Arenhövel, Z. Phys. A 280 (1977) 349

[189] H. Arenhövel and D. Drechsel, Phys. Rev. C 20 (1979) 1965

[190] K.-M. Schmitt and H. Arenhövel, Z. Phys. A 320 (1985) 311

[191] G.E. Brown, M. Bolsterli, Phys. Rev. Lett. 3 (1959) 472

[192] A. Bohr and B.R. Mottelson , Nuclear Structure, Vol. II Nuclear Deformations, W.A. Benjamin Reading, Massachusetts (1975) 477

[193] M.-Th. Hütt and A.I. Milstein, Phys. Rev. C 57 (1998) 305

[194] T. deForest, J.D. Walecka, Adv. Phys. 15 (1966) 1

[195] M.L. Goldberger and F.E. Low, Phys. Rev. 176 (1968) 1778

[196] V.S. Barashenkov and H.J. Kaiser, Fortschr. Phys. 10 (1962) 33

[197] V.A. Petrun'kin, Nucl. Phys. 55 (1964) 197

[198] A. Veyssière, H. Beil, R. Bergère, P. Carlos, A. Leprêtre, Nucl. Phys. 159 (1970) 561

[199] F.E. Bertrand, Ann Rev. Nucl. Sci. 26 (1976) 457; A. van der Woude, in [204] p. 65

[200] B.L. Berman, R.E. Pywell, S.S. Dietrich, M.N. Thompson, K.G. McNeill, J.W. Jury, Phys. Rev C 36 (1987) 1286

[201] D.S. Dale, A.M. Nathan, F.J. Federspiel, S.D. Hoblit, J. Hughes, and D. Wells, Phys. Lett. B 214 (1988) 329

[202] R.R. Harvey, J.T. Caldwell, R.L. Bramblett, S.C. Fultz, Phys. Rev. B 136 (1964) 126

[203] L.M. Young, Ph.D. thesis, University of Illinois at Urbana-Champaign, 1972 (unpublished)

[204] Giant Multipole Resonances, ed. F.E. Bertrand, Harwood academic publisher, Chur, London, New York (1980)

[205] R.M. Laszewski, P. Rullhusen, S.D. Hoblit, S.F. LeBrun, Phys. Rev. Lett. 54 (1985) 530

[206] K. Wienhard, K. Ackermann, K. Bangert, U.E.P. Berg, C. Bläsing, W. Naatz, A. Ruckelshausen, D. Rück, R.K.M. Schneider, R. Stock, Phys. Rev. Lett. 49 (1982) 18

[207] R. Pitthan, Th. Walcher, Phys. Lett. 36B (1971) 563

[208] A. Van Der Woude, in [204] p. 69

[209] R. Pitthan, in [204] p. 161

[210] D.M. Drake, S. Joly, L. Nilsson, S.A. Wender, K. Aniol, I. Halpern, D. Storm, Phys. Rev. Lett 47 (1981) 1581

[211] R. Zorro, I. Bergqvist, S. Crona, A. Hakansson, A. Likar, A. Lindholm, L. Nilsson, N. Olsson, Nucl. Phys. A 472 (1987) 125

[212] I. Bergqvist, R. Zorro, A. Hakansson, A. Lindholm, L. Nilsson, N. Olsson, A. Likar, Nucl. Phys. A 419 (1984) 509

[213] C.M. Laymon, R.O. Nelson, S.A. Wender, L.R. Nilsson, Phys. Rev. C 46 (1992) 1880

[214] D.A. Sims, G.J. O'Keefe, R.P. Rassool, A. Kuzin, M.N. Thompson, J.O. Adler, B.-E. Andersson, K.G. Fissum, K. Hansen, L. Isaksson, B. Nilsson, H. Ruijter, A. Sandell, B. Schröder, J.R.M. Annand, G.I. Crawford, P.D. Harty, J.C. McGeorge, G.J. Miller, Phys. Rev. C 55 (1997) 1288

[215] A. Migdal, Journ. Phys. USSR 8 (1944) 331

[216] J.S. Levinger, *Nuclear Photo-Disintegration* (Oxford University Press, 1960)

[217] A.M. Baldin, Nucl. Phys. 18 (1960) 318;
L.I. Lapidus, Sov. Phys. JETP 16 (1963) 964

[218] J.L. Friar, S. Fallieros, Am. J. Phys. 49 (1981) 847

[219] A.I. L'vov, Nucl. Phys. A 638 (1998) 756

[220] J.S. Levinger, Phys. Lett. B82 (1979) 181

[221] J.M. Laget, Nucl. Phys. A312 (1978) 265

[222] A.I. L'vov, preprint Lebedev Phys. Inst. 344 (1987) (unpublished)

[223] R. Weiner and W. Weise, Phys. Lett. B 159 (1985) 85

[224] V. Bernard, N. Kaiser and U.-G. Meissner, Int. J. Mod. Phys. E 4 (1995) 193

[225] M. Damashek and F.J. Gilman, Phys. Rev. D1 (1970) 1319

[226] A.I. L'vov, V.A. Petrun'kin and S.A. Startzev, Sov. J. Nucl. Phys. 29 (1979) 651

[227] D. Babusci, G. Giordano and G. Matone, Phys. Rev. C 57 (1998) 291

[228] D. Babusci, G. Giordano, A.I. L'vov, G. Matone and A.M. Nathan, Phys. Rev. C 58 (1998) 1013

[229] A. Hünger, J. Peise, A. Robbiano, J. Ahrens, I. Antony, H.-J. Arends, R. Beck, G.P, Capitani, B. Dolbilkin, H. Falkenberg,G. Galler, S.J. Hall, J.D. Kellie, R. Kondratjev, R. Kordsmeier, V. Lisin, A.I. L'vov, G.J. Miller, C. Molinari, P. Ottonello, A.R. Reolon, M. Sanzone, M. Schmitz, M. Schneider, M. Schumacher, O. Selke, Th. Walcher, F. Wissmann, S. Wolf, A. Zucchiatti, Nucl. Phys. A. 620 (1997) 385

[230] R.A. Arndt, I.I. Strakovsky and R.L. Workman, Phys. Rev. C 56 (1997) 577

[231] O. Hanstein, D. Drechsel and L. Tiator, Nucl. Phys. A 632 (1998) 561

[232] R.A. Arndt, I.I. Strakovsky, and R.L. Workman, Phys. Rev. C 53 (1996) 430. The SAID program is accessible at URL http://clsaid.phys.vt.edu/ CAPS/

[233] V.I. Goldansky, O.A. Karpukhin, A.V. Kutsenko and V.V. Pavlovskaya, Nucl. Phys. 18 (1960) 473

[234] P. Baranov, G. Buinov, V. Godin, V. Kuznetsova, V. Petrun'kin, L. Tatarinskaya, V. Shirchenko, L. Shtarkov, V. Yurchenko and Yu. Yanulis, Phys. Lett. B 52 (1974) 122

[235] F.J. Federspiel, R.A. Eisenstein, M.A. Lucas, B.E. MacGibbon, K. Mellendorf, A.M. Nathan, A. O'Neill and D.P. Wells, Phys. Rev. Lett. 67 (1991) 1511

[236] A. Zieger, R. Van de Vyver, D. Christmann, A. De Graeve, C. Van den Abeele and B. Ziegler, Phys. Lett. B 278 (1992) 34

[237] B.E. MacGibbon, G. Garino, M.A. Lucas, A.M. Nathan, G. Feldman and B. Dolbilkin, Phys. Rev. C 52 (1995) 2097

[238] C. Caso et al., Review of Particle Physics, Eur. Phys. J. C 3 (1998) 1

[239] K.W. Rose, B. Zurmuhl, P. Rullhusen, M. Lugwig, A. Baumann, M. Schumacher, J. Ahrens, A. Zieger, D. Christman and B. Ziegler, Nucl. Phys. A 514 (1990) 621

[240] J. Schmiedmayer, P. Riehs, J.A. Harvey and N.W. Hill, Phys. Rev. Lett. 66 (1991) 1015

[241] M. Bawin and S.A. Coon, Phys. Rev. C 55 (1997) 419

[242] L. Koester, W. Waschkowski, L.V. Mytsina, G.S. Samosvat, P. Prokofjevs and J. Tambergs, Phys. Rev. C 51 (1995) 3363

[243] T.L. Enik, L.V. Mitsyna, V.G. Nikolenko, A.B. Popov and G.S. Samosvat, Phys. Atom. Nucl. 60 (1997) 567

[244] F. Wissmann, M.I. Levchuk and M. Schumacher, Eur. J. Phys. A 1 (1998) 193

[245] G. Wormser, in: Lecture Notes in Physics 365, M. Schumacher , G. Tamas Eds., p. 100 Springer (1990)

[246] H. Arenhövel, M. Weyrauch, P.G. Reinhard, Phys. Lett. 155B (1985) 22

[247] J. Vesper, N. Ohtsuka, L. Tiator, D. Drechsel, Phys. Lett. 159B (1985) 233;
J. Vesper, D. Drechsel, N. Ohtsuka, Nucl. Phys. A 466 (1987) 652

[248] F. Lenz, E. J. Moniz, Phys. Rev. C12 (1975) 909

[249] K. Klingenbeck, M.G. Huber, J. Nucl. Phys. G6 (1980) 961

[250] M.G. Huber, B. Ch. Metsch, H.R. Petry, in: Lecture Notes in Physics 365, M. Schumacher , G. Tamas, Eds. Springer (1990)145

[251] E. Oset and L.L. Salcedo, Nucl. Phys. A 468 (1987) 631

[252] G. García-Recio, E. Oset, L.L. Salcedo, D. Strottman and M.J. López, Nucl. Phys. A 526 (1987) 685

[253] T. Udagawa, S.-W. Hong and F. Osterfeld, Phys. Lett. B 245 (1990) 1

[254] R.H. Landau and A.W. Thomas, Nucl. Phys. A 302 (1978) 461

[255] L.D. Landau, Zh. Exp. Teor. Fiz. 35 (1958) 97

[256] C.W. deJager, H. deVries and C. deVries, Nucl. Data Tables 14 (1974) 479

[257] D. Pines and P. Noziéres, Theory of Quantum Liquids, Vol. I (W.A. Benjamin, New York and Amsterdam, 1966)

[258] A.B. Migdal, Theory of Finite Fermi Systems and Applications to Atomic Nuclei (Interscience, New York, 1957)

[259] G. Baym and S.A. Chin, Nucl. Phys. A 262 (1976) 527

[260] W. Bentz, A. Arima, H. Hyuga, K. Shimizu, K. Yazaki, Nucl. Phys. A 436 (1985) 593

[261] M.R. Anastasio and G.E. Brown, Nucl. Phys. A285 (1977) 516

[262] W.H. Dickhoff, A. Fässler, J. Meyer-ter-Vehn and H. Müther, Phys. Rev. C23 (1981) 1154

[263] W.H. Dickhoff, Nucl. Phys. A399 (1983) 287

[264] S.-O. Bäckman and G.E. Brown, Phys. Reports 124 (1985) 1

[265] J.I. Fujita and M. Hirata, Phys. Lett. B 37 (1971) 237

[266] J.I. Fujita, S. Ishida, M. Hirata, Supp. Prog. Theor. Phys. 60 (1976) 73

[267] J.I. Fujita and M. Ichimura, in: Mesons in nuclei, eds. M. Rho and D.H. Wilkinson (North-Holland, Amsterdam, 1979) Chap. 15

[268] H. Hyuga, A. Arima, and K. Shimizu, Nucl. Phys. A 336 (1980) 363

[269] T. Yamazaki, in *Mesons in Nuclei*, edited by M. Rho and D.H. Wilkinson (North-Holland, Amsterdam, 1979) Chap. 16

[270] A. Arima and H. Hyuga, in *Mesons in Nuclei*, edited by M. Rho and D.H. Wilkinson, (North-Holland, Amsterdam, 1979) Chap. 17

[271] Y. Nambu and G. Jona-Lasinio, Phys. Rev. 122 (1961) 345

[272] B.D. Serot, J.D. Walecka, Adv. Nucl. Phys. 16 (1986) 1

[273] M. Rho, "Chiral Symmetry in Nuclear Physics" nucl-th/9812012

[274] M. Jacob and G.C. Wick, Ann. Phys. (N.Y.) 7 (1959) 404

[275] Y. Hara, Prog. Theor. Phys. Suppl. 51 (1972) 96

[276] A. Erdélyi, "Higher Transcendental Functions", McGraw-Hill 1953

[277] F.A. Berends, A. Donnachie and D.L. Weaver, Nucl. Phys. B4 (1967) 1

[278] P. Stichel and E. Werner, Nucl. Phys. A145 (1970) 257

[279] J.S. O'Connell, in: "Photonuclear Reactions and Applications", B.L. Berman Ed., Pacific Grove 1973

[280] E. Hayward, in [204] p. 275

[281] J.L. Friar and S. Fallieros, Phys. Rev. C 15 (1977) 365

[282] P. Christillin, Phys. Lett. B146 (1984) 375

[283] A. Fabrocici and S. Fantoni, Nucl. Phys. A435 (1985) 448

[284] B. Castel, I.S. Towner, "Modern Theories of Nuclear Moments", Oxford Univ. Press 1990

[285] A.I. L'vov and A.I. Milstein, Phys. Lett. A192 (1994) 185

[286] R.P. Feynman and A.R. Hibbs, *Quantum mechanics and path integrals*, McGraw-Hill, New York, 1965

[287] J.S. Levinger, M.L. Rustgi and K. Okamoto, Phys. Rev. 106 (1957) 1191

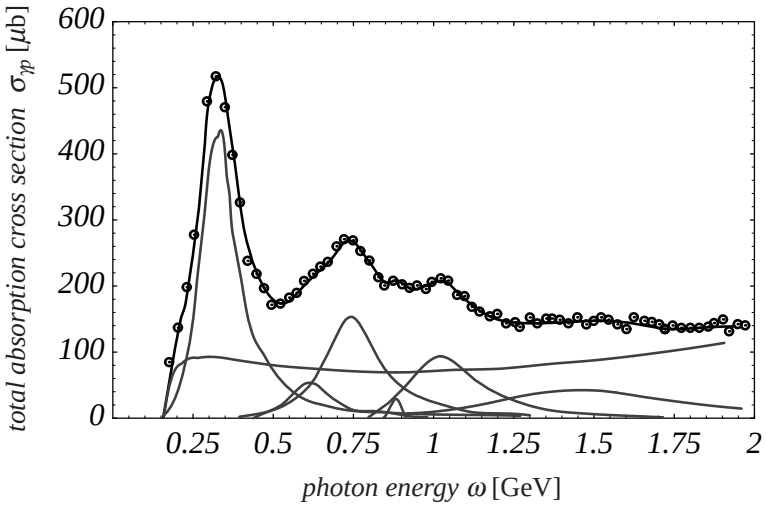

Figure 2.1: *Photoabsorption cross section of the proton schematically separated into partial cross sections [142] containing nucleon resonances and a nonresonant component.*

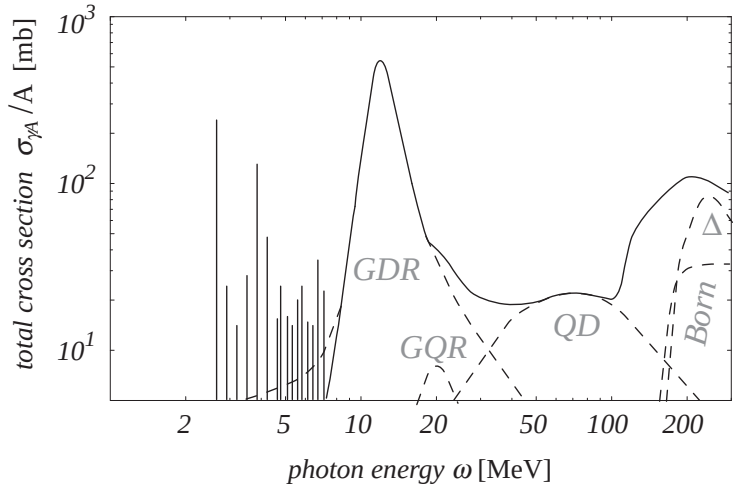

Figure 2.2: *Schematic view of the nuclear photoabsorption cross section of ^{208}Pb from the giant resonance to the Δ resonance range. GDR: giant-dipole resonance, GQR: isovector giant-quadrupole resonance, QD: quasideuteron mode, Δ: Delta resonance of nucleons in the nucleus, Born: nonresonant photoexcitation of nucleons in the nucleus through the Born terms of the photo-pion amplitudes [144].*

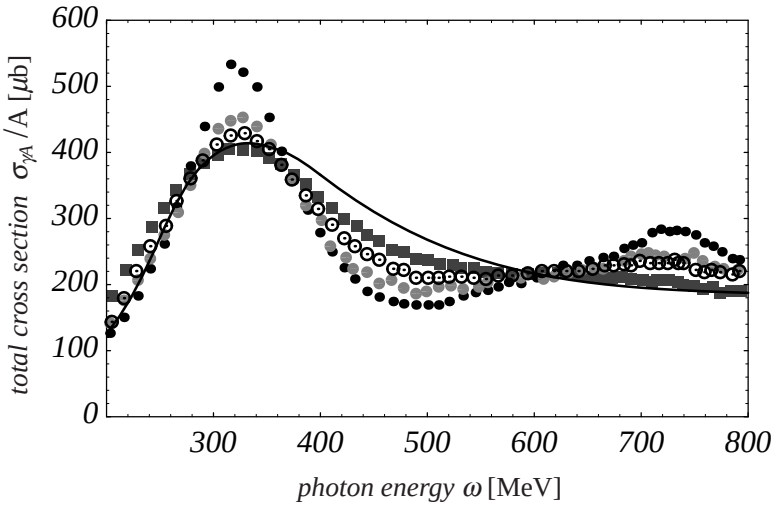

Figure 2.3: *Total photoabsorption cross sections per nucleon. Data are shown for* ^1H *(black circles),* ^2H *(gray circles),* ^3He *(open circles) and* ^4He *(grey squares) [146]. The solid line represents the universal curve for complex nuclei.*

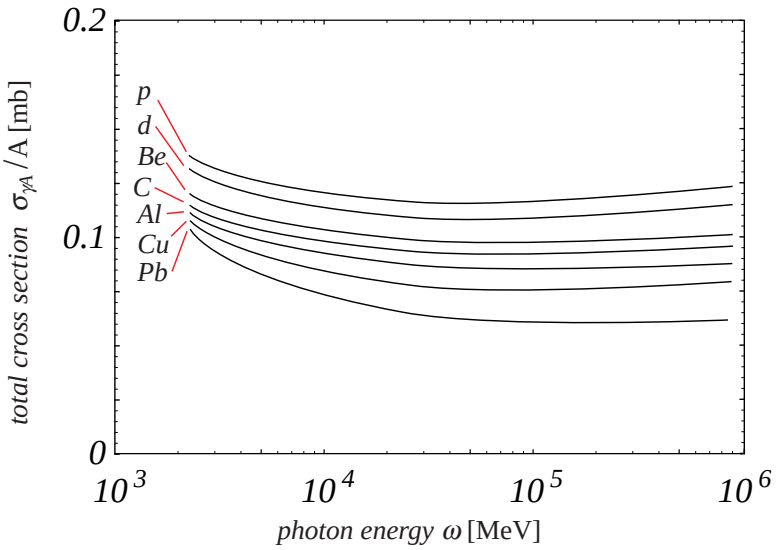

Figure 2.4: *Fits to the total nuclear photoabsorption cross sections per nucleon as an example of shadowing in the asymptotic region [148].*

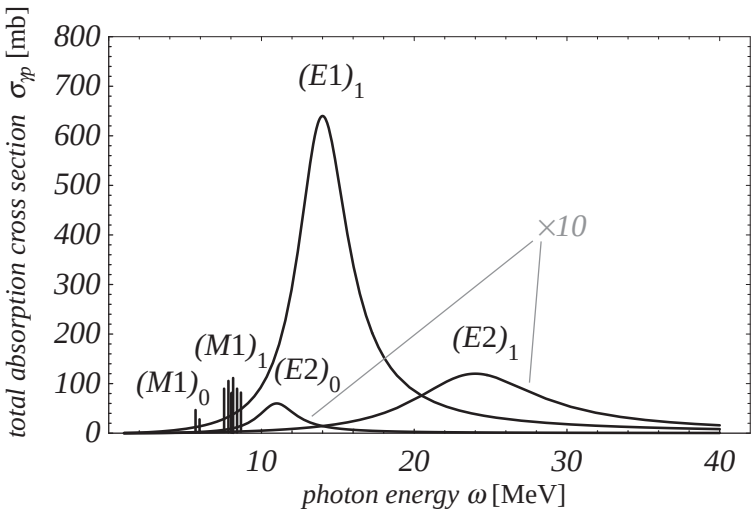

Figure 2.5: *Schematic representation of giant resonance multipoles for ^{208}Pb. $(E1)_1$: isovector giant electric-dipole resonance (GDR), $(M1)_0$: isoscalar giant magnetic-dipole resonance, $(M1)_1$: isovector giant magnetic-dipole resonance,$(E2)_0$: isoscalar giant electric-quadrupole resonance, $(E2)_1$: isovector giant electric-quadrupole resonance [95].*

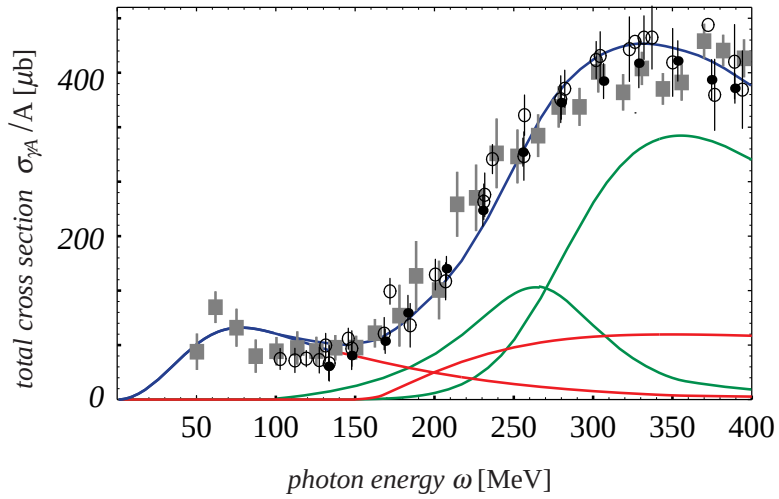

Figure 2.6: *Total nuclear photoabsorption cross sections per nucleon. Data are shown for nuclei between ^4He and ^{238}U [148]. In addition the result of a model calculation for the universal photoabsorption curve is shown [157]. The left curve extending underneath the Δ resonance is the QD cross section. The Δ-resonance cross section is partitioned into two curves, into a non-mesonic part (left resonant curve) and a mesonic part (right resonant curve). The nonresonant curve in the Δ range corresponds to the Born term of meson photoproduction.*

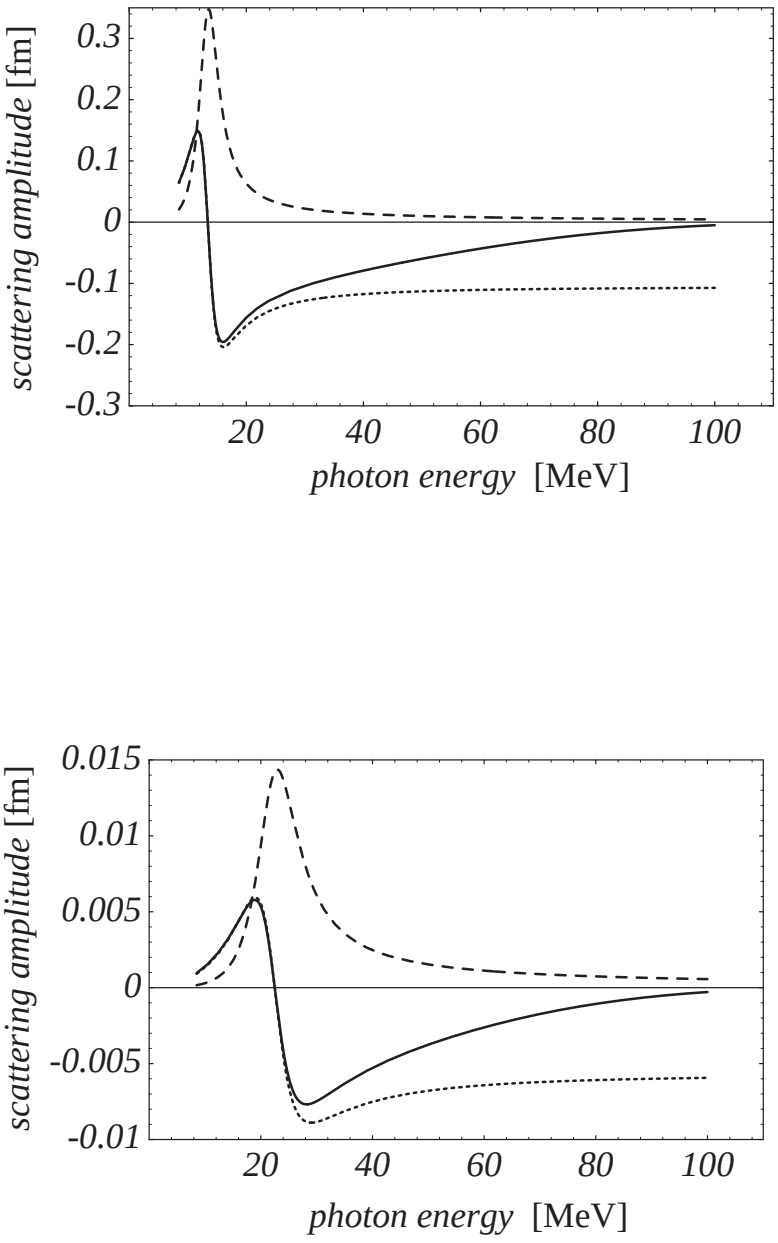

Figure 4.1: *Scattering amplitudes for the giant-dipole resonances (upper figure) and isovector giant-quadrupole resonance (lower figure) of ^{208}Pb in the forward direction: Im $R^{\lambda L}(\omega, \theta = 0)$ (dashed), Re $\tilde{R}^{\lambda L}(\omega, \theta = 0)$ (dotted) and Re $\hat{R}^{\lambda L}(\omega, \theta = 0)$ (solid).*

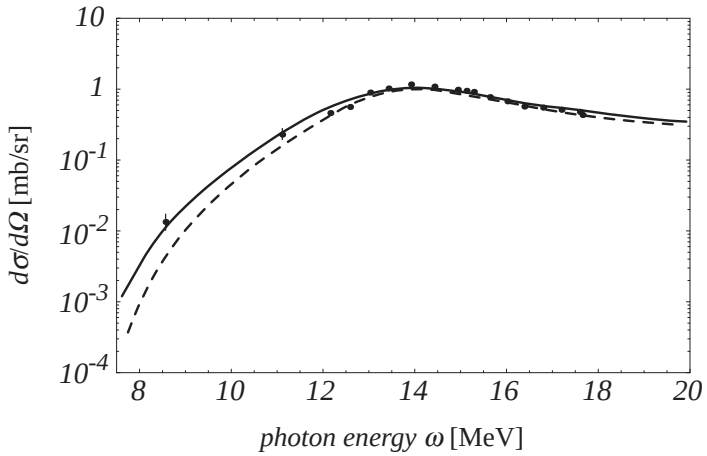

Figure 4.2: *Differential cross sections for Compton scattering by* ^{209}Bi*. Scattering angle* $\theta = 135°$*. Data points at 9.0, 11.4 and 17.74 MeV are measured by [63]. Other data points are measured by [201]. Solid curve: calculated using the GDR parameters of [63]. Dashed curve: calculated using the GDR parameters of [201].*

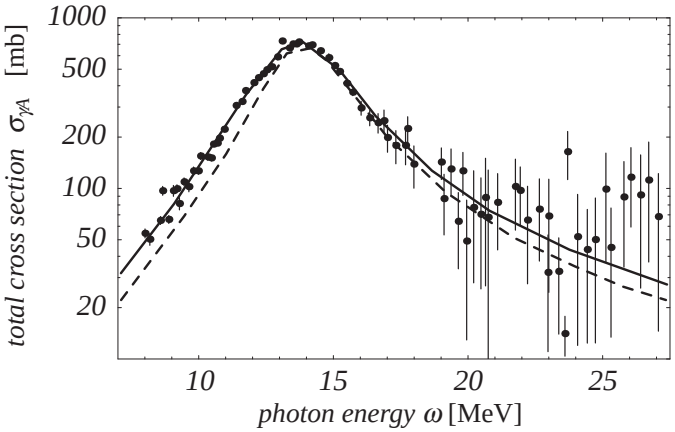

Figure 4.3: *Photoabsorption cross sections for* ^{209}Bi *measured by [202] multiplied by a scaling factor of 1.35. Solid curve: calculated using the GDR parameters of [63]. Dashed curve: calculated using the GDR parameters of [201].*

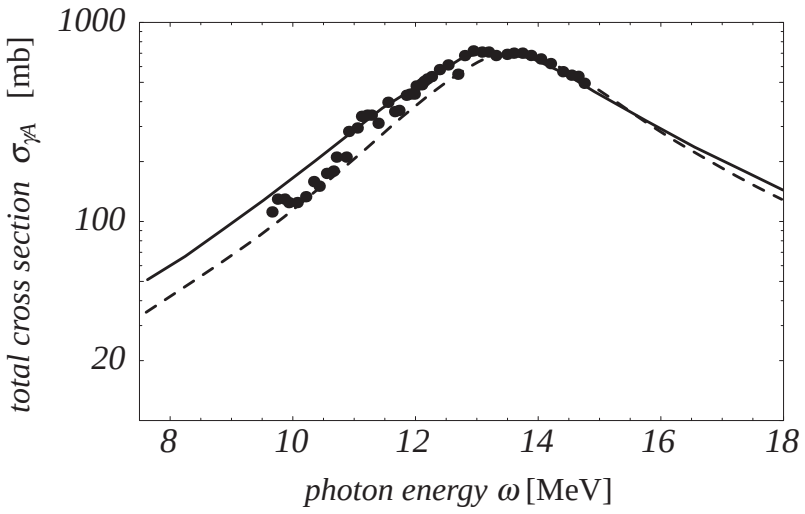

Figure 4.4: *Photoabsorption cross sections for ^{209}Bi measured by [203] multiplied by a scaling factor of 1.09. Solid curve: calculated using the GDR parameters of [63]. Dashed curve: calculated using the GDR parameters of [201].*

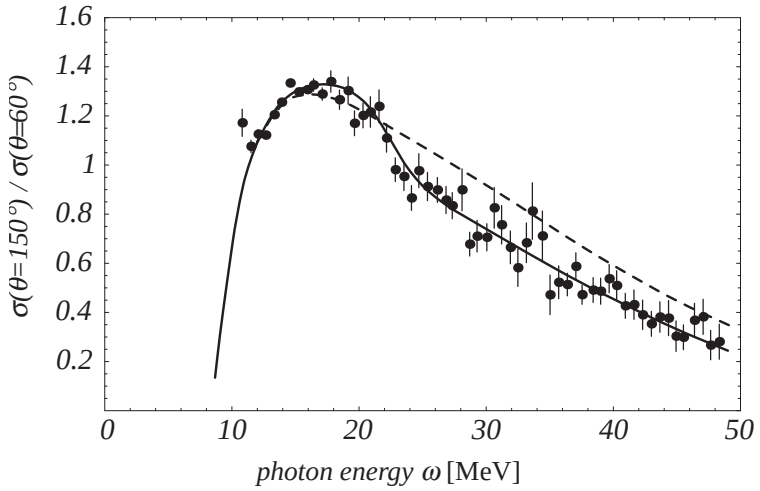

Figure 4.5: *Cross-section ration $\sigma(\theta = 150°)/\sigma(\theta = 60°)$ for Compton scattering of unpolarized photons by ^{208}Pb [25]. Solid line: Calculated including the IVGQR. Dashed line: Calculated not including the IVGQR. The IVGQR shows up as interference of the $E2$ amplitude with the predominant $E1$ amplitude from the GDR.*

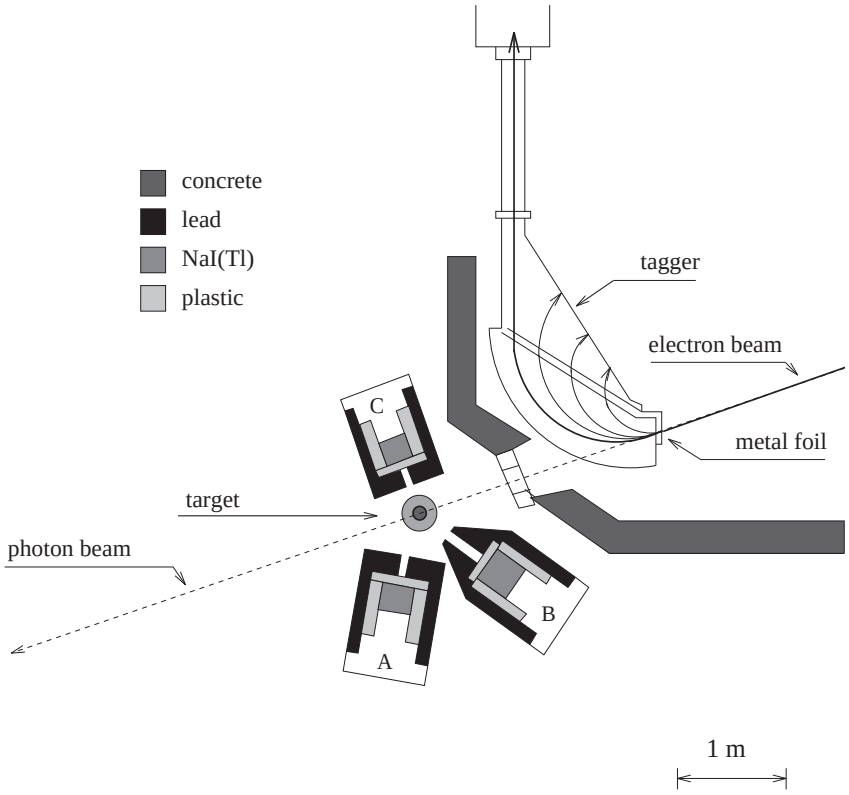

Figure 5.1: *Typical experimental arrangement as used at the MAX laboratory of the university of Lund (Sweden) [51,52]. The photon beam having an energy of about 100 MeV hits a thin metal foil serving as a bremsstrahlung radiator. Quasi monochromatic photons are produced through a coincidence condition between an event in one of the NaI(Tl) detectors (A, B, C) and an event in the tagger.*

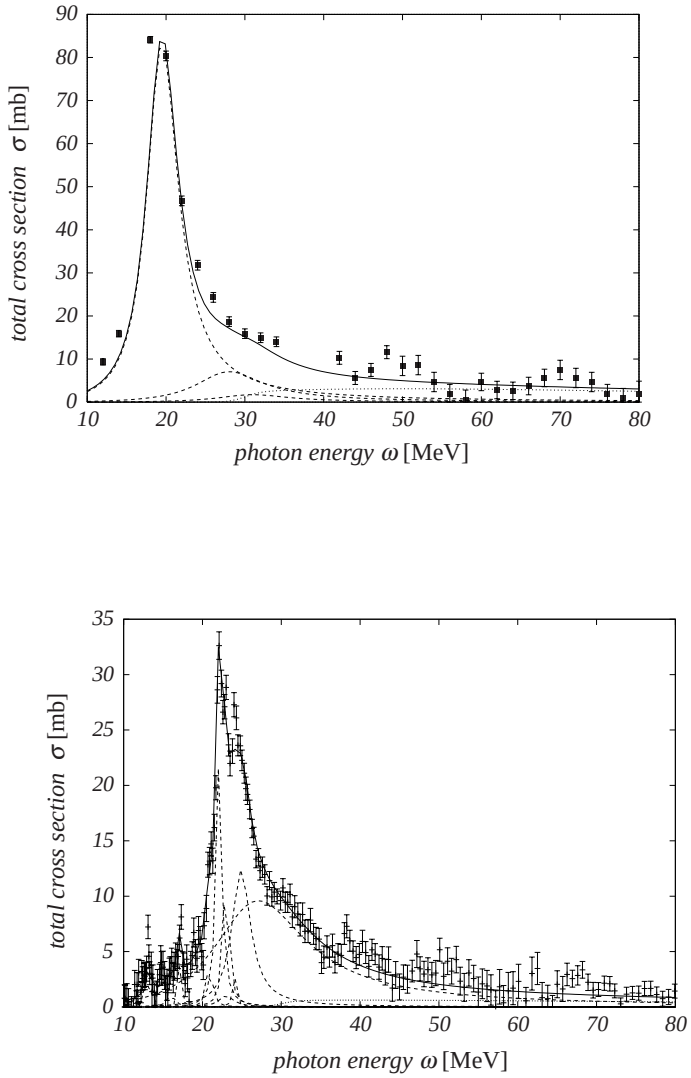

Figure 5.2: *Total photoabsorption cross sections [84] for ^{40}Ca (upper figure) and ^{16}O (lower figure) partitioned into components having Lorentzian shapes. Dashed curves: GR components. Dotted curves: QD components.*

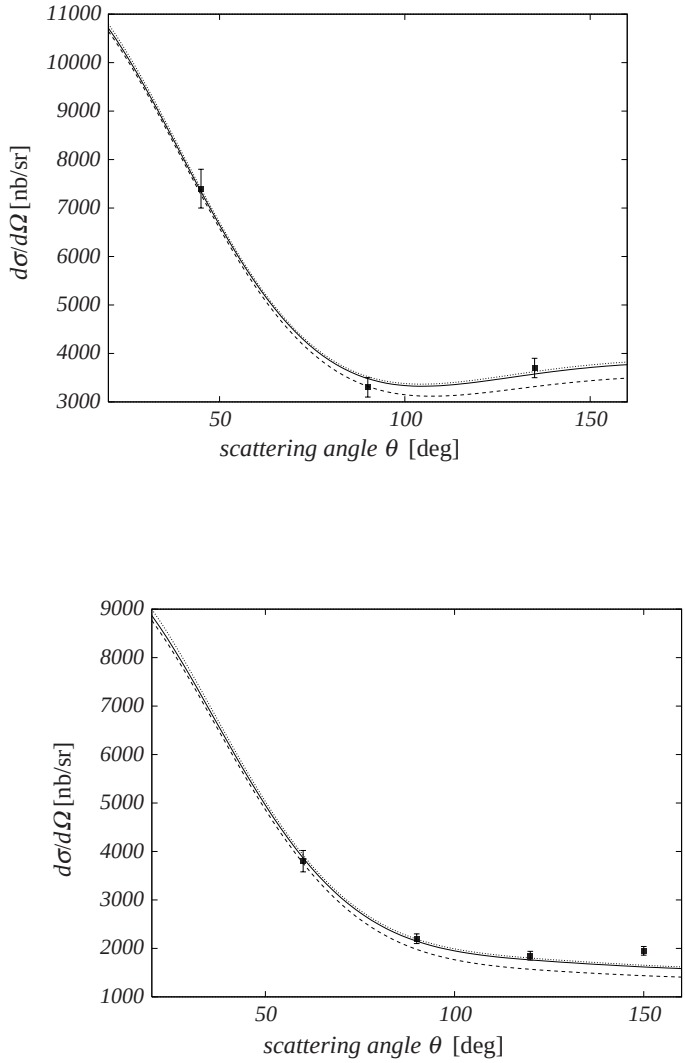

Figure 5.3: *Experimental elastic differential cross sections [42, 47, 48] for* ^{40}Ca *versus scattering angle compared with predictions.* $E_\gamma = 58\ MeV$ *(upper Figure),* $E_\gamma = 75\ MeV$ *(lower Figure). The curves are calculated for (i) the free-nucleon electromagnetic polarizabilities (dashed), (ii) the free-nucleon electromagnetic polarizabilities supplemented by meson exchange corrections predicted for the finite nucleus (solid), and (iii) the free-nucleon electromagnetic polarizabilities supplemented by meson exchange corrections predicted for nuclear matter (dotted).*

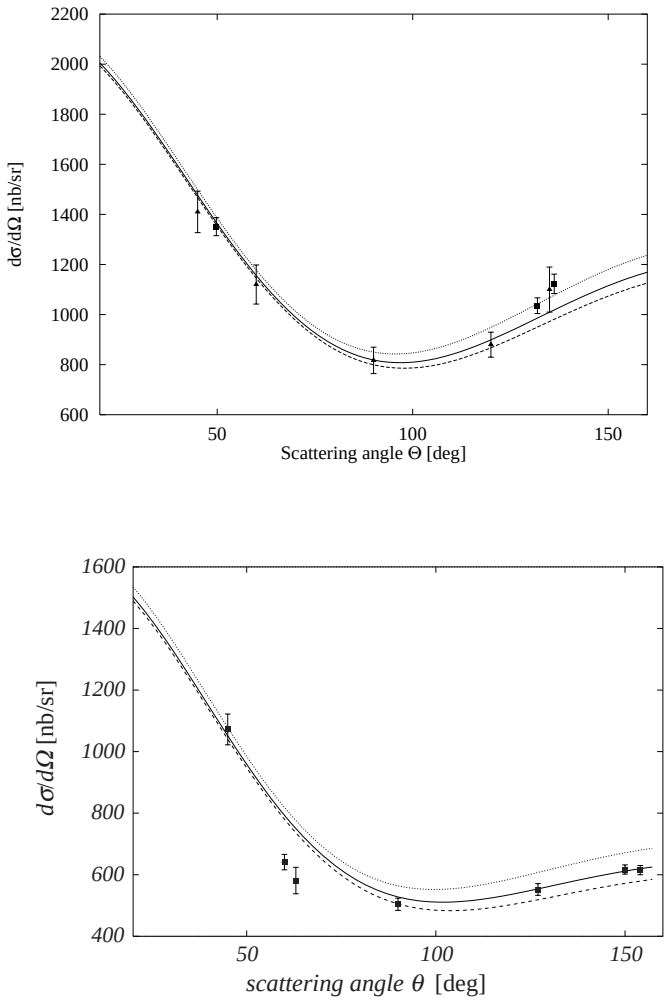

Figure 5.4: *Differential cross sections [39, 47, 48] for Compton scattering by* ^{16}O *versus scattering angle compared with predictions.* $E_\gamma = 58$ *MeV (upper figure);* $E_\gamma = 75$ *MeV (lower figure). The curves are calculated for (i) the free-nucleon electromagnetic polarizabilities (dashed), (ii) the free-nucleon electromagnetic polarizabilities supplemented by meson exchange corrections predicted for the finite nucleus (solid), and (iii) the free-nucleon electromagnetic polarizabilities supplemented by meson exchange corrections predicted for nuclear matter (dotted).*

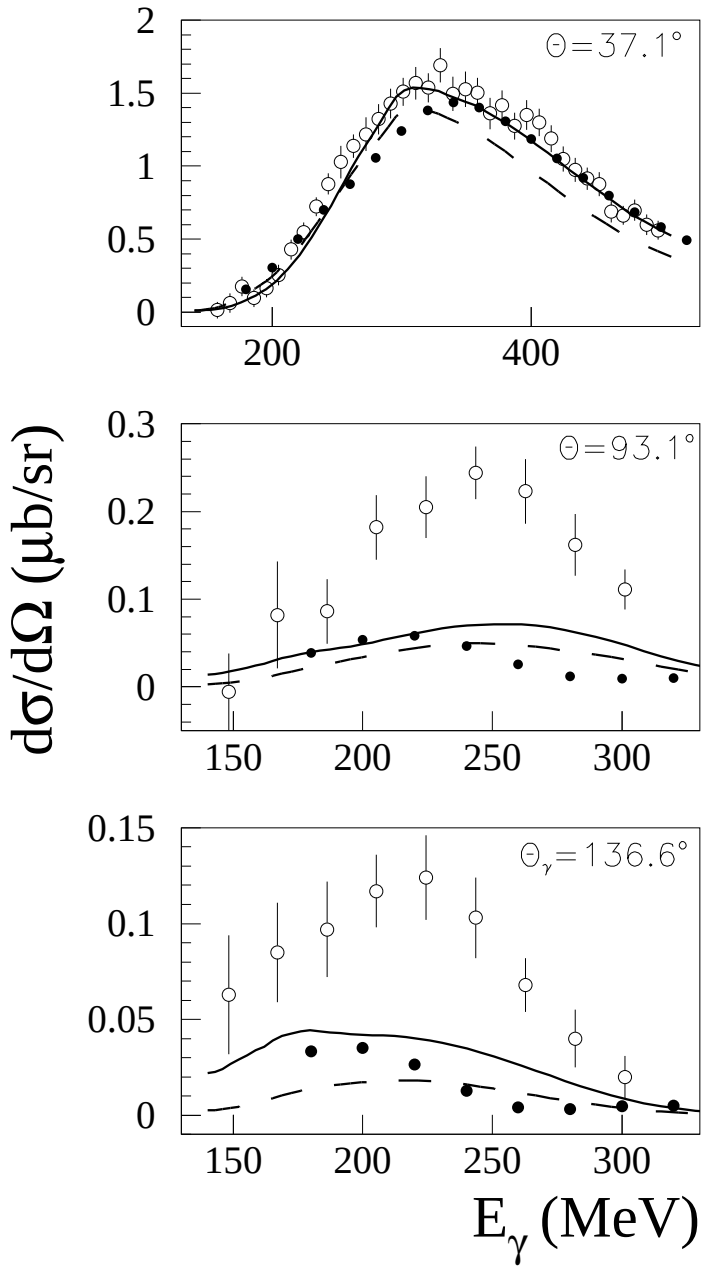

Figure 6.1: *Differential cross sections* $(d\sigma/d\Omega)_{LAB}$ *for Compton scattering by* ^{4}*He [46] compared with predictions. The full circles are calculated within the* Δ*-hole model including the seagull amplitudes [46]. The results of the schematic model (dashed) and the extended schematic model (solid) are also shown [46].*

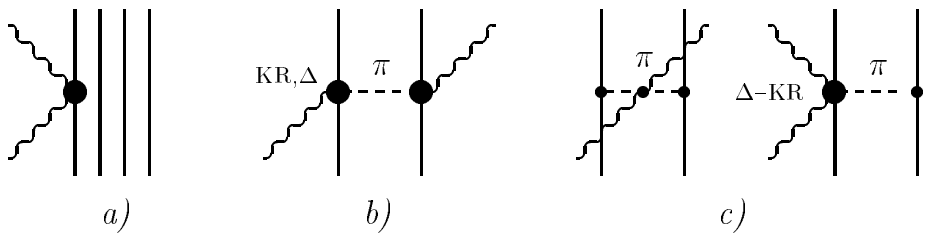

Figure 6.2: *One- and two-body contributions to nuclear Compton scattering. Diagram a is the impulse approximation. Diagram b describes real pion production followed by pion absorption. Diagrams c are required by the gauge invariance; in particular, the last diagram contains the contact $\gamma\pi N\Delta$ vertex.*

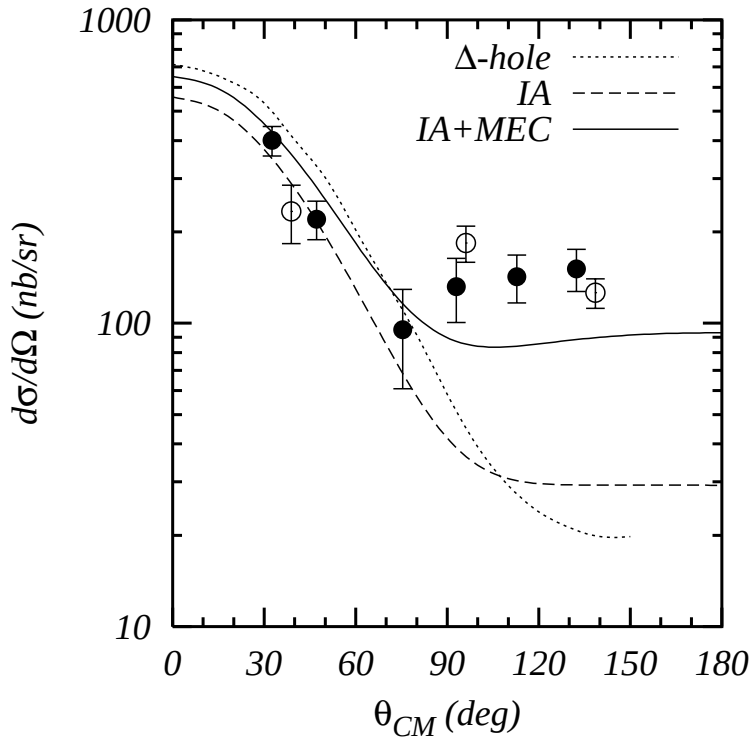

Figure 6.3: *Differential cross sections $(d\sigma/d\Omega)_{CM}$ for Compton scattering by ^4He at $E_\gamma = 206$ MeV. Data are from [45] (solid circles) and from [46] (open circles). Shown are predictions of the Δ-hole model in the local-density approximation [109], impulse approximation, Eq. (6.7), and the total contribution including the two-body MEC, Eq. (6.13).*

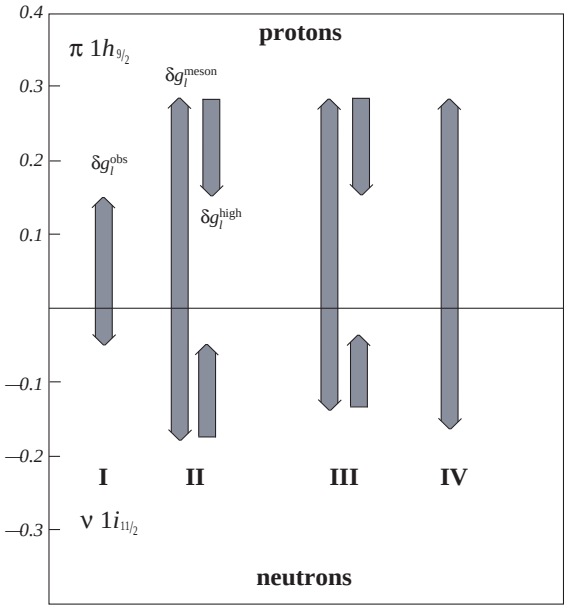

Figure 7.1: *Summary of results on the Fujita-Hirata relation. Column I: Experimental result of Yamazaki [269]. Column II: δg_L^{meson} calculated from the experimental $\mathring{\kappa}^{GDR}$ and δg_L^{high} obtained as a difference between δ_l^{meson} of column II and δg_L^{obs} of column I. Column III: Predictions of Hyuga et al. [268]. Column IV: Predictions of Brown and Rho [87].*

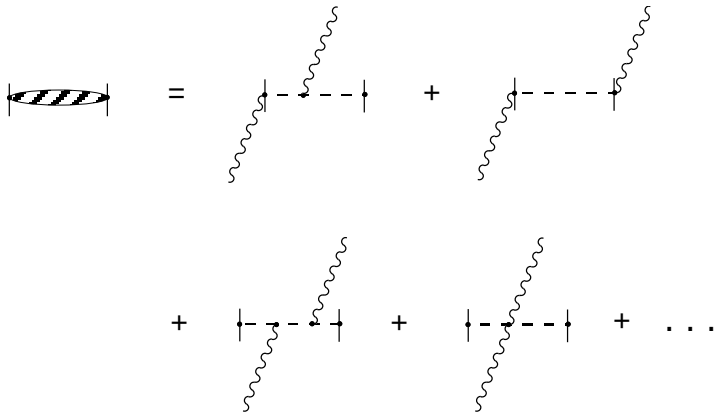

Figure 9.1: *Typical diagrams contributing to $\mathcal{T}_{(\pi)}^{ij}$. The wavy lines denote photons and dashed lines denote pions. The amputation indicates that T^{ij} contains only the nucleon vertices, but not its wave functions.*

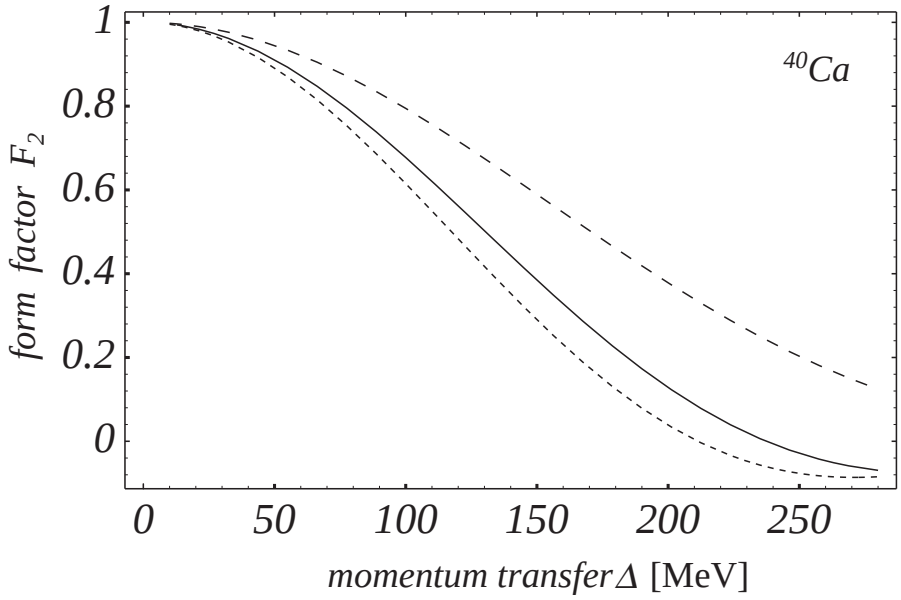

Figure 9.2: *Comparison of the form factors from Eqs. (9.8) (dotted curve) and (9.9) (full curve) for the case of* ^{40}Ca*. The approximation* $F_1^2(q/2)$ *is shown as a dashed curve.*

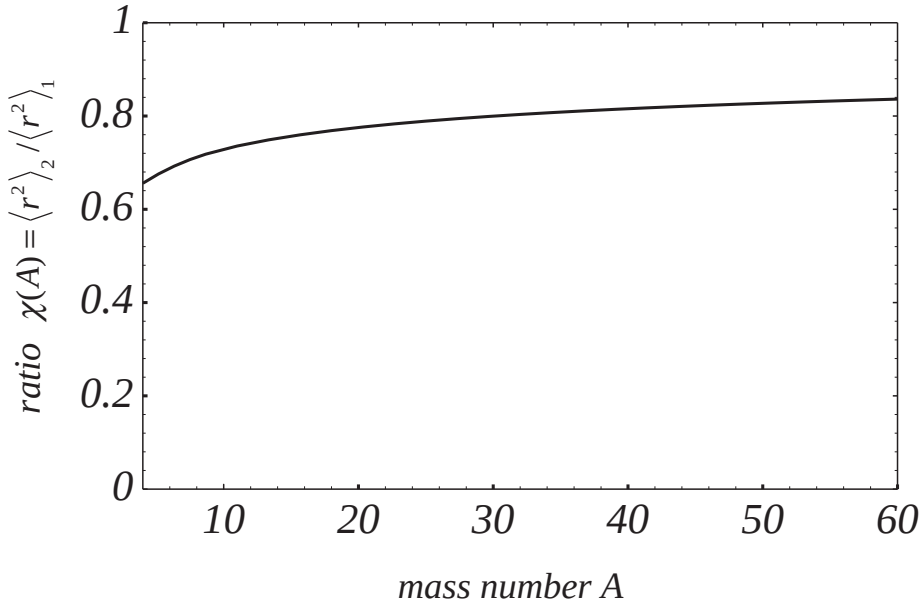

Figure 9.3: *Ratio* $\chi(A) = \langle r^2 \rangle_2 / \langle r^2 \rangle_1$ *as a function of the nuclear mass number A*

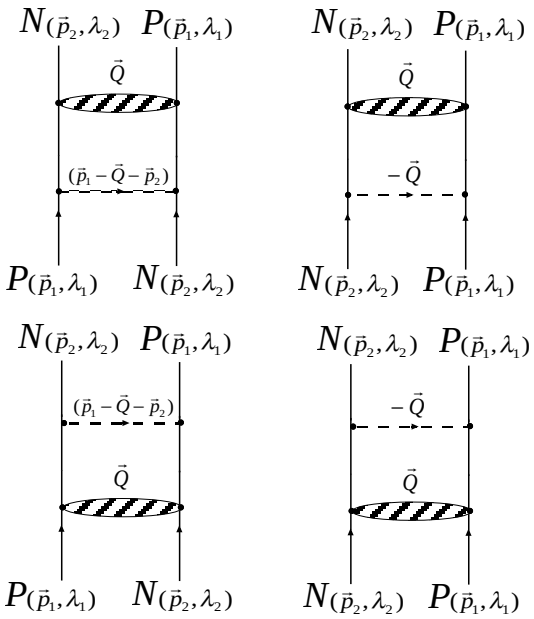

Figure 9.4: *Set of diagrams, from which the two-body correction to the correlator is extracted. Here the same symbolic abbreviation is used as in Fig. 9.1. The nucleon spin projections are denoted by* λ_i.

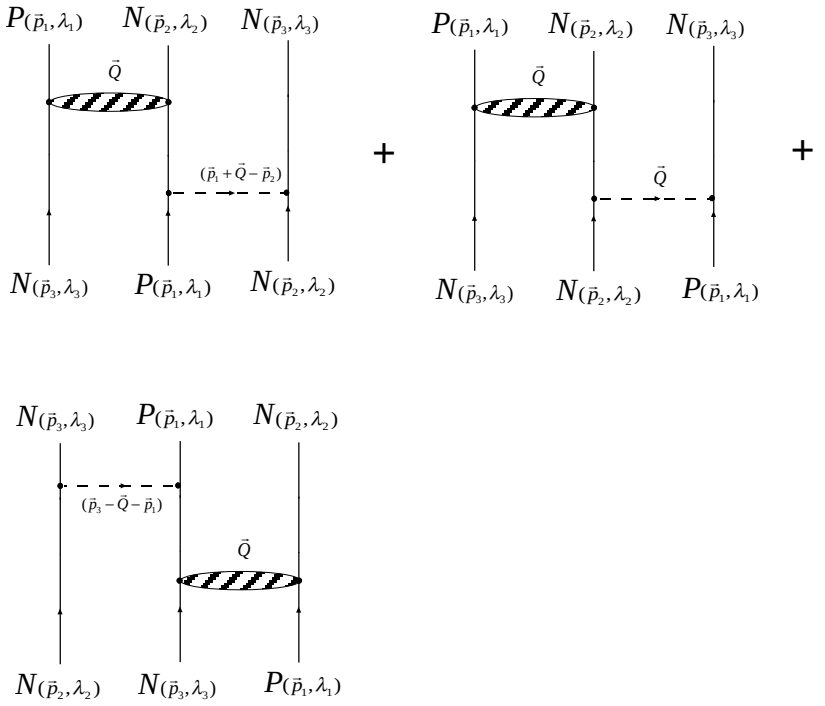

Figure 9.5: *Three-body diagrams yielding an additional correction to the correlator, which is of the same order in* f/m_π *as the two-body diagrams shown in Fig. 9.4. The notations are the same as in Fig. 9.1 and Fig. 9.4.*

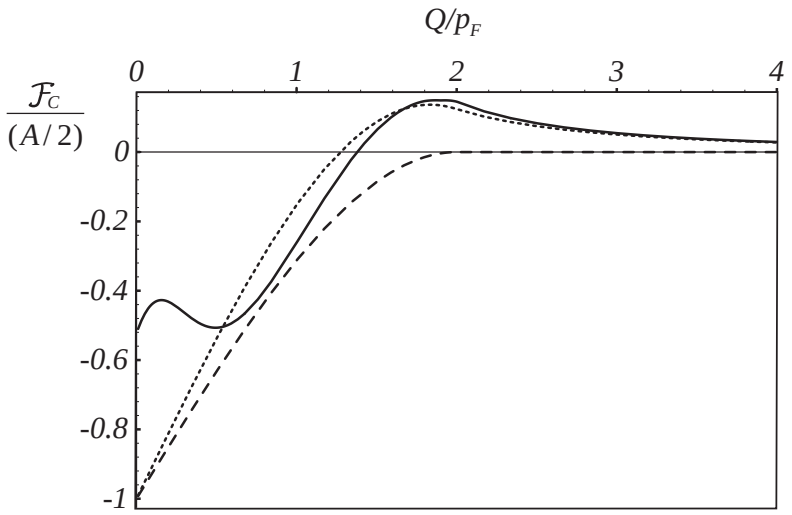

Figure 9.6: *Central part of the correlator with three-body corrections (full curve), without three-body corrections (dotted curve) and Fermi correlator without any corrections (dashed curve).*

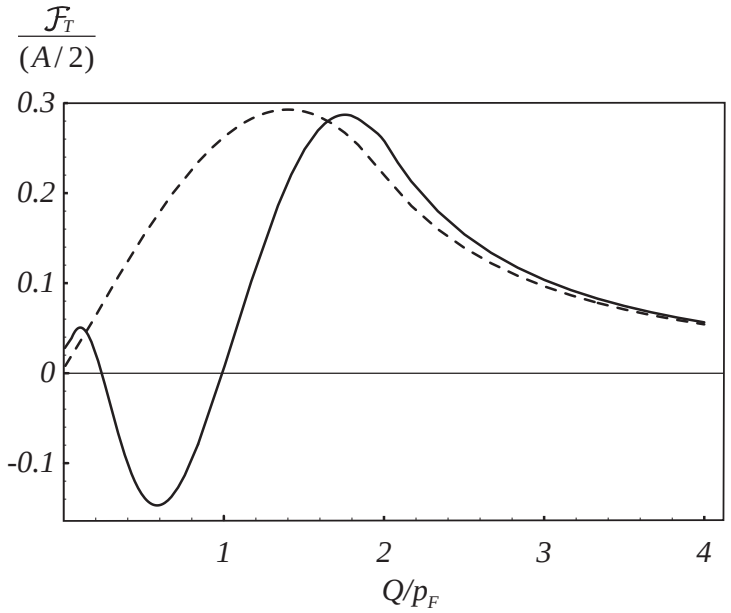

Figure 9.7: *Tensor part of the correlator with three-body corrections (full curve) and without three-body corrections (dashed curve).*

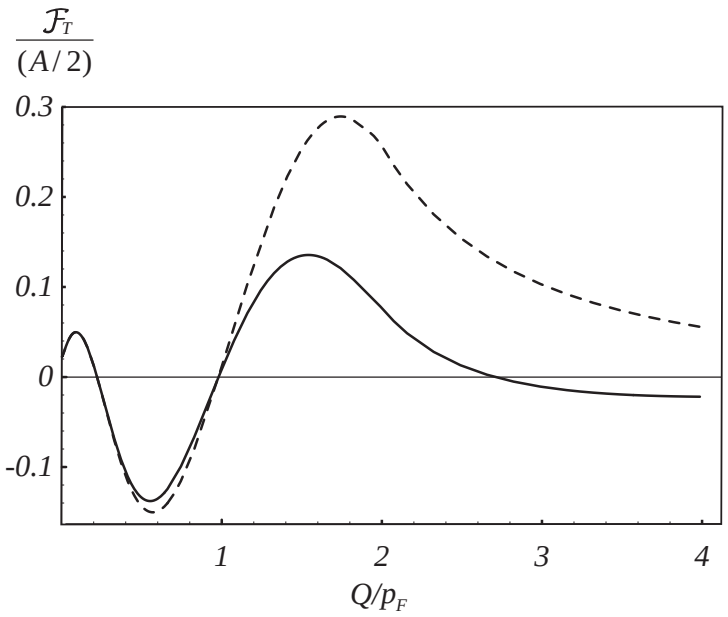

Figure 9.8: *Comparison of the tensor part of the correlator with (full curve) and without (dashed curve) the ρ-meson contribution.*

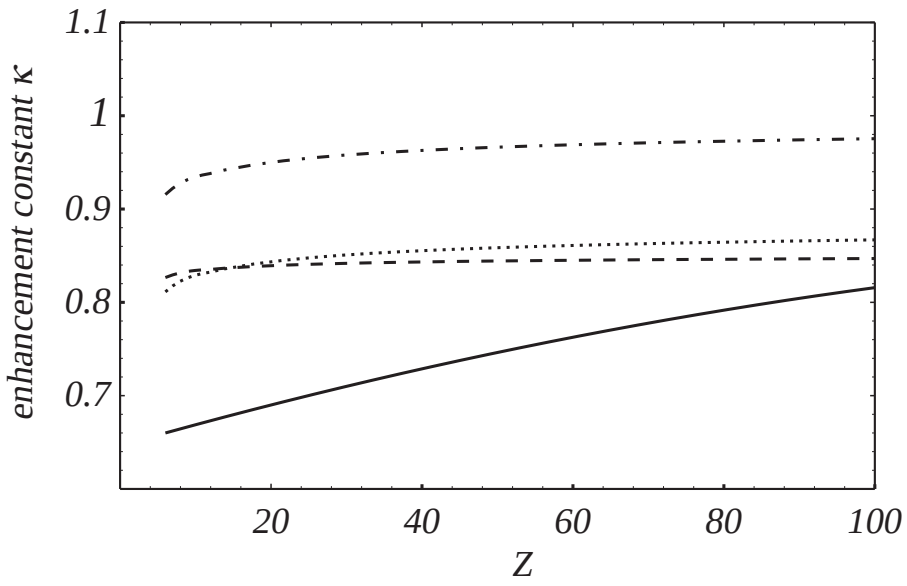

Figure 9.9: *Dependence of enhancement constant κ on proton number Z. The dashed curve corresponds to the pionic tensor contribution κ_T^π, the dash-dotted curve includes also the central contribution κ_C^π and the dotted curve gives the total κ, including the contribution from ρ-meson exchange. The realistic-density result $\kappa^{(rd)}$ for the full enhancement constant (cf. Eq. (9.30)) is shown as a full curve.*

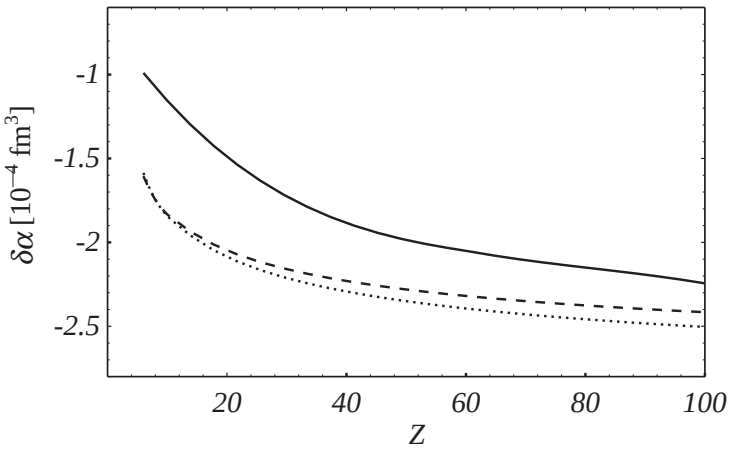

Figure 9.10: *Pion-exchange contribution to electric polarizability $\delta\alpha$ as a function of Z. The dashed curve corresponds to the central contribution $\delta\alpha_C$ and the dotted curve gives the total $\delta\alpha = \delta\alpha_C + \delta\alpha_T$. The use of a realistic density leads to the full curve.*

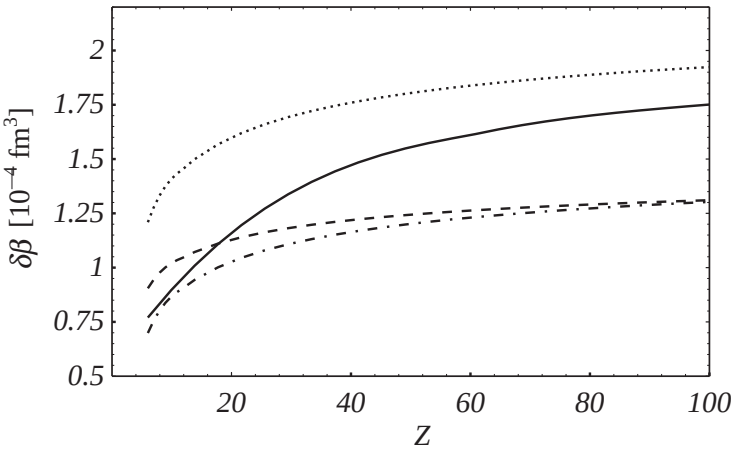

Figure 9.11: *Pion-exchange contribution to magnetic polarizability $\delta\beta$ as a function of Z. The dashed curve corresponds to the central contribution $\delta\beta_C$ and the dash-dotted curve gives the sum $\delta\beta_C + \delta\beta_T$. Adding the contribution of the Δ-isobar excitation as given in Eq. (9.29) leads to the total value of $\delta\beta$ given as the dotted curve. The use of a realistic density leads to the full curve.*

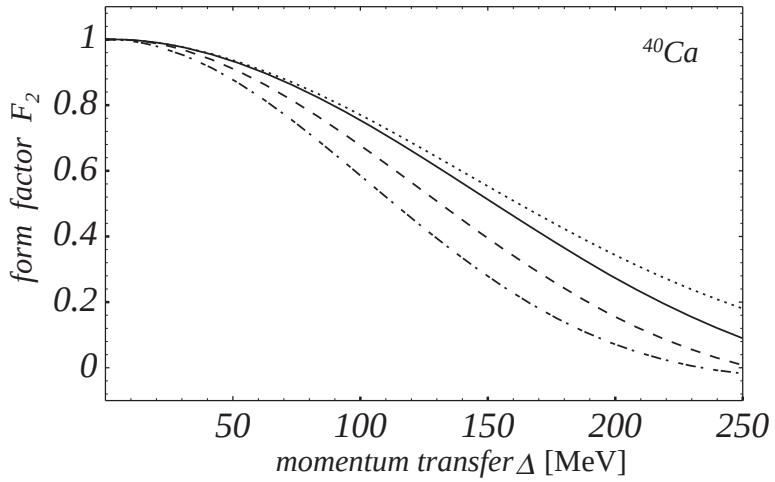

Figure 9.12: *Form factors $F_2^{(i)}(\Delta)$ for ^{40}Ca. The dashed curve is $F_2^{(1)}$ and the full curve is $F_2^{(2)}$. For comparison the (experimental) charge form factor F_1 is also shown (dash-dotted curve), as well as the function $F_1^2(\Delta/2)$ (dotted curve).*

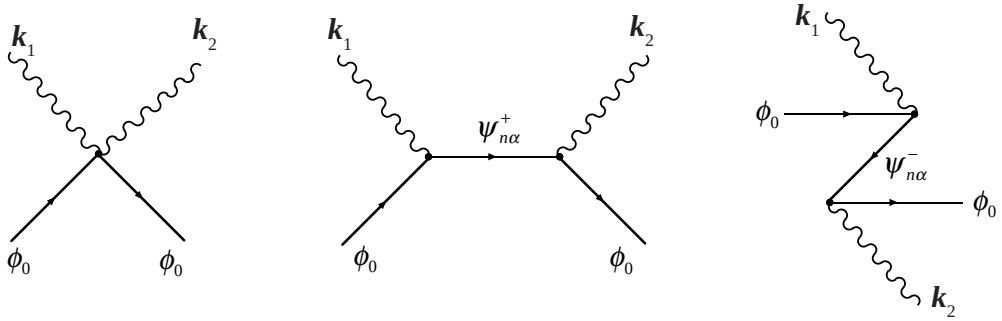

Figure 10.1: *Diagrams of Compton scattering off the relativistic oscillator (crossed terms are not shown)*

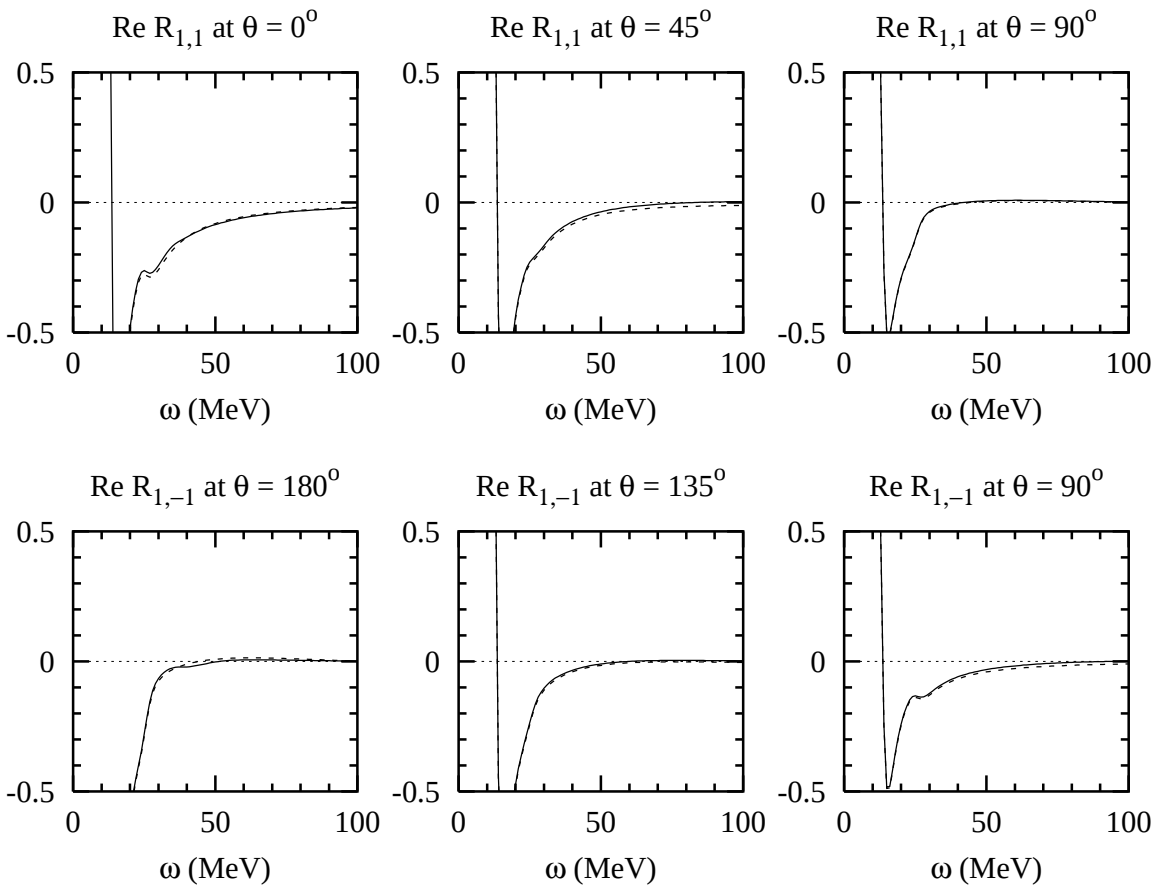

Figure 10.2: *Phenomenological, Eq. (10.73), (dashed lines) and exact (solid lines) amplitudes R_{GR} in the relativistic oscillator model at $\omega_0 = (13.4 - 2.1i)$ MeV and $\eta = 0.06$. Units are e^2/E_0.*

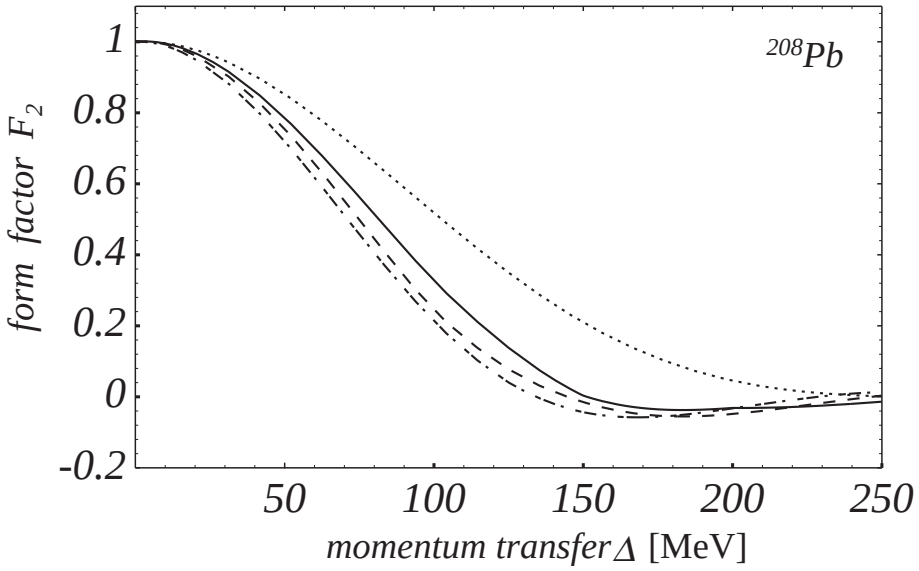

Figure B.1: *Exchange form factors $F_2^{(i)}(q)$ for the case of ^{208}Pb. The dashed curve represents $F_2^{(1)}$, while the full curve corresponds to $F_2^{(2)}$. For comparison the (experimental) charge form factor F_1 (dash-dotted curve) and the function $F_1^2(q/2)$ (dotted curve) are also shown. The parameters for the form factor F_1 were taken from ref. [256].*

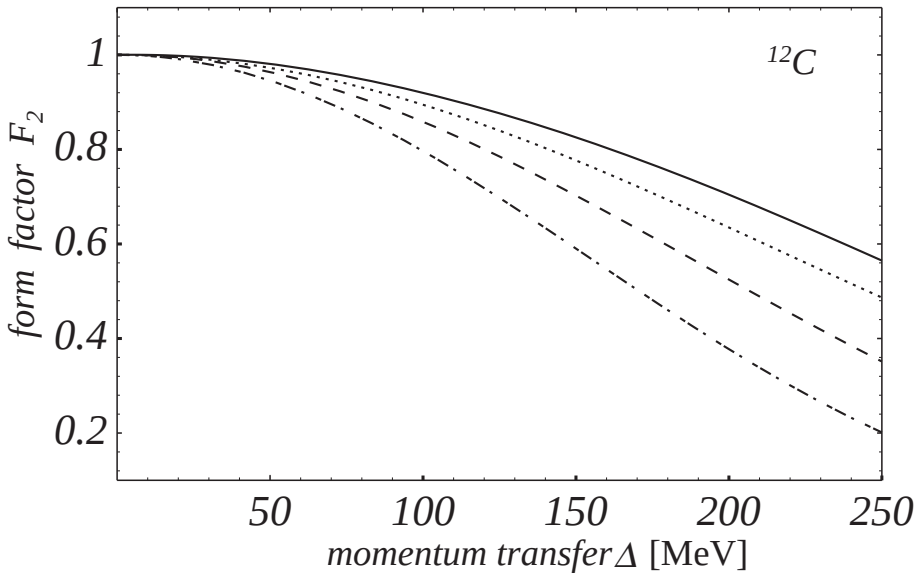

Figure B.2: *Same as Fig. B.1, but for ^{12}C.*

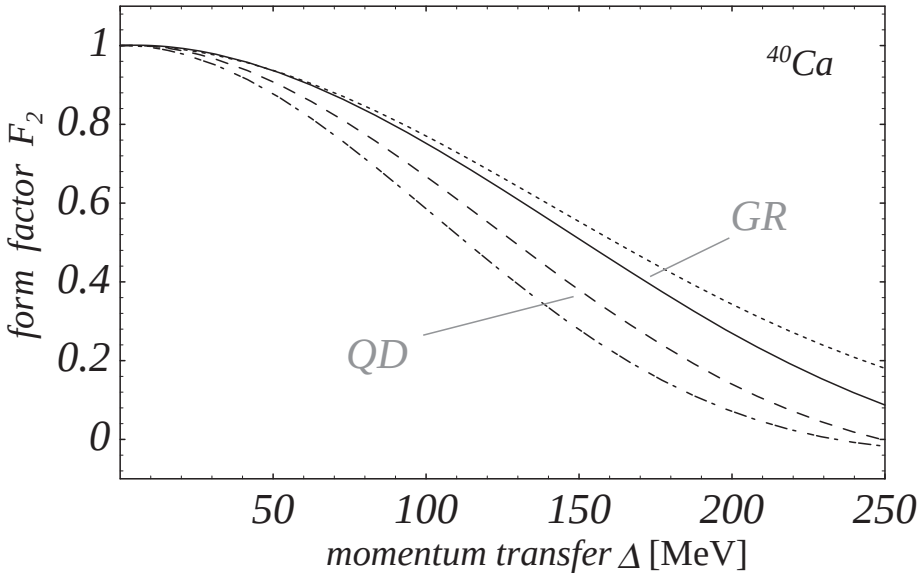

Figure B.3: *Form factors* $F_2^{(GR)}(\Delta)$ *and* $F_2^{(QD)}(\Delta)$*for* ^{40}*Ca. The dashed curve is* $F_2^{(QD)}$ *and the full curve is* $F_2^{(GR)}$*. In addition, the (experimental) charge form factor* F_1 *(dash-dotted curve) and the function* $F_1^2(\Delta/2)$ *(dotted curve) are shown for the sake of comparison.*

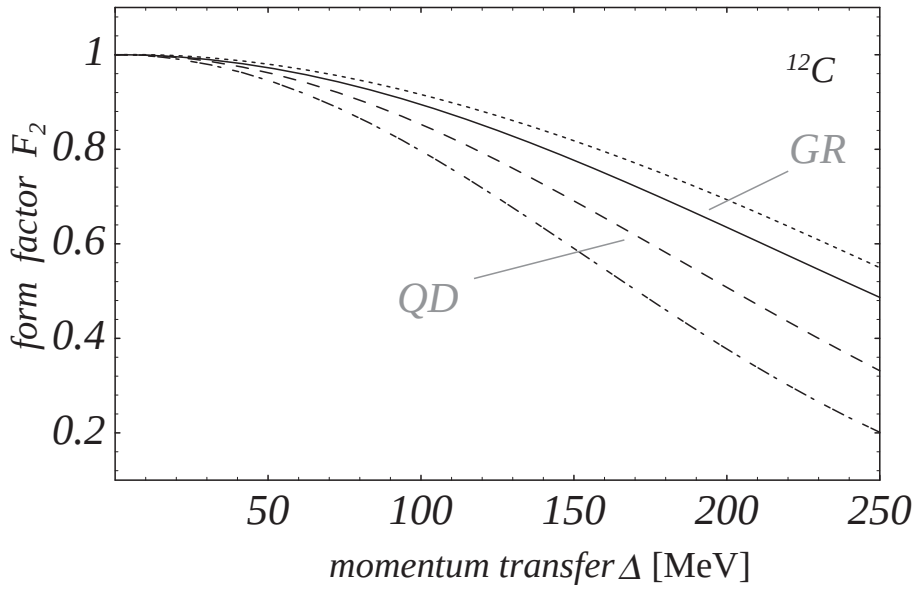

Figure B.4: *Same as Fig. B.3, but for* ^{12}*C.*